



Università degli Studi di Milano
Dipartimento di Chimica

Doctorate School in Chemical Sciences and Technologies
Doctorate in Chemical Sciences
XXVII cycle

CHIRAL ELECTROCHEMISTRY IN IONIC LIQUIDS

CHIM-02

Serena Arnaboldi

R09646

Supervisor: Prof. Patrizia Romana Mussini

Co-supervisor: Prof. Armando Gennaro

School Director: Prof. Emanuela Licandro

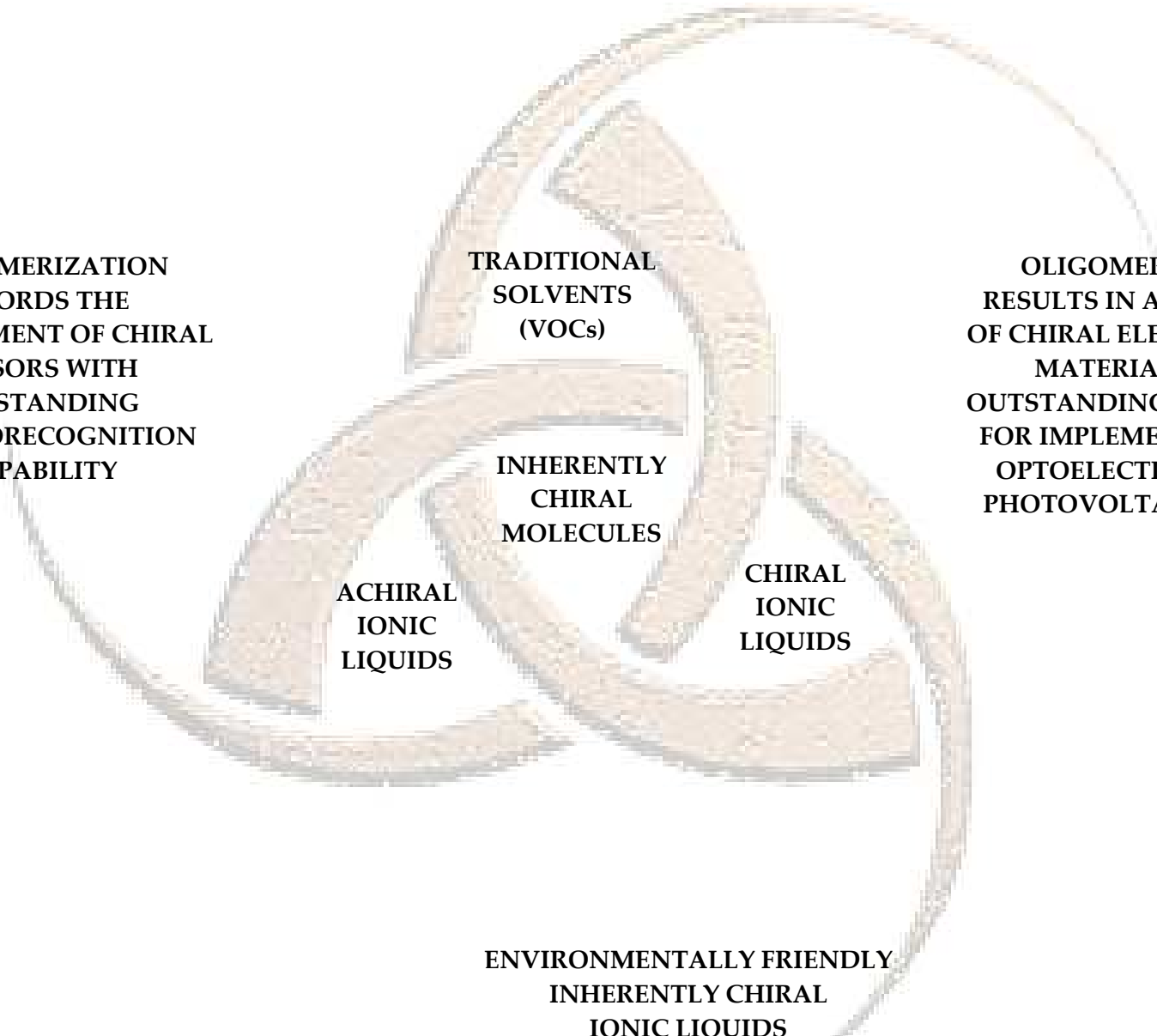
Academic Year 2013/2014

Index

General Remarks	1
1. Introduction.....	4
1.1 Conjugated Conducting Polymers	6
1.2 Electrochemistry of Conductive Polymers	11
1.2.1 General Mechanism.....	11
1.2.2 Charging-Discharging of Conductive Polymers.....	14
1.2.3. Specific n-doping Process	17
1.2.4. Factors that Affect the Electropolymerization Process.....	18
1.3 What is an Ionic Liquid? And Why use it in Electrodeposition?	20
1.4 Chirality in Conducting Polymers: Current Approaches	23
1.4.1 An Innovative Approach: Inherent Chirality in Atropisomeric Bi-heteroaromatic Scaffold.....	27
1.4.2 The Forefather of the Inherently Chiral Family	29
1.4.3 The Family Grows I: Inherently Chiral Molecular Materials with Thiophene-based Atropisomeric Scaffolds.....	31
1.4.4 The Family Grows II: Inherently Chiral Molecular Materials with Pyrrole-based Atropisomeric Scaffolds.....	33
1.4.5 The Same Concept in All-thiophene Materials: Inherently Chiral Spider-Like Oligothiophenes (β,β' -bithiophene core)	34
1.4.6 Chirality coupled with Ionic Liquids: Inherently Chiral Ionic Liquids	36
1.5 Electroreductive Cleavage of the Carbon Halogen Bond in Organic Halides	40
1.6 Guidelines and Targets of the PhD Thesis	42
References	45
2. Experimental.....	48
2.1 Voltammetry.....	48
2.1.1 Voltammetric Study of The Chemical Reactivity of Inherently Chiral Monomers in Traditional Solvents	48
2.1.2 Enantiorecognition Tests of Enantiopure Thiophene-based Oligomers	50
2.1.3 Characterization of Cyclic Oligothiophenes and Enantiorecognition Tests.....	50
2.1.4 Differential Pulse Voltammetry (DPV) to Study the Racemization Barrier of Monomers with 3,3'-Bis-indole Core.....	51
2.1.5 DPV to Check Probe Enantiomeric Excess on Homochiral Films.....	51
2.1.6 Study of the DET Process in the Reductive Cleavage of Carbon-Halogen Bond.....	52
2.1.7 Protocol Employed for Chloride Impurities Abatement.....	53

2.2 An Introduction to Less Common Techniques	55
2.2.1 Electrochemical Impedance Spectroscopy (EIS).....	55
2.2.2 Principles of Electrochemical Impedance Spectroscopy (EIS) Measurements.....	57
2.2.3 Equivalent Circuit Elements.....	60
2.2.4 Common Equivalent Circuit models	62
2.2.5 The Experimental Setup and the Analysis Protocol.....	64
2.2.5 Circular Dichroism Spectroscopy (CD)	66
2.3 Other Experimental Techniques	70
References	74
3. Results and Discussion.....	75
3.1 Inherently Chiral Molecules with thiophene-based Atropisomeric Scaffolds.....	75
3.1.1 The Forefather T ₄ BT ₂	75
3.1.2. Enantiorecognition Tests: Traditional Solvents vs Ionic Liquids.....	83
3.1.3 Enantiorecognition Tests through Electrochemical Impedance Spectroscopy (EIS).....	91
3.1.4. Confirming the Enantiorecognition Capability using Drugs	97
3.1.5 Confirming the Concept of Inherent Chirality Varying the Terminal Bi-thiophenic Units.....	103
3.2 Inherently Chiral Molecules with Pyrrole-based Atropisomeric Scaffolds.....	124
3.2.1 Confirming the Concept of Inherent Chirality Varying the Chemical Nature of the Atropisomeric Scaffold	124
3.2.2 A Corollary Study: Temperature Effect on Rotational Barrier of Indole-based Monomer with 3,3'-Connectivity.....	132
3.3 Inherently chiral spider-like oligothiophenes with β,β'-bithiophene core	133
3.3.1 Enantiorecognition Tests.....	139
3.4 Inherently Chiral Electroactive Macrocycles	144
3.4.1 Chiroptical Proprieties of Enantiopure Ringlets	151
3.4.2 Electrochemistry of Chiral Macrocycles in BMIMPF ₆	156
3.4.3 Characterization of Cavities also as Racemates: Electrochemistry of Racemate Macrocycles in Traditional Solvents	157
3.4.4 Focusing on Linear Dimers.....	161
3.4.5 Racemic Trimer Tested as a Donor in a Bulk-heterojunction Solar Cell.....	164
3.5 Study of the DET Process of Model Organic Halides in BMIMPF ₆ Ionic Liquid	167
3.5.1 Electrochemical characterization: BMIMPF ₆ vs ACN	169
3.5.2 EIS Characterization: BMIMPF ₆ vs ACN	172
3.6 Inherently Chiral Ionic Liquids	176

3.6.1 1,1' Bis-benzimidazole-based Inherently Chiral Ionic Liquids	177
3.6.1.1 2,2'-Dialkyl-1,1'-Bis-benzimidazole Scaffolds	177
3.6.1.2 1,1' Bis-benzimidazolium Salts	194
3.6.2 2,2' Bis-benzimidazole-based Inherently Chiral Ionic Liquids	195
3.6.2.1 2,2' Bis-benzimidazole Scaffolds.....	195
3.6.2.2 2,2' Bis-benzimidazolium Salts	197
3.6.3 3,3'-Bis-Collidine Scaffold	198
3.6.3.1 3,3' Bis-collidinium Salts	200
3.6.4 Electrochemical Characterization of Biheteroaromatic Scaffolds.....	201
3.6.5 ICILs vs Scaffolds	204
3.6.6 First Electrooligomerization Test using a 3,3'-Bis-collidinium Derivative as Supporting Electrolyte	206
References.....	210
4. Appendix: Removal of Cl ⁻ Impurities from Ionic Liquids by AgCl Deposition on Silver Electrode	213
References.....	219
Conclusions.....	220



**OLIGOMERIZATION
AFFORDS THE
DEVELOPMENT OF CHIRAL
SENSORS WITH
OUTSTANDING
ENANTIORECOGNITION
CAPABILITY**

**TRADITIONAL
SOLVENTS
(VOCs)**

**OLIGOMERIZATION
RESULTS IN A NEW CLASS
OF CHIRAL ELECTROACTIVE
MATERIALS WITH
OUTSTANDING PROPERTIES
FOR IMPLEMENTATION IN
OPTOELECTRONIC AND
PHOTOVOLTAIC DEVICES**

**INHERENTLY
CHIRAL
MOLECULES**

**ACHIRAL
IONIC
LIQUIDS**

**CHIRAL
IONIC
LIQUIDS**

**ENVIRONMENTALLY FRIENDLY
INHERENTLY CHIRAL
IONIC LIQUIDS**

General Remarks

The development of environmentally friendly and more sustainable methodologies of synthesis has become one of the main objectives of organic chemistry, in particular for the requirements of chemical industry. In this perspective, electrochemical methods appear most promising since they allow to control the selectivity of electron transfers at a molecular level and hence the formation of the reactive intermediates (besides their intrinsically very mild operating conditions); these advantages can be further enhanced by the use of active electrode surfaces (electrocatalysis).

However, a typical drawback of electrochemical processes consists in the employment of volatile organic solvents (VOCs), which imply safety problems and require the addition of high amounts of a supporting electrolyte to obtain the necessary conductivity. Both problems could be overcome by shifting to non-conventional media such as room temperature ionic liquids (RTILs). In fact, RTILs present various desirable advantages over molecular solvents, including negligible vapour pressure, high intrinsic conductivity without addition of supporting electrolyte (in fact they are both solvent and electrolyte) and easy recyclability. Accordingly, an increasing number of electrochemical studies in ionic liquids is appearing in the literature, pointing to attractive potentialities and suggesting the opportunity of mechanistic investigations on selected model cases of fundamental and applicative interest.

In this context, this thesis has been initially aimed at carrying out a study of molecular electrochemistry and electrocatalysis in ionic liquids, particularly focusing on the combined effects of the ionic liquid molecular structure and the nature of the electrode surface, considering two model processes:

- the electroreductive cleavage of the carbon halogen bond in organic halides, of great interest in the synthetic, analytical, and environmental fields;

- the electrooxidative coupling of thiophene-based monomers, affording electrodeposition of conducting materials for application in photovoltaic, optoelectronic, and sensor devices.

Besides their great applicative interest, the two processes are convenient model cases for electron transfer studies in ionic liquids, one reductive (via radical anion) and one oxidative (via radical cation), both of them presenting a radical coupling as a preferential outcome as well as being significantly influenced by the electrode material and tunable through the reaction medium.

However, the 3-year research results actually went well beyond these initial targets, with the discovery of the outstanding properties of inherently chiral electroactive thiophene-based oligomers, on which we then concentrated most of our efforts.

In particular:

- electrooligomerization in ionic liquids of 'inherently chiral' thiophene-based monomers, developed by Prof. Sannicolò's partner group, afforded the preparation of enantiopure chiral electrodes of new concept and unprecedented enantiodiscrimination ability, affording neat separation of chiral probe antipode signals of different probes, also of pharmaceutical interest, in different media and operating conditions;
- such oligomers turned out to be mostly cyclic, idealizing chiral conducting polymers without ends, displaying a pool of extraordinary properties, both as racemates (promising performance in organic solar cells, photoactivity, electrochromism, ability to complex other semiconductors, outstanding comonomers for copolymerizations of functional monomers of poor polymerization ability...) and as enantiopure antipodes (chirality tunable with electric potential, unprecedented enantiodiscrimination ability as electrodes, circularly polarized luminescence, possibility of preparation as self-supported membranes)
- considering the outstanding enantioselectivity granted by the inherent chirality concept in semiconductor films, a new research line has been started, aimed to the development of the first inherently chiral ionic liquids.

Furthermore, having verified the general validity and effectiveness of the inherent chirality concept, and considering our concern for ionic liquid media, we have started, again in cooperation with Professor Sannicolò's group, a further research line, aimed to the implementation of inherent chirality in new-concept ionic liquids, with the target of obtaining new, attractive media for chemical and electrochemical processes, possibly of cheap and simple synthesis, affording safe, mild and environmentally friendly operating conditions, intrinsic to the ionic liquid class, combined with powerful chirality manifestations. Three approaches, all based on the implementation of inherent chirality in the ionic liquid cation, are being developed and compared. As a valuable ancillary research product, a very simple 'Egg of Columbus' protocol has been developed, providing an effective solution to the important issue of halide impurity removal from ionic liquid media.

1. Introduction

The process on which a large part of this work has been based, the electrooxidative coupling of thiophene-based conjugated molecules, is of extreme importance for the obtainment of conducting polymers (CPs) for applications in energetics (*i.e.* photovoltaics), optoelectronics, and sensoristics, their properties being widely and finely modulable by convenient molecular design.

There are at least four major classes of semiconducting polymers that have been developed so far. They include *i)* conjugated conducting polymers, *ii)* charge transfer polymers, *iii)* ionically conducting polymers and *iv)* conductively filled polymers.

The conductively filled polymers were first made in 1930 for the prevention of corona discharge. The potential uses for conductively filled polymers have since been multiplied due to their ease of processing, good environmental stability and wide range of electrical properties. Being multi-phase systems in nature, however, the lack of homogeneity and reproducibility has been an inherent weakness for this type of polymers. Therefore, controlling the quality of dispersion to obtain homogeneous conducting polymer composites is critically important.

Since 1975, various ionically conducting polymers or polymer electrolytes have been prepared for a wide range of applications ranging from rechargeable batteries to smart windows. Polymer electrolytes are also highly processable. The ionic conduction mechanism requires the dissociation of opposite ionic charges and the subsequent ion migration between coordination sites, which are generated by the slow motion of polymer chain segments. Consequently, polymer electrolytes normally show a low conductivity and high sensitivity to humidity. They often become electrically non-conducting upon drying.

The discovery by Akamatu *et al.* in 1954 of electrical conductivity in molecular charge transfer (CT) complexes, which led to subsequent findings of superconductivity in molecular CT complexes in 1980 (Jerome *et al.*) and with fullerene in 1986 (Iqbal *et al.* 1986), promoted the development of conducting CT polymers. The conductivity in CT complexes arises from the formation of appropriate segregated stacks of electron donor and acceptor molecules and a certain degree of charge transfer between the stacks. A desired crystal structure is, therefore, essential for good conductivity in the molecular CT complexes. However, the resultant materials are often brittle and unprocessable. To overcome this problem, attempts have been made to attach electron donor and/or acceptor moieties onto polymer backbones to produce charge transfer polymers with good processability and stacking properties.

Along with all of the activities described above, various conjugated polymers showing excellent electrical properties have been synthesized during the past 25 years or so. Owing to the delocalization of electrons in a continuously overlapped π -orbital along the polymer backbone, certain conjugated polymers also possess interesting optical and magnetic properties. These unusual optoelectronic properties allow conjugated polymers to be used for a large number of applications, including protecting coatings from corrosion, sensing devices, artificial actuators, all-plastic transistors, non-linear optical devices and light emitting displays. Due to the backbone rigidity intrinsically associated with the delocalized conjugated structure, however, most un-functionalized conjugated polymers are intractable (*i.e.* insoluble, infusible and brittle). Some of them are even unstable in air [1].

1.1 Conjugated Conducting Polymers

The first example of conducting polymer (CP) as insoluble material appeared almost 150 years ago. In 1862, Letheby reported the anodic oxidation of aniline in a solution of diluted sulphuric acid and that the blue-black shiny powder was insoluble in water.

The modern development of conducting polymers began in 1977 as the American scientists Heeger and MacDiarmid and their Japanese colleague Shirakawa discovered that doping chainlike polyacetylene (PA) with iodine endowed the polymer with metal-like properties, producing copper colored films with an increase of conductivity of 10 orders of magnitude. Polyacetylene is considered the archetype of conducting polymers, and the discovery of its conductive properties represented a great breakthrough in the fields of chemistry and material chemistry, so that the Heeger, MacDiarmid and Shirakawa were awarded the Nobel Prize in Chemistry in 2000. These unconventional properties of an organic material stimulated worldwide efforts to find applications such as batteries or electronic devices. However, PA was not stable and was easily destroyed by oxidative degradation. Therefore, numerous other conducting polymers with properties similar to those of PA were synthesized, such as polyphenylene (PP), polyphenylenevinylene, polypyrrole (PPy), polythiophene (PTh), and, last but not least, polyaniline (PANI).(Figure 1) [2].

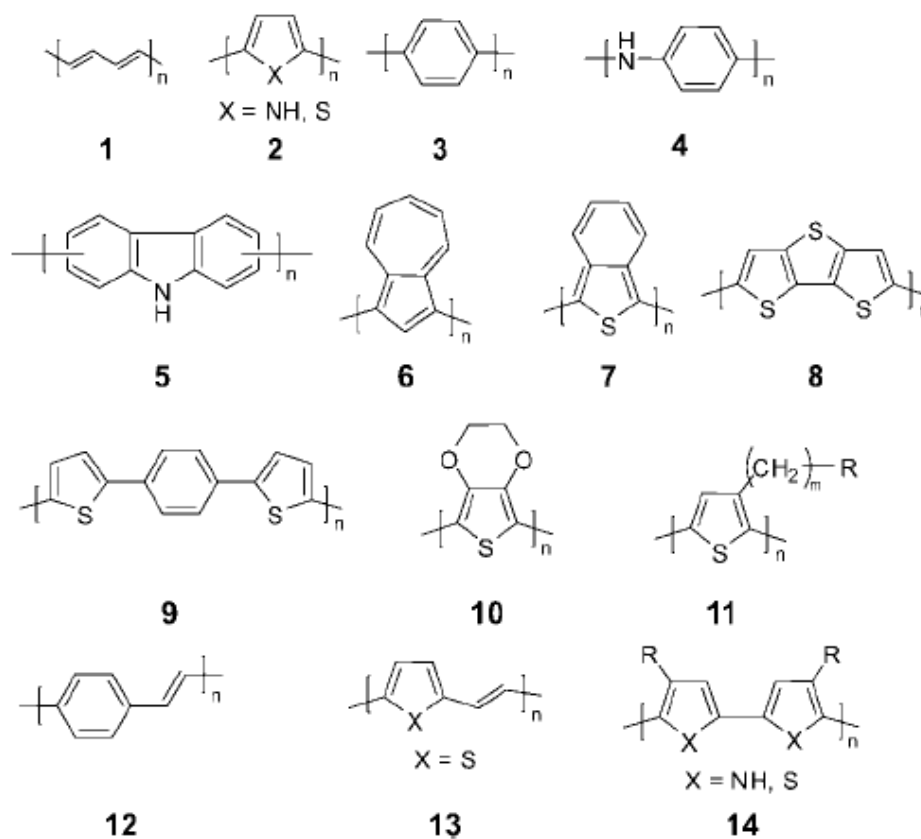


Figure 1. Some examples of conducting polymers:

1, polyacetylene (PA), 2 polypyrrole (PPy), polythiophene (PTh); 3, poly-p-phenylene (PPP); 4, polyaniline (PANI); 5, polycarbazole; 6, polyazulene; 7, poly(isothionaphthalene); 8, poly(dithienothiophene); 9, poly(dithienylbenzene); 10, poly(ethylenedioxythiophene) (PEDOT); 11, poly(3-alkylthiophene); 12, poly(phenylenevinylene) (PPV); 13, poly(thienylenevinylene); 14, poly(bipyrrole), poly(bithiophene).

There are two essential conditions for the polymer to become conductive:

- the conjugated structure with alternating single and double bonds or conjugated segments coupled with atoms providing π -orbitals for a continuous orbital overlap (e.g. N, S). This is because just as metals have high conductivity due to the free movement of electrons through their structure, in order for polymers to be electronically conductive they must possess not only charge carriers but also an orbital system that allows the charge carriers to move. The conjugated structure can meet the second requirement through a continuous overlapping of π -orbitals along the polymer backbone.

- the doping process. Since most organic polymers do not have intrinsic charge carriers, they may be provided by partial oxidation (p-doping) of the polymer chain with electron acceptors (*e.g.* I₂, AsF₅) or by partial reduction (n-doping) with electron donors (*e.g.* Na, K). Through such a doping process, charged defects (*e.g.* polaron, bipolaron and soliton) are introduced, which could then be available as charge carriers.

The simple band theory can provide some useful information about the doping-induced changes in electronic structure.

According to band theory [3], the electrical properties of direct gap inorganic semiconductors are determined by their electronic structures, and the electrons move within discrete energy states called bands. By analogy, the bonding and antibonding π orbitals of the sp² hybridized π -electron materials (*e.g.* polyenes) generate energy bands, which are fully occupied (π -band) and empty (π^* -band).

The highest occupied band is called the valence band, and the lowest unoccupied band is the conduction band. The energy difference between them is called band gap.

Electrons must have certain energy to occupy a given band and need extra energy to move from the valence band to the conduction band. Moreover, the bands should be partially filled in order to be electrically conducting, as neither empty nor full bands can carry electricity. Owing to the presence of partially filled energy bands, metals have high conductivities (Figure 2 (a)). The energy bands of insulators and semiconductors, however, are either completely full or completely empty. For instance, most conventional polymers have full valence bands and empty conduction bands, which are separated from each other by a wide energy band gap (Figure 2 (b)). In contrast, conjugated polymers have narrower band gaps (Figure 2 (c)) and doping can change their band structures by either taking electrons from the valence band (p doping) or adding electrons to the conduction band (n-doping).

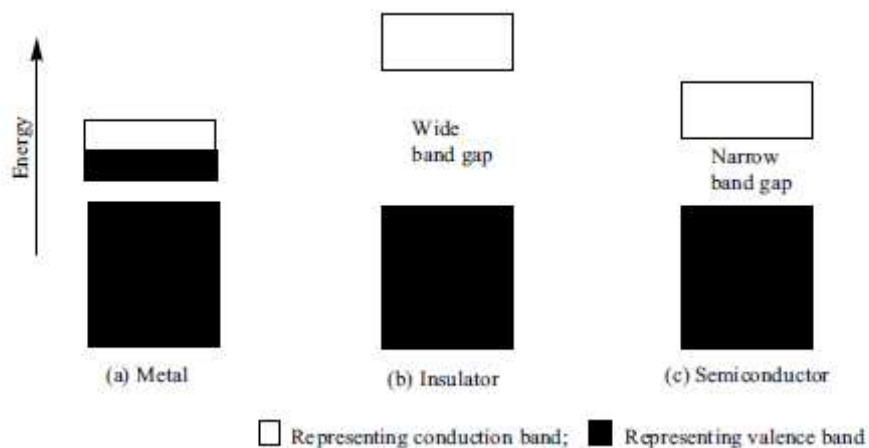


Figure 2. Energy gaps in (a) metal; (b) insulator; (c) semiconductor.

When an electron is added (or removed) to the bottom of the conduction band (or removed from the top of the valence band) of a conjugated polymer (Figure 3(a)), the conduction (valence) band ends up being partially filled and a radical anion (cation), commonly termed as a polaron [4], is created (Figure 3(b)). The formation of polarons causes the injection of states from the bottom of the conduction band and top of the valence band into the band gap. A polaron is characterized both by spin ($1/2$) and charge ($1e$). Addition (removal) of a second electron on a chain already having a negative (positive) polaron results in the formation of a bipolaron (spinless) through dimerization of two polarons, which can lower the total energy (Figure 3(c)). In conjugated polymers with a degenerate ground state (*i.e.* two equivalent resonance forms), like *trans*-polyacetylene, the bipolarons can further lower their energy by dissociating into two spinless solitons at one-half of the gap energy (Figure 3(d)). Solitons do not form in conjugated polymers with non-degenerate ground states, such as in polypyrrole, polythiophene and polyaniline. The population of polarons, bipolarons, and/or solitons increases with the doping level. At high doping levels, the localized polarons, bipolarons or solitons near to individual dopant ions could overlap, leading to new energy bands between and even overlapping the valence and conduction bands, through which electrons can flow.

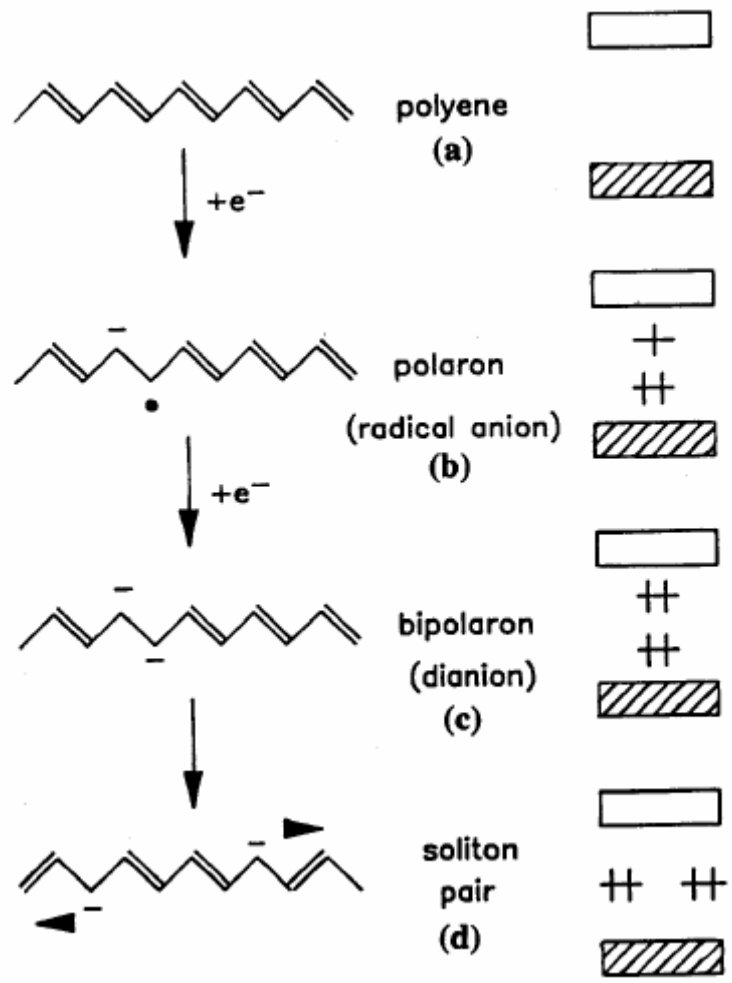
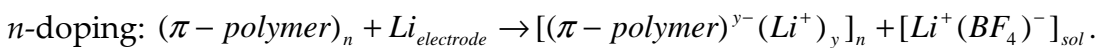
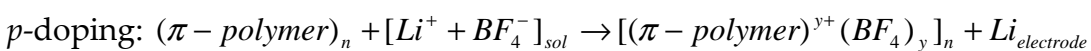


Figure 3. Illustration of the formation of polaron, bipolaron, and soliton pair on a trans-polyacetylene chain by doping

There are different types of doping methods:

i) chemical doping; *ii)* electrochemical doping; *iii)* photo-doping; *iv)* charge injection doping; *v)* non-redox doping; *vi)* secondary doping.

In particular in the electrochemical doping the electrode supplies the required redox charge to the conducting polymer, by applying an appropriate potential, positive or negative:



1.2 Electrochemistry of Conductive Polymers [2, 5]

1.2.1 General Mechanism

This work is focused on the electrochemistry of polythiophene systems. In our case, the conducting polymers are obtained by means of cyclic voltammetry electrooxidizing the corresponding monomer, by cycling the potential around its oxidation peak.

The generally accepted electropolymerization mechanism involves the formation of radical cations, that couple together or with the starting monomer, as illustrated in the following Figure 4:

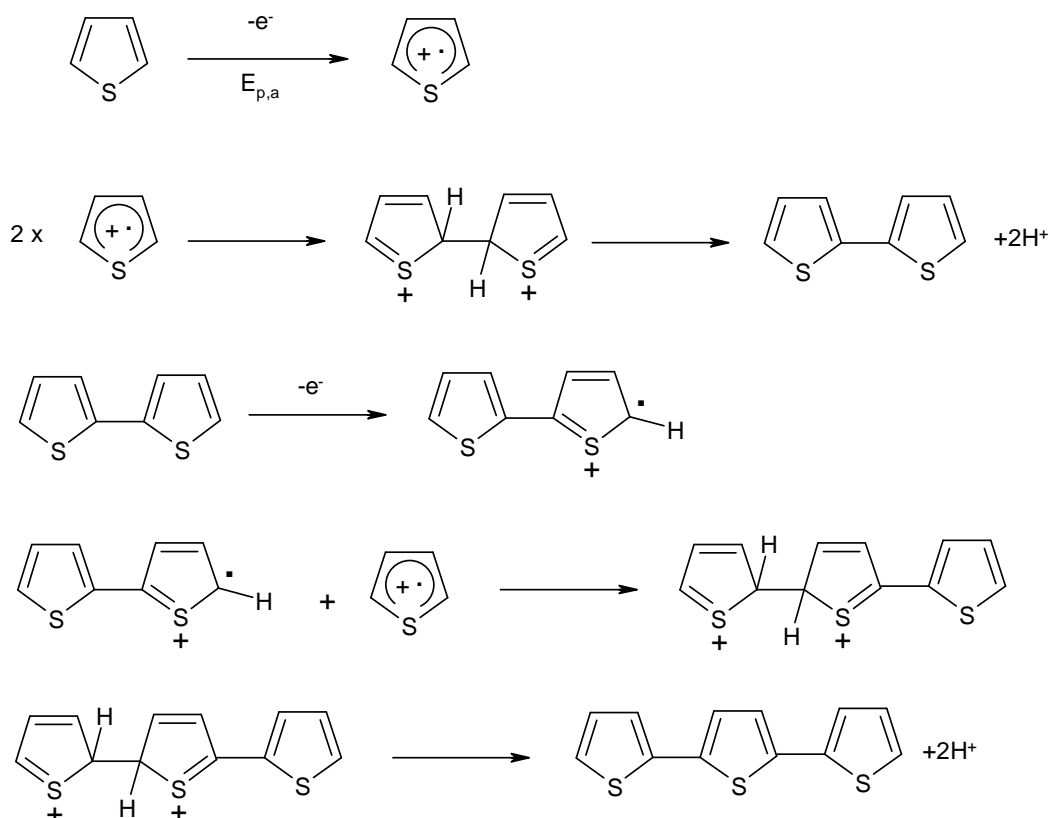
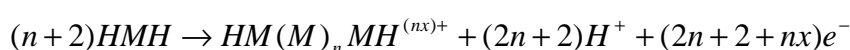


Figure 4. Electropolymerization mechanism for thiophene monomer

This process involves a coupling reaction sequence in which the electrochemical stoichiometry of the reacting monomer is 2.07-2.6 F mol⁻¹. This means that the film-forming process needs two electrons per molecule (*i.e.* 2 F mol⁻¹) while the additional charge normally serves the partial reversible oxidation of the rising conjugated species. It is worthwhile noticing that, since the polymer is longer than the monomer, and thus its conjugation is more extended, its oxidation occurs at less positive potential than the monomer, so the two processes, the polymer formation and its doping, occur simultaneously. The complete reaction equation of the process is:



(2n+2) electrons are used for the polymerization process itself, while the remaining *nx* electrons are required for the doping process. Generally, *x* is between 0.07 and 0.6, *i.e.*, every third to fourth monomeric subunit has been charged at the end of polymerization. Higher levels of doping could be forced, by applying a more positive potential, but this extra energy could lead to overoxidation of thiophenes, and consequently to a degradation of the physico-chemical and mechanical properties of the polymer film.

The oxidation of the monomer in the α position generates a radical cation, that couples with another radical cation, generating a doubly charged σ -dimer. The elimination of two protons (which is the rate determining step) and the consequent rearomatization of the system (which is the driving force of the elimination reaction) generate a neutral dimer. As it is more conjugated than the monomer, it is immediately oxidized and its cation undergoes a next coupling step, and so on. The mechanism is essentially a sort of chain propagation reaction, with a series of E(CCE)_n steps, with E denoting an electrochemical process and C a chemical follow-up reaction.

In the very first step a radical ion dimerization of the monomeric starting molecules took place but the coupling tendency between charged oligomers and a monomer radical cation decreased as a function of the oligomeric chain length.

This is due to:

i) the rate constants of radical cation coupling. It is extremely higher, even at low monomer concentrations, for the dimerization of the monomeric cations than for the coupling of superior oligomers:

ii) the rate constants of protons elimination from the intermediate σ -dimers. As a consequence of the diminished acidity of the growing charged intermediate σ -dimers (function of their lengths due to the resonant stabilizing effect of a large conjugated oligomer), the elimination rates decreased for longer intermediates.

And what about intermediates formed during the electropolymerization process?

Saveant *et al.* [6] proposed that radical cations of the starting compound and their oligomeric intermediates be involved in the oligomerization reaction and then preferably couple between themselves. Studies by Heinze *et al.* on donor-substituted thiophenes such as methylsulfanyl- or methoxy-substituted derivatives confirm these findings [7].

A peculiar aspect regards the so-called *nucleation loop* which was first described by Pletcher [8]. This phenomenon is normally observed on the reverse sweep of the very first voltammetric cycle during a potentiodynamic electropolymerization experiment (Figure 5).

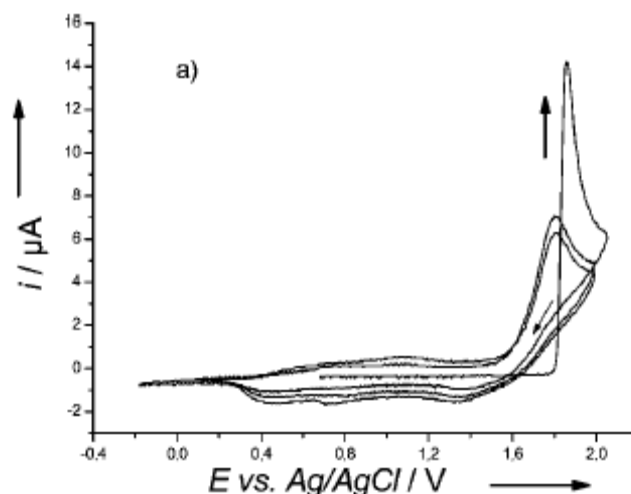


Figure 5. 'Nucleation loop' of thiophene: $v = 0.1 \text{ V s}^{-1}$; $c = 3 \times 10^{-3} \text{ M}$, cyclic voltammetry in 1-hexyl-3-methyl-3*H*-imidazol-1-iumtris(pentafluoroethyl)trifluorophosphate) [HMIM][PF₃(C₂F₅)₃]

This phenomenon has been interpreted as the start of the nucleation process of the corresponding polymer.

In summary, the electropolymerization involves three different stages:

- oxidation of the monomer at the electrode, formation of soluble oligomers in the diffusion layer (preferably by successive dimerization steps);
- deposition of oligomers involving nucleation and growth processes;
- solid state polymerization, producing longer chains and cross-linked materials.

1.2.2 Charging-Discharging of Conductive Polymers

As before mentioned, the doping process correspond to an oxidation / reduction, and ions from the supporting electrolyte play an active role, in order to maintain the electroneutrality of the film. Cyclic voltammetry is a useful tool to monitor this phenomenon.

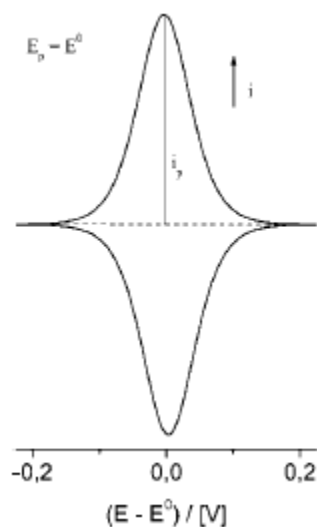


Figure 6. Theoretical cyclic voltammogram for a thin layer film with one redox centre.

In the case of a simple one-electron transfer, reversible cyclic voltammogram for a thin layer film should show completely symmetrical and mirror-image anodic and cathodic waves with identical peak potentials and current levels (Figure 6).

The current in the reversible case is then (eq 1):

$$i = \frac{n^2 F^2 A \Gamma_T v \exp \theta}{RT(1 + \exp \theta)^2} \quad \text{where} \quad \theta = \frac{nF}{RT}(E - E^0) \quad \text{and}$$

$\Gamma_T = \Gamma_{ox} + \Gamma_{red}$ correspond to the total surface covered by reduced and oxidized states.

Increasing film thickness, the voltammetric response gradually shifts from mirror symmetrical diagrams to the classic, asymmetrical shape with I proportional to $v^{1/2}$. Characteristic voltammetric features of conducting polymers are a steep anodic wave at the start of charging, followed by a broad and flat

plateau as potential increases. In the reverse scan a potential-shifted cathodic wave appears at the negative end of the capacity-like plateau (Figure7).

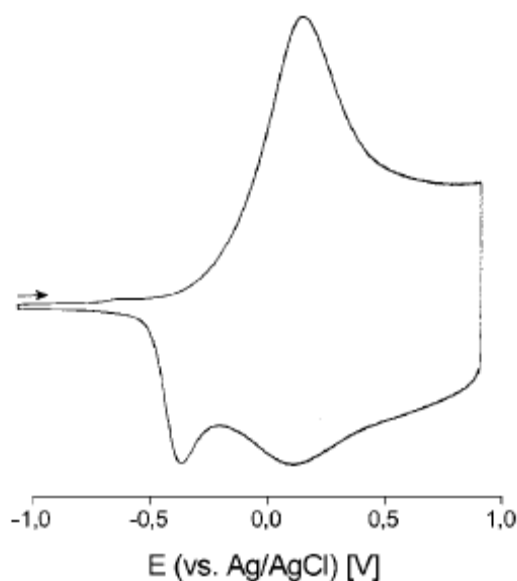


Figure 7. Cyclic voltammogram of the oxidation of poly(4,4'-dimethoxy-bithiophene) in $\text{CH}_2\text{Cl}_2/0.1 \text{ M TBAPF}_6$, $T = 273 \text{ K}$, $v = 0.2 \text{ V s}^{-1}$.

The number of accessible redox states increases with increasing chain length of the system, resulting in the superposition of redox states over a broad potential range for long chain lengths. Therefore, the capacity-like plateau is referred to faradaic redox processes. Moreover, the voltammetric signal of the steep anodic wave at the beginning of the charging certainly belongs to a close superposition of several redox states.

A very unusual phenomenon that is often observed during charging/discharging of CPs is the so-called *memory* or *first cycle effect* [9]. It implies that after a waiting time in the discharged state of a polymeric film the first voltammetric cycle differs in shape and peak position from subsequent cycles. While the anodic wave of the very first cycle is normally both steep and sharp, all subsequent anodic scans show broadened waves which are significantly shifted toward negative potentials (Figure 8).

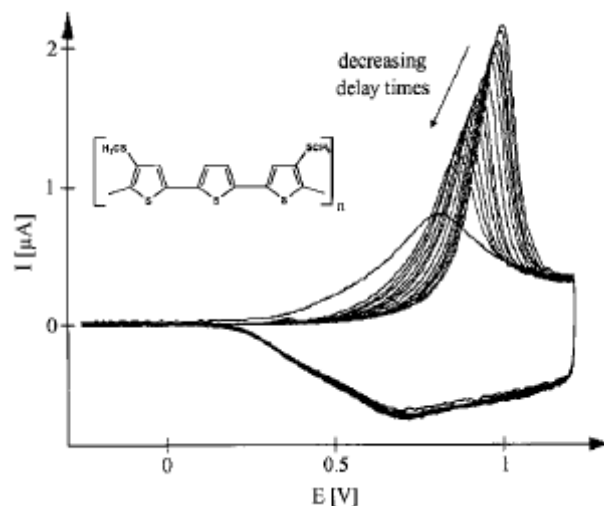


Figure 8. Memory effect of poly(4,4''-dithiomethyl-2,2',2''-terthiophene) in $\text{CH}_3\text{CN} + \text{TBAPF}_6$ 0.1 M for different waiting times τ (top down): 30, 15, 10, 8, 6, 4, 2, and 1 min; 45, 30, 15, 10, and 5 s; $v = 60 \text{ V s}^{-1}$, $T = 298 \text{ K}$, Pt disk electrode ($r = 12.5 \mu\text{m}$).

In the so called stability process [9] the polymer underwent a series of few redox cycles around the first oxidative potential, with the shape and position of the cathodic discharging waves remaining unchanged during all cycles.

The phrase 'memory effect' refers to the electrochemical response during charging of polymeric films that depends on the history of foregoing electrochemical events. In fact during charging/discharging of CPs, a rearrangement of the chain configuration took place, which was followed by the incorporation and extraction of counterions. Thus, during reduction, expulsion of counterions occurs from opened channels that get closed slowly as a function of waiting time.

1.2.3. Specific n-doping Process

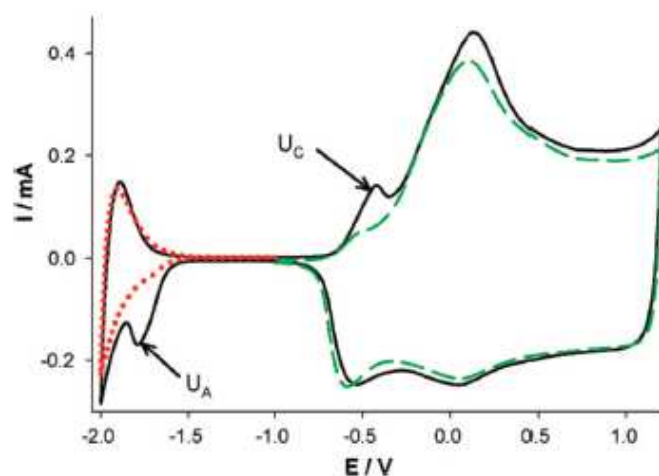


Figure 9. Cyclic voltammetry of a PEDOT film in 0.1 M TEABF₄/CH₃CN: responses of film cycled through both n- and p-doping regions (black line), through the p-doping region (green line) and through the n-doping region (red line). From A. R. Hillman, S. J. Daisley, S. Bruckenstein, *Electrochim. Acta* **2008**, 53, 3763

A peculiar phenomenon that concerns the n-doping is the so-called *charge trapping effect*. The negative charge, injected at a given potential, is released only at much more positive potentials in the reverse scan. This effect could be attributed to structural modifications in the polymer network (*i.e.* the generation of quinone-like redox states), that, analogously as the memory effect, requires more energy to restore the initial conformation.

In the case of PEDOT charging, here illustrated in Figure 9, ion trapping occurs during consecutive p- and n-doping cycles. It is likely that the discharging processes of this polymer are incomplete and regions of conducting material and associated anions/cations are isolated within an insulating matrix of undoped polymer. With this model, kinetic control at the completion of the undoping process must be assumed, which may be caused by changes in the polymer structure.

1.2.4. Factors that Affect the Electropolymerization Process

Variations of experimental parameters such as temperature, potential, electrode nature, or concentration of the starting monomer creates significant changes of physical and chemical characteristics.

Both experimental parameters and the preparation technique determine the properties of the resulting polymers.

a) Polymerization Technique

Potentiodynamic, potentiostatic, and galvanostatic polymerizations are the three most important techniques that can be used to electrosynthesize a conducting polymer. Potentiodynamic polymerization (*i.e.* cyclic voltammetry) is characterized by a cyclic, time-regular change of the electrode potential during the deposition of the conducting polymer onto the electrode. The growing polymer film following the potential changes continuously switches between its neutral (insulating) and its doped (conducting) states, which is accompanied by a continuous exchange of electrolyte and solvent through the freshly deposited polymer. Conducting polymers made by potentiodynamic polymerization are generally obtained in their neutral state at the end of the experiment, on the contrary potentiostatic and galvanostatic methods lead to polymers in their doped state.

Generally a polymer obtained by cyclic voltammetry is more irregular than the one obtained by the other two techniques. This is due to the ingress/egress of the solvent and ions that create volume expansions and structure defects. However the quality of the deposited film is strongly dependent to the monomer system. For this reason for each monomer, the optimal electrochemical technique must be tested to carry out an efficient CP electrosynthesis.

b) Experimental Conditions

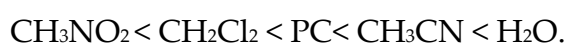
Experimental conditions such as potential (current), solvent, and temperature are also important for the quality and the properties of CPs.

Potential (Current): the choice of the correct potential (current) value determines the chain length and the structure of CP. Very high oxidation potentials or currents imply generation of highly charged and reactive intermediates and consequently lead to defects and formation of cross-linked materials. At low potentials, *vice versa*, the oligomeric intermediates are weakly charged, and consequently, the electropolymerization may end at an oligomeric level.

Temperature: at low temperatures systems with shorter chain lengths are favoured and well-ordered structures with high conductivities are formed.

Solvent and Supporting Electrolyte: solvents with high polarity minimize Coulombic repulsions during cationic coupling steps but their nucleophilicity should be low.

In the case of conventional solvents, it rises in the following order:



Water can only be used for the generation of polymers for which the oxidation potentials of their monomers are low, to avoid solvent discharge reaction.

The influence of type and size of the electrolyte ions on the polymerization, the subsequent charging/discharging properties, and the morphology is considerable. Thus, even the magnitude of conductivity of electrogenerated CPs is affected by counterions.

In recent years the utilization of ionic liquids (ILs) for the synthesis and use of conducting polymers brings together two of the most exciting and promising areas of research. They are both solvent and supporting electrolyte and present various desirable advantages over traditional organic solvents as for example their extremely low nucleophilicity.

1.3 What is an Ionic Liquid? And Why use it in Electrodeposition? [10]

One of the aims of this PhD thesis was to study the electrooxidative coupling of oligothiophenes or thiophene-based conjugated molecules to give conductive polymer films in ionic liquids (ILs), verifying the IL effects on the redox properties of the monomer, the polymerization rate, and the electrochemical, morphological and mechanical properties of the resulting conducting films.

For this reason it is convenient to start with a brief introduction on the potentialities of ILs as a media for CPs electrodepositions.

The recognized definition of ionic liquid is 'an ionic material that is liquid below 100 °C'.

ILs offer a unique combination of chemical and physical properties that make them exploitable as electrolyte and solvent at the same time. Many of the anions of the supporting electrolytes that produce high conductivities in CPs are also the same ones that commonly occur in ionic liquid compounds (as in our case: PF_6^- ; BF_4^- ; ClO_4^-). Thus appropriate ILs provide a superb source of the dopant anions.

It is worthwhile noticing that the anion of the IL should have a peculiar impact on the growth and properties of the conducting films, since it must cyclically enter and exit the forming polymer network, for sake of electroneutrality. This results in an opening/closing of the polymeric structure and an increase/decrease in its volume. The size and nature of the dopant counterion incorporated during synthesis can have a dramatic effect on the ion movement occurring during redox processes.

ILs can modulate many aspects of the general electropolymerization mechanism (describe in the paragraph 1.2.1) for example:

- 1) The **stabilization of charged polymerization intermediates** due to the polar nature of IL;

- 2) The **oligomer solubility** and **the extent to which they diffuse away from the electrode**; these factors may be influenced by viscosity, conductivity, solubilization ability of ILs.
- 3) The **polymer doping level** which might be higher on account of the much higher ion availability in ILs.
- 4) The **degree of solvent swelling** of the polymer films (which should be lower in ILs), significantly impacting on the **ion mobility within the polymer** and thus on the latter's electrochemical activity.
- 5) Also **reconditioning of the conducting film network after storage should be less critical**, since there would be no solvent evaporation and electrolyte concentration within the film.

Summarizing, possible improvements (still to be fully investigated) in the process of electrodeposition and successive treatments of the CP films are:

i) increased doping level; *ii)* increased film smoothness; *iii)* increased conductivity; *iv)* decreased overoxidation; *v)* improved electrochemical stability; *vi)* better stability upon storage.

There are different ionic liquids readily available, either commercially or through straightforward laboratory synthesis, some of these are reported in Figure 10.

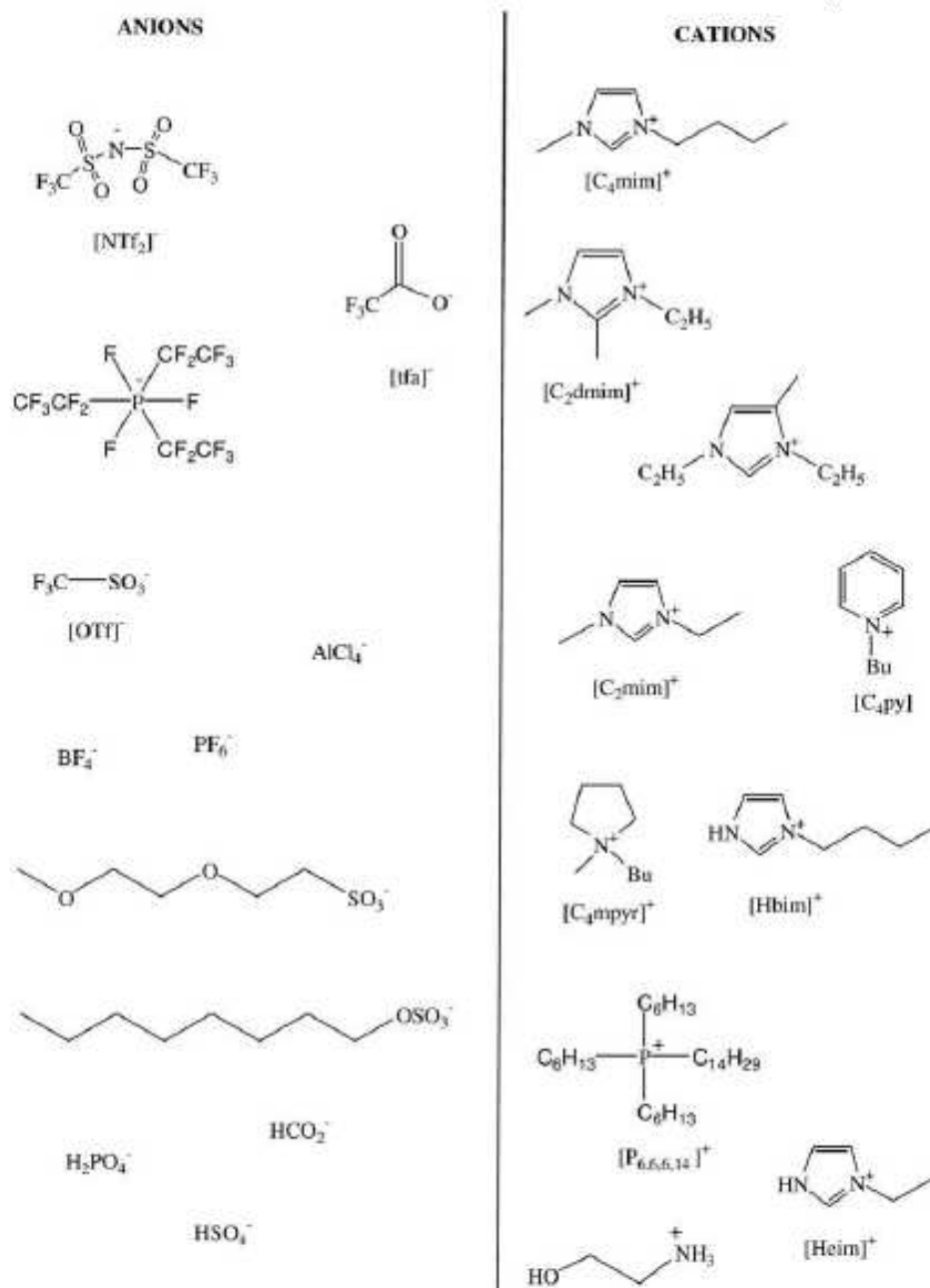


Figure 10. Examples of ILs used for CPs electrosynthesis

When we choose an IL for a given process we must consider some important aspects. First, both the cation and anion must be chemically and electrochemically stable. High viscosity and low conductivity may be problematic, in fact viscosity of the IL affects the conductivity and the rate of ion diffusion with some impact on the electropolymerization process. The viscosity is easily tailored by changing the cation and anion.

Second, the monomer must be soluble in the ionic liquid at adequate concentrations.

Finally, the size and nature of the ionic liquid ions are expected to influence the extent to which they are incorporated into the polymer during growth or electrochemical cycling. The size of the cation can be easily tailored by modifying the length of the alkyl substituents, and choice of a planar aromatic cation, such as imidazolium, rather than non-planar aliphatic species such as pyrrolidinium or phosphonium, may also enhance cation intercalation.

Considering the significant influence that the medium has on the electrochemical and morphological features of CPs we have developed a completely new and potentially promising class of chiral ionic liquids, as a further exploitation of the concept of inherent chirality. They maintain the classical features of just described commercially available ILs but in addition they possess a 'pervasive' chirality guaranteed by the implementation of the innovative concept of *inherent chirality*, largely described in the following pages for the development of monomers and materials of impressive chirality manifestations. Accordingly, we have started the development of inherently chiral ionic liquids, with the aim of obtaining high enantioselectivity, competitive with that of so far available chiral ionic liquids, designed along current concepts.

The study of this family of inherently chiral ILs (ICILs) will be presented in much more details in the chapter 1.4.6.

1.4 Chirality in Conducting Polymers: Current Approaches

The introduction of chirality in organic conjugated polymers displaying electro-conductive properties has been considered for a wide variety of purposes:

i) the ordered spontaneous chain assembling [11]; *ii)* the applications for second order nonlinear optical, due to the absence of centrosymmetry of such materials [12]; *iii)* the

discrimination between antipodes, as required in sensors designed for the detection of chiral analytes, mostly, but not necessarily, of biological origin [13].

Chirality is generally introduced in the polymer by attaching chiral pendants to the electroactive conjugated backbone through suitable linkers [11-14,16-18] even though, alternatively and more rarely, blends of electroactive materials and chiral enantiopure compounds are employed [15]. A great variety of chiral substituents have been employed either chosen from the natural chiral pool, like sugars [16] and amino-acids [17], or manmade, designed and synthesized for specific applications. The presence of carbon stereocenters invariably characterizes the chiral substituents. The enantiodiscrimination properties transmitted to the backbone by the substituents depend upon the functional groups characterizing them, upon their density and distance from the electroconducting chain and upon the nature of the linker.

An example [18] regards the synthesis of a thiophene-based polymer obtained by usual synthetic route (oxidation by FeCl_3) resulting in a random polymerization process with loss of the global supramolecular chirality (poly 1 in Figure 11 (a)).

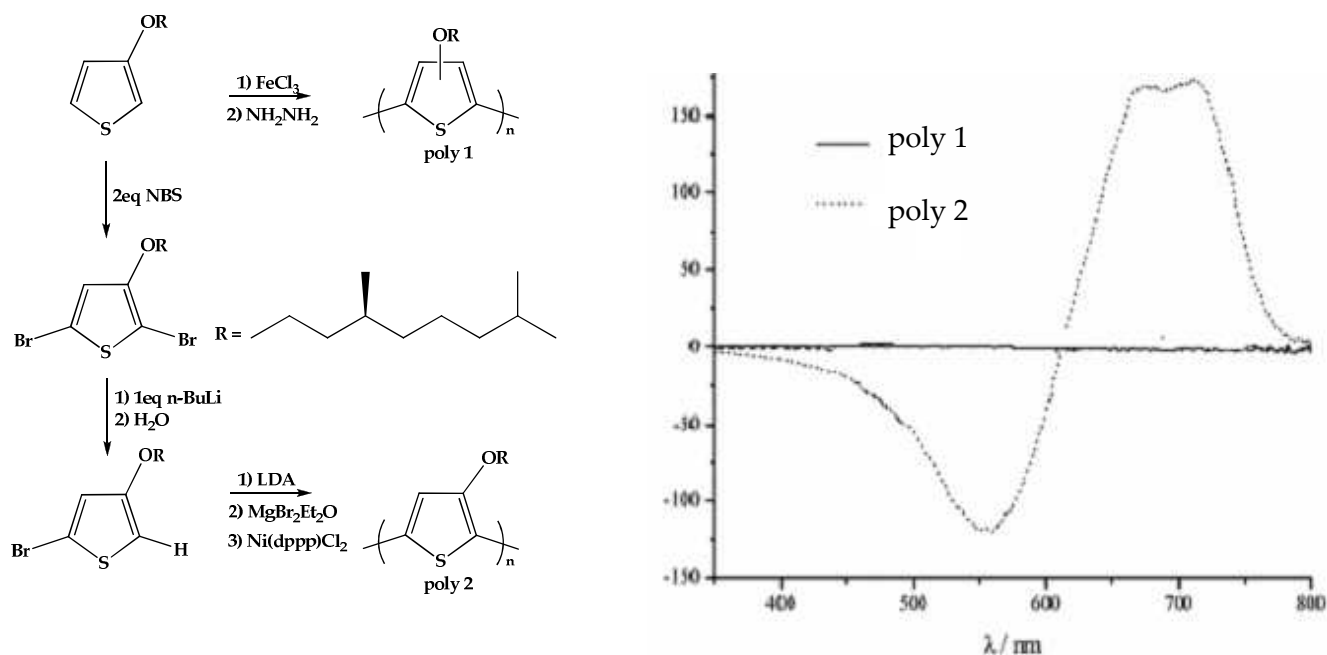


Figure 11. (a) Synthetic routes for the obtainment of poly 1 (random polymer) and poly 2 (regioregular polymer). (b) Circular dichroism spectra of poly 1 (full line) and poly 2 (dotted line)

Only much more refined and expensive synthetic routes can give regioregular polymerization (poly 2 in Figure 11(a)) and therefore a macroscopically chiral material.

This difference is depicted in the circular dichroism spectra in Figure 11 (b): the dotted curve corresponds to high supramolecular chirality obtained by the stereoregular polymerization, and the full line to null one resulting from random polymerization.

Another approach [19], evidencing the dramatic effects of the absence of regioregularity in the growing polymer, is to synthesize monomers with C_2 symmetry featuring two identical stereocentres, as the example reported in Figure 12:

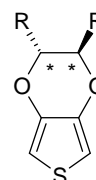


Figure 12. An example of (dissymmetric) chiral C_2 symmetry monomer

in this case, the polymer obtained both by chemical or electrochemical oxidation is regioregular, but, on the other

hand, the chirality of the resulting materials depends on the aggregation state of the polymer chains and can be easily lost changing external conditions, as well demonstrated by Langeveld-Voss and coworkers [20].

In particular they examined the molecule depicted in Figure 13:

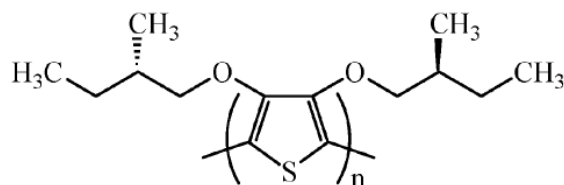


Figure 13. Optically active regioregular polythiophene

The results are very interesting: the chirality of such materials strictly depends on the aggregation state of the polymer chains and the observed optical activity is attributed to intermolecular helical packing of predominantly planar chains as illustrated below.

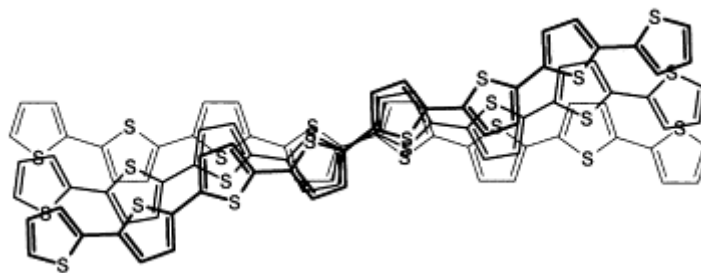


Figure 14. Helical packing of predominantly planar chains in polythiophenes

Moreover chirality is completely lost by changing polarity of the system (decreasing mass percentage of methanol) and by raising the temperature (Figure 15).

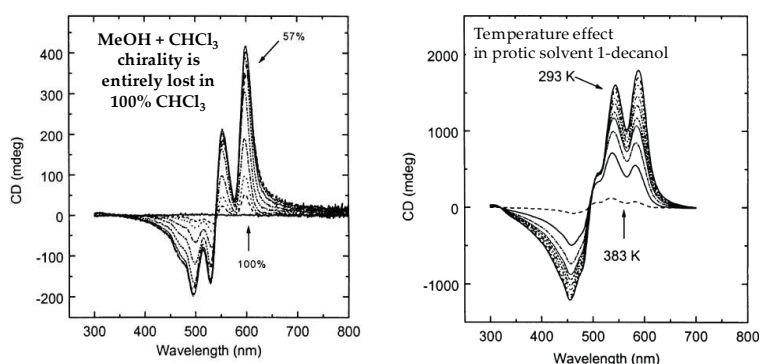


Figure 15. Circular Dichroism spectra of polymer illustrated in Figure 13
(a) Effect of solvent polarity, (b) Effect of raising temperature

Alternative approaches to introduce chirality in polymers imply external chirality sources, such as:

- 1) Chiral counteranions: an example is the electrooxidative polymerization of 2-methoxyaniline in the presence of aqueous (+) and (-) camphorsulfonic acid (HCSA) [21];
- 2) Biopolymers as templating media: *e.g.*, developing a supramolecular chiral insulated 'molecular wire' by self-assembly between an achiral water-soluble polythiophene and a natural polysaccharide, schizophyllan (SPG) [22];

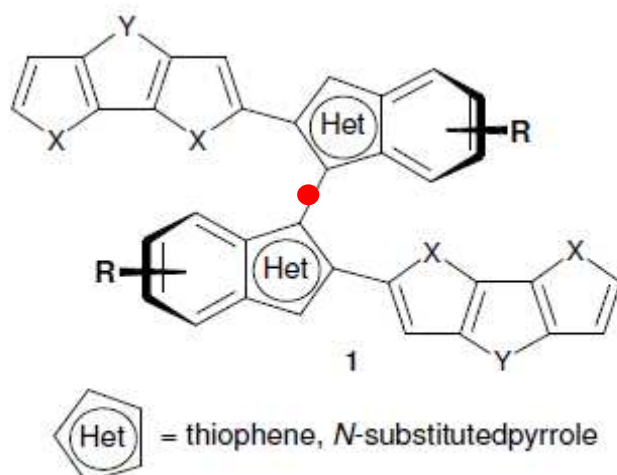
- 3) Molecular imprinting by chiral templates, implying *inter alia* material overoxidation: an example from literature is the enantioselective uptake of glutamic acid into a polypyrrole-based molecularly imprinted polymer [23].

In all cases chirality is however not intrinsic to the polymer backbone.

1.4.1 An Innovative Approach: Inherent Chirality in Atropisomeric Bi-heteroaromatic Scaffold

In this context, in cooperation with the group of Professor Sannicolò [24], we have recently planned and presented a revolutionary concept in the preparation of chiral electroactive polymers by designing, preparing and characterizing oligomerizable chiral thiophene-or pyrrole-based monomers, having the general formula represented in Figure 16, in which chirality results from a tailored torsion internally produced along the conductive backbone (from here the appellative of *inherently chiral* monomers), rather than from the presence of one or more stereogenic centres external to the α -conjugated sequence.

These poly-heterocycles were prepared by chemical or electrochemical oxidation of monomers having the general structure depicted in Figure 16. Importantly, the same conjugated system responsible for the optical and electrochemical properties of these materials is also responsible for the molecular chirality, thus implying that the chiroptical and the enantio-recognition properties of the material are strictly correlated to the electrochemical ones.



X = S, NR'; Y = 2H, CR₂'', NR'''; R = functional group

Figure 16. General structure of the proposed inherently chiral monomers

The molecular design was developed following these guidelines:

- a) chirality results from an internal torsion in the conjugated backbone (as said above);
 - b) a suitably substituted atropisomeric bi-heteroaromatic scaffold (a bi-thiophene or a bi-pyrrole system) is responsible for chain torsion;
 - c) the stereogenic unit is tailored so as to conjugatively interconnect the two 2-(5,2'-bithienyl) moieties;
 - d) a 'node' (depicted with • in Figure 16) [25] is located on the interannular bond, but distortion from coplanarity of the two halves should not preclude conjugative interaction.
- In addition, the three-dimensional (3D) structure of the monomer (transferred to the related polyconjugated network) is important for amplifying the electro-optical performance of organic semiconductors [26];
- e) the C₂ symmetry of these molecules makes homotopic the thiophene α-positions involved in the oxidative coupling, thus assuring complete regioselectivity in the products. Each propagation step (dimerization, trimerization, etc.) invariably results in C₂ symmetric materials.

The result of this innovative approach was the creation of a new family of inherently chiral molecules, where the bi-heteroaromatic central core is constituted, depending on the case, by a bis-benzothiophene (a), a bis-indole (b) or a bi-(2,2'-dimethylthiophene) as shown in figure 17.

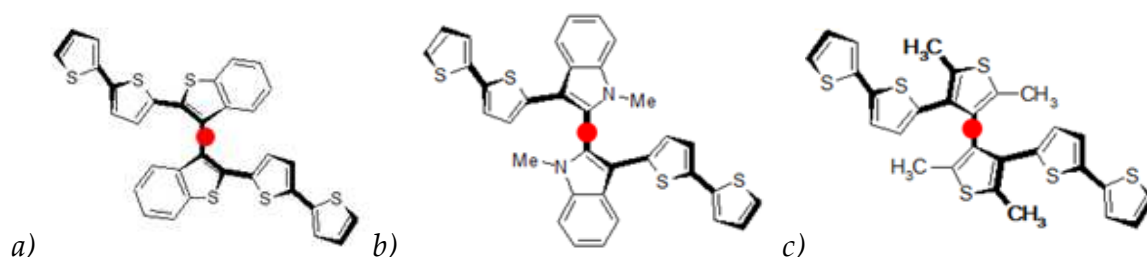


Figure 17. Examples of inherently chiral molecules with: a) bis-benzothiophene core, b) bis-indole core c) bis-(2,2'-dimethylthiophene) core.

From Figure 17 it is possible to deduce that the atropisomerism generated by the distortion around the node arises in case a) from the interactions between the *peri*-hydrogen of each benzene and the thiophene rings, and in cases b) and c) from the interactions between methyls and thiophene groups.

1.4.2 The Forefather of the Inherently Chiral Family

The first forefather, represented in Figure 18, was the 2,2'-bis(2,2'-bithiophene-5-yl)-3,3'-bi-1-benzothiophene (acronym T₄BT₂). The T₄BT₂ molecule was designed in the frame of a collaboration with Prof. W. Kutner of the Institute of Physical Chemistry of the Polish Academy of Sciences (Warsaw), to act as a cross-linker in the development of Molecularly Imprinted Polymer (MIP) sensors to form copolymers with monomers having functional groups suitable for sensoristic applications but recalcitrant to polymerization [27].

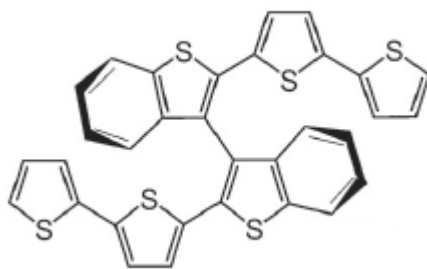


Figure 18. Structure of the inherently chiral T₄BT₂

The resulted copolymer films have shown excellent mechanical properties. In fact, the derived melamine piezomicrogravimetric chemosensor has given excellent performances in terms of linear concentration range, detection limit, and selectivity.

According to the strategic guidelines mentioned above, T₄BT₂ has a bis-benzothiophene as a central scaffold and it is constituted by two equal moieties, each one being approximately planar and thus of high effective conjugation. Moreover it has very interesting and peculiar properties as:

a) Intrinsic 3D character: bulky substituents on both ortho positions of the biaryl rings induce formation of a central node between the two moieties, controlling the barrier of the stereomerization process (enantiomerization).

b) Intrinsic regioregularity in polymerization: there are only two sites available for polymerization, reciprocally far away, symmetrical, and easily accessible. These two α -positions are homotopic; thus full regioregularity and chirality, of the polymer during electrodeposition are guaranteed.

c) Inherent dissymmetry: in spite of including no stereogenic center, the whole molecule is chiral, exhibiting a C₂ symmetry axis. Molecular Mechanics (MM) calculations, performed by progressively varying the torsional angle between the two thianaphtene units, suggested the racemisation barrier to be comprised between 50 and 65 kcal mol⁻¹.

Thus, the energy barrier is sufficiently high to guarantee a racemisation half-life time of several centuries. Therefore, stable enantiomers of T₄BT₂ can be separated and stored.

1.4.3 The Family Grows I: Inherently Chiral Molecular Materials with Thiophene-based Atropisomeric Scaffolds

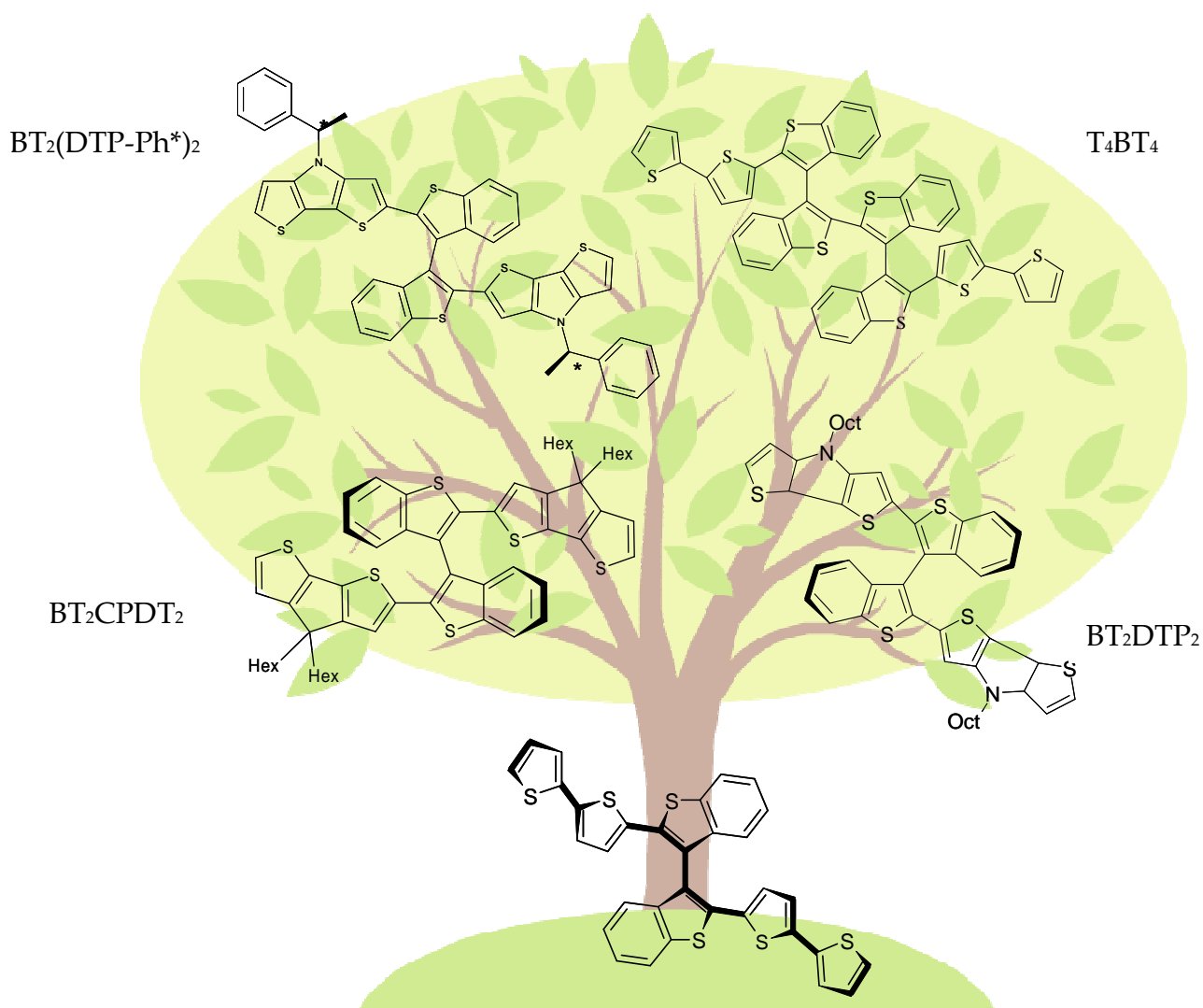


Figure 19. The inherently chiral bi-thianaphtene-based monomer ‘tree’

Starting from the roots of the tree, where the founder is located (T_4BT_2), other unconventional monomers with sterical and electronic tunability have been synthesized. The electronic availability of the monomers depends on the electronic richness of the heterocyclic system used as scaffold. For this reason, the introduction of a pyrrole ring on the two side chains (BT_2DTP_2 molecule in Figure 19) flanking the central α -conjugated

backbone should produce a much electron richer system than its bithiophene-based analogous. Furthermore, a methylene bridge between the two pendant rings can increase their electronic availability by forcing co-planarization and reducing conformational freedom (BT₂CPDT₂ molecule in Figure 19). The methylene bridge can be functionalized in turn with groups able to confer special physicochemical properties to the material; double substitution with long alkyl chains should be beneficial for solubility, without affecting constitutional and sterical order.

The nitrogen atoms of a bi-pyrrole system could develop a multiple function:

a) when substituted by linear or branched alkyl chains, they could cooperate to increase solubility (BT₂-DTP₂ in Figure 19); *b)* when functionalized by chiral enantiopure units, they could be very helpful in the resolution step of the racemates (BT₂-(DTP-Ph*)₂ molecule in Figure 19).

Finally in the T₄BT₄ molecule (Figure 19) a second stereogenic axis was added in order to facilitate the separation of the resulting diastereoisomers through achiral HPLC (high performance liquid chromatography).

1.4.4 The Family Grows II: Inherently Chiral Molecular Materials with Pyrrole-based Atropisomeric Scaffolds

In cooperation with Università degli Studi dell' Insubria we have synthesized molecules with general structures represented in Figure 20, where the atropisomeric scaffold is a bis-indole.

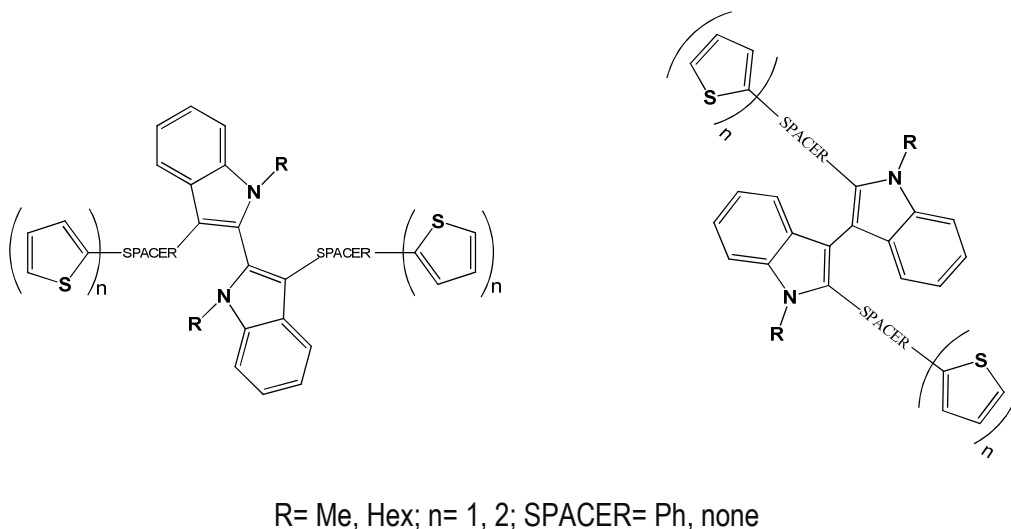


Figure 20. General structures of inherently chiral molecules with a bis-indole core

The stereogenic axis is characterized by two interconnected suitably substituted pyrrole moieties, since that polyheterocycles based on pyrrole display remarkable electroactivity properties. The pyrrole structure offers the possibility, not allowed in the case of thiophene, of locating the heteroatom in position ortho to the interanular bond, since a bulky substituent at nitrogen can be active in hindering rotation thus stabilizing atropisomers. Moreover the geometries of pyrrole and thiophene are rather different, playing a primary role in hindering the rotation around the interanular axis. For example, enantiomerization is much easier in 2,2'- or 3,3'-disubstituted bis-indoles than in the analogous thianaphthene derivatives.

1.4.5 The Same Concept in All-thiophene Materials: Inherently Chiral Spider-Like Oligothiophenes (β,β' -bithiophene core)

Multi-thiophene molecules have attracted considerable attention on account of their outstanding stability, resistance under repetitive electrochemical cycling, even at negative potentials, similarity of spectroscopic properties in solution and in the solid state, remarkable solubility in organic non-polar solvents and space-filling capacity. For these reasons in the last years, together with Professor Sannicolò's group, we started to synthesize and characterize two series of 'spider-like' oligothiophenes [28] (Figure 21), with the aim both of developing novel functional materials with attractive properties for energetic and sensoristic applications, and of throwing new light on the structure/reactivity relationships in the important class of branched oligothiophene semiconductors.

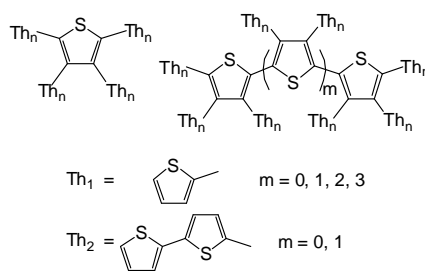


Figure 21. General structure of 'spider like' oligothiophenes with α,α' connections

In particular, we have shown that the electronic properties of these oligomers do not depend upon the overall number of thiophene units, but (i) on the number of conjugated thiophene units in the longest α -linked chain in the molecule, and (ii) on the number of 'nodes', *i.e.* bonds between thiophene rings capable of distortion from planarity of these rings, along the same α -conjugated chain. In fact the conjugation efficiency regularly increases, and the energy gap decreases, with the increase of the number of α -linked thiophene rings in the main backbone and with the decrease of the node density along it. Nevertheless the gaps tend to flatten for chains longer than five or six conjugated units, making the effort to synthesize more complex structures actually useless. On the other

hand, at constant length of the α -thiophene conjugated backbone the conjugation is impaired by an increasing node density along the conjugated chain [25]

More recently, we successfully applied the concept of *inherent chirality* to the achiral 'spider-like' oligothiophene family. In this frame, we have synthesized the C_2 symmetric 2,2',4,4',5,5'-tetra(2-thienyl)-3,3'-bithiophene named (T8)₃ (Figure 22).

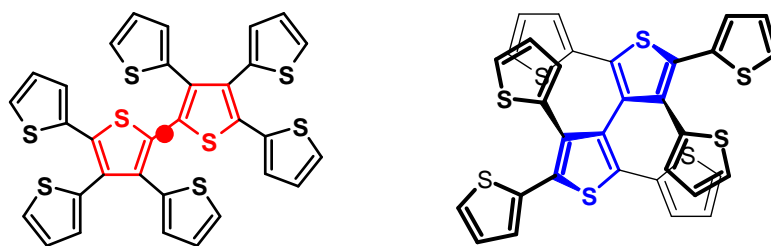


Figure 22. A comparison between the previous spider (T8)₄ on the left and of the new inherently chiral spider (T8)₃ on the right

This molecule differs from all the analogues described in the previous paragraphs 1.4.2, 1.4.3, 1.4.4 for the lack of sterically hindered 2-thienyl units in position *ortho* to the bond containing the stereogenic axis responsible for the atropisomerism. In fact it is entirely constituted by thiophene units and the chirality is generated from the presence of the β,β' link between the two α -terthiophene equal moieties that confers to the system an high racemization barrier. The situation is completely different from the case of 'spider like' molecules (Figure 22 on the left) where the sulphur atom in the position *ortho* to the α,α' interanular bond is not sufficiently sterically demanding to impede the rotation.

The same β,β' conjugated system implies also impressive chiroptical properties tunable with electric potential and an outstanding enantio recognition capability (presented in paragraph 3.3).

1.4.6 Chirality coupled with Ionic Liquids: Inherently Chiral Ionic Liquids

Chiral Ionic Liquids (CILs) constitute a class of chiral solvents which got a steadily increasing importance in the last ten years on account of some peculiar interesting properties just mentioned in the paragraph 1.3 which elevate them above the level of the traditional chiral organic solvent.

The ILs result from the association of generally large organic cations (imidazolium, ammonium, oxazolinium, thiazolinium) with weakly coordinating inorganic anions (BF_4^- , PF_6^- , SbF_6^- , TfO^- , etc.). It is expected that the physical and chemical properties of ILs could be significantly modified by changing the nature of the cations and/or the anions, offering to the designer the possibility of modulating the reactivity and the selectivity of a process according to specific needs.

The secret of the behaviour of the CILs is related to the high degree of supramolecular organization which induces a significant chirality transfer from the solvent to the dissolved species. It is suggested that ILs, and CILs in particular, would display a behaviour similar to that shown by highly organized liquid polymers, where a tridimensional network of hydrogen bonds between anion and cations aligns and orients the molecules in solution according to a highly ordered texture.

The chiral structuration of CILs is at the basis of molecular recognition and is exploited to induce stereoselective reactions. CILs are used as chiral solvent for asymmetric synthesis and for stereoselective polymerization, as chiral phases for gas chromatography, as chiral shift reagents in NMR spectroscopy and, in some cases, when the molecular geometry is suitably tailored, they are used to generate cholesteric liquid crystals.

The current general design of CILs follows rather intuitive strategies: the use of a chiral anion (lactic acid, α -aminoacids, 10-camphorsulfonic acid, 1,1'-binaphthylphosphoric acid) is a simple strategy, not particularly challenging since based on the use of compounds widely employed in other areas and scarcely rewarding from the point of view of possible innovation. The use of chiral cations offers an infinite range of possibilities, starting from

those based on aminoacids and aminoalcohols deriving from the chiral pool. Oxazolines and their quaternary salts can be easily prepared from the aminoalcohols obtained by reduction of the carboxy group of α -aminoacids. Ephedrine and its derivatives are largely available starting materials for preparing quaternary ammonium salts.

Imidazolium and thiazolium cations are characterized by the presence of a chiral pendant on the heterocyclic ring. The substituent which confers chirality to the CILs displays very different structures: the classical 1-phenylethyl group is widely employed, but derivatives of tartaric acid, pinene, myrntanol, citronellol, menthol, carvone etc are also popular.

All the CILs have a structural feature in common: they are characterized by chiral substituents having one or several stereocenters as stereogenic elements (Figure 23) [29,30].

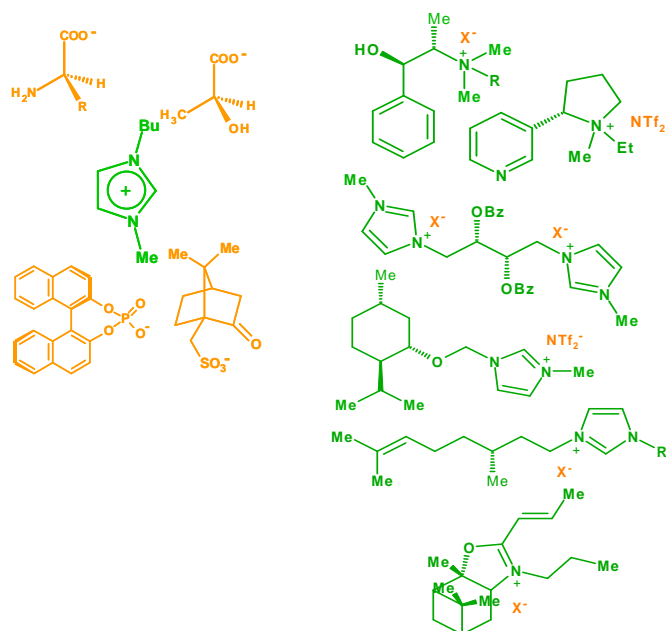


Figure 23. Literature examples of CILs having stereocenters as stereogenic elements

There are only two exceptions to this classical design:

1- Only a couple of very similar examples is reported in literature exhibiting planar stereogenicity (Figure 24: a, b). The heterocyclophane scaffold is made asymmetric by the presence of the methyl group in position 4 of the imidazole ring. It is not surprising that the enantirecognition properties of this CIL is modest.

2- Axial stereogenicity was employed in one case only: a series of C_1 symmetric CILs based on a pyridinium salt as cation, carrying a 5-alkylidene-1,3-dioxane ring in γ -position was synthesized in an enantiomerically enriched form by an enantioselective dehydrobromination promoted by *N,N'*-dimethylnorephedrine (Figure 24: c).

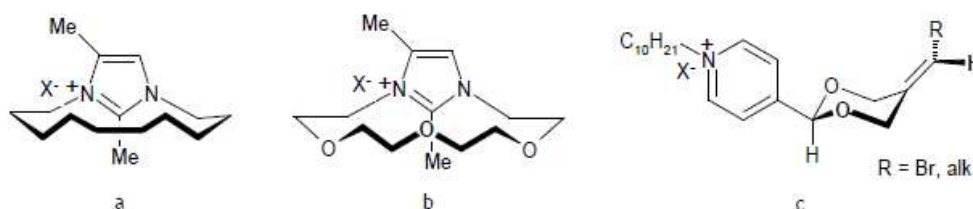


Figure 24. Exceptional molecular structures to the classical design of CILs

The rod-like core was designed in order to confer to these compounds the behaviour of liquid crystals. Cholesteric mesophases are found only in a couple of cases and with very special counteranions, provided that the CILs would be enantiopure. Surprisingly, the scalar physical properties characterizing the CILs (glass transition temperature, melting point and mesomorphic transitions) do not significantly depend upon enantiomeric composition. The scarce relevance of this crucial parameter indicates that the stereogenic core is not able to induce strong chirality effects in these molecules. The stereogenic alkylidenic moiety is too far from the ionic site and its influence on the rotational properties of the molecule is consequently weak.

In this context, together with Professor Sannicolò's group we started to design, synthesize, characterize and test in electrochemical oxoreduction processes a new and revolutionary family of CILs, which we have defined as *inherently chiral* ('inherently chiral ionic liquids, ICILs') In fact, we have demonstrated that the concept of inherent chirality is a general concept which does not depend from the chemical nature of the molecule; thus, considering the exciting results achieved with electroactive inherently chiral oligomer films (see further on) we have planned to exploit the same concept also in the field of ILs.

The rationale for the structural design is based on the following considerations:

1. The CIL cation should include an atropisomeric scaffold, such as a bi-imidazolium or bi-pyridinium unit, determining both chirality (stemming from a stereogenic axis) and ionic liquid properties (Figure 23); such inherently dissymmetric chromophore should be endowed with relevant enantiodiscrimination ability and high chiroptical properties, as demonstrated by our recent results on inherently chiral oligomers based on the same concept [24,31,32].

2. The symmetry is C_2 , so that the two systems (imidazolium and pyridinium) and the substituents are homotopic. In other words, they are absolutely identical and chemically and physically indistinguishable. This symmetry should guarantee a much higher level of intermolecular organization of the molecules and a much more easy supramolecular interaction between solvent and dissolved species than in C_1 symmetric CILs.

3. The ortho-substituents with respect to the interanular bond have a double function: to stabilise the stereogenic axis, avoiding the free rotation around the interanular bond, and to modulate the IL physical properties.

Three examples of atropisomeric scaffolds and related CILs are reported in Figure 25.

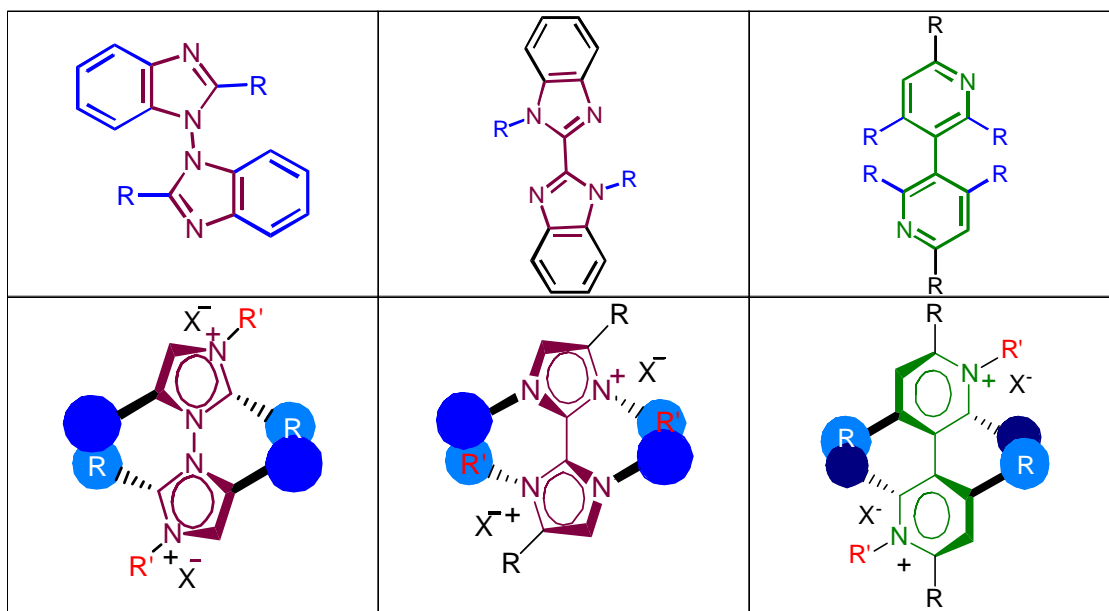


Figure 25. Three possible designs of atropisomeric scaffolds and of related CILs cations

The synthetic access to such systems appeared feasible, taking into account that a partner group from Università degli Studi dell'Isabria had already successfully prepared biheteroaromatic systems for applications in homogeneous stereoselective catalysis and in the field of chiral electroactive materials. Moreover, the starting materials are commercially available and inexpensive.

1.5 Electroreductive Cleavage of the Carbon Halogen Bond in Organic Halides

As already mentioned, the initial research plan implied the study in ionic liquids of two model electrochemical processes, respectively hinging on a radical cation and a radical anion intermediate, and possibly more affected by the ionic liquid anion and the ionic liquid cation, respectively. Thus, together with the electrooxidative coupling of the α -thiophene positions in thiophene-based molecules, affording electrodeposition of conducting materials (which turned out to be the most important part of the thesis, on account of the outstanding properties of such materials), the electroreductive cleavage of the carbon halogen bond in organic halides was parallelly investigated in ACN + 0.1 M TBAPF₆ and in BMIMPF₆ ionic liquid, on catalytic and non-catalytic electrodes.

The electroreduction of organic halides is of great prominence in the synthetic, analytical, and environmental domains, and in all of these three cases conspicuous benefits are obtained from the use of such electrocatalytic materials as silver (Ag) or palladium (Pd), and to a lesser extent gold (Au), which, by deeply modifying the reaction mechanism with respect to the non-catalytic case (*e.g.*, the glassy carbon one) thanks to the specific interaction between metal and halide [33], result in a positive shift of the reduction potential depending on the molecular structure (aliphatic, aromatic, benzyl halide; chloride, bromide, iodide leaving group) [34], even greater than 1 V. Thus in the synthetic field one gets very mild operating conditions, high selectivity and interesting alternative

reaction products [35]; in the analytical field, an amplified and much more differentiated range of detectable halides; and, in the environmental field, the direct and selective dehalogenation of halides, while totally preventing the occurrence of dangerous byproducts [36].

From the mechanistic point of view the electrocatalytic process has been rationalised in the latest years in cooperation with Università degli Studi di Padova.

It is the first example of detailed mechanistic study of an electrocatalytic process involving complex organic molecules. After focusing our studies on the role of molecular structure, quite recently we analyzed in detail the role of the medium, *i.e.*, supporting electrolyte [37] and solvent [38], both of them emerging as determining factors on the electron transfer (ET), particularly conspicuous when the electronic material is catalytic. In particular, the catalytic effects are seen to increase regularly with decreasing steric hindrance of the supporting electrolyte cation [37] and with decreasing 'primary medium effect' on the leaving halide group (corresponding to increasing aptitude of the solvent to solvate such an anion) [39], and these effects are particularly high with the protic solvents (alcohols) and especially with water, a convenient and attractive feature for analytical and environmental applications [38].

Considering our expertise in this field we decided to continue the study of the electroreductive cleavage in commercial ionic liquids in order to: *i)* verify if the catalytic effects also persist in commercial achiral ionic liquids, to which extent, and in which relationship with the electrode materials; and *(ii)* verify if in such media the dissociative electron transfer mechanisms (DET) and the relations between catalytic effects and molecular structure of the organic halide are the same observed in traditional solvents in the recent years [38].

This work is also propaedeutic to DETs studies in chiral conditions involving organohalides, to be performed in the next future in the new inherently chiral ionic liquids synthesized by the group of Professor Sannicolò, described in the paragraphs 1.4.6 and 3.6.

1.6 Guidelines and Targets of the PhD Thesis

This PhD thesis, as said before, was initially focused on studying in ionic liquid media two processes of fundamental importance in electrochemistry, respectively hinging on a radical cation and a radical anion intermediate:

(a) the electrooxidative coupling of thiophene-based conjugated molecules, with characterization and exploitation of their resulting products;

(b) the electroreductive cleavage of the carbon-halogen bond, particularly on catalytic surfaces (which had been the object of our former mechanistic studies in a wide range of organic solvents).

However, line (a), in cooperation with Prof. Sannicolò's research group, soon led us to evidence outstanding properties for thiophene-based 'inherently chiral' conducting films electrodeposited in ionic liquid. This prompted us to focus most of our attention and efforts on the study, exploitation and generalization of the 'inherent chirality' concept in electroactive molecular materials (a study also supported by Fondazione Cariplo, grant no. 2011-0417; actually the new oligomer class is so important that it has been recently patented). Moreover, since the 'inherent chirality' concept proved to be of general value, considering our interest for ionic liquids we added a further, new research line:

(c) development and electrochemical characterization of inherently chiral ionic liquids, also in cooperation with Prof. Sannicolò's research group.

a) Electrooxidative coupling of thiophene-based conjugated molecules in ionic liquids (resulting in discovery of outstanding properties of a new class of 'inherently chiral' electroactive materials)

The electrooxidative coupling of thiophene-based conjugated monomers to give conductive oligomer films has been studied in ionic liquids (commercial *achiral* ILs and synthesized *inherently chiral* ILs), to verify their effects on the redox properties of the

monomer, the polymerization rate, and the electrochemical and mechanical properties of the conducting films by means of cyclic voltammetry (CV) electrochemical impedance spectroscopy (EIS), scanning electron microscopy (SEM), *UV-visible* spectroelectrochemistry, photoelectrochemistry and in the case of enantiopure materials chiroptical spectroscopy.

The central thread of this thesis is the use of innovative and commercial ionic liquids to electrodeposit enantiopure oligomer films endowed with both homogeneity, regularity and reproducibility for the development of electrochemical sensors for chiral molecules, two attractive applications being *e.g.* their use as postchromatographic chiral electrochemical sensors or as a tool to estimate the enantiomeric purity of chiral analytes. In the last case it would be possible to directly evaluate the stereoselectivity of a chemical reaction without time consuming separation and purification procedures.

The outstanding chirality manifestations of the new electroactive oligomers also include the reversible tunability of the torsion angle and of the chirality manifestations with the electric potential (*breathing chirality*), electrochromism, and circularly polarized luminescence. Quite attractively, they can be obtained also in form of self-standing membranes.

Moreover these materials could find interesting applications also as racemates, *e.g.* in organic photovoltaics as an economically convenient donor replacing the common but more expensive poly-(3-hexyl-thiophene), or as complexing cavities (even for other semiconductors), or as comonomers to promote polymerizations of functional monomers of low intrinsic oligomerization ability. It is worthwhile underlying that in particular the cyclic oligomers can be regarded as idealizing conducting polymers without ends.

b) Cleavage of the carbon-halogen bond in ionic liquids

For this line, we have studied model molecules of alkyl- and aryl- bromides on glassy carbon GC, Au and Ag electrodes (non-catalytic, moderately catalytic, and highly catalytic

respectively), by two electrochemical techniques: cyclic voltammetry and electrochemical impedance spectroscopy. In particular we have compared the DET process for model organohalides studied in the latest years in traditional solvents using different electrode surfaces, with the DET process in a commercial ionic liquid.

It is worthwhile mentioning that the EIS technique has been used for the first time in the study of a DET mechanism and the data obtained suggest that it is a useful and complementary tool for the investigation of this process.

c) Development of inherently chiral ionic liquids

We have started this new line, in cooperation with professor Sannicolò, and supported by Fondazione Cariplo, grant no. 2011-1851, to verify the potentialities of new classes of ionic liquids endowed with the same 'inherent chirality' property as the outstanding electroactive films developed in line (a). In the first steps of this research, electrochemistry has mainly been applied to the characterization of the molecules developed by the organic partners, in a feedback scheme, to rationalize and optimize structure-properties relationships; but we are also going to test the new molecule effect on the model electrochemical processes studied in lines (a) and (b), exploiting the knowledge acquired while studying them in common achiral ionic liquids.

As a quite useful by-product of this research line, we have also developed an 'egg of Columbus' simple, mild and convenient protocol for abatement of halide traces in commercial ionic liquids.

References

- [1] Liming Dai PhD, *Intelligent Macromolecules for Smart Device. From Materials Synthesis to Device Applications*, 2004, Springer Link, ISBN 978-1-85233-510-6
- [2] J. Heinze, B.A. Frontana-Uribe, S. Ludwigs, *Chem. Rev.*, **2010**, 110, 4724
- [3] W.A Harrison, *Solid State Theory*, **1979**
- [4] J. L.Brédas, R. R.Chance, R. Silbey, *Phys. Rev. B*, **1982**, 26, 5843; J. L. Brédas, G. B. Street, *Acc. Chem. Res.* **1985**, 18, 308
- [5] I.F. Perepichka, D.F. Perepichka, *Handbook of Thiophene-based materials: Applications in Organic Electronics and Photonics*, **2009**, Wiley, Chichester, ISBN 978-0-470-05732-2
- [6] C.P. Andrieux, P. Audebert, P. Hapiot, J.M. Savéant, *J. Phys. Chem.*, **1991**, 95, 10158
- [7] J. Heinze, H. John, M. Dietrich, P. Tschuncky, *Synth. Met.* **2001**, 119, 49
- [8] S. Asavapiriyant, G. K. Chandler, G. A. Gunawardena, D. Pletcher, *J. Electroanal. Chem.* **1984**, 177, 229
- [9] B. Villeret, M. Nechtschein, *Phys. Rev. Lett.* **1989**, 63, 1285; G. Inzelt, *Electrochim. Acta* **1989**, 34, 83; K. Kalaji, L. Nyholm,; L. M. Peter, *J. Electroanal. Chem.* **1992**, 325, 269
- [10] F. Endres, A.P. Abbott, D.R. MacFarlane, *Electrodeposition from Ionic Liquids*, **2008**, Wiley-VCH: Weinheim, Germany, ISBN 978-3-527-31565-9
- [11] A. S. Ribeiro, L. M. O. Ribeiro, S. M. M. Leite, J. G. Da Silva Jr., J. C. Ramos, M. C. Navarro, J. Tonholo, *Polymer*, **2006**, 47, 8430; J. R. Matthews, F. Goldoni, H. Kooijman, A. L. Spek, A. P. H. J. Schenning, E. W. Meijer, *Macromol. Rapid. Commun.*, **2007**, 28, 1809
- [12] T. Verbiest, S. Sioncke, G. Koeckelberghs, C. Samyn, A. Persoons, E. Botek, J.M. André, B. Campagne, *Chem. Phys. Lett.*, **2005**, 404, 112
- [13] M. Lemaire, D. Delabouglise, R. Garreau, A. Guy, J. Roncali, *J. Chem. Soc. Chem. Commun.* **1988**, 658; J. Huang, V.M. Egan, H. Guo, J.Y. Yoon, A.L. Briseno, I.E. Rauda, R. Garrell, C.M. Knobler, F. Zhou, R.B. Kaner, *Adv. Mater.*, **2003**, 15, 1158; B. P. J. De Lacy Costello, N. M. Ratcliffe, P.S. Sivanand, *Synth. Met.*, **2003**, 139, 43
- [14] L.A.P. Kane-Maguire, G.G. Wallace, *Chemical Society Reviews*, **2010**, 39, 2545

- [15] E. J. Severin, R. D. Sanner, B. J. Doleman, N. S. Lewis, *Anal. Chem.*, **1998**, 70, 1440; J.A. Switzer, H.M. Kothari, P. Poizot, S. Nakanishi, E.W. Bohannan, *Nature*, **2003**, 425, 490
- [16]. L. Torsi, G. M. Farinola, F. Marinelli, M. C. Tanese, O. H. Omar, L. Valli, F. Babudri, F. Palmisano, P. G. Zambonin, F. Naso, *Nature materials*, **2008**, 7, 412
- [17] C.D. McTiernan, K. Omri, M. Chahma, *J. Org. Chem.*, **2010**, 75, 6096
- [18] G. Bidan, S. Guillerez and V. Sorokin, *Adv. Mater.*, **1996**, 8, 157
- [19] D. Caras-Quintero, P. Bäuerle, *Chem. Comm.*, **2004**, 926-927
- [20] B. M. W. Langeveld-Voss, R. A. J. Janssen and E. W. Meijer, *J. Mol. Struct.*, **2000**, 521, 285
- [21] I. D. Norris, L. A. P. Kane-Maguire and G. G. Wallace, *Macromolecules*, **2000**, 33, 3237
- [22] C. Li, M. Numata, A.-H. Bae, K. Sakurai and S. Shinkai, *J. Am. Chem. Soc.*, **2005**, 127, 4548
- [23] B. Deore, Z. Chen and T. Nagaoka, *Anal. Chem.*, **2000**, 72, 3989
- [24] F. Sannicolo, S. Rizzo, T. Benincori, W. Kutner, K. Noworyta, J. W. Sobczak, V. Bonometti, L. Falciola, P. R. Mussini, M. Pierini, *Electrochimica Acta*, **2010**, 55(27), 8352
- [25] T. Benincori, V. Bonometti, F. De Angelis, L. Falciola, M. Muccini, P. R. Mussini, T. Pilati, G. Rampinini, S. Rizzo, F. Sannicolò, S. Toffanin, *Chem. Eur. J.*, **2010**, 16, 9086
- [26] J. Roncali, P. Leriche, A. Cravino, *Adv. Mater.*, **2007**, 19, 2045
- [27] A. Pietrzyk, W. Kutner, R. Chitta, M. E. Zandler, F. D'Souza, F. Sannicolò, P. R. Mussini, *Anal. Chem.*, **2009**, 81, 10061
- [28] T. Benincori, M. Capaccio, F. De Angelis, L. Falciola, M. Muccini, P. Mussini, A. Ponti, S. Toffanin, P. Traldi, F. Sannicolo, *Chem. Eur. J.*, **2008**, 14, 459
- [29] J. Ding, D. W. Armstrong, *Chirality*, **2005**, 17, 281
- [30] C. Baudequin, D. Bregeon, J. Levillain, F. Guillen, J.-C. Plaquevent, and A.-C. Gaumont, *Tetrahedron: Asym.*, **2005**, 16, 3921
- [31] F. Sannicolò, S. Arnaboldi, T. Benincori, V. Bonometti, R. Cirilli, L. Dunsch, W. Kutner, G. Longhi, P. R. Mussini, M. Panigati, M. Pierini, and S. Rizzo, *Angew Chem. Int. Ed.*, **2014**, 53, 2623

- [32] F. Sannicolò; P. Mussini; T. Benincori; R. Cirilli; S. Abbate; S. Arnaboldi, S. Casolo; E. Castiglioni; G. Longhi; R. Martinazzo; M. Panigati; M. Pappini; E. Q. Procopio; S. Rizzo, *Chemistry A European J.*, **2014**, 10, 15261
- [33] A. A. Isse, P. R. Mussini, A. Gennaro, *J. of Phys. Chem. C* , **2009**, 113, 14983
- [34] A. A. Isse, G. Berzi, L. Falciola, M. Rossi, P. R. Mussini, A. Gennaro, *J. of Appl. Electrochem.*, **2009**, 39, 2217
- [35] M. Guerrini, P. Mussini, S. Rondinini, G. Torri; E. Vismara, *Chem. Comm.*, **1998**, 15, 1575; S.Rondinini, P.R.Mussini, P.Muttini, G.Sello, *Electrochimica Acta*, **2001**, 46, 3245
- [36] S. Rondinini, P. R. Mussini, M. Specchia, A. Vertova, *Journal of the Electrochemical Society*, **2001**, 148, D102; G. Fiori, S. Rondinini, G. Sello, A. Vertova, M. Cirja, L. Conti, *J. of Appl. Electrochem.*, 2005, 35, 363
- [37] A. Gennaro; A. A. Isse,; E. Giussani, P. R. Mussini; I. Primerano; M. Rossi, *Electrochimica Acta*, **2013**, 89, 52
- [38] S. Arnaboldi, A. Gennaro, A. A. Isse, P. R. Mussini, *Electrochimica Acta*, **2014**, submitted
- [39] L. Falciola, A. Gennaro, A. Ahmed Isse, P. R. Mussini, M. Rossi, *J. of Electroanal. Chem.* **2006**, 593, 47

2. Experimental

2.1 Voltammetry

2.1.1 Voltammetric Study of The Chemical Reactivity of Inherently Chiral Monomers in Traditional Solvents [1,2,3]

All the materials were characterized by cyclic voltammetry, at scan rates ranging from 0.02 to 2 V·s⁻¹, using an Autolab PGSTAT potentiostat of Eco-Chemie (Utrecht, The Netherlands), run by a PC with the GPES or NOVA software of the same manufacturer. The substrate working solutions (3 or 4 cm³) were 5·10⁻⁴ - 1·10⁻³ M in methylene dichloride (CH₂Cl₂, Sigma Aldrich analytical grade) or in acetonitrile (ACN, Sigma-Aldrich, analytical grade on molecular sieves) with 0.1 M tetrabutylammonium hexafluorophosphate, TBAPF₆, (Fluka, electrochemical grade) or tetraethylammonium tetrafluoroborate, TEABF₄, (Fluka, electrochemical grade) as supporting electrolytes; they were de-aerated by N₂ purging before each experiment, the cell being equipped with a presaturator to grant constant working volume. In the case of the ionic liquid (1-butyl-3-methylimidazolium hexafluorophosphate, BMIMPF₆, Sigma-Aldrich ≥97.0%, HPLC), obviously the supporting electrolyte is not necessary, and the concentration of the monomer was 0.012M. The working electrodes (WE) was either *i*) a 0.031 cm² glassy carbon (GC) disk embedded in glass of Metrohm *ii*) a 0.031 cm² gold (Au) disk embedded in Teflon® of Amel, *iii*) a 0.031 cm² platinum (Pt) disk embedded in glass, *iv*) a 1.44 cm² platinum foil for bulk depositions, *v*) an indium-doped tin oxide (ITO) coated glass slide of Sigma-Aldrich (sheet resistance 9–12 Ω/sq.). The optimized finishing procedure for the disk electrodes consisted in surface polishing with a diamond powder of 1 μm diameter (Aldrich) on a wet DP-Nap cloth (Struers®). The counter electrode (CE) was a platinum one. The reference electrode (RE) was an aqueous saturated calomel electrode (SCE) operating in a double bridge, filled with the working medium, to avoid water and KCl leakage into the working solution. The ohmic potential drop was compensated by the

positive feedback technique. The conducting oligomer films were electrodeposited from racemic or enantiopure monomer solutions, by repeated oxidative potential cycling at 0.2 V s⁻¹ around the monomer first oxidation peaks, followed by repeated stability cycles in a monomer-free solution.

In view of applications in photovoltaic or optoelectronic devices, determinations of the electrochemical higher occupied molecular orbital (HOMO) and lower unoccupied molecular orbital (LUMO) levels, and of the electrochemical HOMO-LUMO gaps were carried out (to be compared with the spectroscopic and the theoretical ones).

There are two different methods to calculate the HOMO-LUMO gap and the single values of the HOMO and LUMO states: the *onset criterion* (conformation of highest efficiency) and the *maxima criterion* (conformation of most abundant population).

The *onset potentials* of oxidation and reduction are determined from intersection of the tangents between the baseline and the signal current. The use of a reference compound is required (ferrocenium|ferrocene redox standard couple in our case) and the comparison of the potential values for the two materials, with subsequent conversion to vacuum level, provides the HOMO and the LUMO energy levels and the band gap, E_g of the analyzed material, according to these formulas [4]:

$$E_{HOMO}(eV) = -1e \cdot [E_{p,(onset),a}(V \text{ vs } Fc^+ | Fc) + 4.8(V \text{ } Fc^+ | Fc \text{ vs zero})],$$

$$E_{LUMO}(eV) = -1e \cdot [E_{p,(onset),c}(V \text{ vs } Fc^+ | Fc) + 4.8(V \text{ } Fc^+ | Fc \text{ vs zero})].$$

Usually the electrochemical band gaps of the polymer films are higher than the values extracted from the optical absorption spectra ($E_g = h \text{ (Js}^{-1}) \cdot c \text{ (ms}^{-1}) / \lambda_{\text{max}} \text{ (m)} \cdot q_e \text{ (C)}$), due to electrode-film interface charge barrier. The usual practice is to calculate the energy of the LUMO level by subtracting the electrochemically obtained HOMO value from the optical band gap; the HOMO corresponds to ionization potential, whereas the LUMO refers to an excited state and the optical measurement should be more meaningful.

2.1.2 Enantiorecognition Tests of Enantiopure Thiophene-based Oligomers [2]

The enantiorecognition tests on a 'model probe' were performed using the BMIMPF₆ ionic liquid as the medium granting high reproducibility and regularity of oligomer deposition while providing the same counter anion as in the previous experiments in traditional medium (PF₆⁻). (*R*) and (*S*) enantiopure conducting oligomer films were electrodeposited from the respective 0.012 M monomer solutions on gold screen-printed working electrodes (Metrohm 61208210 or Dropsens®) by repeated oxidative CV cycling at 0.05 V s⁻¹ scan rate, followed by several potential cycles in a monomer-free blank medium, after which the CV characteristics of (*S*)- and (*R*)-*N,N*-dimethyl-1-ferrocenylethylamine probes (or their racemate) (Sigma-Aldrich, ≥ 97%) were recorded, intercalating repeated stability potential cycles in the monomer-free solution to regenerate a probe-free film.

For other enantiorecognition tests the classical 3-electrodes minicell was employed, with GC embedded in glass (*S* = 0.031 cm²) as working electrode, a Pt disk as a counter one and an aqueous saturated calomel as a reference electrode always inserted into a glass jacket filled with the same cell background solution. The electrodeposition and stabilization medium in these cases was ACN with TBAPF₆ 0.1 M as supporting electrolyte.

The chiral probes were: *i*) (*R*) and (*S*) ofloxacin (the (*S*) enantiomer was purchased from Sigma-, ≥ 98.0%, the more expensive (*R*) enantiomer from Carbosynth) dissolved in ACN + TBAPF₆ 0.1 M, and *ii*) (*L*) and (*D*) DOPA (3,4-dihydroxy-*L*-phenylalanine and 3,4-dihydroxy-*D*-phenylalanine, Sigma-Aldrich, ≥ 98%) dissolved in water (for trace analysis, Sigma-Aldrich) with 0.05 M of hydrochloric acid (≥ 37%, for trace analysis Sigma-Aldrich).

2.1.3 Characterization of Cyclic Oligothiophenes and Enantiorecognition Tests [3]

In this case racemic or enantiopure substrate films were deposited by drop casting from solutions of racemic or enantiopure cyclic oligothiophenes in CH₂Cl₂ on the gold working

electrode of screen printed electrode minicells (Dropsens®), also featuring a carbon counter electrode and a silver pseudoreference electrode.

The solid-state CV features of the film-coated electrodes were recorded in the ionic liquid BMIMPF₆, by cyclic voltammetry performing redox cycles at different scan rates (from 0.010 V s⁻¹ to 2 V s⁻¹) using the same AutolabPGSTAT potentiostat of Eco-Chemie.

On the enantiopure electrode surfaces enantio-recognition tests were performed in the same conditions, using 0.012 M solutions of (*S*) and (*R*)-*N,N*-dimethyl-1-ferrocenylethylamine probes or their racemate in BMIMPF₆ working medium.

2.1.4 Differential Pulse Voltammetry (DPV) to Study the Racemization Barrier of Monomers with 3,3'-Bis-indole Core

Monomers in concentration of 0.0005 M were dissolved in ACN or CH₂Cl₂ with TBAPF₆ 0.1 M. Measurements were carried out in a 3-electrode minicell with GC as a working electrode, Pt disk as a counter one and an aqueous saturated calomel as a reference inserted into the same aforementioned a double bridge. The cell was put in a thermostatic bath where dry ice was mixed with methanol. In this way very low temperatures were reached. The temperature was monitored by means of a mercury thermometer. Differential pulse voltammetric responses were measured every 5-10 °C in order to reveal any changes in the distance between the two first anodic peaks.

2.1.5 DPV to Check Probe Enantiomeric Excess on Homochiral Films

After the electrodeposition of (*S*) and (*R*) chiral surfaces in BMIMPF₆ ionic liquid on screen printed gold electrodes, enantiopure films were tested with different mixtures of (*S*)- and (*R*)-*N,N*-dimethyl-1-ferrocenylethylamine probes containing these enantiomeric ratios: *i*)

1:1; *ii*) 1:1.5 and *iii*) 1:2.3, and the specular ones. The measurements were conducted using differential pulse voltammetry.

2.1.6 Study of the DET Process in the Reductive Cleavage of Carbon-Halogen Bond

All measurements were carried out in a classic three-electrode configuration (GC, as working electrode; platinum sheet as counter electrode; saturated calomel electrode, as reference) with 3-4 cm³ of working solution; we chose ACN with TBAPF₆ 0.1 M as supporting electrolyte for the experiments in traditional VOC medium, while for the experiments in RTIL we chose BMIMPF₆. The sample concentration was 0.00075 M in ACN and ten times higher in BMIMPF₆.

The organic halides studied, in ascending order of κ parameter, were: bromo-acetonitrile (the only aliphatic molecule), bromobenzene, 9-bromophenanthrene, 9-bromoanthracene, 4-bromo-benzophenone (all purchased from Sigma-Aldrich).

Intersolvental normalization was achieved referring the potential scales to the intersolvental redox couple Fc⁺|Fc (ferrocenium|ferrocene).

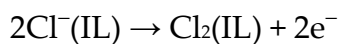
2.1.7 Protocol Employed for Chloride Impurities Abatement

Voltammetric measurements (cyclic voltammetry, differential pulse voltammetry, cathodic stripping voltammetry, CSV) and constant potential electrolyses were performed using a Autolab PGSTAT128 or PGSTAT302N potentiostat/galvanostat (EcoChemie, The Netherlands), managed by a PC with GPES software. All experiments were carried out in a three-electrode mini-cell with 3 or 4 cm³ of commercially available ionic liquids. Two samples of different purity of 1-butyl-3-methylimidazolium hexafluorophosphate, BMIMPF₆ (≥97.0%, Aldrich; and ≥98.5%, Fluka) and one of the corresponding tetrafluoroborate salt, BMIMBF₄ (≥98% 'BASF-Quality', Aldrich) were considered.

Voltammetric measurements employed a Teflon-embedded Ag disk (Amel, $S = 0.071 \text{ cm}^2$) or glass-embedded GC disk (Metrohm, $S = 0.031 \text{ cm}^2$) as working electrode, a Pt wire as counter electrode and an aqueous saturated calomel (SCE, to which all reported potentials are referred) as reference electrode inserted into a glass jacket, filled with IL, ending in a porous frit to prevent water and chloride leakage in the working solution. Calibration plots for the quantification of IL chloride impurities were obtained starting from the purest BMIMPF₆ commercially available (the 98.5% Fluka one), over a wide range of added chloride concentrations ($5 \cdot 10^{-6} \div 3 \cdot 10^{-2} \text{ mol dm}^{-3}$) obtained from a standard solution of tetraethylammonium chloride TEACl (98.0%, Fluka) dissolved in the same IL. Techniques of decreasing sensitivity with increasing chloride concentration were applied, *i.e.* CSV, DPV, and CV, on Ag electrode, exploiting the oxidation process, either as accumulation step in CSV, or as direct diffusive peak, at $E_{p,Ag} = -0.15 \text{ V}$ (*vs.* SCE) in DPV (yielding simple peaks in the lower concentration range and more complex ones at the higher concentrations) and in CV. The pulsed technique parameters were: conditioning potential -0.4 V (*vs.* SCE) for 30 seconds, equilibration time 5 s, modulation time 0.05 s, modulation amplitude 0.05 V, interval time 0.1 s, step potential 0.001 V; for the stripping analysis after the conditioning period a preconcentration step was performed at +0.4 or

+0.1 V (*vs.* SCE) for a specified time period. Cyclic voltammeteries were recorded at 0.2 V s⁻¹ scan rate potential.

In the highest concentration range, GC was also employed, since it implies the reaction:



at $E_{p,GC} = +1.25$ V (*vs.* SCE)

For electrolyses a Ag pigtail wire (1 mm diameter, 13-15 cm length) was employed as anode and, when necessary as discussed below, the Pt wire was inserted into a second jacket in order to obtain a separated cathodic compartment. Both electrolyses and CSV preconcentration steps were carried out under constant stirring, while there is no need of deaeration.

2.2 An Introduction to Less Common Techniques

2.2.1 Electrochemical Impedance Spectroscopy (EIS) [5]

The electrical resistance is the ability of a circuit element to resist to the flow of electrical current. Ohm's law defines resistance, R , in terms of the ratio between voltage, E , and current, I :

$$R = \frac{E}{I}$$

The use of this relationship is limited to an ideal resistor that has several properties as: *i*) it follows Ohm's law at all current and voltage levels, *ii*) its resistance value is independent of frequency, *iii*) AC current and voltage signals through a resistor are in phase with each other. However, a real system contains circuit elements that exhibit much more complex behaviour; for this reason another more general parameter named impedance, Z , is used. Like resistance, impedance is a measure of the ability of a circuit to resist the flow of electrical current, but unlike resistance, it is not limited by the simplifying properties listed above.

Electrochemical impedance is usually measured by applying an AC potential to an electrochemical cell and then measuring the current through the cell. The response to a sinusoidal potential excitation is an AC current signal that can be analysed as a sum of sinusoidal functions (a Fourier series).

Electrochemical impedance is normally measured using a small excitation signal. The cell response is pseudo-linear and the current response to a sinusoidal potential will be a sinusoid at the same frequency but shifted in phase.

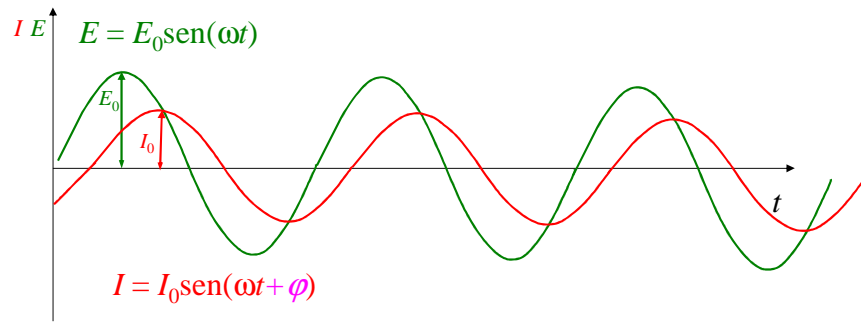


Figure 1. Sinusoidal current response in a linear system

The excitation signal, expressed as a function of time, has the form:

$$E = E_0 \sin(\omega t)$$

where E is the potential at time t , E_0 is the amplitude of the signal, and ω is the radial frequency. The relationship between radial frequency ω (expressed in radian/second) and frequency f (expressed in Hertz) is:

$$\omega = 2\pi f$$

In a linear system, the response signal, I , is shifted in phase (φ) and has a different amplitude, I_0 .

$$I = I_0 \sin(\omega t + \varphi)$$

An expression analogous to Ohm's law allows us to calculate the impedance of the system:

$$Z = \frac{E_t}{I_t} = \frac{E_0 \sin(\omega t)}{I_0 \sin(\omega t + \varphi)} = Z_0 \frac{\sin(\omega t)}{\sin(\omega t + \varphi)}$$

The impedance is therefore expressed in terms of a magnitude, Z_0 , and a phase shift, φ .

From Euler's relationship:

$$\exp(j\varphi) = \cos \varphi + j \sin \varphi$$

it is possible to express the impedance as a complex function.

The potential is described as:

$$E_t = E_0 \exp(j\omega t)$$

and the current response as:

$$I_t = I_0 \exp(j\omega t - \varphi)$$

The impedance is then represented as a complex number:

$$Z(\omega) = \frac{E}{I} = Z_0 \exp(j\varphi) = Z_0(\cos \varphi + j \sin \varphi).$$

2.2.2 Principles of Electrochemical Impedance Spectroscopy (EIS) Measurements

An electrochemical system opposes a number of obstacles to the current circulating under a given potential, including:

- the resistance to charge transport in solution;
 - the problem of mass transport to the electrode for the reactant species;
 - the capacitive reactance of the electrical double layer at the electrode/solution interphase;
 - the overpotential for the electron transfer between molecule and electrode,
- and many possible others, according to the specific case.

Therefore analysis of the electrochemical system impedance can afford valuable information concerning each of the above steps/obstacles.

The necessary condition is to be able to discriminate within the global impedance each single contribution and assign it to the right step/obstacle, or identify a circuit model corresponding to the electrochemical system and providing a simulated impedance spectrum faithfully reproducing the experimental one.

To this aim it is necessary to repeat the impedance measurement at different frequencies (*i.e.*, on a whole frequency spectrum) of the alternating voltage; in fact all resistive terms in the circuit, excepting ohmic resistances, have their own dependency on frequency; for instance, capacitive reactance tends to zero at high frequencies.

Any of these steps/obstacles can be modelled as an electric circuit element or element combination.

Electrical circuit theory distinguishes between linear and non-linear systems where impedance analysis of linear circuits is much easier than analysis of non-linear ones.

Unfortunately electrochemical cells are not linear in fact doubling the voltage will not necessarily double the current.

However, Figure 2 shows how electrochemical systems can be pseudo-linear. The I vs E curve at a small enough portion appears to be linear.

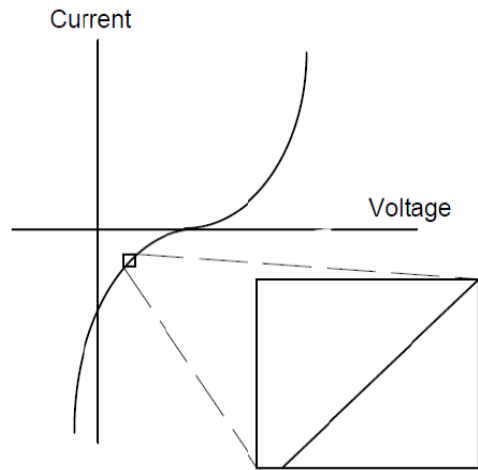


Figure 2. Pseudo-linearity in an electrochemical system

In normal EIS practice, the system is polarized at the chosen potential, and on this fixed potential an alternating voltage is superimposed with a convenient amplitude (a small AC signal 1 to 10 mV) that corresponds to a pseudo-linear system. The large non-linear response of the cell to the DC potential is not visible because only cell current at the excitation frequency is measured. The resulting alternating current is analysed in terms of amplitude and phase angle. The same determination is repeated in a wide frequency range, from very high ones (MHz) to very low ones (mHz) (typically 100 kHz – 0.1 Hz).

The necessary time for obtaining the impedance spectrum dramatically increases with increasingly lower frequency limit.

The expression for $Z(\omega)$ is composed of a real and an imaginary part. If the real part is plotted on the X-axis and the imaginary part is plotted on the Y-axis of a chart, a 'Nyquist plot' is obtained (see Figure 3). Notice that in this plot the Y-axis is negative and that each point on the Nyquist plot is the impedance at one frequency.

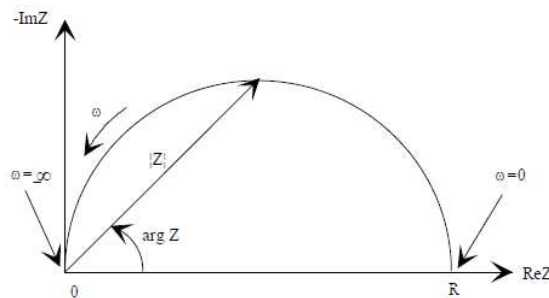


Figure 3. Nyquist plot

Figure 3 has been annotated to show that low frequency data are on the right side of the plot and higher frequencies are on the left. On the Nyquist plot the impedance can be represented as a vector (arrow) of length $|Z|$. The angle between this vector and the X-axis, commonly called the 'phase angle', is ϕ ($=\arg Z$).

The Nyquist plot in Figure 3 results from the electrical circuit of Figure 4. The semicircle is characteristic of a single 'time constant'. Electrochemical impedance plots often contain several semicircles but only a portion of a semicircle is seen.

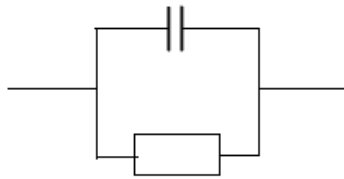


Figure 4. Simple equivalent circuit with one time constant

Another popular presentation method are Bode plots (Figure 5).

The impedance is plotted with log frequency on the X-axis and both the absolute values of the impedance ($|Z|=Z_0$) and the phase-shift on the Y-axis (Bode modulus and Bode phase respectively).

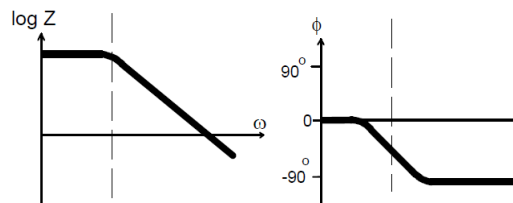


Figure 5. Bode plots

'Lissajous figure' (Figure 6) can be obtained applying sinusoidal signal $E(t)$ on the X-axis of a graph and the sinusoidal response signal $I(t)$ on the Y-axis. Analysis of Lissajous figures on oscilloscope screen was the accepted method of impedance measurement prior to the availability of modern EIS instrumentation.

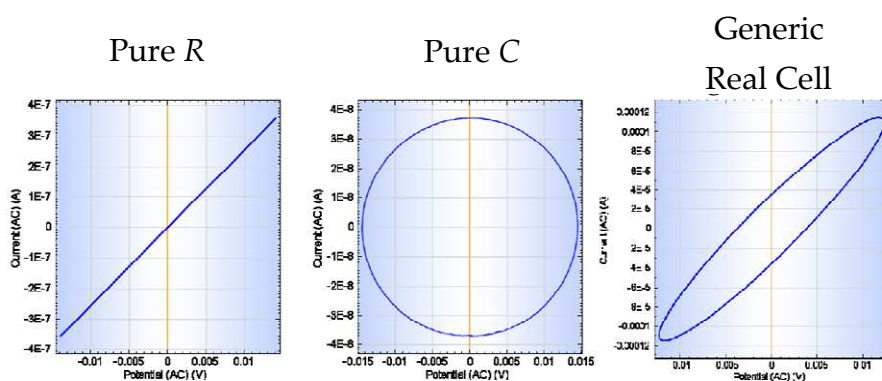


Figure 6. Lissajous figures

2.2.3 Equivalent Circuit Elements

EIS data is commonly analysed by fitting it to an equivalent electrical circuit model. Most of the circuit elements in the model are common electrical elements such as resistors, capacitors, and inductors. To be useful, the elements in the model should have basis in the physical electrochemistry of the system.

Table 1 lists the common equivalent elements that represent the possible obstacles to current flow in an electrochemical system.

Equivalent Element	Admittance	Impedance
R	$1/R$	R
C	$j\omega C$	$1/j\omega C$
L	$1/j\omega L$	$j\omega L$
W (infinite Warburg)	$Y_0\sqrt{(j\omega)}$	$1/Y_0\sqrt{(j\omega)}$
O (finite Warburg)	$Y_0\sqrt{(j\omega)}\text{Coth}(B\sqrt{(j\omega)})$	$\text{Tanh}(B\sqrt{(j\omega)})/Y_0\sqrt{(j\omega)}$
Q (CPE)	$Y_0(j\omega)^\alpha$	$1/Y_0(j\omega)^\alpha$

Table 1. Circuit elements and related admittance and impedance frequency functions

Each parameter will be analysed in detail in the following pages.

The R parameter in the first line in table 1 represents the solution resistance that is often a significant factor in the impedance of an electrochemical cell.

During the cell modelization for a generic 3-electrode system it is necessary to take into account the resistance between the reference electrode and the working one. The resistance of an ionic solution depends on the ionic concentration, ions type, temperature, and the cell geometry according to the second Ohm law.

The C parameter corresponds to the double layer capacitance. An electrical double layer exists on the interface between an electrode and its surrounding electrolyte.

However capacitors in EIS experiments often do not behave ideally; for this reason a constant phase element (CPE) is introduced.

The impedance of a real capacitor can be expressed as:

$$Z_{CPE} = \frac{1}{(j\omega)^\alpha Y_0}$$

where,

$Y_0 = C = \text{capacitance}$

$\alpha = \text{generally } 0.9-1.0 (\alpha=1 \text{ for an ideal capacitor})$

For a constant phase element, the exponent α is less than one. The 'double layer capacitor' on real cells often behaves like a CPE, not a capacitor.

Polarization resistance or charge transfer resistance is the R parameter in table 1. When an electrode is polarized, it can cause current to flow through electrochemical reactions that occur at the electrode surface. The amount of current is controlled by the kinetics of the reactions and the diffusion of reactants both towards and away from the electrode.

Diffusion is also correlated to the so called Warburg impedance. As said before, the impedance depends on the frequency of the potential perturbation. At high frequencies, the Warburg impedance is small since diffusing reactants do not have to move very far. At low frequencies, the reactants have to diffuse farther, increasing the Warburg impedance.

The equation for the 'infinite' Warburg impedance is:

$$Z_w = \sigma(\omega^{-\frac{1}{2}})(1 - j)$$

σ is the Warburg coefficient explicated by this equation:

$$\sigma = \frac{RT}{n^2 F^2 A \sqrt{2}} \left(\frac{1}{C^{*O} \sqrt{D_O}} + \frac{1}{C^{*R} \sqrt{D_R}} \right)$$

in which:

ω = radial frequency

D_O = diffusion coefficient of the oxidant

D_R = diffusion coefficient of the reductant

A = surface electrode area

n = number of the electron involved in the reaction

On a Nyquist plot the Warburg impedance appears as a diagonal line with a slope of 45°, complementary on a Bode plot, the Warburg impedance exhibits a phase shift of 45°.

This form of the Warburg impedance is only valid if the diffusion layer has an infinite thickness. Quite often, however, this is not the case. If the diffusion layer is bounded, the impedance at lower frequencies no longer obeys the equation above. Instead, we get the form:

$$Z_w = \sigma (\omega^{-1/2}) (1 - j) \tanh\left(\delta \left(\frac{j\omega}{D}\right)^{1/2}\right)$$

with,

δ = Nernst diffusion layer thickness

D = average value of the diffusion coefficients of the diffusing species

This more general equation is called the 'finite' Warburg. For high frequencies where $\omega \rightarrow \infty$, or for an infinite thickness of the diffusion layer where $\delta \rightarrow \infty$, $\tanh[\delta (j\omega/D)^{1/2}] \rightarrow 1$ and the equation above simplifies to the infinite Warburg impedance.

2.2.4 Common Equivalent Circuit models

Simplified Randles cell

The simplified Randles cell is one of most common cell models. It includes a solution resistance, a double layer capacitor and a charge transfer (or polarization resistance). The

double layer capacitance is in parallel with the charge transfer resistance. In addition to being a useful model the simplified Randles cell is the starting point for other more complex models.

The equivalent circuit for a simplified Randles Cell is shown in Figure 7.

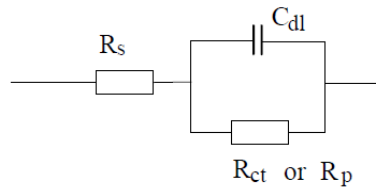


Figure 7. Simplified Randles circuit

The Nyquist plot for a simplified Randles cell is always a semicircle (Figure 8). The solution resistance can be measured by reading the real axis value at the high frequency intercept (R_s , the one near to the origin of the plot).

The real axis value at the other (low frequency) intercept is the sum of the polarization resistance and the solution resistance (R_s+R_{ct}). The diameter of the semicircle is therefore equal to the polarization resistance.

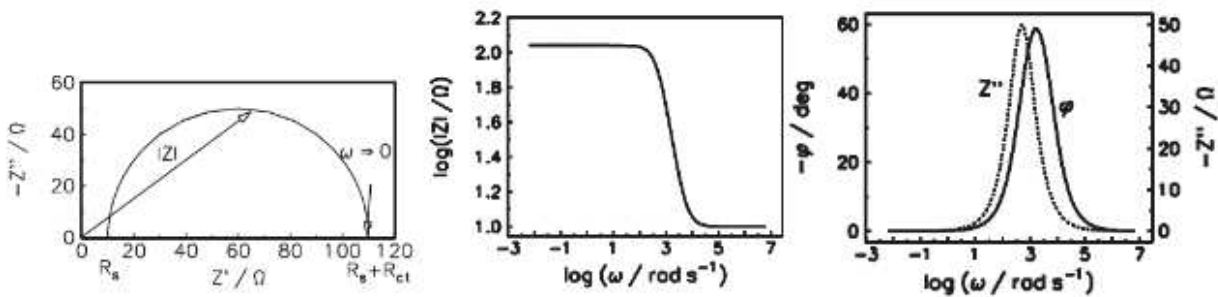


Figure 8. From left to right: Nyquist, Bode modulus and Bode phase plots for a simplified Randles circuit

Equivalent circuit with mixed kinetic and charge transfer control

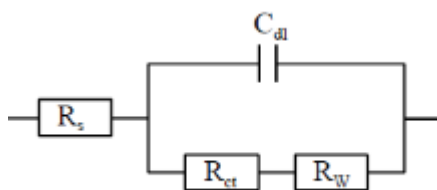


Figure 9. Randles cell: equivalent circuit with mixed kinetic and charge transfer control

This circuit describes an electron transfer at the interphase with both charge transfer and mass transfer control. With decreasing frequency (stationary conditions, as in a potentiostatic electrolysis) the reagent diffusion to the electrode becomes determining and is accounted for by the 'Warburg' straight line (Figure 10).

On the contrary, with increasing frequency the reactant diffusion becomes negligible with respect to charge transfer resistance and double layer polarization (half circle, Figure 10); finally at the highest frequencies also these processes are excluded, and the solution ohmic resistance can be observed alone, as the small real segment in proximity to the origin.

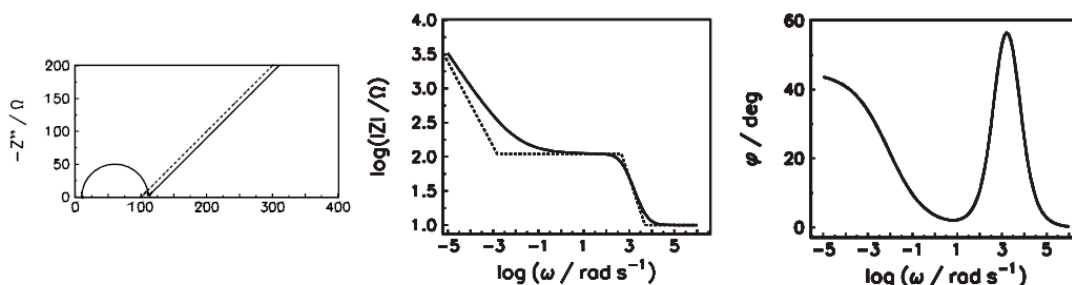


Figure 10. From left to right: Nyquist, Bode modulus and Bode phase plots for a modified Randles circuit

2.2.5 The Experimental Setup and the Analysis Protocol

Protocol to highlight differences between racemic and enantiomeric films of our inherently chiral surfaces

After electrodeposition and stabilization by cyclic voltammetry, the polymer films were also studied in monomer-free solution by comparing their electrochemical impedance at different potential values, representative of different doping states, in particular: at the

neutral state, at the onset and at the potential where the polymer is in the highest doping state.

Measurements were carried out in a classic three-electrode configuration (glassy carbon, GC, as working electrode; platinum sheet as counter electrode; saturated calomel electrode, SCE, as reference) with 3 cm³ of working solution (ACN and TBAPF₆ 0.1 M). The potentiostat was a PGSTAT302N equipped with the FRA2 module.

Protocol to study enantiorecognition ability of our enantiomeric perfectly specular surfaces

After electrodeposition of the suitable enantiopure antipodes and stabilization of the resulting films in BMIMPF₆ on gold screen printed electrode by CV, the enantiorecognition capability of these chiral electrodes were tested by EIS using solutions of each chiral ferrocene-based probe dissolved in pure ionic liquid. The apparatus was the same as above (potentiostat PGSTAT302N equipped with the FRA2 module).

The chosen potentials were: *i*) in the potential window where both probes are inactive, and *ii*) at the peak potential of each enantiomers.

Protocol to investigate the DET in carbon-halogen cleavage process

All measurements were carried out in a classic three-electrode configuration (GC, Au, Ag as working electrodes; platinum sheet as counter electrode; saturated calomel electrode, as reference) with 3-4 cm³ of working solution; we chose ACN with 0.1 M TBAPF₆ as supporting electrolyte for the experiments in traditional VOC medium, while for the experiments in RTIL we chose BMIMPF₆. The sample concentration was 0.00075 M in ACN and ten times higher in BMIMPF₆.

The organic halides studied were: bromo-acetonitrile (the only aliphatic molecule), bromobenzene, 9-bromophenanthrene, 9-bromoanthracene, 4-bromo-acetophenone.

For each molecule the EIS study was carried out at three different potentials corresponding, more or less, to the first reduction peak (associated with reductive cleavage), half-height potential and onset.

2.2.5 Circular Dichroism Spectroscopy (CD) [6]

Linearly polarized light is light whose oscillations are confined to a single plane. All polarized light states can be described as a sum of two linearly polarized states at right angles to each other, usually referenced to the viewer as vertically and horizontally polarized light. This is shown in the Figure11 below:

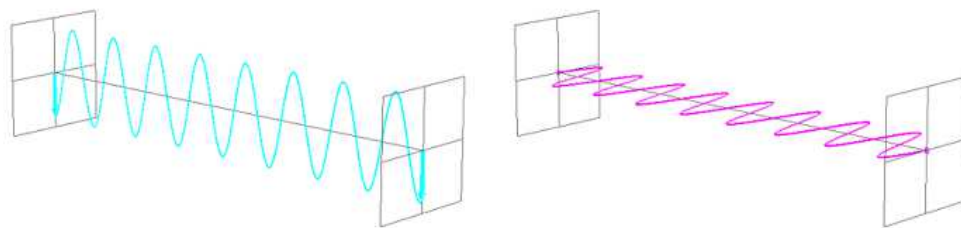


Figure 11. Vertically (on the left) and horizontally (on the right) polarized light

If horizontally and vertically polarized light waves of equal amplitude that are in phase with each other are taken, the resultant light wave (red) is linearly polarized at 45° , as shown in the Figure 12:

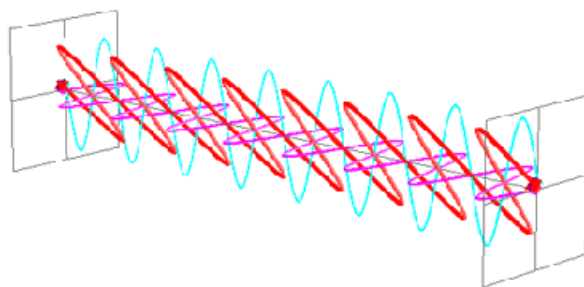


Figure 12. 45° linearly polarized light

If the two polarization states are out of phase, the resultant wave ceases to be linearly polarized. For example, if one of the polarized states is out of phase with the other by a

quarter-wave, the resultant will be a helix and is known as circularly polarized light (CPL). The helices can be either right-handed (*R-CPL*) or left-handed (*L-CPL*) and are non-superimposable mirror images (Figure 13).

The optical element that converts between linearly polarized light and circularly polarized light is termed a quarter-wave plate. A quarter-wave plate is birefringent, *i.e.* the refractive indices seen by horizontally and vertically polarized light are different. A suitably oriented plate will convert linearly polarized light into circularly polarized light by slowing one of the linear components of the beam with respect to the other so that they are one quarter-wave out of phase. This will produce a beam of either left- or right-CPL.

The difference in absorbance of left-hand and right-hand circularly polarized light is the basis of circular dichroism. A molecule that absorbs *L-CP* and *R-CP* light differently is optically active, or chiral.

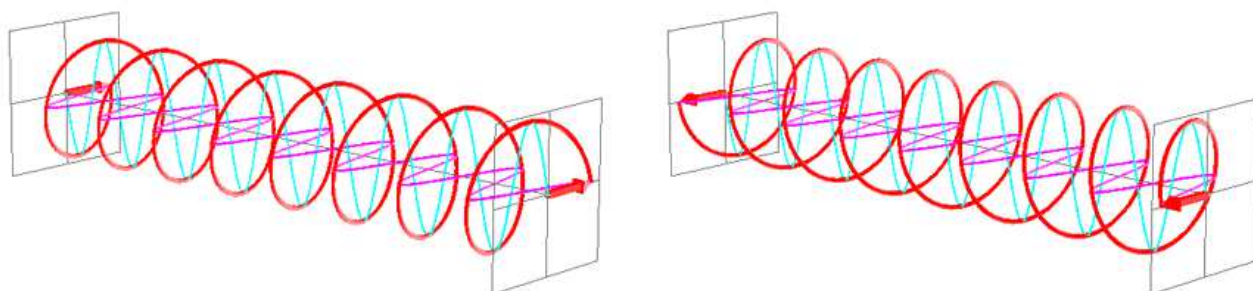


Figure 13. Left circularly polarized (*L-CP*) light (on the left) and right circularly polarized (*R-CP*) light (on the right)

Circular dichroism (CD) is the difference in the absorption of left-handed circularly polarized light (*L-CPL*) and right-handed circularly polarized light (*R-CPL*) and occurs when a molecule contains one or more chiral chromophores (light-absorbing groups):

$CD = \Delta A(\lambda) = A(\lambda)_{L-CPL} - A(\lambda)_{R-CPL}$, where λ is the wavelength

Another way to represent the CD signal is by molar circular dichroism parameter $\Delta\epsilon$:

$$\Delta\epsilon = \epsilon_{LCP} - \epsilon_{RCP} = \frac{A_{LCP} - A_{RCP}}{cl}$$

where ϵ is the molar extinction coefficient, c is the molar concentration, l is the path length in centimeter.

Measurements carried out in the visible and ultra-violet region of the electro-magnetic spectrum monitor electronic transitions, and, if the molecule under study contains chiral chromophores then one CPL state will be absorbed to a greater extent than the other and the CD signal over the corresponding wavelengths will be non-zero. A circular dichroism signal can be positive or negative, depending on whether *L*-CPL is absorbed to a greater extent than *R*-CPL (CD signal positive) or to a lesser extent (CD signal negative).

CD spectroscopy is a spectroscopic technique where the CD of molecules is measured over a range of wavelengths. CD spectroscopy is used extensively to study chiral molecules of all types and sizes, but it is in the study of large biological molecules where it finds its most important applications. A primary use is in analyzing the secondary structure or conformation of macromolecules, particularly proteins. As secondary structure is sensitive to its environment, temperature or pH, circular dichroism can be used to observe how secondary structure changes with environmental conditions or on interaction with other molecules. Structural, kinetic and thermodynamic information about macromolecules can be derived from circular dichroism spectroscopy.

Chiral molecules exist as pairs of mirror-image isomers. These mirror image isomers are not super-imposable and are known as enantiomers. The physical and chemical properties of a pair of enantiomers are identical with two exceptions: the way that they interact with polarized light and the way that they interact with other chiral molecules.

Circular birefringence and optical rotation

Chiral molecules exhibit circular birefringence, which means that a solution of a chiral substance presents an anisotropic medium through which *L*-CPL and *R*-CPL propagate at different speeds. A linearly polarized wave can be thought of as the resultant of the superposition of two circularly polarized waves, one left-circularly polarized, the other right-circularly polarized. On traversing the circularly birefringent medium, the phase relationship between the circularly polarized waves changes and the resultant linearly polarized wave rotates. This is the origin of the phenomenon known as optical rotation,

which is measured using a polarimeter. Measuring optical rotation as a function of wavelength is termed optical rotatory dispersion (ORD) spectroscopy.

In this context the equation for the determination of the specific rotation is:

$$[\alpha]_{\lambda}^T = \frac{\alpha}{l \times c}$$

where α is the measured rotation in degrees, l is the path length in decimeters, c is the concentration of the sample expressed in g/cm^3 , T is the temperature at which the measurement is taken (in degrees Celsius), and λ is the wavelength in nanometers.

Circular dichroism

Unlike optical rotation, circular dichroism only occurs at wavelengths of light that can be absorbed by a chiral molecule. At these wavelengths left- and right-circularly polarized light will be absorbed to different extents.

Although ORD spectra and CD spectra can theoretically provide equivalent information, each technique has been used for very distinct applications. Optical rotation at a single wavelength is used as a general measurement tool for chiral molecules, to determine concentration and as a determinant of chiral purity compared to a known standard. The simplicity and low-cost of the experiment and instrumentation makes it ideal for this application. Circular dichroism spectra on the other hand are better spectrally resolved than ORD spectra, and consequently more suitable for advanced spectral analysis.

In this frame it is important to introduce the vibrational circular dichroism (VCD) that is an extension of circular dichroism spectroscopy into the infrared and near infrared ranges. Because VCD is sensitive to the mutual orientation of distinct groups in a molecule, it provides three-dimensional structural information. VCD spectra of enantiomers can be simulated using *ab initio* calculations, thereby allowing the identification of absolute configurations of small molecules in solution from VCD spectra.

Circular dichroism, in situ CD spectroelectrochemistry, vibrational circular dichroism and circularly polarized luminescence were performed in cooperation with Prof. Giovanna Longhi, Prof. Ettore Castiglioni and Prof. Sergio Abbate, Dipartimento di Medicina Molecolare e Traslazionale, Università degli Studi di Brescia, Italy

The circular dichroism (CD) spectra of the inherently chiral monomers were recorded by using a Jasco Model J-700 spectropolarimeter. The spectra are average computed over three instrumental scans and the intensities are presented in terms of ellipticity values (mdeg).

In situ CD spectroelectrochemistry was performed on enantiopure oligomer films electrodeposited on ITO coated glass slides (8-12 Ω /sq, Sigma Aldrich), in a 1 cm path length quartz cuvette also including a mini SCE reference electrode and a platinum wire counter electrode. A JASCO 815SE spectrometer equipped with a photomultiplier extended to the NIR range was employed. The spectra for each potential value were obtained with one scan at 1000 nm/min scan rate, 0.25 s response time, slit width 300 nm.

Circularly polarized luminescence spectra were recorded using a homemade instrument [7,8]. The excitation radiation was brought to the cell from a Jasco FP8200 fluorimeter through an optical fiber containing water, a 90° scattering geometry was chosen, the incident radiation has been polarized parallel to the collection direction, five scans were taken for each enantiomer. Spectral response has been corrected using a reference lamp.

2.3 Other Experimental Techniques

Chiral HPLC and polarimetry, performed by Dr. Roberto Cirilli, Dipartimento del Farmaco, Istituto Superiore di Sanità, Rome, Italy

HPLC enantioseparations were performed by using the stainless-steel Chiralpak IB-3 analytical (250 mm \times 4.6 mm i.d.) and semi-preparative (250 mm \times 10 mm i.d.) columns (Chiral Technologies Europe, Illkirch, France). All chemicals, solvents for HPLC and

syntheses and spectral grade solvents were purchased from Aldrich (Italy) and used without further purification.

The analytical HPLC apparatus consisted of a PerkinElmer (Norwalk, CT, USA) 200 lc pump equipped with a Rheodyne (Cotati, CA, USA) injector, a 20- μ L sample loop, a HPLC Dionex CC-100 oven (Sunnyvale, CA, USA) and a Jasco (Jasco, Tokyo, Japan) Model CD 2095 Plus UV/CD detector. For semi-preparative separations, a PerkinElmer 200 LC pump equipped with a Rheodyne injector, a 500 μ L sample loop, a PerkinElmer LC 101 oven and Waters 484 detector (Waters Corporation, Milford, MA, USA) were used. The signal was acquired and processed by the Clarity software (DataApex, Prague, The Czech Republic).

For polarimetric measurements specific rotations were measured at 589 nm by a PerkinElmer polarimeter model 241 equipped with a Na/Hg lamp. The volume of the cell was 1 cm³ and the optical path was 10 cm. The system was set at a temperature of 20 °C.

Photophysical characterization and UV-visible spectroelectrochemistry performed in cooperation with Dr. Monica Panigati and Dr. Elsa Quartapelle Procopio, Università degli Studi di Milano, Italy

Absorption spectra were measured with an Agilent 8543 spectrometer at room temperature. Steady-state emission spectra were recorded on a HORIBA Jobin-Yvon Fluorolog 3 spectrometer equipped with a 450W Xenon arc lamp and a Hamamatsu R928P photomultiplier tube as detector. Emission and excitation spectra were corrected for source intensity (lamp and grating) and emission spectral response (detector and grating) by standard correction curves. For fluid solution state samples, luminescence quantum yields (PLQY) were measured in optically dilute solution and compared to reference emitters by the method of Demas and Crosby [9]. The fluorescein in NaOH 0.1 M solution at room temperature was used as reference ($\Phi_F = 0.95$) [10]. All the PLQYs values fallen in a $\pm 5\%$ range.

A quartz cuvette for UV-Vis spectroelectrochemistry was filled with the working solution; an ITO electrode, covered by a polymer film was the WE and was inserted in the cuvette, pinned to the cuvette wall with an alligator clip; a thin Pt wire was the CE and a small-diameter SCE was the reference electrode. On account of the small dimension of the system, it was not possible to de-aerate the working solution. However, this should have not influenced the measurement, since the potential scans concerned mainly the anodic region, *i.e.* not involving the reduction of the molecular oxygen.

LDI spectra analysis performed by M.Sc Marco Pappini, Università degli Studi di Milano, Centro Interdipartimentale Grandi Apparecchiature, Italy

LDI experiments were performed with a Bruker Microflex LT spectrometer both at low- and high resolution level.

High resolution LDI data were used to determine the relative abundance of cyclic *vs.* open-chain oligomers. To this end the mass spectra $I(x)$ (where x is the mass/charge ratio) were fitted to a (positive) superposition of basis signals S^i

$$I(x) = \sum_i \gamma_i^2 S^i(x - \eta)$$

one for each possible isomer i . Optimization was performed by minimizing the standard euclidean distance in the space of squared-integrable functions, defined for each oligomer in an appropriate spectral range (*e.g.* [1180-1198] m/z for the dimer and [1775-1980] m/z for the trimer). Quadrature of the integrals was performed over the fine mass grid available from our instrument.

The basis signals S^i were obtained by the isotopologue abundances (as computed from the relevant elemental isotope abundances) upon Lorentzian broadening the theoretical δ -peaked distributions, using a common broadening factor for each signal.

A shift term η was added to the functional form to allow for a possible drift of the mass signal. It was optimized in the fitting procedure, along with the broadening factor above and the coefficients γ_i , and always turned out to be much smaller than 1 m/z unit.

SEM imaging, performed together with M.Sc. Benedetta Sacchi, Università degli Studi di Milano, Milan, Italy

ITO or screen-printed electrodes (WE: GC, Pt and Au), covered by electrodeposited polymer films, were sputtered with a layer of gold to ensure the necessary electrical conductivity, required by the technique. SEM micrographs have been taken with a scanning electron microscopy SEM-EDS (Energy-Dispersive Spectroscopy).

¹H NMR and proton decoupled ¹³C NMR performed by Dr. Elsa Quartapelle Procopio, Dr. Simona Rizzo and Dr. Voichita Mihali

¹H NMR and proton decoupled ¹³C NMR spectra were recorded at 300 and 400 MHz ($T = 300$ K) on a Bruker Avance-300 and -400 instruments. Chemical shifts (δ) for ¹H spectra are expressed in ppm relative to internal Me₄Si as standard. Signals were abbreviated as s, singlet; d, doublet; t, triplet; q, quartet; dd, double doublet.

References

- [1] F. Sannicolò, S. Rizzo, T. Benincori, W. Kutner, K. Noworyta, J. W. Sobczak, V. Bonometti, L. Falciola, P. R. Mussini, M. Pierini, *Electrochimica Acta*, **2010**, 55(27), 8352
- [2] F. Sannicolò, S. Arnaboldi, T. Benincori, V. Bonometti, R. Cirilli, L. Dunsch, W. Kutner, G. Longhi, P. R. Mussini, M. Panigati, M. Pierini, and S. Rizzo, *Angew Chem. Int. Ed.*, **2014**, 53, 2623
- [3] F. Sannicolò; P. Mussini; T. Benincori; R. Cirilli; S. Abbate; S. Arnaboldi, S. Casolo; E. Castiglioni; G. Longhi; R. Martinazzo; M. Panigati; M. Pappini; E. Q. Procopio; S. Rizzo, *Chemistry A European J.*, **2014**, 10, 15261
- [4] S. Trasatti, *Pure Appl. Chem.*, **1986**, 58, 955
- [5] A. Lasia, *Electrochemical Impedance Spectroscopy and its Applications in Modern Aspect of Electrochemistry*, edited by B.E.Conway, J. O'M. Bockris, and R.E. White, vol. 32, p.143-248, Kluwer Academic/Pleum Publisher, New York, **1999**, ISBN 978-0-306-45964-1; Gamry Instruments, *Electrochemical Impedance Spectroscopy Primer*, www.gamry.com
- [6] A. Roger, B. Nordén, *Circular dichroism and Linear Dichroism*, Oxford Chemistry Masters, Oxford University Press, **1997**, ISBN 0-19-855897-X; <http://www.photophysics.com/tutorials/circular-dichroism-cd-spectroscopy/1-understanding-circular-dichroism>
- [7] E. Castiglioni, S. Abbate, G. Longhi, *Appl. Spectrosc.*, **2010**, 64, 1416.
- [8]. E. Castiglioni, S. Abbate, F. Lebon, G. Longhi, *Chirality*, **2012**, 24, 725
- [9] M. Takayanagi, T. Gejo, I. Hanazaki, *J. Phys. Chem.*, **1994**, 98, 12893
- [10] G. A. Crosby, J. N. Demas, *J. Am. Chem. Soc.*, **1970**, 92, 7262

3. Results and Discussion

3.1 Inherently Chiral Molecules with thiophene-based Atropisomeric Scaffolds

3.1.1 The Forefather T₄BT₂

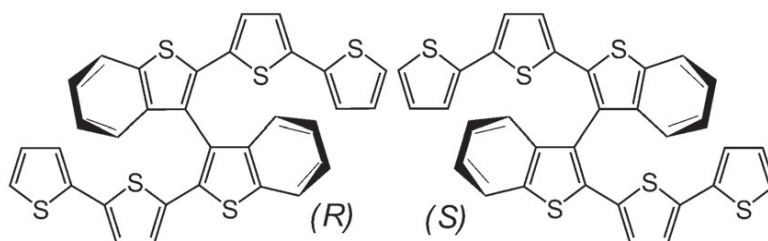
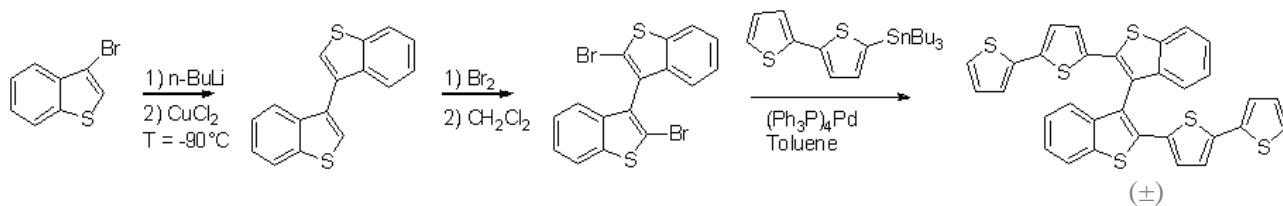


Figure 1. Structures of the T₄BT₂ enantiomers, in particular the *R* antipode on the left and the *S* one on the right

The 2,2'-bis-(2,2'-bithiophene-5-yl)-3,3'-bi-1-benzothiophene (acronym T₄BT₂) is the forefather of our inherently chiral family. The structural properties are well described in the chapter 1 at the paragraph 1.4.2. Interestingly, the 3,3'-junction of the internal thiophene units, generally considered a defective connection in polyconjugated systems, does play the essential role of granting electronic communication between the two halves of the molecule and at the same time of preventing the racemisation process. T₄BT₂ can be easily synthesized [1], according to the scheme 1, from commercially starting available materials as a racemate ((±)-T₄BT₂), according to the scheme 1, which can be perfectly separated into enantiomers (Figure 1) at the semi-preparative scale level by HPLC on a chiral stationary phase (Figure 2). The elution time between the two enantiomers is of the order of few minutes [2].



Scheme 1. Reaction scheme for the production of T₄BT₂ racemate

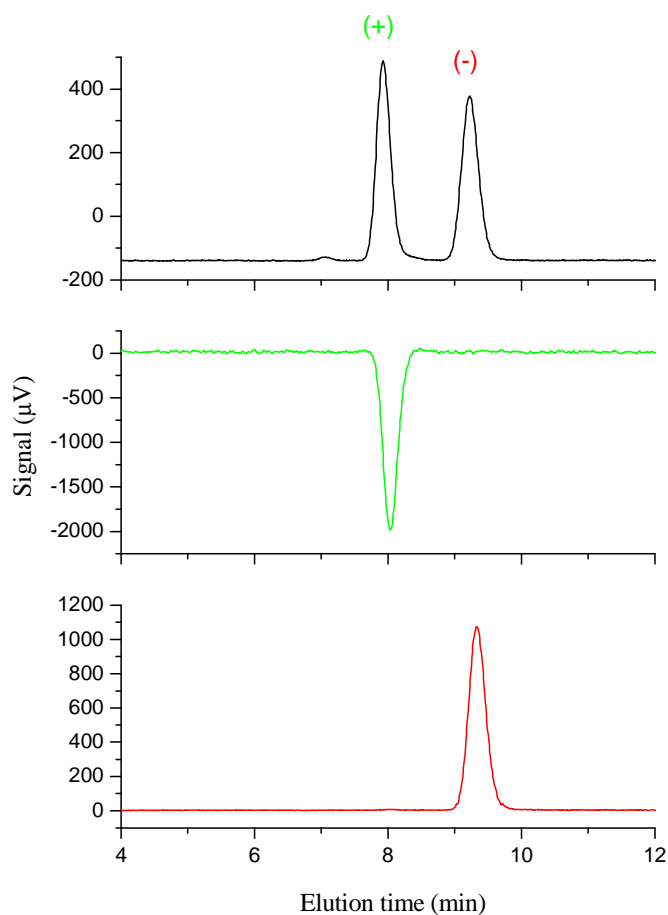


Figure 2. Analytical HPLC resolution of racemic T₄BT₂ and purity check of the enantiomers isolated on a semipreparative scale. Column: Chiralpak IB-3 (250 × 4.6 mm I.D.); eluent: *n*-hexane/CH₂Cl₂/EtOH=100:5:0.2 (v/v/v); T=25°C; (detector UV at λ=360 nm, detector CD at λ=360 nm). Black: racemic T₄BT₂; green: first eluted enantiomer, (+)-T₄BT₂; red: second eluted enantiomer, (-)-T₄BT₂

In order to clarify the chemical reactivity, the electrochemical behaviour and the interconnection between the two thianaphthenic units of the (\pm)-T₄BT₂, the half of the forefather 2-[5-(2,5'-bithienyl)]thianaphthene, named T₂BT, has been characterized by means of cyclic voltammetry.

The results were compared with that obtained for the T₄BT₂ in the same conditions (Figure 3). The analysis were conducted in CH₂Cl₂ and ACN in a 3-electrode minicell on glassy carbon as working electrode as explain in the experimental part, paragraph 2.1.1.

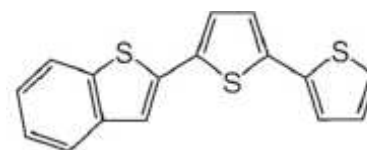


Figura 3.
Chemical structure
of T₂BT

In the first row of Figure 3, characterization of the monomers of T₄BT₂ and T₂BT in CH₂Cl₂ are represented. The anodic CV pattern (at all potential scan rates) of T₄BT₂ consists of two nearly merging peaks (with $E_{pa,I} = 0.62V$ vs. Fc⁺|Fc and $E_{pa,II} = 0.78V$ vs. Fc⁺|Fc). They all point to two equal, slightly interacting conjugated sites, resembling α -terthiophene, with some enhancement in the effective conjugation. This enhancement is a consequence of the presence of the condensed benzene ring and/or of some residual interaction with the adjacent twin π system (the dihedral angle at this node being significantly less than 90°).

The electrochemical energy gaps, determined from either the difference of the first anodic and the first cathodic peak potential ($E_{g,ECmax} = 3.20$ eV) or onsets ($E_{g,EC\ onset} = 2.93$ eV) are similar, albeit not coincident, with the spectroscopic gaps, determined from the absorption wavelength maximum ($E_{g,UV-vis\ max} = 3.32$ eV) or onset ($E_{g,UV-vis\ onset} = 2.79$ eV). The obtained values are intermediate between the literature values for linear α -terthiophene (α T₃: $E_{g,UV-vis\ max} = 3.50$ eV, $E_{g,UV-vis\ onset} = 3.04$ eV [2], $E_{g,EC} = 3.10$ eV [3]) and linear α -tetrathiophene (α T₄; $E_{g,UV-vis\ max} = 3.28$ eV, $E_{g,UV-vis\ onset} = 2.71$ eV [2]; $E_{g,EC} = 2.77$ eV [3]).

These considerations are confirmed by data obtained in the case of the half molecule T₂BT, featuring only one oxidation peak at all scan rates.

Very interesting is when the solvent is changed from CH₂Cl₂ to ACN; in fact a single peak is observed to account for the two redox sites, only widening at higher scan rates. This can be justified considering that, on account of its higher polarity, acetonitrile tends to shield

the positive charges generated during the oxidation process and as a consequence the two equivalent redox sites are more independent.

Oligomerization of T₄BT₂ and T₂BT monomers is very fast, regular and virtually unlimited even at low monomer concentration; in both cases resulting films are stable upon various oxidative redox cycles. The first oxidation peak for the racemic oligo-T₄BT₂ film (Figure 3, second row, on the left) is significantly less positive with respect to that of the monomer, thus pointing to an increased effective conjugation. Moreover, there is a small reduction peak at ~ -1.90 V *vs.* Fc⁺|Fc, the corresponding charge being released at the symmetrical sharp reoxidation peak occurring at ~ -0.01 V *vs.* Fc⁺|Fc, before the regular first oxidation peak of the oligomer (Figure 3, fourth row).

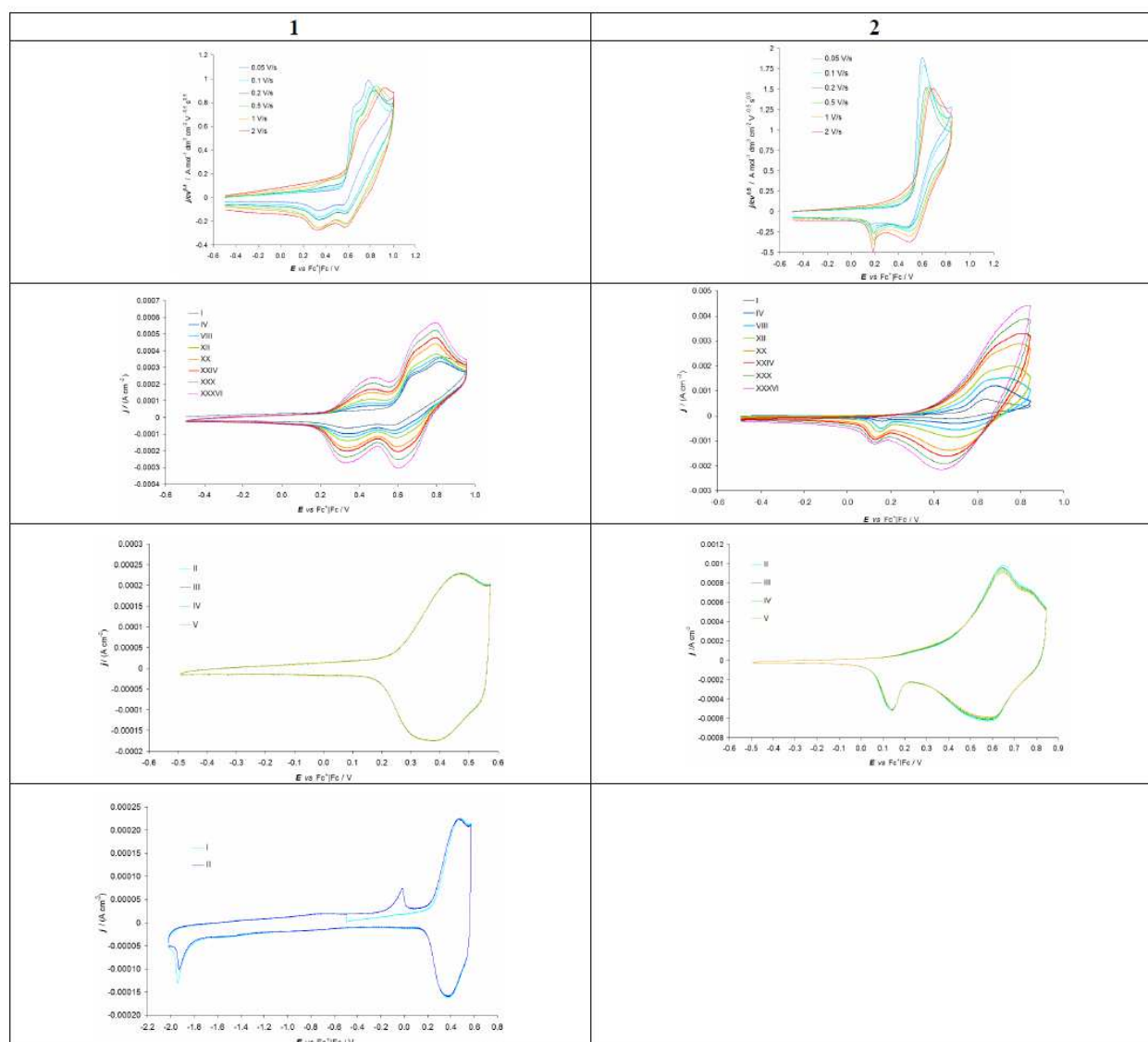


Figure 3. CV characterization of 0.001 M T₄BT₂ monomer (1) and T₂BT (2) on GC electrode in CH₂Cl₂ + 0.1 M TBAPF₆ medium: monomer at different potential scan rates, with ohmic drop compensation (first row); electrodeposition of the conducting films (second row); film stability upon oxidative redox cycles in monomer-free solution (third row); charge trapping upon potential cycling in monomer-free solution (fourth row)

Chiroptical properties of the enantiopure antipodes

The chiroptical properties of the enantiopure antipodes (*R*)-T₄BT₂ and (*S*)-T₄BT₂ have been determined: impressive is the specific rotation value, in accordance with the presence in the molecule of an inherently dissymmetrical chromophore ($[\alpha]_D^{20} = +1001$ ($c = 0.1\%$, CHCl₃); $[\alpha]_D^{20} = -991$ ($c = 0.1\%$, CHCl₃)). The DFT calculations provided an evaluation of the stereochemical properties of (*S*)-T₄BT₂. It appeared that the favored dihedral angle is

about 80° (the angle value computed by averaging those found within the two most representative conformations of (*S*)-T₄BT₂, characterized by a relative Boltzmann population of 74% and 26%) and the enantiomerization barrier, related to rotation around the bond connecting the thianaphthene units, is close to 167 kJ mol⁻¹, thus indicating a high configurational stability of the enantiomers even at high temperatures. Absolute configuration was assigned to the enantiomers by comparison of the experimental CD curves with that calculated for the (*S*)-enantiomer (Figure 4).

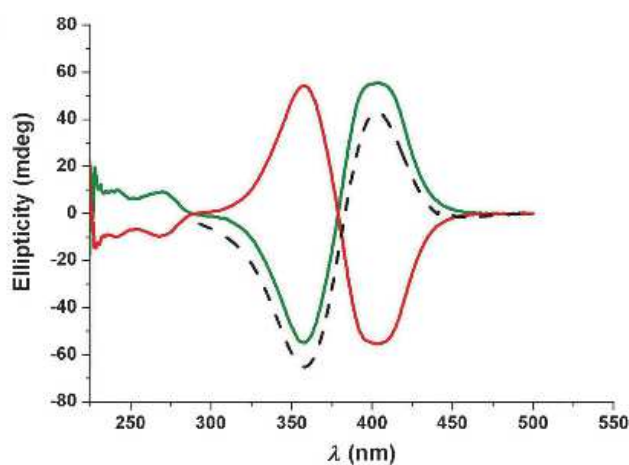


Figure 4. CD spectra (CHCl₃, $c=0.14$ mgcm⁻³) of (*S*)-(+)-T₄BT₂ (green) and (*R*)-(-)-T₄BT₂ (red). Dotted black curve: calculated CD spectrum for (*S*)-T₄BT₂

Pseudo-scalar properties

The most interesting features of these materials is related to their pseudo-scalar properties, above all the CD and enantioselection properties.

The CD spectra of the films demonstrate that chirality and its CD sign are fully transferred from monomers to the oligomers. The bisignate spectra of the oligomers are very similar to those shown by the original monomers, with ellipticity maxima strongly shifted toward higher wavelengths, in accordance with the increased conjugation extent gained with polymerization (Figure 5). This result gives a proof of the great differences existing between these non-conventional, inherently chiral oligomers and the traditional ones,

which exhibit CD manifestations only in particular chain aggregation states, but are completely silent under ordinary conditions [4].

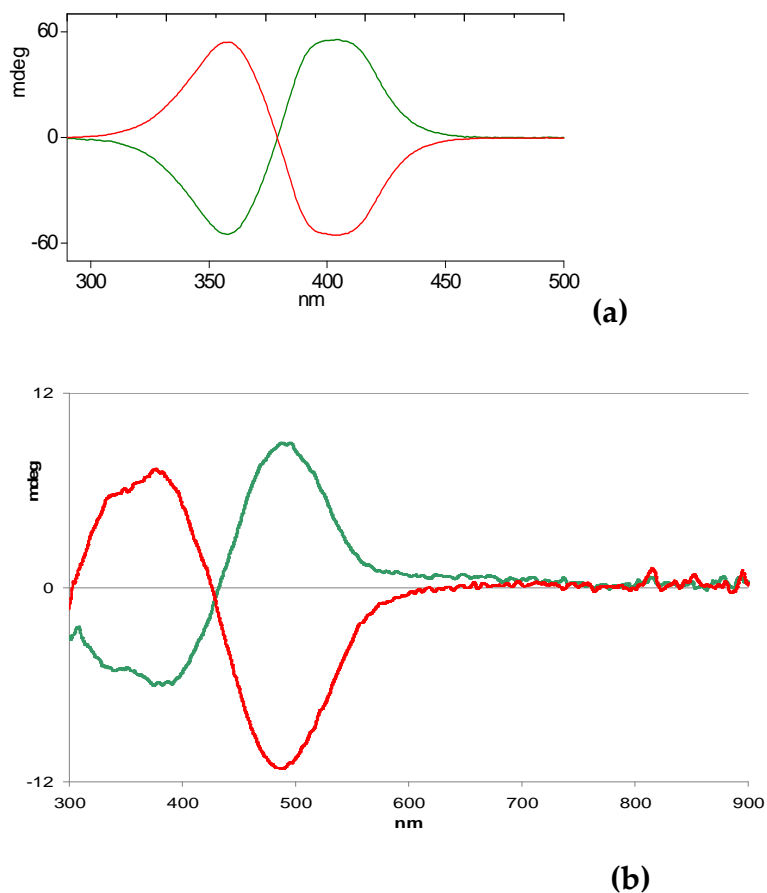
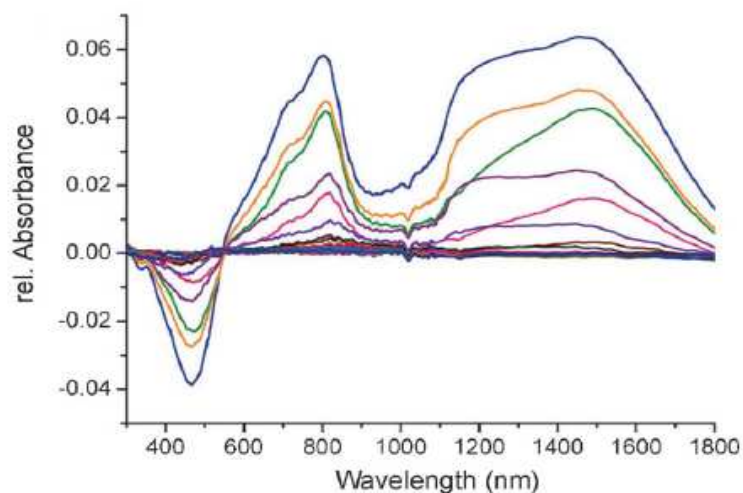
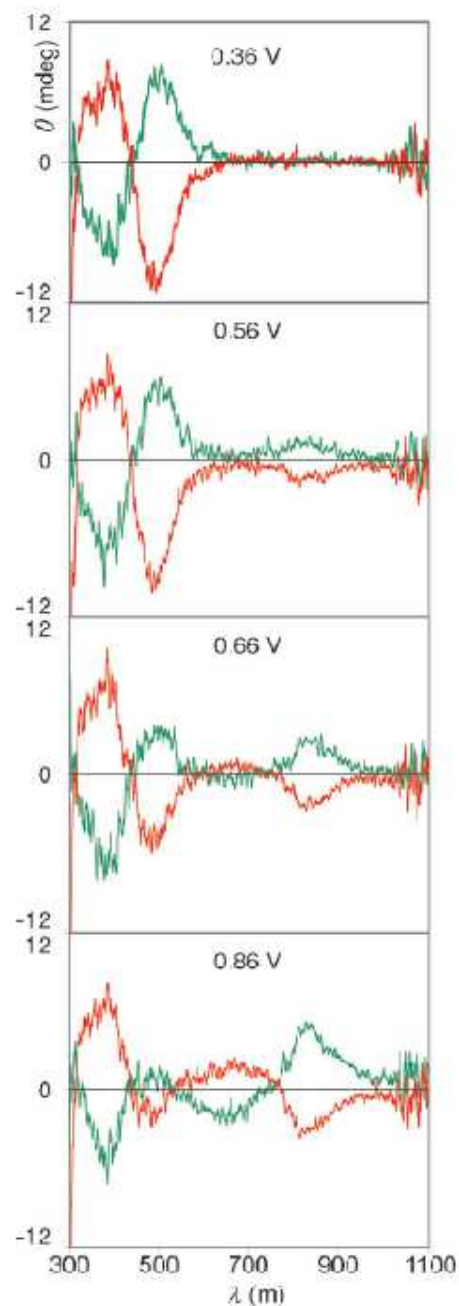


Figure 5. CD spectra of films of oligo-(R)-(-)-T₄BT₂ (red) and oligo-(S)-(+)-T₄BT₂ (green) on an ITO electrode d. (a): enantiopure monomers in solution; (b): enantiopure oligomer films deposited on ITO glass electrodes

The changes in the CD spectrum of the chiral films [5] resulting from potential variations (Figure 6 (b)) provide insight into the electronic state of the material. For these experiments, a quartz cuvette was adapted to serve as the three-electrode cell fitted with an indium tin oxide (ITO) working electrode coated by either a film of electrodeposited oligo-(S)-(+)-T₄BT₂ or oligo-(R)-(-)-T₄BT₂, together with a saturated calomel electrode (SCE) and a Pt wire as the reference and counter electrode, respectively. The CD spectra of the films, recorded at different applied potentials, parallel the UV spectra (Figure 6 (a)): they progressively decrease in their lower energy component with the potential increase, while new signals grow in at higher wavelengths, as expected on the basis of the UV data.



(a)



(b)

Figure 6. (a) Combined Vis/NIR data collected by in situ spectroelectrochemistry spectra on a (-)-T₄BT₂ film deposited on a Pt electrode grid during a slow CV cycle (5 mV s⁻¹). Potentials are referred to the Fc⁺|Fc couple. Vis/NIR are reported at constant potential intervals and plotted as differences with respect to the spectrum of the neutral film. (b) CD spectra of films of oligo-(R)-(-)-T₄BT₂ (red) and oligo-(S)-(+)-T₄BT₂ (green) on an ITO electrode during an anodic cycle in 0.1M TBAPF₆ in acetonitrile. Potentials are referred to the Fc⁺|Fc couple

Interestingly, the ellipticity of the new signals is considerably lower than the original one, thus indicating a decrease in the chirality in the oxidized state. Injection of holes would force the two thianaphthene rings to co-planarize to gain electronic conjugation with some loss in the stereogenic efficacy of the atropisomeric core. The two interconnected heteroaromatic units, however, cannot become coplanar in the heavily doped state, otherwise enantiomeric purity would be lost, whereas the signal is fully recovered when the oligomer is reduced back to its neutral state. This process was perfectly reversible and indefinitely repeatable and suggested us the figure of a *breathing system*.

This suggestion is supported by the DFT calculations [5], indicating that a remarkable dihedral angle decrease from 80° to 71° is caused by abstraction of one electron from (S)-T₄BT₂.

3.1.2. Enantiorecognition Tests: Traditional Solvents *vs* Ionic Liquids

As mentioned in the introduction, the most important achievement in this work has been the preparation of chiral surfaces able to discriminate between the two enantiomers of a chiral analyte for their final employment in chiral sensors. A prerequisite for this study is the preparation of electrode surfaces which are fully reproducible in size, shape, morphology, and thickness.

Moreover, suitable chiral electroactive probe molecules (the potential chiral analytes) must be selected on account of their redox potential, considering the level of polymer doping/undoping, and their steric hindrance *i.e.* probe capability to diffuse within the film. For these reasons the commercially available (S)-(-)- and (R)-(+)-N,N-dimethyl-1-ferrocenylethylamine (represented in Figure 7) have been chosen.

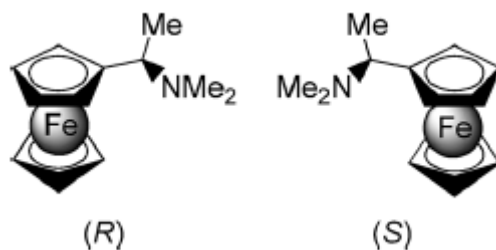


Figure 7. Molecular structures of available (*S*)-(-)- and (*R*)-(+)-*N,N*-dimethyl-1-ferrocenylethylamine

Preliminary enantioselectivity tests were performed in acetonitrile as solvent with 0.1M TBAPF₆ as supporting electrolyte in a classic three electrode mini-cell (Figure 8) using a glassy carbon disk embedded in glass as working electrode, a platinum disk as counter and an aqueous saturated calomel as reference.

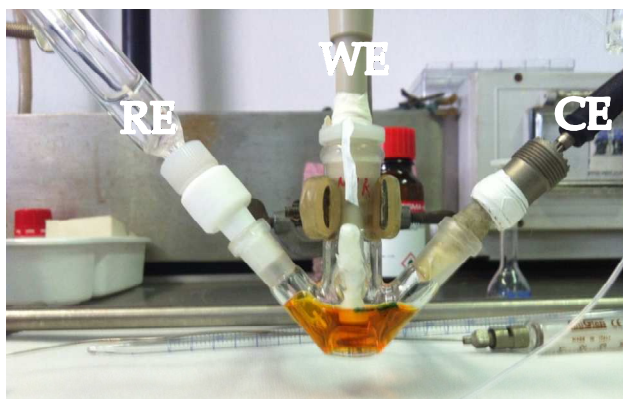


Figure 8. The three electrode mini-cell used for preliminary enantioselectivity tests

Unfortunately the electrodeposited enantiopure films obtained in these conditions displayed an unsatisfactory reproducibility probably due to small variations of the reciprocal electrode position and variations in the monomer concentration notwithstanding the presence of a presaturator. In this way the enantioselectivity capability of the obtained homochiral films remained nearly unexploited.

In order to overcome such limitations, we decided to work on screen printed electrodes (SPEs), granting the highest cell geometry reproducibility in

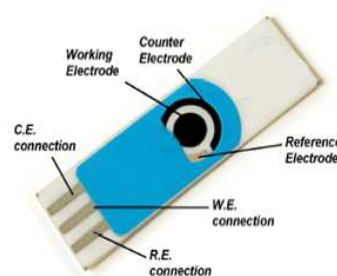


Figure 9. A screen printed mini-cell:
WE: GC, Au or Pt; CE: carbon; pseudoRE: Ag

combination with an ionic liquid, granting very regular electrodeposition on account of high viscosity, and constant monomer concentration on account of low volatility, besides being chemically compatible, unlike ACN, with the insulating paint used in commercial SPE fabrication.

A screen printed electrode is represented in figure 9, it is a real electrochemical cell with the three classic electrodes used in cyclic voltammetry. These mini-cells allowed to work in a drop of ionic liquid media (20 μ l) with much higher monomer concentration (about 10⁻² M).

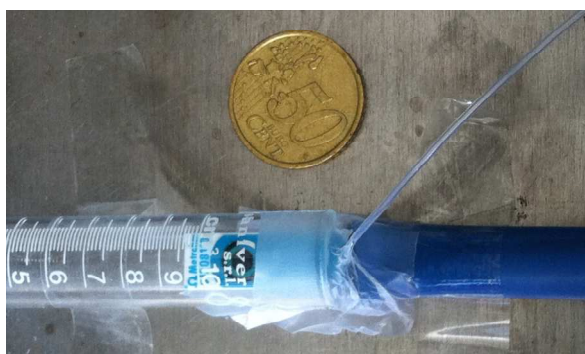


Figure 10. Deaerated microchamber for electropolymerization from 20 μ L solution deposited on screen printed electrodes (Working: Au, Pt, or GC disk, Ag pseudoreference, carbon counter electrode)

As mentioned in the introduction (paragraph 1.3) ionic liquid media can modulate many aspects of the general electropolymerization mechanism [6]. Preliminary literature evidences point to ILs possibly imparting many improvements to electrodeposited conducting polymers [7].

For the enantiorecognition tests the 1-butyl-3-methylimidazolium hexafluorophosphate (BMIMPF₆, Figure 11) ionic liquid was chosen for different reasons:

i) it has the same counter anion adopted in the former and parallel works in molecular solvents; *ii)* previous literature studies account for good performance in thiophene-based monomer electropolymerizations [8].

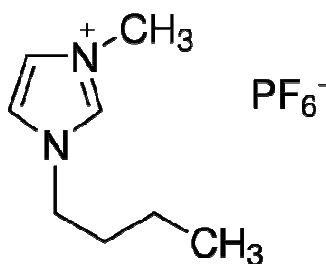


Figure 11. Molecular structure of BMIMPF₆ ionic liquid

The electro-oligomerization was efficient in molecular solvents as just said at the beginning of this paragraph, [1] while in BMIMPF₆ ionic liquid it has required significantly higher monomer concentrations. Under these conditions, the oligomerization of enantiopure T₄BT₂ was slower than that of the racemate. This appears consistent with the lower freedom degrees and higher stereospecificity of the enantiomer cases (Figure 12).

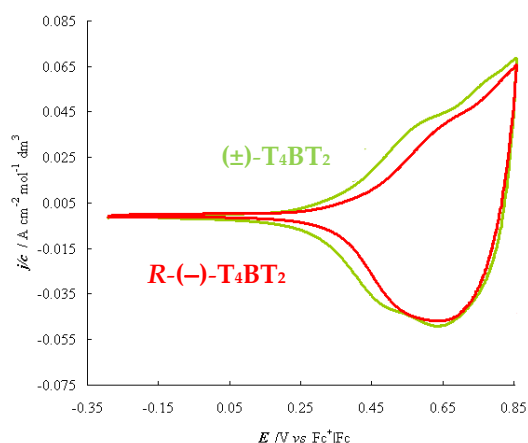


Figure 12. Electro-oligomerization of (±)-T₄BT₂ (green line) and R-(-)-T₄BT₂ (red line) in BMIMPF₆ on gold screen printed electrodes

As a preliminary test for the enantiorecognition ability of the enantiomeric films in ionic liquids [5], the CV curves of commercial (S)-(-)- and (R)-(+)- chiral ferrocene based probes were recorded on a bare gold screen printed electrode (Figure 14) and on two gold screen printed electrodes, one coated with the film of oligo-(R)-(-)-T₄BT₂ and the other with that of oligo-(S)-(+)-T₄BT₂. Such films were very regular and homogeneous as depicted by SEM micrographs in Figure 13.

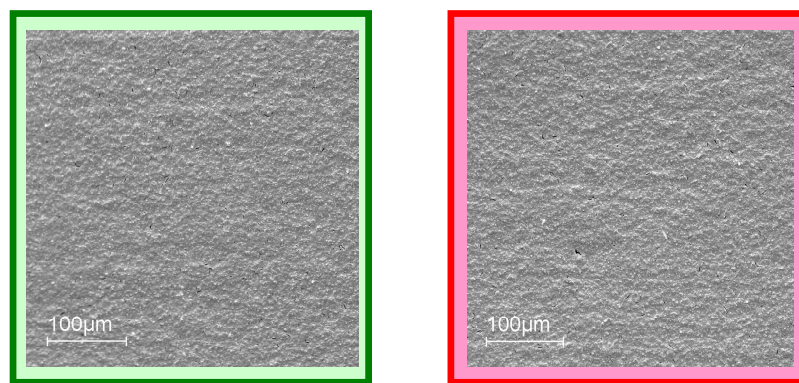


Figure 13. SEM micrographs of oligo-(*S*)-(+)-T₄BT₂ and oligo-(*R*)-(-)-T₄BT₂ electrodeposited from pure BMIMPF₆ on gold screen printed electrode

On the bare Au electrode, a typical diffusion-controlled reversible peak couple was observed for both (*S*)- and (*R*)-enantiomeric probes. Both CV curves showed peaks at formal potential $E^{\circ'} = -0.01$ V *vs.* Fc⁺|Fc with about 60 mV half-peak width and approximately a 60 mV anodic-to-cathodic peak potential separation, as expected for a reversible one-electron transfer (Figure 14).

On the oligomer-film-coated electrodes (36 oligomerization potential cycles at 50 mV s⁻¹) the enantiomeric oligo-(*R*)-(-)-T₄BT₂ and oligo-(*S*)-(+)-T₄BT₂ films displayed an outstanding, perfectly specular enantiodiscrimination ability towards the (*R*)- and (*S*)-chiral probes, with a formal potential difference of about 0.10 V between the two enantiomers (Figure 15):

- 1) on the oligo-(*S*)-(+)-T₄BT₂ film coated electrode, the formal redox potentials are +0.07 and +0.17 V *vs.* Fc⁺|Fc for (*S*)- and (*R*)-chiral probes, respectively (Figure 15 a);
- 2) on the oligo-(*R*)-(-)-T₄BT₂ film coated electrode, the formal redox potentials are +0.07 and +0.17 V *vs.* Fc⁺|Fc for (*R*)- and (*S*)-chiral probes, respectively (Figure 15 b).
- 3) separation of formal potentials is even larger for racemic (±)-probe (Figure 15 c).

Considering that the formal potential of the probes falls in the potential range in which the film is neutral, the electron transfer process must take place at the interphase between the metal electrode and the probe molecule, within the chiral film. Actually the redox peaks remain fully reversible on the film-coated electrode, albeit shifted to more positive

potentials, and the potential difference between forward and backward peaks significantly decreases. Both these features point to an electron-transfer process within the chiral film. This information implies that the latter differently affects, through diastereomeric interactions, the energetics of the electron-transfer process in both thermodynamic and kinetic terms.

Moreover, we verified that the impressive enantiodiscrimination effect exerted by the chirotopic electrode surface towards the antipodes of the probes is reversible. In fact, the probe-free film can be easily recovered by performing a few CV cycles around the first oxidation potential in a blank solution. This recovery enabled us to perform multiple subsequent enantio-recognition tests, alternating the (*S*) and (*R*) probes, on both the enantiomorphous surfaces starting from either enantiomer.

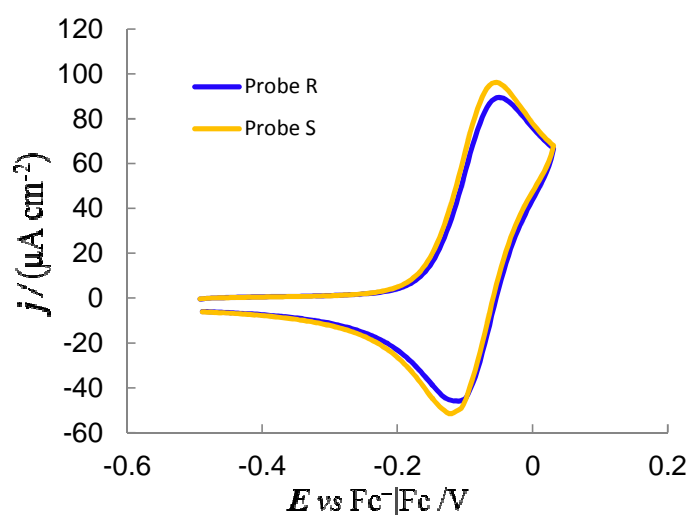


Figure 14. CV patterns of probe (*S*)-(yellow curve) and probe (*R*)-(blue curve) recorded on gold screen printed electrodes in BMIMPF₆ ionic liquid at 50 mVs⁻¹ scan rate

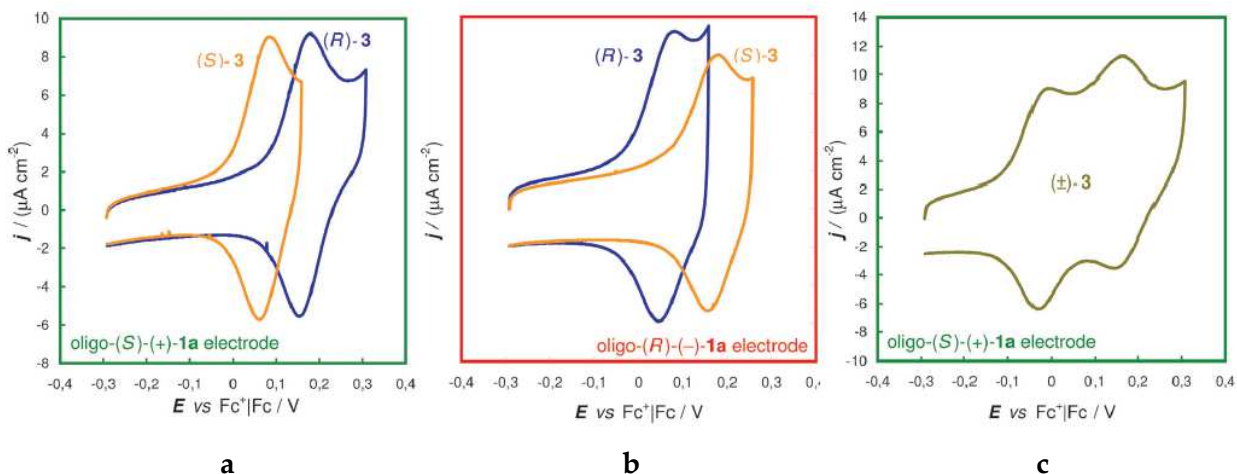


Figure 15. Enantioselective CV tests for the oligo-(S)-(+)-T₄BT₂ (a) and oligo-(R)-(-)-T₄BT₂ (b) film coated Au electrodes with (R)- and (S)-chiral redox probes (8 mM). c) Data also shown for the oligo-(S)-(+)-T₄BT₂ film coated Au electrode with the (±)-racemic redox probe. Potential scan rate: 50 mV s⁻¹

Very interesting is that these homochiral films were also able to discriminate at quantitative level mixture containing different enantiomeric excess (*ee*) of the two probe antipodes as depicted in Figure 16. Experiments were carried out on the oligo-(S)-(+)-T₄BT₂ in BMIMPF₆ ionic liquid by means of differential pulse voltammetry.

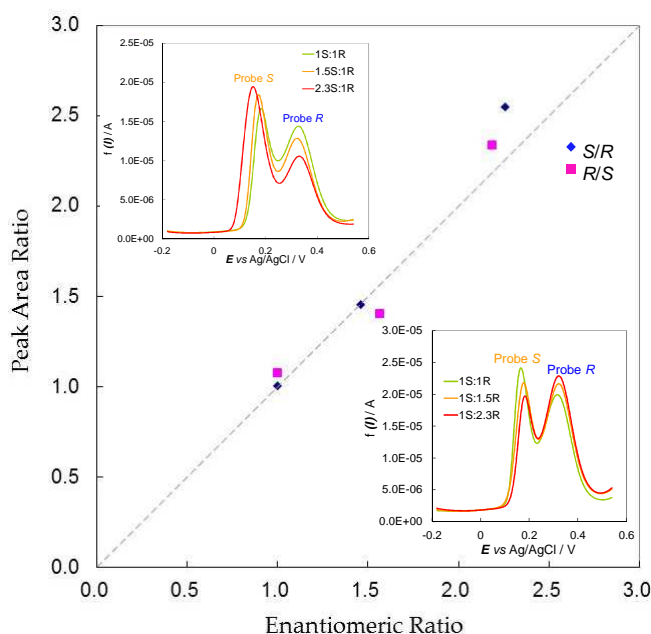


Figure 16. Probe enantiomeric excess study on (+)-T₄BT₂ homochiral films

The term enantiomeric excess was introduced in 1971 by Morrison and Mosher in their publication *Asymmetric Organic Reactions* [9]. It is a measurement of purity used for chiral substances [10] and reflects the degree to which a sample contains one enantiomer in greater amounts than the other. A racemic mixture has an *ee* of 0%, while a single completely pure enantiomer has an *ee* of 100%.

Enantiomeric excess is defined as the absolute difference between the mole fraction (*F*) of each enantiomer:

$$ee = |F_+ - F_-|$$

where

$$F_+ + F_- = 1$$

In practice, it is most often expressed as a percentage:

$$ee = ([\alpha]_{\text{obs}}/[\alpha]_{\text{max}}) \times 100$$

Enantiomeric excess is used as one of the indicators of the success of an asymmetric synthesis. For mixtures of diastereomers, there are analogous definitions and uses for diastereomeric excess and percent diastereomeric excess.

A non-racemic mixture of two enantiomers will have a net optical rotation. It is possible to determine the specific rotation of the mixture and, with knowledge of the specific rotation of the pure enantiomer, the optical purity can be determined [10].

$$\text{optical purity (\%)} = \frac{[\alpha]_{\text{observed}}}{[\alpha]_{\text{maximal}}} \times 100$$

Ideally, the contribution of each component of the mixture to the total optical rotation is directly proportional to its mole fraction, and as a result the numerical value of the optical purity is identical to the *ee*. This has led to informal use the two terms as interchangeable, especially because optical purity was the traditional way of measuring enantiomeric excess. However, other methods such as chiral column chromatography and NMR spectroscopy can now be used for measuring the amount of each enantiomer individually.

From Figure 16 is clear that the relationship between the peak area ratio and the enantiomeric ratio is linear taking into account six mixture of the probe antipodes.

It is a unique example in literature of homochiral surfaces able to discriminate chiral analytes through peak potential considering that other works regard enantio recognition in term of current. In the latter case is practically impossible to evaluate the enantiomeric purity of an antipode mixture. Moreover voltammetric techniques were used for the first time as a tool to estimate this parameter using disposable economical supports.

3.1.3 Enantio recognition Tests through Electrochemical Impedance Spectroscopy (EIS)

Before proceeding with the presentation of the enantio recognition results is useful to briefly introduce the model case of a conductive polymer studied by means of electrochemical impedance spectroscopy in order to better understand the subsequent data.

Study of conductive polymers by EIS: the model

A kinetic model for an electrode coated with a redox polymer layer in contact with a solution containing no redox couple has been proposed by Gabrielli *et al.* [11].

This model is schematically represented in Figure 17:

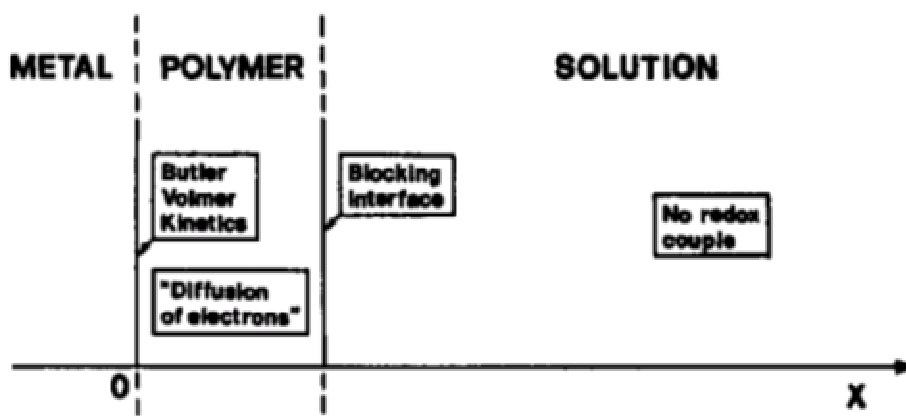


Figure 17. Scheme of hypothesis used for calculating the *ac* impedance of a redox polymer film in contact with a solution without a redox couple

This hypothesis can be described (in the absence of a redox couple in solution) with a Randles equivalent circuit in which the Z_w (Warburg impedance, corresponding to the mass transport in a semi-infinite diffusion) is replaced with Z_D , or a Warburg impedance for finite reflective boundaries; this can be simulated with two limit circuits, a Warburg impedance at higher frequencies and a capacitor at lower frequencies.

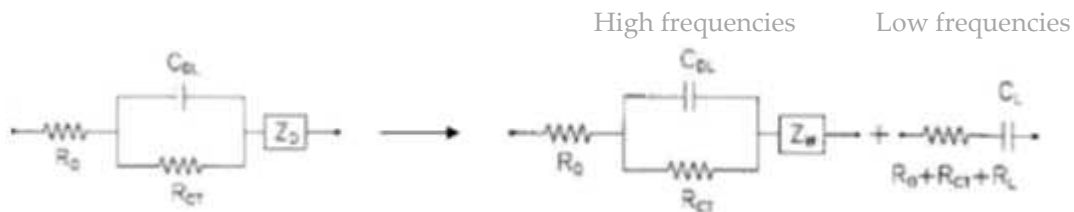


Figure 18. Modified Randles circuit (with limit cases) modeling the impedance of a conductive polymer

In such circuit, which corresponds to the Nyquist diagram in Figure 19, can model an electrochemical system including [12]:

- an electrode|polymer interphase that is related to a parallel between the capacitance C (in Figure 19 classified as 'capacity at high frequencies', C_{HF}) and the resistance R_{CT} (corresponding to the electron transfer which can be expressed in term of the classic Butler and Volmer equation). It corresponds to the semi-circle in Figure 19 whose diameter is the R_{CT} of the system, and the frequency at the maximum of $-Z''$ coordinate is equal to: $\omega = 1/(R_{CT}C)$.
- a polymer phase corresponding to a finite electron and ion diffusion layer, which is represented at mid-high frequencies by Warburg element (in Figure 19 the straight line with a slope of 45°) and at low frequencies by a capacity (defined 'capacity at low frequency' C_{LF} , proportional to the polymer thickness and to the redox center concentration) in series with a resistance (defined 'resistance of the polymer' R_p). These elements correspond to the vertical line at low frequencies in Figure 19. The projection on the real axis of this segment is described by the expression: $\Phi^2 / (3D_E C_{LF})$ where Φ is the film thickness D_E is the charge diffusion coefficient within the polymer.

- the uncompensated resistance of the electrolyte (R_E) is the small segment of the real axis between the origin and the beginning of the semicircle at the higher frequencies.

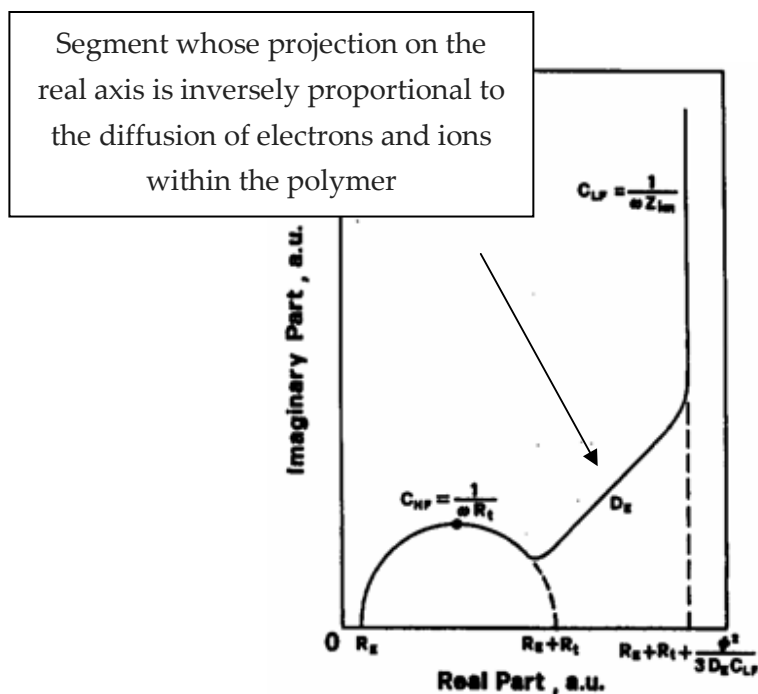


Figure 19. Typical *ac* impedance diagram (Nyquist plot) for a conductive polymer

In summary, the Nyquist diagram consists of three frequency domains:

1. at high frequencies a semicircle is observed due to the parallel combination of the charge transfer resistance of the redox process: $Q + e^- \rightarrow P$ and the capacity of the double layer at the metal|polymer interface.
2. the straight line of 45° at medium frequencies corresponds to the Warburg impedance that describes the charge transport within the film by electron diffusion.
3. at low frequencies the vertical line is attributable to the capacitive behavior.

Impedance of conducting polymers such as polypyrrole, polyaniline, polythiophenes and polycarbazoles gives a response similar to that of the redox polymers. For these systems, the capacitive behavior is observed at higher frequencies than the redox polymers; in fact conductive polymers promote a more rapid propagation of charge within their network.

The Warburg frequency domain can be more or less significant, depending on the nature of the polymer and on the applied potential.

Bode plots are represented in Figure 20:

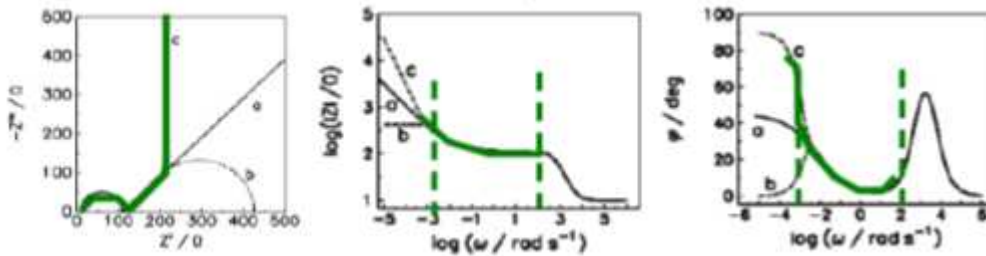


Figure 20. Bode magnitude (2) and Bode phase (3) plots correlated to the Nyquist diagram (1): case a: semi-infinite diffusion, case b: finite transmissive diffusion; case c: finite reflective diffusion.

The situation of interest is highlighted in green and corresponds to the c case

Enantiorecognition tests

The enantiorecognition test were carried out following the procedure described in chapter 2 at paragraph 2.2.5. Results obtained are depicted in Figure 21:

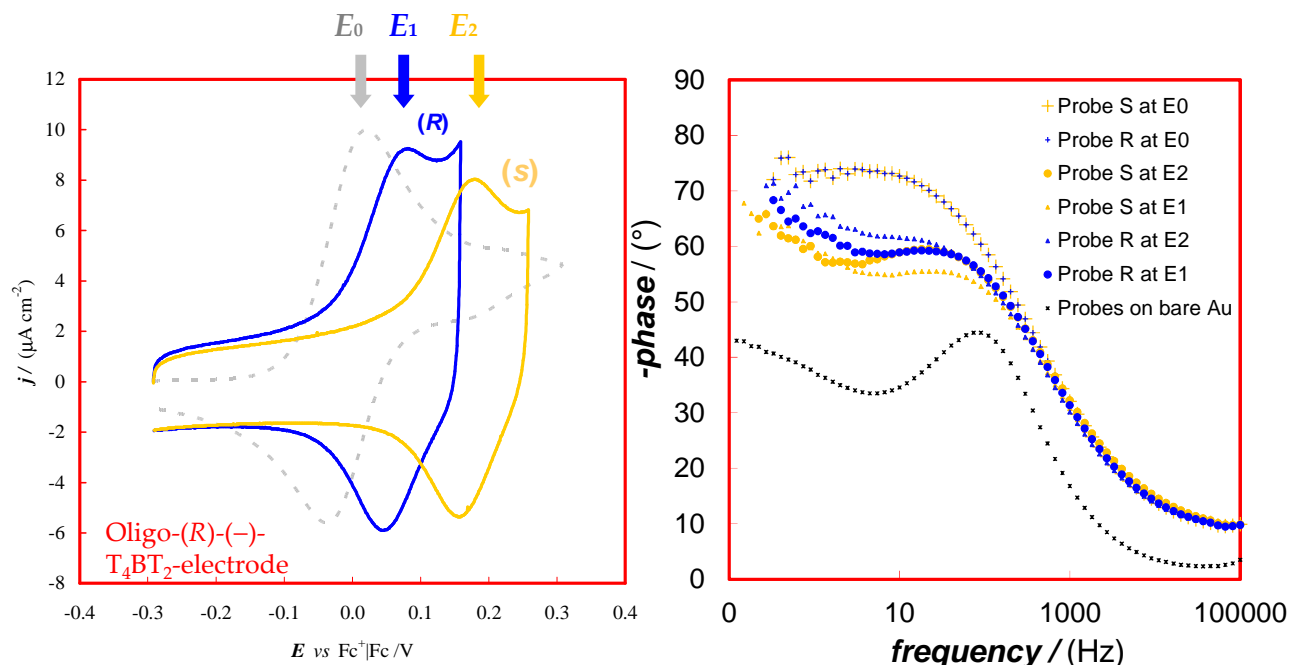


Figure 21. On the left: CV patterns recorded on electrode covered by (R)-(-)- T_4BT_2 film in presence of the ferrocene based probe enantiomers (blue and yellow lines) in BMIMPF₆.

For comparison probe signal on bare electrode is depicted (grey line) in BMIMPF₆.

On the right: Bode phase plots representative of enantiorecognition tests conducted on oligo-(R)-(-)- T_4BT_2 electrodes in the same conditions.

Spectra were recorded at different potential values named E_0 , E_1 , E_2 representative respectively of: the peak potential of chiral probes on bare electrode ($E_0 = 0.01 \text{ V vs Fc}^+/\text{Fc}$) and the peak potential of each probe enantiomer ($E_1 = 0.07 \text{ V vs Fc}^+/\text{Fc}$ V and $E_2 = 0.17 \text{ V vs Fc}^+/\text{Fc}$) recorded on electrode covered by T_4BT_2 homochiral films.

For comparison it is moreover indicated the spectra of (R) and (S) probes recorded on gold bare electrode.

Only Bode spectra are here reported because of higher significance and better comprehension respect to Nyquist plots. Measurements were conducted on screen printed cells endowed with fixed position of electrodes granting perfectly reproducible films, but this geometry has made difficult the interpretation of the Nyquist diagrams.

Results obtained from Bode plots have confirmed the enantiorecognition capability of T_4BT_2 homochiral films.

For Bode spectra recorded at E_0 value (Figure 21) on chiral electrode surfaces in presence of first (R) and then (S) probes the signals obtained are perfectly superimposable and display features depicted in Figure 20 in c case. In fact the E_0 value falls in the region where the film is neutral and redox probes are not yet active so films recall the situation of an electrode coated with a conductive polymer layer in contact with a solution containing no redox couple.

When spectra are recorded at E_1 and E_2 values (Figure 21) corresponding to the peak potentials of each probe enantiomer (*i.e.* in the region where each probe is active) it is interesting to note that they are perfectly superimposed notwithstanding plots have been recorded at different potential values. This means that both chiral probes are involved in a charge transfer process characterized by the same time constant.

This interpretation is also confirmed when Bode spectra are recorded on the same surface for each enantiomer at the other enantiomer's own potential (*i.e.* E_1 for probe S and E_2 for probe R); in this case the EIS diagram are not superimposable, consistently with the former assumptions.

For comparison in Figure 21 spectrum of chiral probes on bare electrode is represented. It resembles the theoretical behavior characterized by a charge transfer process at mid frequencies and by a Warburg behavior at low frequencies.

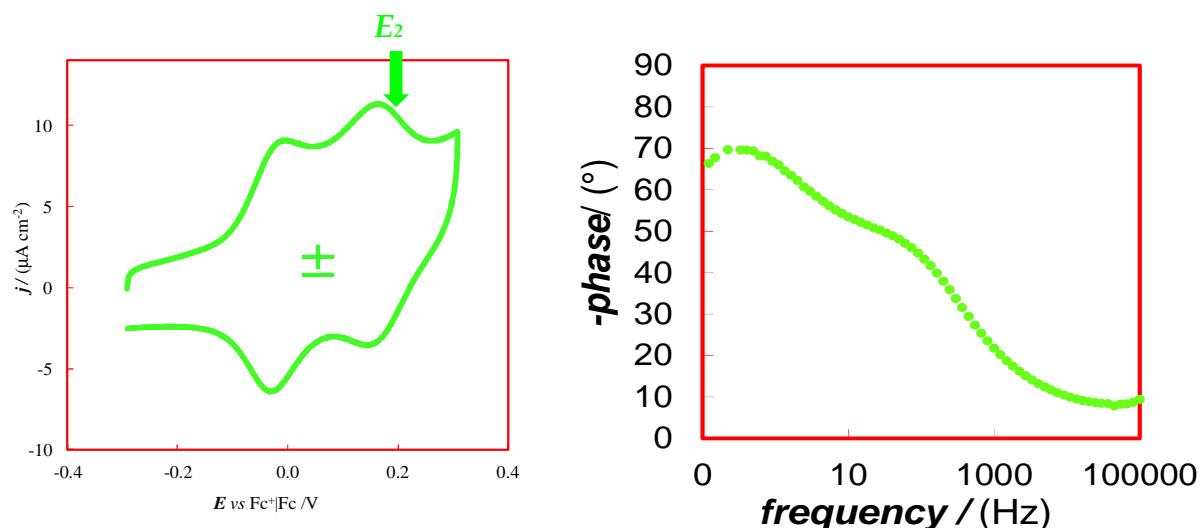


Figure 22. On the left: enantiorecognition tests on (R)-(-)-T₄BT₂ homochiral film in presence of racemic probe in BMIMPF₆. On the right: Bode plot recorded in the same conditions

Enantioselectivity tests were also carried out by means of EIS on the same (*R*)-(-)-T₄BT₂ homochiral surface in presence of a racemic mixture of chiral ferrocene based probes. In the Bode diagram in Figure 22 it is appreciable the presence of two phase peaks. The potential applied is the E_2 value necessary to activate both redox probes.

The first peak possibly corresponds to the favorite electron transfer process involving the (*R*) probe and the second one is related to (*S*) probe according to a higher time constant.

3.1.4. Confirming the Enantioselectivity Capability using Drugs

Considering the very good results obtained with the 'model' ferrocene-based chiral probe in term of both peak potential separation of the antipodes and impressive discrimination of enantiomeric excess mixtures, the next goal has been to verify whether the same films would display comparable enantioselectivity towards other probes of different bulkiness and/or active in potential windows where the film is charged.

To this aim it has been decided to focus the attention on electroactive probes of practical interest, such as pharmaceutical molecules. Electrodeposited oligo-(*R*)- and oligo-(*S*)-T₄BT₂ homochiral films were tested with two chiral drugs, namely DOPA (3,4-dihydroxy-phenylalanine) and ofloxacin. The amino acid-derivate DOPA is a drug generally employed for the treatment of Parkinson disease while ofloxacin is used in medicine for its antibiotic capacity.

Since neither of these molecules was appropriate for working in the optimal ionic liquid medium, it has been necessary to turn to conventional media and conventional electrodes (ACN being not compatible with the insulating paints adopted in commercial SPEs). This provided a further good test of general validity for the inherent chirality approach to enantioselectivity.

Thus, enantiodiscrimination tests were performed on 0.004 M solutions of (*L*)-DOPA and (*D*)-DOPA in acidic aqueous medium (H₂O + 0.05 M HCl), working on (*S*)- and (*R*)-T₄BT₂

films electrodeposited on conventional GC disk electrode from 0.0005 M solutions of the starting monomers in ACN + TBAPF₆ 0.1 M.

On the bare GC electrodes the DOPA first oxidation peaks, corresponding to a complex quinone-like redox process with a combination of electrochemical and chemical steps, were of course perfectly coincident for the two enantiomers (Figure 23, upper section). Instead an impressive discrimination was obtained on the same electrodes after functionalization with the inherently chiral oligomers (in spite of the less optimal medium and electrode support) with a distance of about 90 mV between the first enantiomer and the second one. Moreover as expected the enantiomer sequence and CV patterns were specular on the two enantiopure surfaces. (Figure 23).

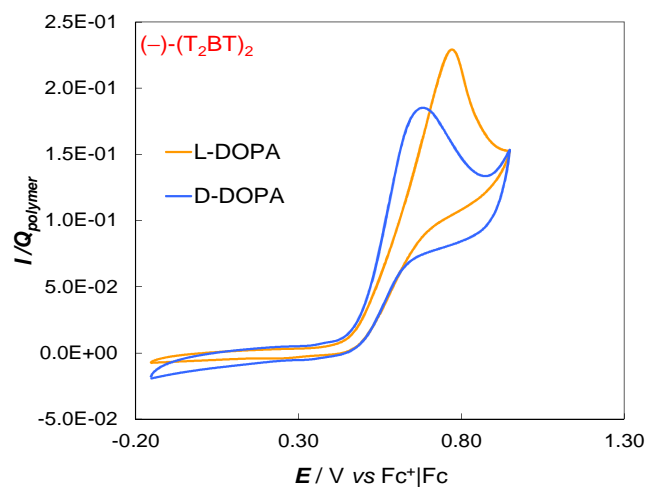
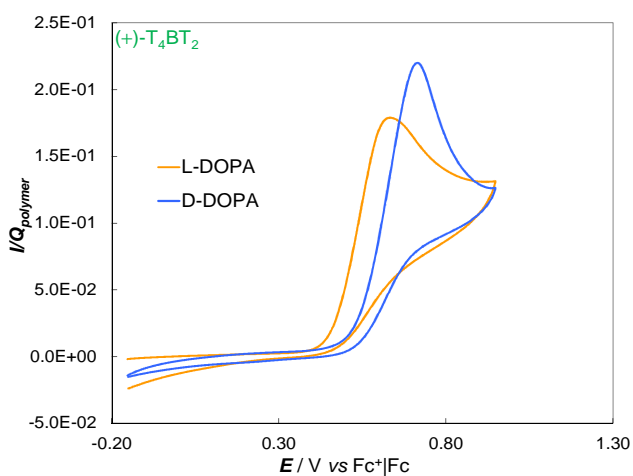
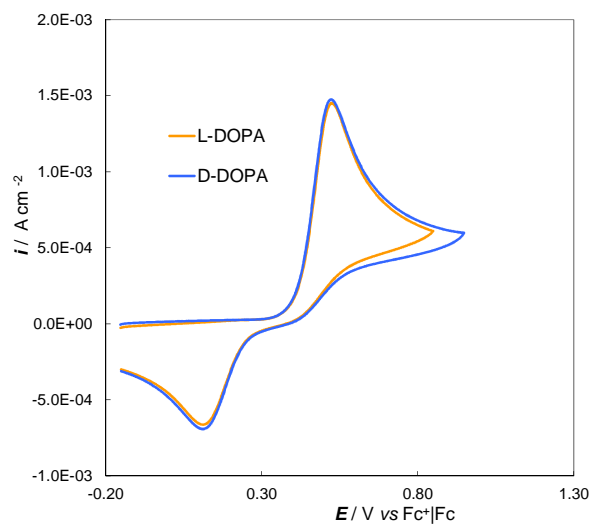
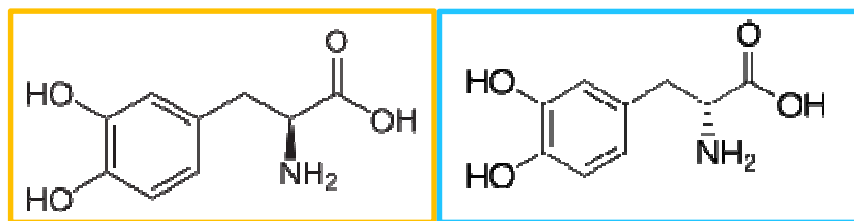


Figure 23. Spectral discrimination of (*D*)- and (*L*)-DOPA enantiomers (0.004 M in H₂O + 0.05 M HCl) on specular oligo-(*S*)- and oligo-(*R*)-T₄BT₂ electrode surfaces electrodeposited on GC disk electrode from ACN + TBAPF₆ 0.1 M

Enantioselectivity tests were also performed on ofloxacin enantiomer solutions, 0.0035 M for the *dextro* enantiomer and 0.0035–0.008 M for the more available (and less expensive)

levo one, in the same ACN + TBAPF₆ 0.1 M medium used in the chiral oligomer film electrodeposition (on GC disk support).

In such working conditions, the ofloxacin first oxidation peak is located at the onset of the oligomer oxidation (*i.e.* superimposed to polymer pattern). To overcome this 'problematic' condition implied to work at high probe concentrations, or to turn to DPV and/or to apply background subtraction to enhance the signal-to-background ratio. Again, however, a neat difference of about 80 mV is observed between the oxidation peak of a given enantiomer (here the *L*-ofloxacin, available at higher concentrations) on the (*S*) and (*R*) surfaces (Figures 24a and 24b, green *vs* red thick lines). Notwithstanding the low accessible concentration the separation of the 0.0035 M (*L*)- and (*D*)- enantiomers on the (*S*) surface can be observed, too, by background subtraction (Figure 24c).

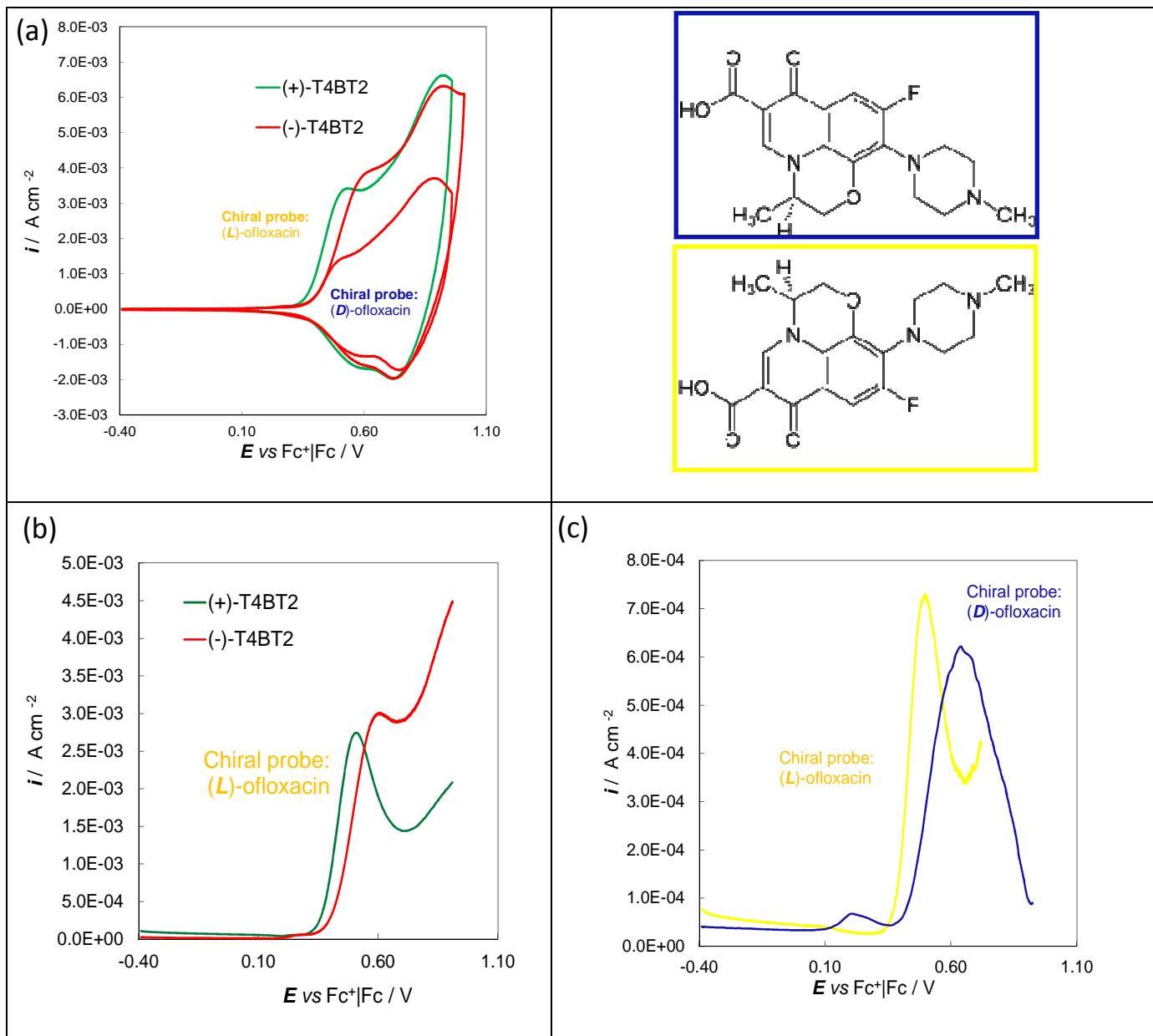


Figure 24. Discrimination of ofloxacin enantiomers on oligo-(*S*)- and oligo-(*R*)-T4BT₂ electrode surfaces electrodeposited on GC disk electrode, in ACN + 0.1 M TBAPF₆ medium. (a) CV and (b) Background-subtracted CV patterns recorded for 0.008 M *L*-ofloxacin on (*S*) and (*R*) electrodes (green and red thick lines) (c) Background-subtracted CV patterns for 0.0035 M *L*- and *D*-ofloxacin on a (*S*) electrode

Finally, some preliminary tests have also been devoted to quantitative analysis issues, particularly aiming to verify the existence of a linear dynamic range for peak currents recorded on the chiral oligomer surfaces.

For this purpose CV patterns were recorded on the oligo-(S)-T₄BT₂ surface with *L*-ofloxacin at increasing concentrations in ACN + 0.1 M TBAPF₆. In spite of the ofloxacin first oxidation peak being localized at the onset of the film oxidation, a regular increase of the CV peak current with analyte concentration can be observed, yielding a neatly linear calibration plot in a concentration range from 0.001 M to 0.01 M (Figure 25), thus confirming the linear response of the chiral surface, to be possibly exploited for quantitative analysis.

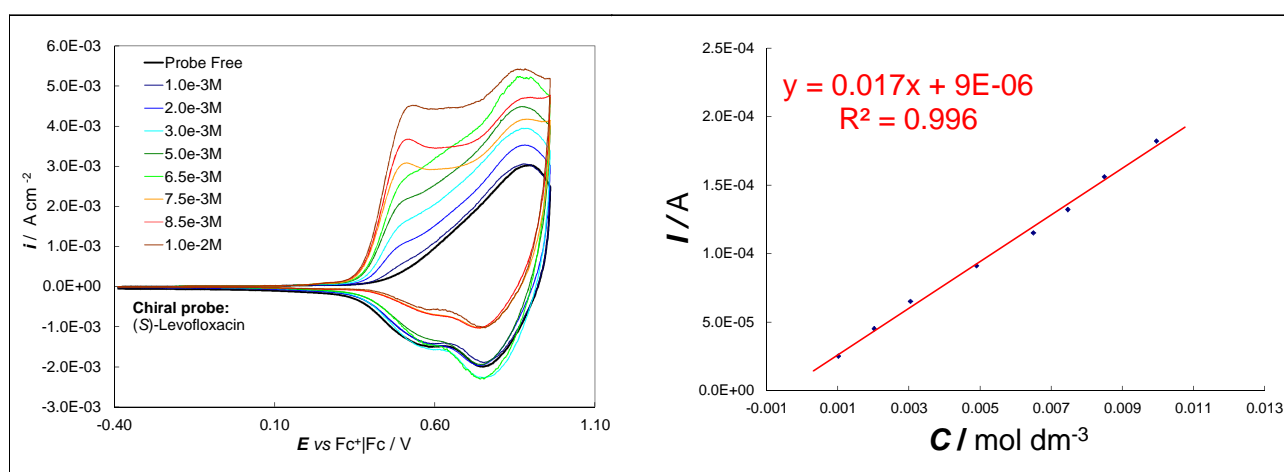


Figure 25. On the left: patterns of preliminary CV quantitative analysis tests on oligo-(S)-T₄BT₂ surface. On the right: CV linear dynamic range for *L*-ofloxacin antibiotic on oligo-(S)-T₄BT₂ electrodeposited on GC disk, in ACN + 0.1 M TBAPF₆

In conclusion the impressive enantiodiscrimination aptitude of oligo-T₄BT₂ inherently chiral surfaces affords neat separation of enantiomer voltammetry peaks of chiral probes of quite different chemical and electrochemical properties, and of quite different structural features. Moreover, such aptitude can be exploited, when necessary, in organic and aqueous media and on common electrode supports, besides the optimal combination of ionic liquid medium and screen printed electrodes. Finally, the peak currents recorded on the inherently chiral surfaces display a good linear dynamic range.

3.1.5 Confirming the Concept of Inherent Chirality Varying the Terminal Bi-thiophenic Units

As explained in the Introduction at paragraph 1.4.3, several monomers were synthesized in order to confirm the generality of the inherent chirality concept. In particular this section is dedicated to the description of the properties and features displayed by monomers obtained maintaining the bis-benzothiophene core but varying the chemical nature of the terminal bi-thiophenic units.

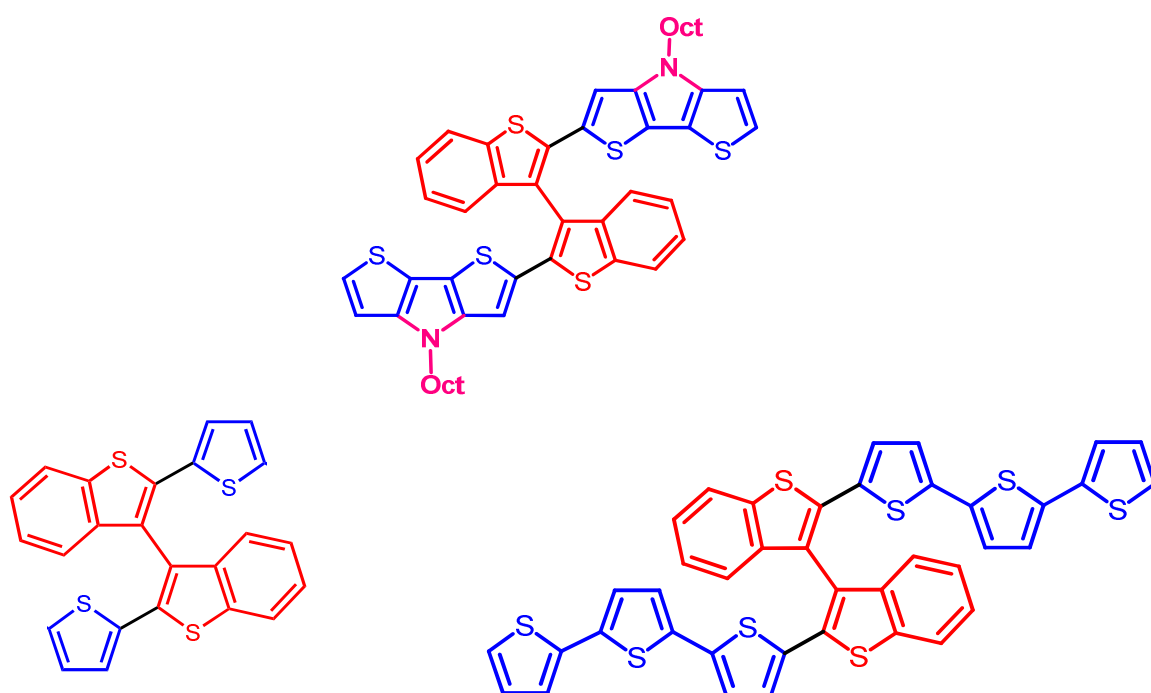
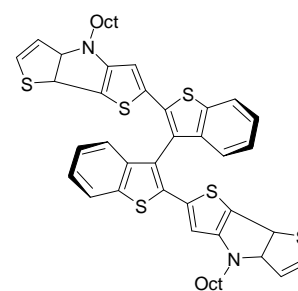


Figure 26. General structure of: BT₂DTP₂ upward, T₂BT₂ down on the left and T₆BT₂ down on the right

BT₂DTP₂ monomer

The BT₂DTP₂ monomer was well characterized in a previous PhD work some years ago [13]. However, in order to test its enantioselective recognition capability some experiments were repeated and extended with the obtainment of interesting results.

Each DTP nitrogen atom is substituted with an *n*-octyl group in



order to improve the solubility of the resulting polymer. The bithiophene side chains of the T₄BT₂ benchmark are closed with a nitrogen atom improving the whole system planarity and the electron donating ability.

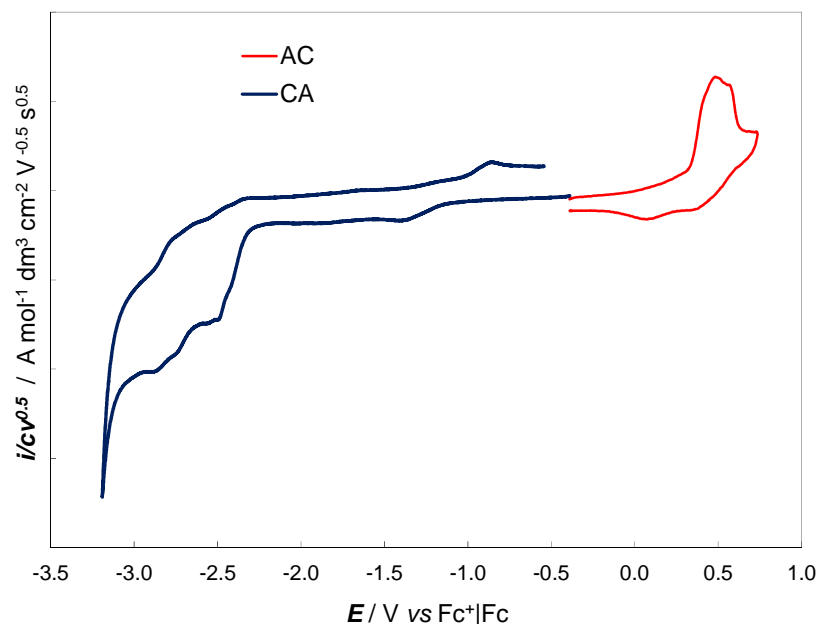


Figure 27. CV features of BT₂DTP₂ monomer ($5 \cdot 10^{-4}$ M) in ACN+TBAPF₆ 0.1 M, on GC electrode at 200 mV s⁻¹

The electrochemical characterization of the BT₂DTP₂ monomer (Figure 27) shows two nearly equivalent peaks, corresponding to the two active terminal units involved in the electrooxidative process, separated by the central node but still communicating through the conjugated system. The oxidation potential is less positive with respect to T₄-BT₂ monomer because of the presence of the electron-rich *N*-octyl dithienopyrrole groups and the higher conjugation efficiency due to the planarization. The distance between the two oxidation peaks is lower than in the T₄BT₂ system meaning that the two redox sites are less interacting. This would seem a contradiction with the higher conjugation of the system but it is probably attributable to a higher torsional angle between the two halves or to a higher attitude of the pyrrole system to localize positive charges.

Electrooligomerization took place fast and regular and resulting films were stable when tested in a monomer free solution (Figure 28). Furthermore widening the potential window in cathodic direction, a reduction peak can be observed, with immediate charge

release, that supports the hypothesis of the formation of an elastic and porous film (Figure 29).

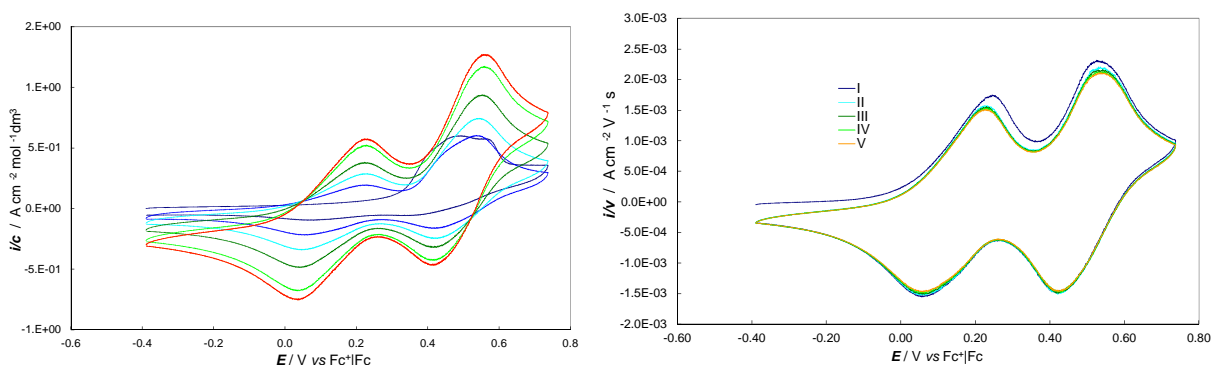


Figure 28. On the left: electrooligomerization, 36 cycles, of BT₂DTP₂ (5·10⁻⁴ M) in ACN+TBAPF₆ 0.1 M on GC electrode, $v=200$ mVs⁻¹; on the right: stability tests in a monomer-free solution

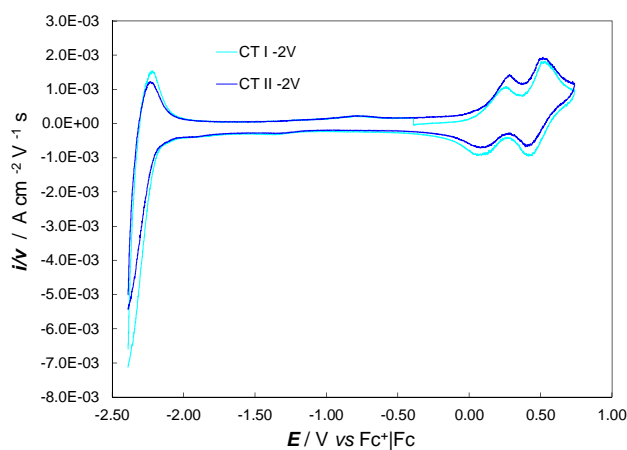


Figure 29. Charge trapping tests on BT₂DTP₂ film opening the potential window in negative direction; BT₂DTP₂ film were deposited in ACN + TBAPF₆ 0.1 M, 36 cycles, on GC electrode, at 200 mV s⁻¹

The enantiopure monomers were obtained by chromatographic separation on a chiral stationary phase, performed by Prof. R. Cirilli from Istituto Superiore di Sanità (Rome). The chiroptical properties of the enantiopure antipodes were evaluated by circular dichroism spectroscopy resulting in perfectly specular bisignate signals, as represented in Figure 30.

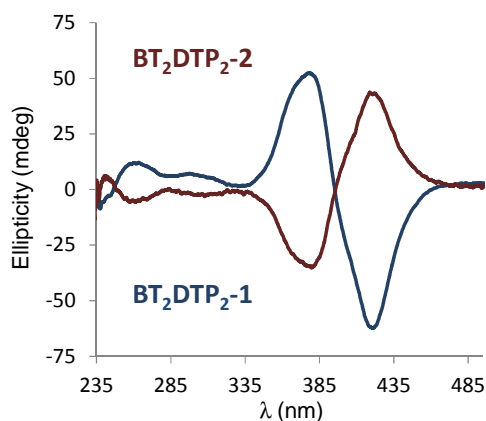


Figure 30. CD spectra (CHCl_3 , $c=0.14 \text{ mgcm}^{-3}$) of (*S*)-(-)- BT_2DTP_2 (blue) and (*R*)-(+)- BT_2DTP_2 (violet).

Very interesting is that BT_2DTP_2 enantiopure films emit circular polarized light (CPL) starting from a linear polarized light like a Fresnel apparatus (Figure 31).

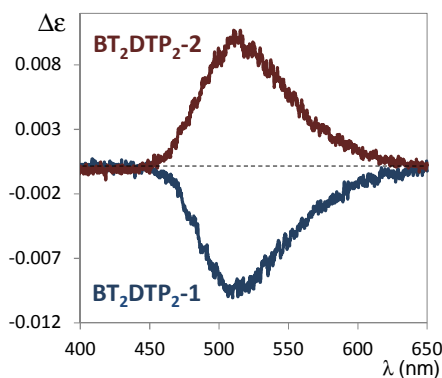


Figure 31. CPL of (*S*)-(-)- BT_2DTP_2 (blue) and (*R*)-(+)- BT_2DTP_2 (violet) in CHCl_3 :
 (*S*)-(-)- BT_2DTP_2 : $1.25 \times 10^{-4} \text{ M}$
 (*R*)-(+)- BT_2DTP_2 : $5.29 \times 10^{-5} \text{ M}$

Measurements of vibrational circular dichroism were performed by Prof. Giovanna Longhi, Università degli Studi di Brescia, dissolving the homochiral films in carbon tetrachloride (CCl_4). Perfectly specular and defined signals were obtained and as a consequence it was possible to assign the absolute configuration comparing the experimental VCD spectra with those calculated theoretically (Figure 32).

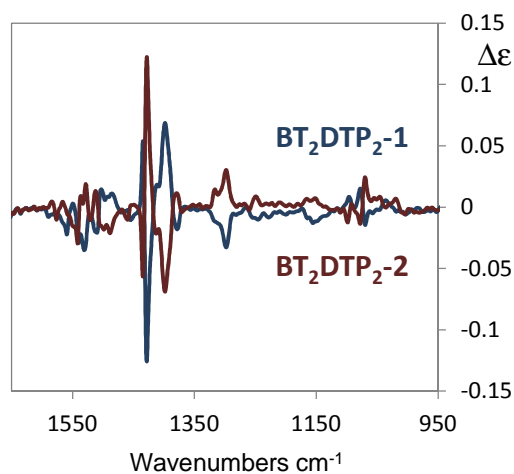


Figure 32. VCD spectra of (*S*)-(-)-BT₂DTP₂ (blue) and (*R*)-(+)-BT₂DTP₂ (violet) in CCl₄:
 (*S*)-(-)-BT₂DTP₂: 0.11 M
 (*R*)-(+)-BT₂DTP₂ 0.09 M

Enantioselective tests were carried out electrodepositing the enantiopure monomers on GC electrode in ACN as solvents (72 cycles, 50 mV s⁻¹) due to the scarce attitude of these materials to electrooligomerize in BMIMPF₆.

For tests pure ionic liquids and ACN + TBAPF₆ 0.1 M were used in presence of ferrocene based chiral probes.

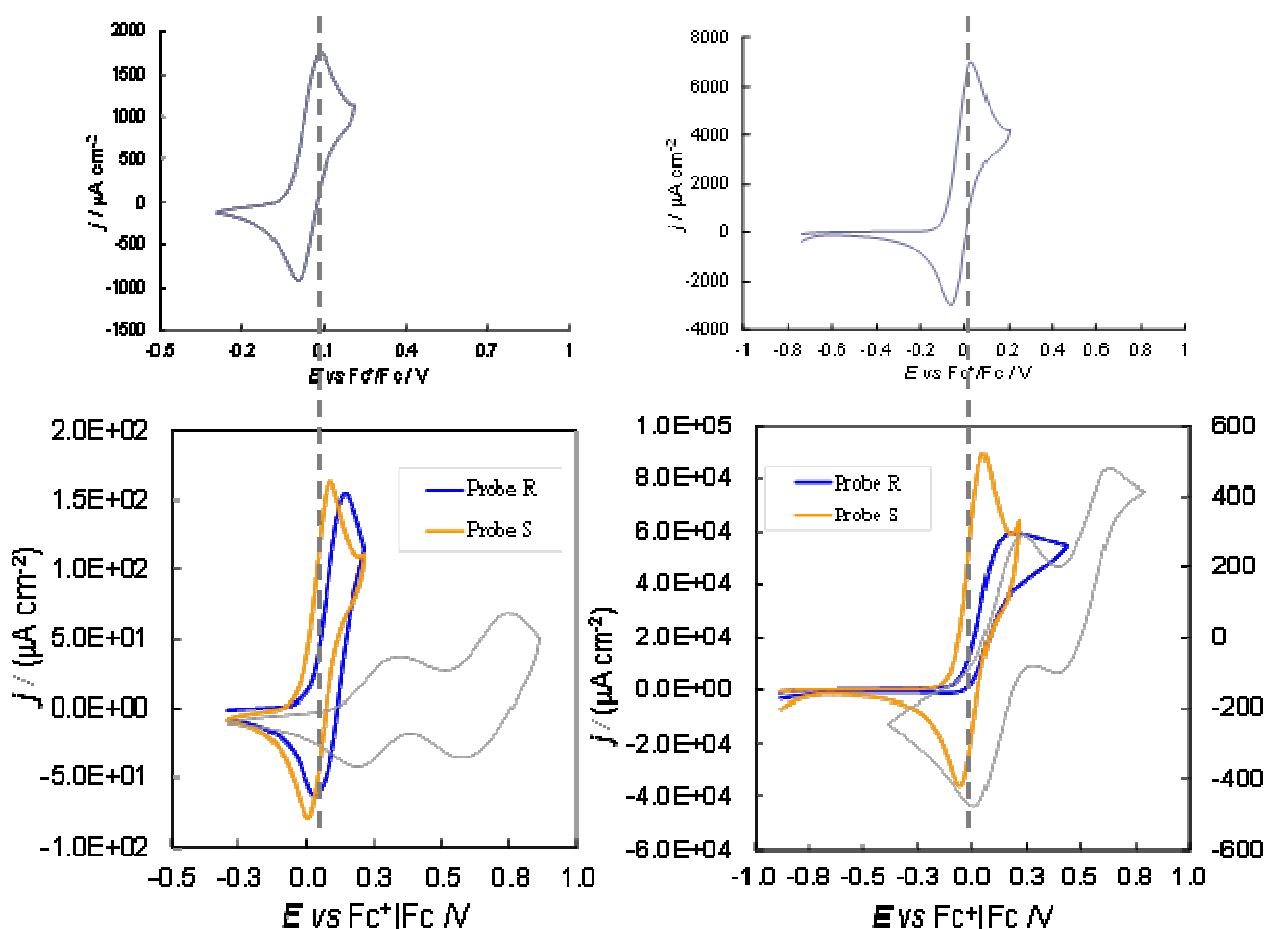


Figure 33. Above: CV patterns of ferrocene based chiral probes recorded on GC bare electrode in BMIMPF₆ (on the left) and in ACN + TBAPF₆ 0.1 M (on the right).

Below: Enantiorecognition tests on (R)-(+)-BT₂DTP₂ in presence of ferrocene based chiral probes on GC electrode. On the left: tests in BMIMPF₆, on the right: tests in ACN + TBAPF₆ 0.1 M.

For comparison CV pattern of the stabilized oligomer film is reported (grey line).

The BT₂DTP₂ chiral surfaces displayed a good enantiorecognition capability especially when enantiopure films were tested in ACN + TBAPF₆ 0.1 M (Figure 33). In the case of BMIMPF₆ the peak separation between the two chiral probes is about 0.049 V; possibly the BT₂DTP₂ films are not very stable in the ionic liquid. Ferrocene signals remain electrochemically and chemically reversible and the mechanism point to a diffusive process, peak values fall in the region where the oligomer is partially charged (at the onset of the film, especially for the R probe), this suggests that the chiral probes could react directly on the film surface, besides within the film (as in the case of T₄BT₂ chiral electrodes when tests were conducted in ionic liquid). On the other hand, when homochiral films

were tested in ACN + TBAPF₆ 0.1 M a separation between the probe enantiomers of about 0.16 V was observed. The mechanism changes completely, with different patterns for the two enantiomers, and probe (*R*) losing the electrochemical and chemical reversibility [14]. The completely different CV pattern of the probe (*R*) is probably due to the position of the probe peak that nearly coincides with the onset of oligomer oxidation.

T₂BT₂ monomer

The synthesis of T₂BT₂ monomer as a racemate is similar to that used in the case of T₄BT₂ molecule.

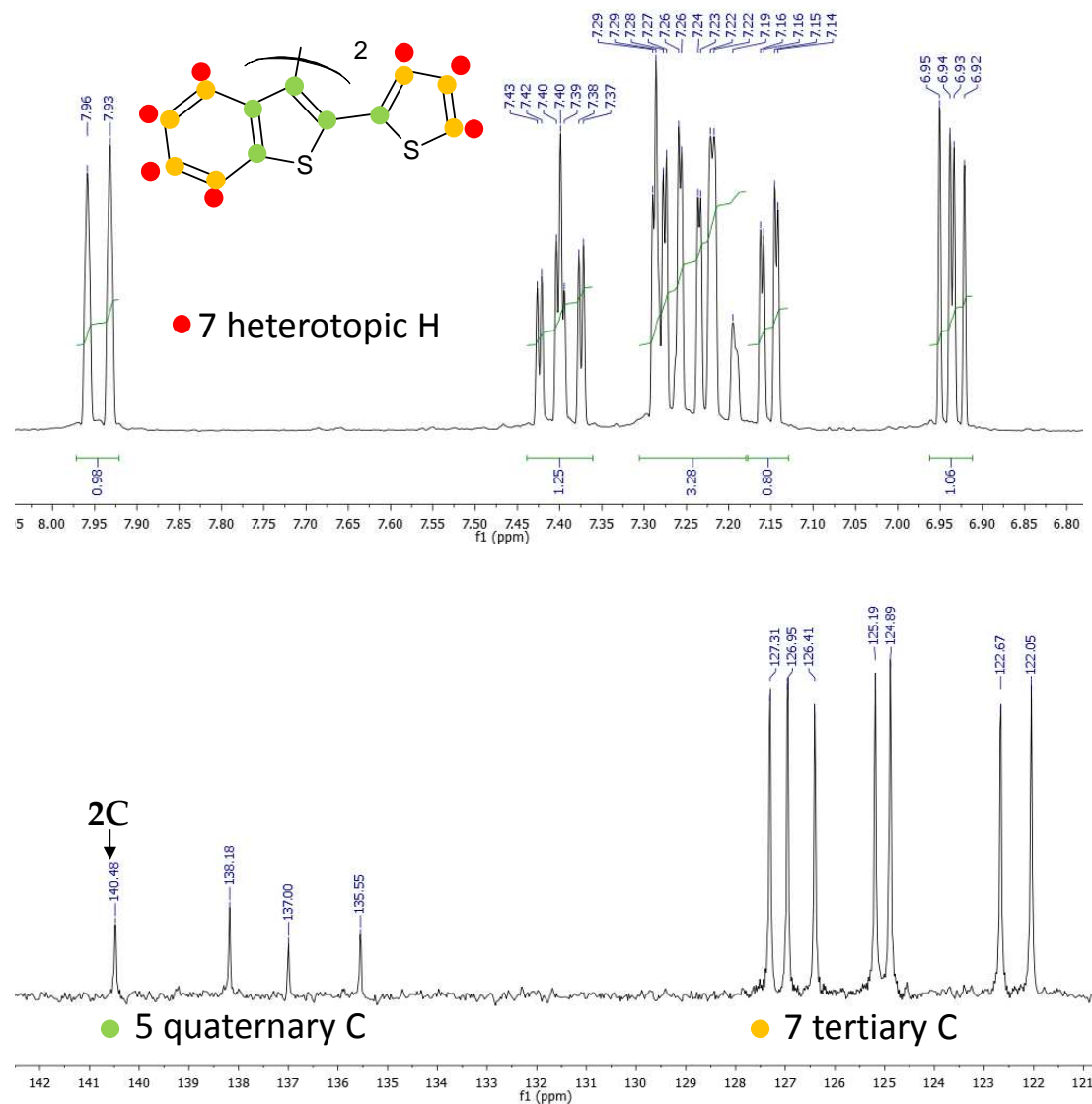


Figure 34. ¹H NMR (above) and proton decoupled ¹³C NMR (below) spectra of T₂BT₂ monomer in CHCl₃

The chemical structure of T₂BT₂ monomer was confirmed by ¹H NMR and proton decoupled ¹³C NMR spectra depicted in Figure 34. In ¹H NMR spectrum there are two doublets and two triplets related to the benzothianaphthenic unit and two doublets and one triplets attributable to the protons of the thiophenic unit. This interpretation was corroborated by the ¹³C NMR spectra.

CV features of the monomer were recorded in CH_2Cl_2 and ACN in order to evaluate the solvent effect. In both cases the HOMO LUMO gap is larger than with T_4BT_2 molecule, on account on the overall lower conjugation efficiency of the system, having thiophene rather than bithiophene side units. Moreover, unlike the T_4BT_2 case, a single oxidation peak is observed not only in ACN, but also in more apolar CH_2Cl_2 pointing to poorer interaction between the two equivalent redox centers. The presence of reduction peaks related to lateral thiophenic units is only perceivable when acetonitrile is used. (Figure 35).

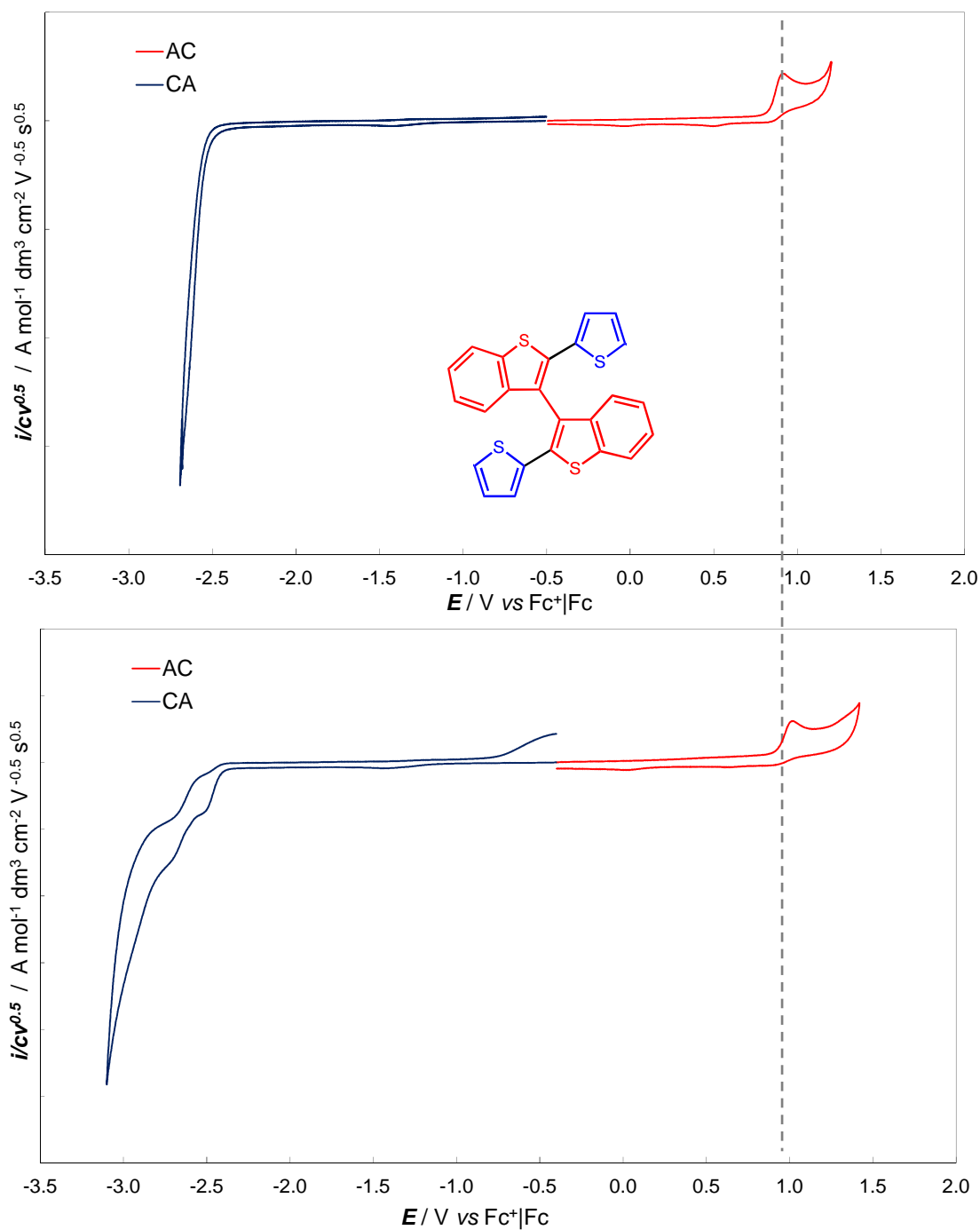


Figure 35. CV features of T₂BT₂ monomer ($5 \cdot 10^{-4}$ M) recorded on GC electrode at $200 mV s^{-1}$ in $CH_2Cl_2 + TBAPF_6$ 0.1 M (above) and in $ACN + TBAPF_6$ 0.1 M (below)

Electrochemical oligomerization did not take place neither in traditional solvents nor in the $BMIMPF_6$. Instead the chemical oxidation with $FeCl_3$ generated a mixture of oligomers (in particular dimers and trimers in the extracted fraction with tetrahydrofuran).

T₆BT₂ monomer

The synthesis of T₆BT₂ monomer as a racemate is similar to that used in the case of T₄BT₂ molecule.

As in the previous case ¹H NMR experiments were carried out in CHCl₃ (Figure 36).

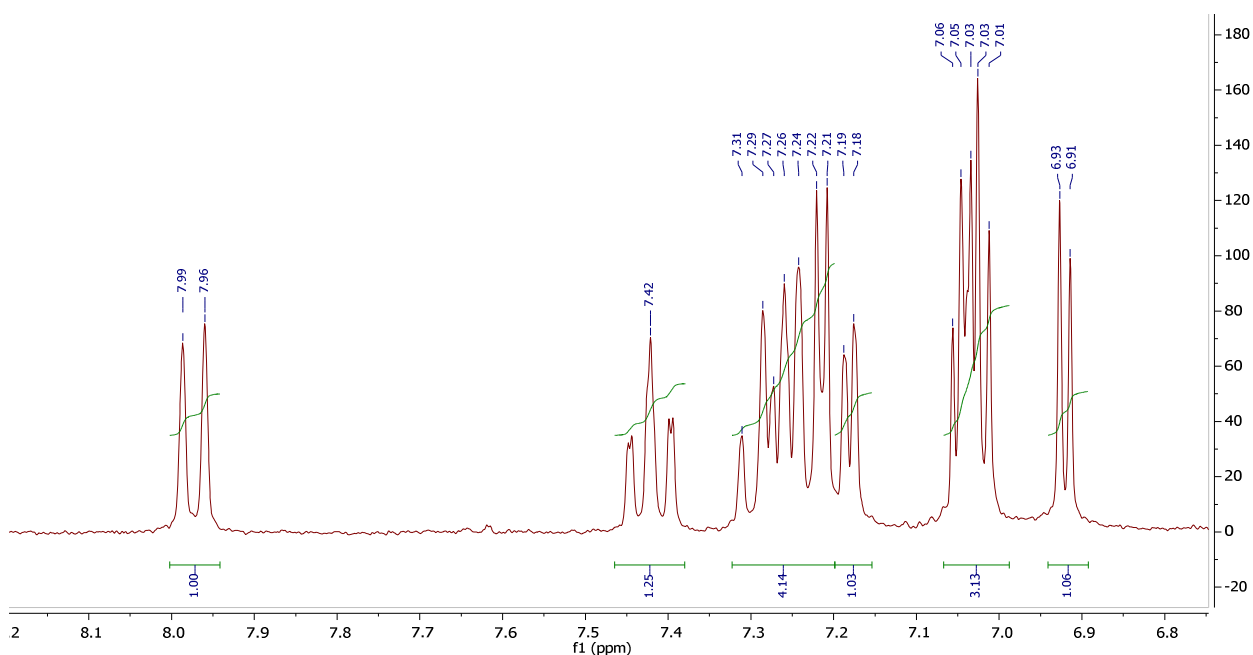
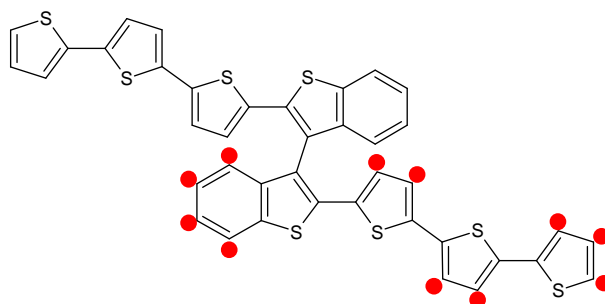


Figure 36. ¹H NMR spectra of T₆BT₂ monomer in CHCl₃

The spectra confirms the presence of eleven constitutionally heterotopic protons. In particular: *i*) two doublets and two triplets relative to the thianaphthenic unit *ii*) and six doublets and one triplet attributable to the protons on the lateral thiophenic chains.

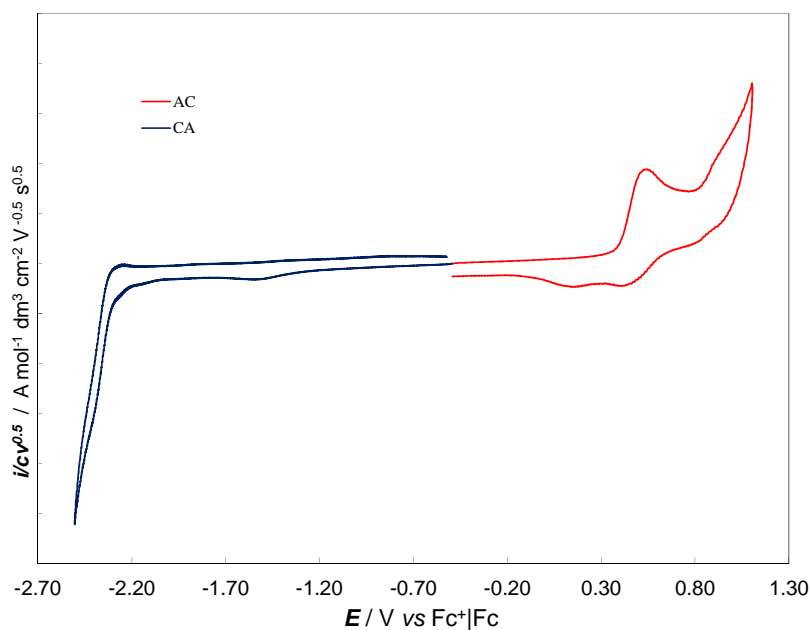


Figure 37. CV features of T₆BT₂ monomer (5·10⁻⁴ M) recorded on GC electrode at 200 mV s⁻¹ in CH₂Cl₂+TBAPF₆ 0.1 M

The electrochemical characterization of T₆BT₂ shows a narrower HOMO-LUMO gap than T₄BT₂, with both first oxidation and first reduction taking place at more advantageous potentials (so that the reduction process becomes visible even in CH₂Cl₂) on account of the improved conjugation. Besides the first oxidation peak, which, according to its broad shape, could correspond to the merging oxidation peaks of the two equivalent moieties only slightly interacting, a second oxidation process can be observed, which could be consistent with the longer conjugated chains in the two moieties (Figure 37).

T₆BT₂ monomer shows fast, regular and virtually unlimited electrooligomerization; resulting films are very stable upon repeated potential scan cycles in a monomer-free solution and display a significant charge trapping effect when opening the potential window in the negative direction (Figure 38).

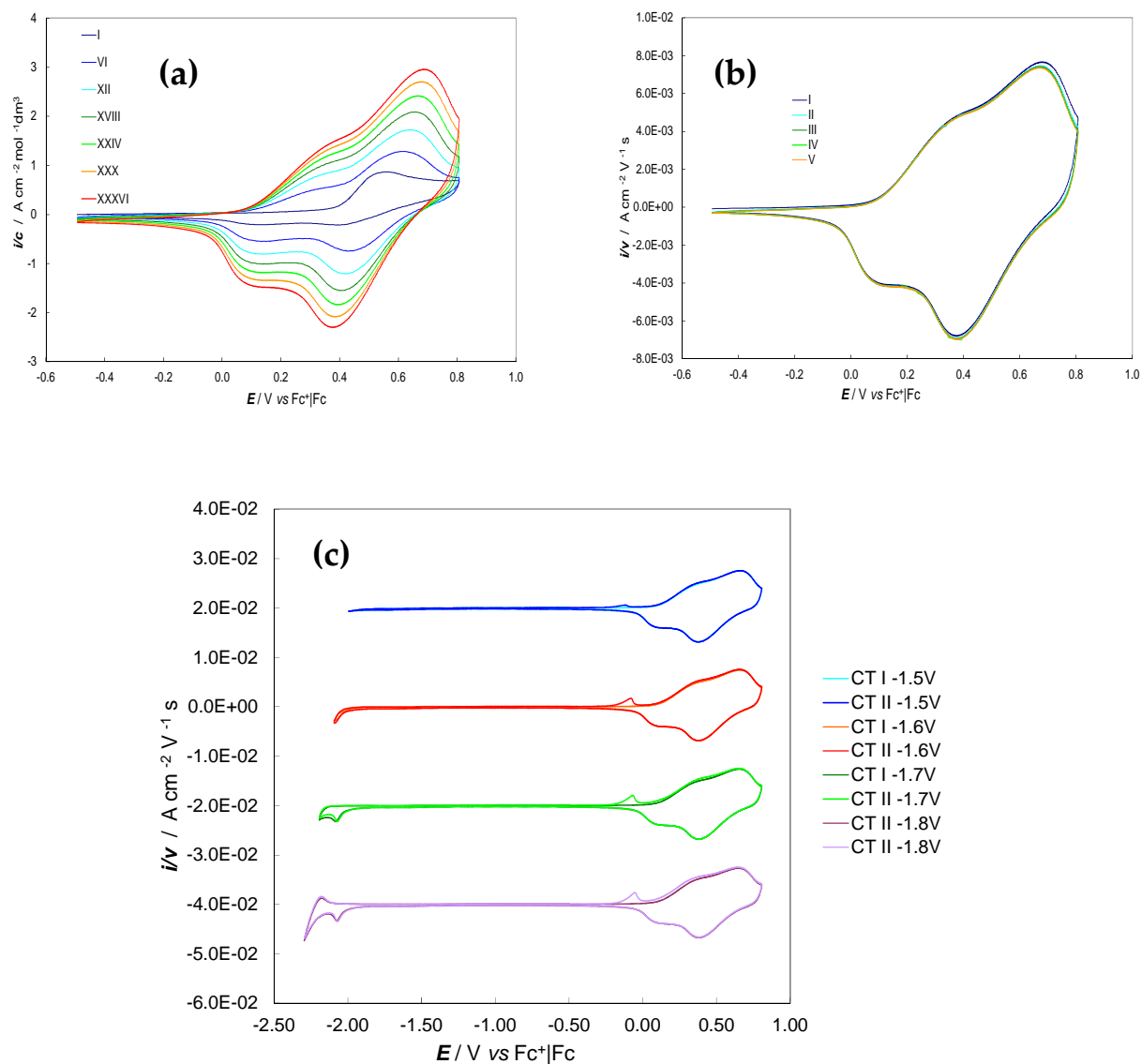


Figure 38. Voltammetric features of T_6BT_2 , on a GC electrode, scan rate 200 mV s^{-1} ,
 a) electrooligomerization, 36 cycles, $[\text{T}_6\text{BT}_2] = 5 \cdot 10^{-4} \text{ M}$ in $\text{CH}_2\text{Cl}_2 + \text{TBAPF}_6 0.1 \text{ M}$
 b) stability test in a monomer free solution
 c) charge trapping effect recorded at different cathodic potentials in a monomer free solution

Separation of T₆BT₂ racemate into enantiomers was performed by Prof. Roberto Cirilli (Figure 39), but they were recovered in small quantities due to difficulties correlated to the separation procedure. However a new method is under study.

The antipode display impressive specific rotation values, higher than that recorded for T₄BT₂ monomer according to the increase in the effective conjugation:

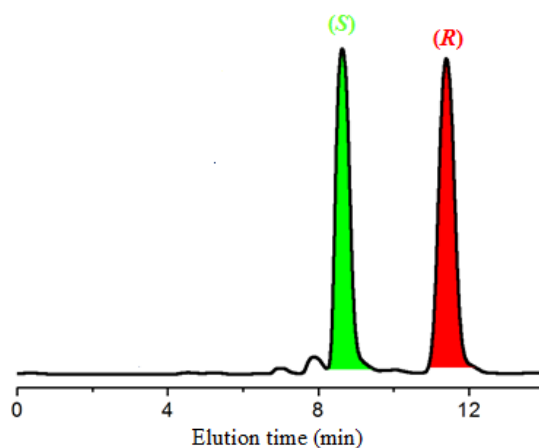


Figure 39. Semipreparative enantioseparation of T₆BT₂.
 CSP: Chiralpak IB 250 mm x 4.6 mm LD
 Eluent: *n*-hexane-dichloromethane-ethanol 90.1:10

T₆BT₂-1: $[\alpha]_{D^{25}}(\text{CHCl}_3) = +1581$

T₄BT₂-1: $[\alpha]_{D^{25}}(\text{CHCl}_3) = +1001$

T₆BT₂-2: $[\alpha]_{D^{25}}(\text{CHCl}_3) = -1368$

vs

T₄BT₂-2: $[\alpha]_{D^{25}}(\text{CHCl}_3) = -991$

Very useful is the comparison between the two just described racemic monomers (T₂BT₂ and T₆BT₂) with the racemic benchmark T₄BT₂. They have in common the same bis-benzothiophene scaffold but differ for the length of the lateral thiophenic chains.

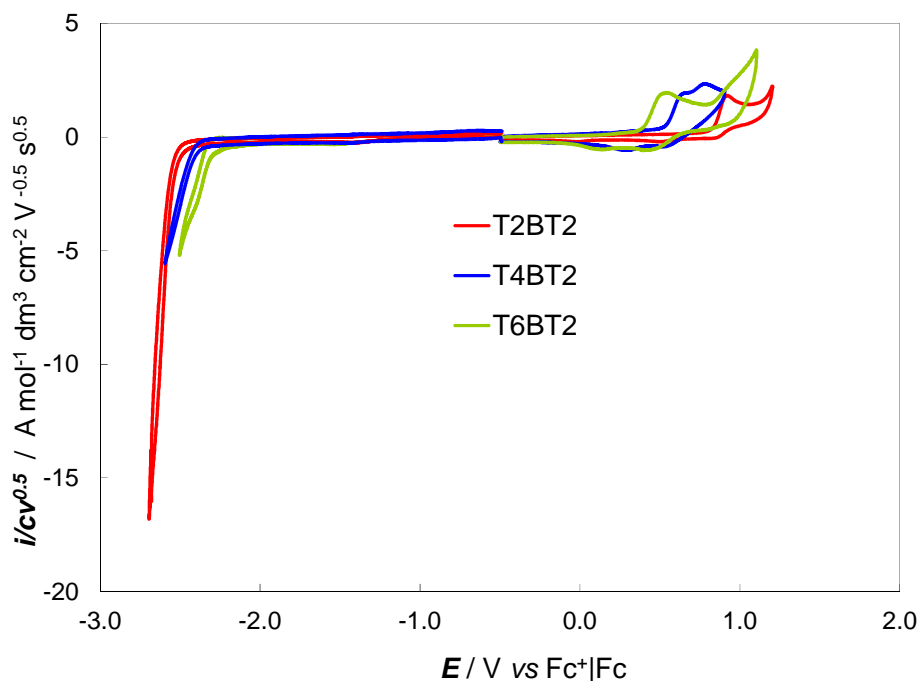


Figure 40. Synopsis of CV patterns of racemic T₂BT₂, T₄BT₂ and T₆BT₂ recorded on GC electrode in CH₂Cl₂ + TBAPF₆ 0.1 M at 200 mV s⁻¹. Monomer concentration: 5·10⁻⁴ M

From Figure 40 it is clear that the effective conjugation of systems increases in the order:

$$T_2BT_2 < T_4BT_2 < T_6BT_2$$

in fact first oxidation and reduction peak potential values of the monomers become less and less extreme in the same order. This corresponds to a decrease in HOMO-LUMO gaps (calculated electrochemically with the onset criterion) for increasingly more conjugated structures (table below).

<i>Onset criterion</i>	$E_{p,a \text{ onset}}$ V/Fc ⁺ Fc	$E_{p,c \text{ onset}}$ V/ Fc ⁺ Fc	$E_{\text{gap max}}$ V	HOMO eV	LUMO eV
T ₂ BT ₂	0.88	-2.53	3.41	-5.23	-1.87
T ₄ BT ₂	0.49	-2.43	2.92	-4.88	-1.96
T ₆ BT ₂	0.32	-2.30	2.62	-4.71	-2.09

In figure 41 T₆BT₂ monomer is also compared with the benchmark T₄BT₂ by means of *UV-vis* spectroscopy.

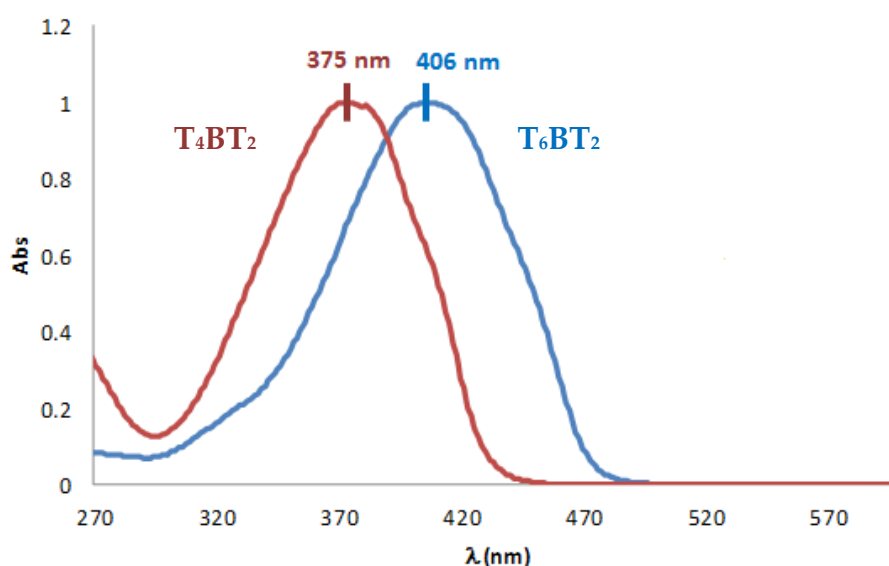


Figure 41. *UV-vis* spectra of T₆BT₂ and T₄BT₂ monomers recorded in CHCl₃

T₆BT₂ *UV-vis* spectrum displays a remarkable bathochromic shift of 29 nm (Figure 41) respect to the T₄BT₂ molecule (*i.e.* conjugation extent increases).

The impressive proprieties showed by racemic T₆BT₂ both as monomer and as oligomer have suggested to compare T₆BT₂ oligomer with the poly(3-hexylthiophene-2,5-diyl), P3HT, a common expensive donor used in bulk heterojunction solar cells.

The first comparison has been done by means of cyclic voltammetry.

Tests were carried out by preparing a solution of P3HT in CH₂Cl₂ + TBAPF₆ 0.1 M subsequently dropcasted on GC electrode. Films were stabilized in a monomer free solution and compared in terms of HOMO values with the last stability cycle of T₆BT₂ oligomer performed in the same conditions (Figure 42). The synthesized oligomer appeared competitive in terms of HOMO value with the P3HT, but not in terms of LUMO one.

In any case in cooperation with Istituto ENI Donegani (Novara) some tests were conducted using T₆BT₂ oligomer as a donor in a bulk-heterojunction solar cell.

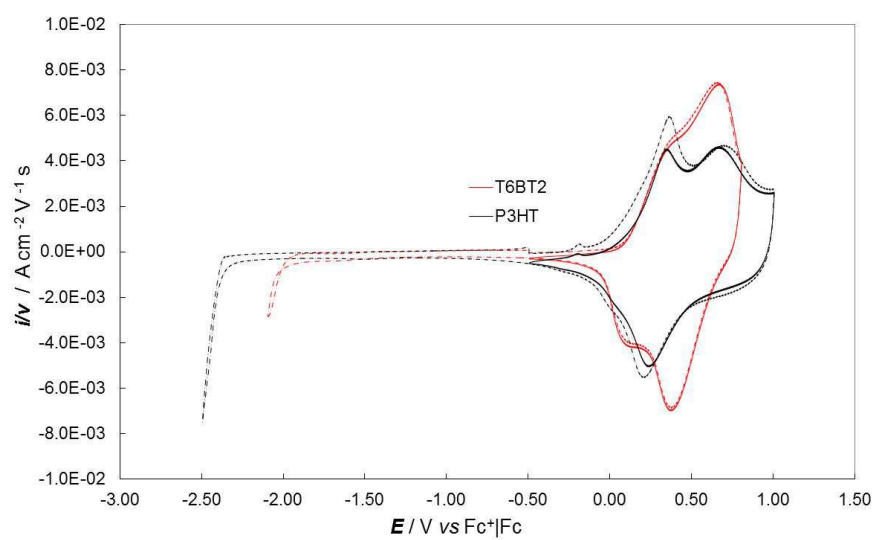


Figure 42. Comparison between the CV patterns of T₆BT₂ oligomer (red line) and P3HT (black line) recorded in CH₂Cl₂ + TBAPF₆ 0.1 M on GC electrode at 200 mVs⁻¹

Organic Photovoltaic devices

An organic solar cell or plastic solar cell is a type of polymer solar cell that uses organic electronics, a branch of electronics that deals with conductive organic polymers or small organic molecules, [15] for light absorption and charge transport to produce electricity from sunlight by the photovoltaic effect.

The plastic used in organic solar cells has low production costs in high volumes. Combined with the flexibility of organic molecules, organic solar cells are potentially cost-effective for photovoltaic applications. Molecular engineering (*e.g.* changing the length and functional group of polymers) affords to modulate the energy gaps and levels of the molecular materials constituting the device, and therefore the device performance. The optical absorption coefficient of organic molecules is high, so a large amount of light can be absorbed with a small amount of materials. The main disadvantages associated with organic photovoltaic cells are low efficiency, low stability and low strength compared to inorganic photovoltaic cells.

In bulk heterojunction cells, the electron donor and acceptor are mixed, forming a polymer blend. If the length scale of the blend is similar to the exciton diffusion length, most of the excitons generated in either material may reach the interface, where excitons split efficiently. Electrons move to the acceptor domains then were carried through the device and collected by one electrode, and holes move in the opposite direction and collected at the other side [16][17][18].

Most bulk heterojunction cells use two components, although three-component cells have been explored. The third component, a secondary p-type donor polymer, acts to absorb light in a different region of the solar spectrum. This in theory increases the amount of

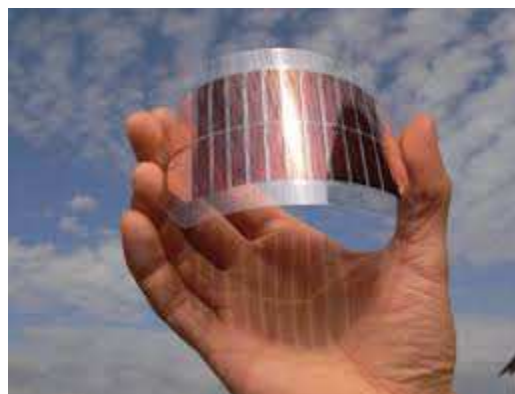


Figure 43. An example of an organic photovoltaic device

absorbed light. These ternary cells operate through one of three distinct mechanisms: charge transfer, energy transfer or parallel-linkage.

In charge transfer, both donors contribute directly to the generation of free charge carriers. Holes pass through only one donor domain before collection at the anode. In energy transfer, only one donor contributes to the production of holes. The second donor acts solely to absorb light, transferring extra energy to the first donor material. In parallel linkage, both donors produce excitons independently, which then migrate to their respective donor/acceptor interfaces and dissociate [19].

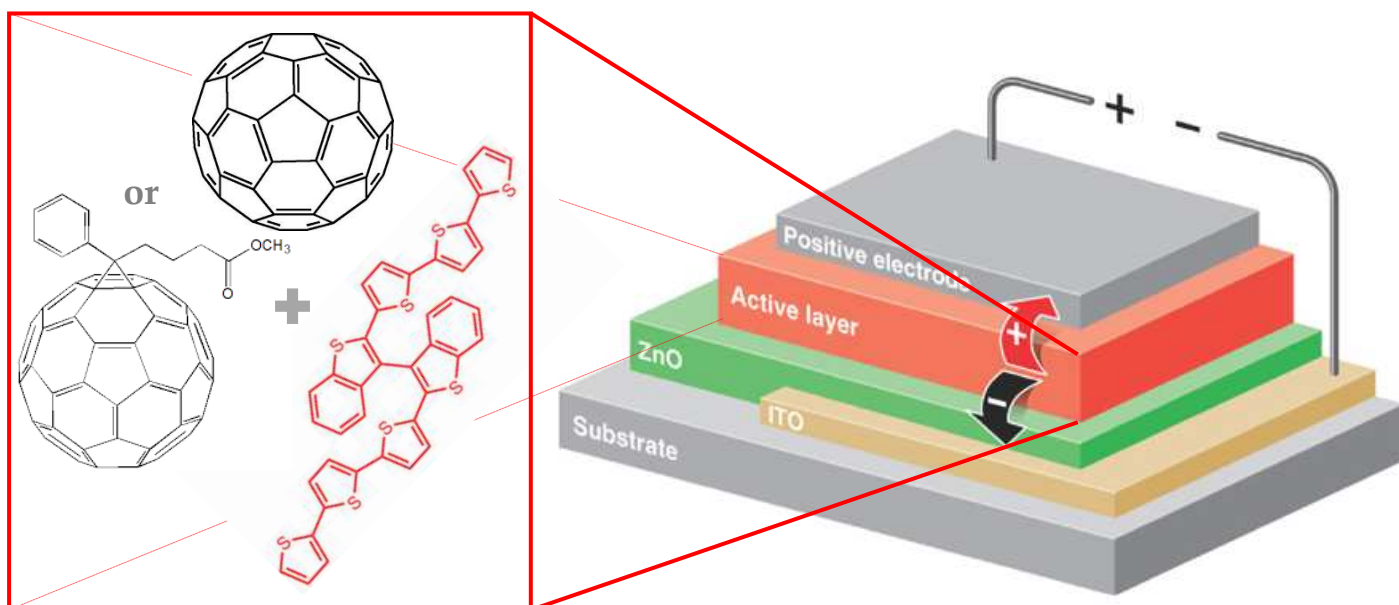


Figure 44. Inverted geometry of a bulk-heterojunction solar cell: the active layer is constituted by a blend of fullerene (C₆₀) or phenyl-C₆₁-butyric acid methyl ester (PCBM) with T₆BT₂ oligomer

Solar cell tests were performed by Istituto ENI Donegani (Novara), using two different acceptors: fullerene (C60) and phenyl-C61-butyric acid methyl ester (PCBM), in both cases blended with T₆BT₂ oligomers. All components have been dissolved in *ortho*-dichlorobenzene in concentration of 20 mg cm⁻³. The active layer was deposited on the support by a spincoater with a speed of 1000 rpm/ 90". The donor *vs* acceptor ratio was 1:1. Six cells have been prepared (two substrates for three devices) for each set of conditions. All results were compared with the model system in which P3HT:PCBM is used as active layer.

The employed inverted architecture was the following: Glass/ ITO/ ZnO/ Active Layer/ MoO₃/ Ag (Figure 45). The dispositive has not been subjected to any heat treatment.

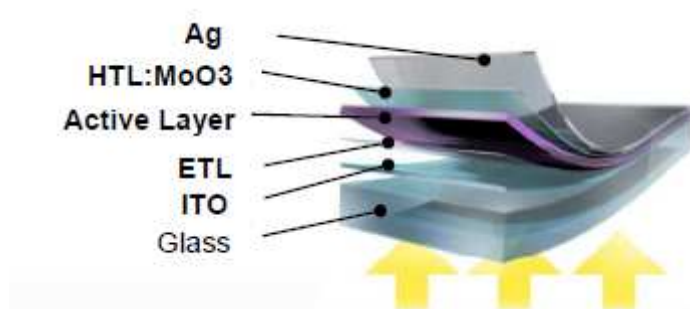


Figure 45. Inverted architecture employed by Istituto ENI Donegani

Although the test was only a preliminary one, with no condition optimization, results appear not to be promising, with an efficiency of 0.24%, to be compared with an efficiency of 3.2% displayed by the benchmark blend P3HT:PCBM. Anyway, in all cases the best results were obtained when T₆BT₂:PCBM mixture is used (Figure 46).

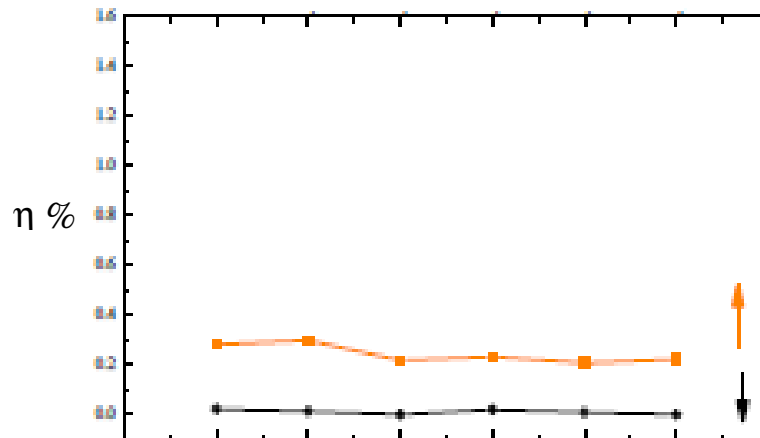


Figure 46. Efficiency values displayed by six cells prepared with two blends: *i)* T₆BT₂:PCBM (orange line) and *ii)* T₆BT₂:C60 (black line)

Moreover, the ENI staff has observed that the films obtained in the above conditions are too rough (RMS factor); in fact the performances increase with the decreasing of the RMS factor (Figure 47).

Much more interesting results were obtained in tests carried out with the same protocol but using other donors; they will be described in the subsequent paragraphs

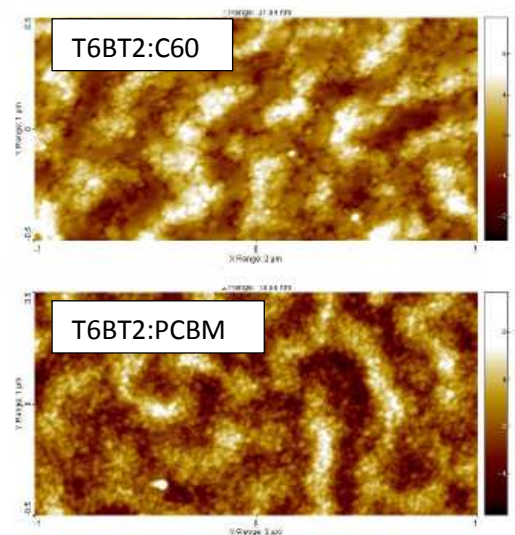


Figure 47. AFM images recorded for the two blends indicated in the picture

3.2 Inherently Chiral Molecules with Pyrrole-based Atropisomeric Scaffolds

3.2.1 Confirming the Concept of Inherent Chirality Varying the Chemical Nature of the Atropisomeric Scaffold

In cooperation with Università degli Studi dell' Insubria Sede di Como monomers with the more electron-rich bis-indole atropisomeric scaffold were also synthesized and characterized (Figure 48).

General features of this class of molecules are well described in the Introduction at the paragraph 1.4.4.

Electrochemical characterization was performed in collaboration with Dr. Elisa Lo Bello and Dr. Sephira Riva: each monomer was studied in ACN and DCM, and on three different working electrodes (GC, Au, Pt).

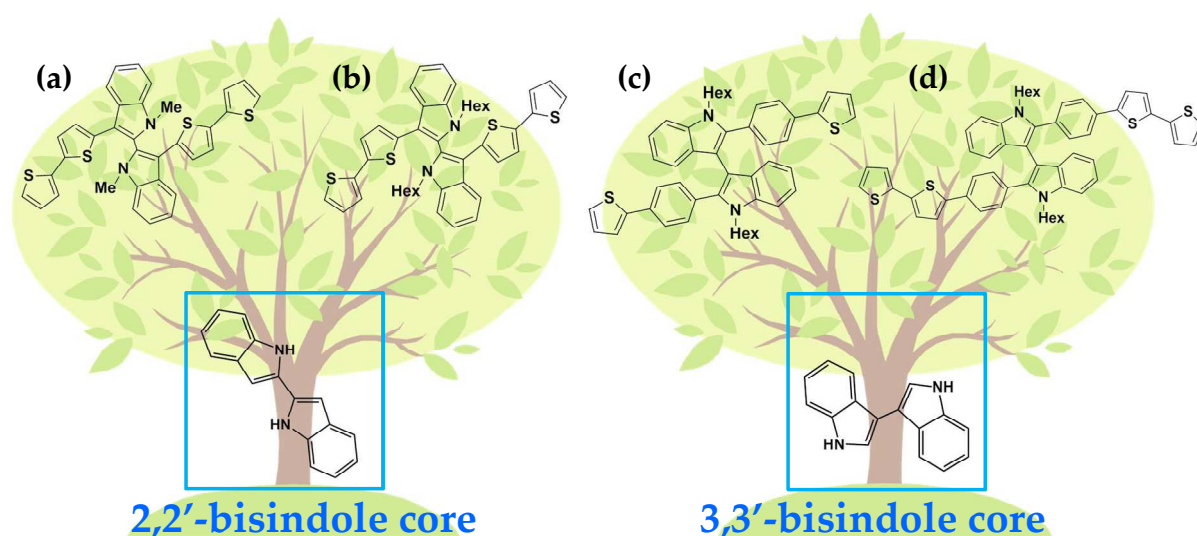


Figure 48. Chemical structures of indole-based monomers.

On the left:

- N,N'-dimethyl-3,3'-bis[2-(5,2'-bithiophenyl)]-2,2'-bis-indole [2,2'-Ind2-T4(N-Me)];
- N,N'-dihexyl-3,3'-bis[2-(5,2'- bithiophenyl)]-2,2'- bis-indole [2,2'-Ind2-T4(N-Hex)].

On the right:

- N,N'- dihexyl -2,2'-bis[4-(2-thiophenyl)-phenyl]-3,3'- bis-indole [3,3'-Ind2-Ph2-T2(N-Hex)];
- N,N'- dihexyl -2,2'-bis{4-[2-(5,2'- bithiophenyl)]phenyl}-3,3'- bis-indole [3,3'-Ind2-Ph2-T4(N-Hex)].

For greater understanding at the roots of the trees the parent scaffold structures are reported:
on the left the 2,2'-bis-indole core and on the right the 3,3'-one

Such monomers afford, *inter alia*, to compare the effect of 2,2' and 3,3' connectivity between the two indolic units on conjugation and redox properties.

In order to promote solubility, aliphatic chains of different length were also added to the indolic nitrogens.

Figure 49 shows a synopsis of CV characteristics for each monomer, analyzed on the same GC electrode surface at the same scan rate (200 mV s^{-1}). Each monomer was characterized in two different solvents, ACN (in blue) and DCM (in red); the corresponding two CV patterns, are superimposed in each figure, and their comparison is meaningful since they have been referred to the $\text{Fc}^+|\text{Fc}$ intersolvental redox couple.

This synopsis enables to create valuable comparisons between the four molecules, in regards to both their electronic and steric properties.

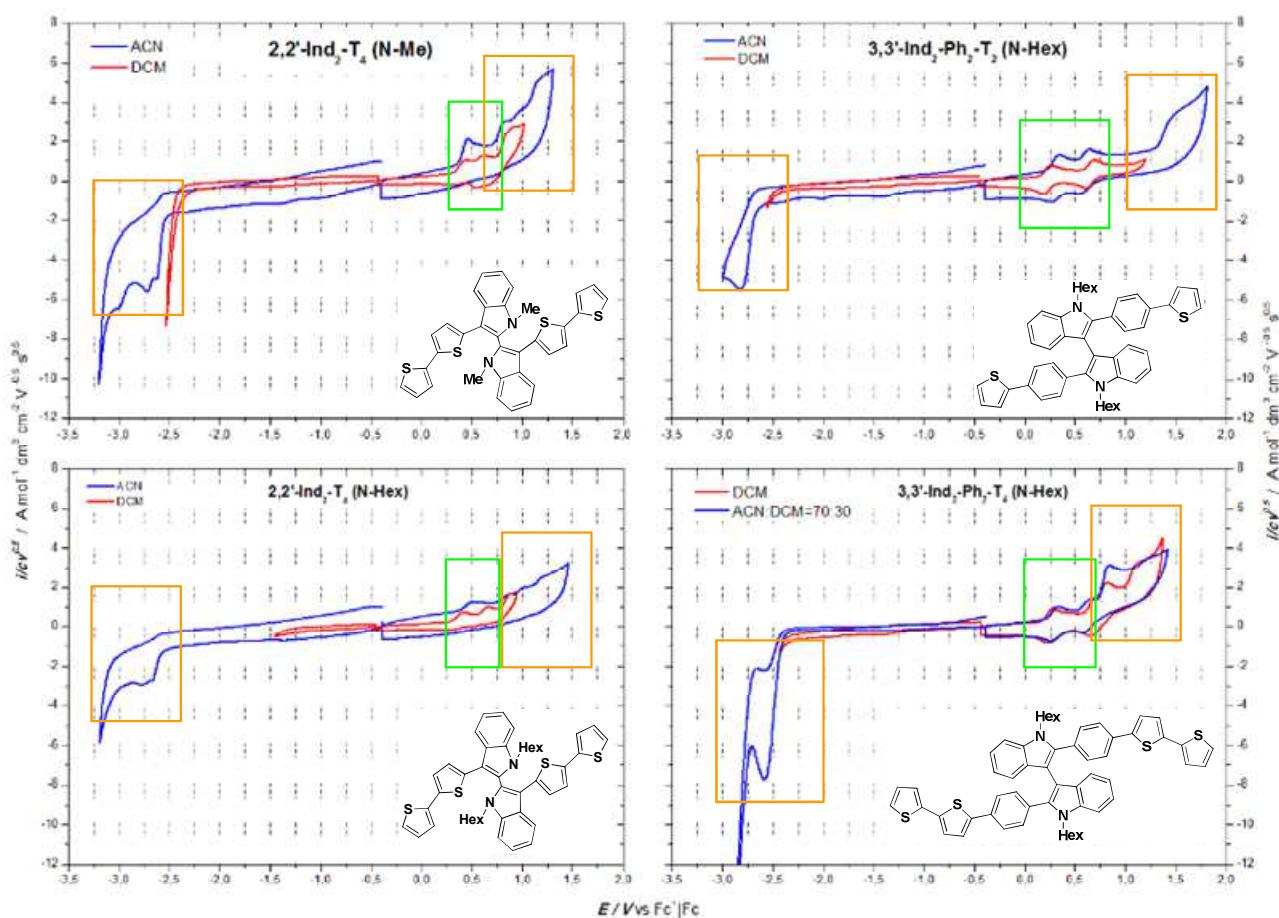


Figure 49. Synopsis of CV patterns of four indole-based monomers of interest. Analyses were carried out in ACN (blue line) and DCM (red line) on GC electrode at 200 mV s^{-1} . Monomer concentration was $5 \cdot 10^{-4} \text{ M}$.

a. Redox sites identification

The first two peaks (sometimes coalescent), framed in green in figure, are to be attributed to the indole sites, which are the electron richest and therefore the most easily oxidized. On the other hand, the successive oxidation peaks and reduction peaks are to be attributed to the thiophene side chains (orange in figure). Their position is confirmed by the oxidation and reduction potential for linear α -oligothiophenes as found in the literature [20], used as comparison.

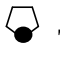
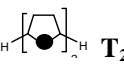
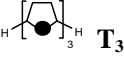
	$E_{cat,2}$ / V (Fc ⁺ Fc)	$E_{cat,1}$ / V (Fc ⁺ Fc)	$E_{an,1}$ / V (Fc ⁺ Fc)	$E_{an,2}$ / V (Fc ⁺ Fc)	E_{gap} / eV
 T₁		-3.73	1.33		5.06
 T₂	-3.47	-2.84	0.88		3.72
 T₃	-2.90	-2.50	0.58	1.53	3.1

Table 1. Peak potential values referred to the standard redox couple Fc⁺|Fc for linear α -oligothiophenes

b. Bis-indolic scaffold connectivity: 2,2' vs 3,3'.

The system consists of two equivalent, partially interacting redox centers. The extent of such interaction depends on two main issues:

- Conjugation efficiency through the central bond, depending on both resonance formulas and torsion angle.
- Solvent ability to coordinate and screen the charges: a polar solvent such as ACN would result in lower interaction between the two halves with respect to an apolar solvent such as DCM. Moreover, the solvent features can result in higher or lower chemical reversibility in the charge transfer process, in case of subsequent chemical reactions possibly involving charge transfer products.

In a CV measurement, two equivalent, reciprocally interacting monoelectronic redox sites generate two peaks. Their distance is directly proportional to their interaction: if they are

completely independent, they will coalesce into a single peak of 0.057 V width and double height.

The conjugation efficiency between the two molecule halves (and therefore of the global conjugated system) also modulates the gap between the first reduction and first oxidation peak (which is directly related to the HOMO-LUMO gap).

In our system, it is worth pointing out that the 3,3'- core twin peaks are more distanced than the 2,2'- ones, and located at less positive potentials (*i.e.*, their oxidation is easier). This suggests a higher conjugation efficiency of 3,3'-bis-indoles, probably related to a lower torsional angle. Recent calculations together with HPLC studies have confirmed this interpretation: the rotation barrier around the central bond is higher for 2,2'-bis-indoles.

The solvent effect is evident for all four molecules: as expected, the twin peaks are closer in polar ACN, on account of its shielding effect between the charged redox centers. Moreover, in the 3,3'- systems the indolic radical cations generated in the electron transfer appear to be stable in both solvents (they show a reversible peak even at low scan rate); whereas for 2,2'- systems reversibility is maintained only at high scan rate (partial at low scan rates) in DCM, and is completely absent in ACN. This suggests that 2,2'- radical cations are less stable, and probably involved in a following chemical step favored by a polar solvent.

c. Conjugation in the oligothiophene side chains.

In the two 2,2'-Ind2-T4 derivatives, the lateral chains are bi-thiophenic. Their oxidation and reduction peaks correspond more or less to those of α linear bi-thiophene (with little variations, imputable to the difference in solvent): 0.79/0.90 V for oxidation and -2.62/-2.67 V for reduction. The conjugation seems to be more effective than that of the linear oligomer, as confirmed by the energy gaps value for chains: 3.53 eV for the Me derivate and 3.62 eV for the Hex derivate; against the 3.72 eV found for the linear oligothiophene.

In the 3,3'-Ind2-Ph2-T4 derivative, a phenyl ring is inserted between the bi-thiophene terminals and the indole core. Conjugation is increased, since the first oxidation peak

moves to 0.83 V, and the first reduction peak to -2.58 V, with the energy gap decreasing to 3.41 eV. The conjugation effect is particularly evident for the first oxidation peak.

Finally, in the 3,3'-Ind2-Ph2-T2, lateral chains consists of a single thiophene, again with a phenyl ring interposed before the indole core. Both oxidation and reduction potentials shift to more extreme values. As a matter of fact, oxidation value is 1.46 V, and reduction value -2.82 V. The energy gap amounts to 4.28 eV, an intermediate value between thiophene and bi-thiophene. This result suggests conjugation to be less effective in a benzene + thiophene oligomer than in a thiophene + thiophene one. Oxidation, in particular, occurs at higher potentials because benzene is less electron-rich than the thiophene, and because conjugation is lower.

All these parameters are summarized in Table 2.

Electrode GC	$E_{I,C}$ / V	$E_{I,C,Onset}$ / V	$E_{I,A}$ / V	$E_{I,A,Onset}$ / V	LUMO _{Max} / eV	HOMO _{Max} / eV	Gap _{Max} / eV	LUMO _{Onset} / eV	HOMO _{Onset} / eV	Gap _{Onset} / eV
2,2'-Ind2-T4 (N-Me)	-2,23	-2,16	0,85	0,74	-2,17	-5,26	3,1	-2,26	-5,16	2,9
2,2'-Ind2-T4 (N-Hex)	-2,29	-2,21	0,90	0,78	-2,12	-5,31	3,2	-2,24	-5,13	2,9
3,3'-Ind2-Ph2-T2 (N-Hex)	-2,37	-2,24	1,83	1,69	-2,03	-6,23	4,2	-2,15	-6,07	3,9
3,3'-Ind2-Ph2-T4 (N-Hex)	-2,19	-2,01	0,71	0,62	-2,22	-5,13	2,9	-2,22	-4,98	2,7

Table 2. Summary of parameters of interest obtained from CV patterns recorded in ACN to elucidate conjugation in the oligothiophene side chains.

All potential values are referred to the standard redox couple $Fc^+|Fc$.

d. Length of the alkyl substituents at the nitrogen atom.

Alkyl substituents were changed from *methyl* to *hexyl* in order to improve solubility. The change has a slight impact on peak potentials which slightly move towards more extreme values, due to the steric increase. Moreover, a decrease in the diffusion coefficient leads to a decrease in the measured current.

The alkyl chain length might also slightly affect the torsional angle and the reciprocal interaction between redox equivalent sites. In any case, they again appear to interact more

both in DCM (in which they appear to be quite distanced) and in ACN (in which they tend to coalesce at low speeds).

The same results are visible on Pt and Au supports (except for few differences related to the high affinity of sulfur for gold).

e. Oligomerization ability

Stable oligomer film formation is only obtained in the case with methyl alkyl substituents on the nitrogen ring [2,2'-Ind2T4(N-Me)], possibly on account of very high solubility conferred by the hexyl chains.

Electrooligomerization of 2,2'-Ind2T4(N-Me) in dichloromethane

As expected, oligomerization does not start when cycling around the first indolic twin peak system, resulting in stable radical cations localized on the molecule core; it only starts by including in the potential cycle the thiophene chains (Figure 50).

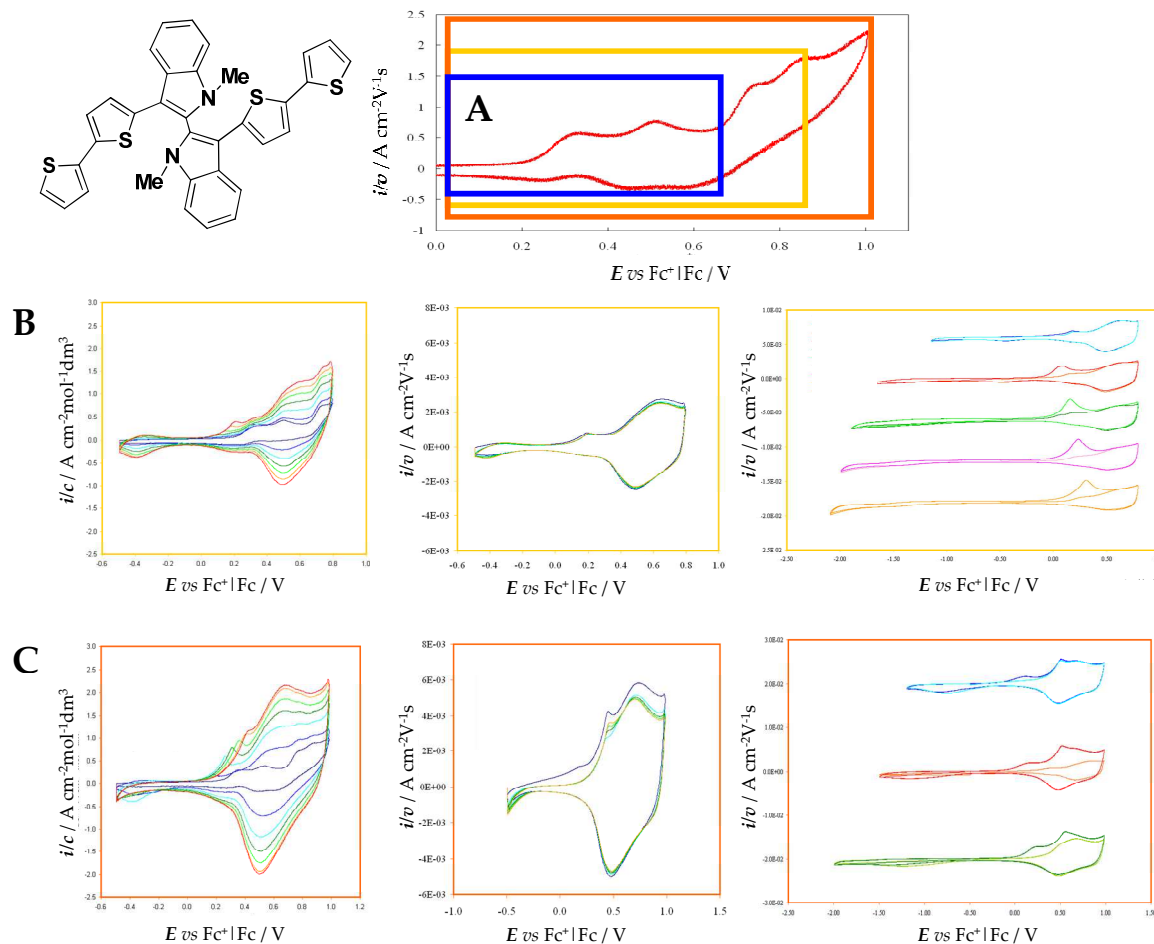


Figure 50. CV patterns of 2,2'-Ind2T4(N-Me) recorded in DCM + TBAPF₆ 0.1 M on GC electrode at 200 mVs⁻¹:

- A) Cycling around the bis-indole twin peaks: no oligomerization;
- B) Cycling around the first of thiophene chain twin peaks; in order from left to right: oligomerization 36 cycles, stability test, and charge trapping phenomenon at different cathodic potentials;
- C) Cycling around the whole thiophene twin peak system, in order from left to right: oligomerization 36 cycles, stability test, and charge trapping phenomenon at different cathodic potentials

2,2'-Ind2T4(N-Me) racemic monomer has shown very fast, regular and virtually unlimited electrooligomerization in DCM + TBAPF₆ 0.1 M on GC as working electrode at 200 mV s⁻¹ potential scan rate both cycling around the third and fourth oxidation peak (Figure 50).

Resulting films were very stable and displayed a very neat charge trapping effect mostly cycling around the whole thiophene twin peak system.

The separation of racemic 2,2'-Ind2T4(N-Me) into the relative enantiomers was successfully achieved in large quantities by Prof. Roberto Cirilli. Work is in progress to prepare enantiopure chiral electrode surfaces as in the cases of T₄BT₂ and BT₂DTP₂ in order to study their enantioselection ability.

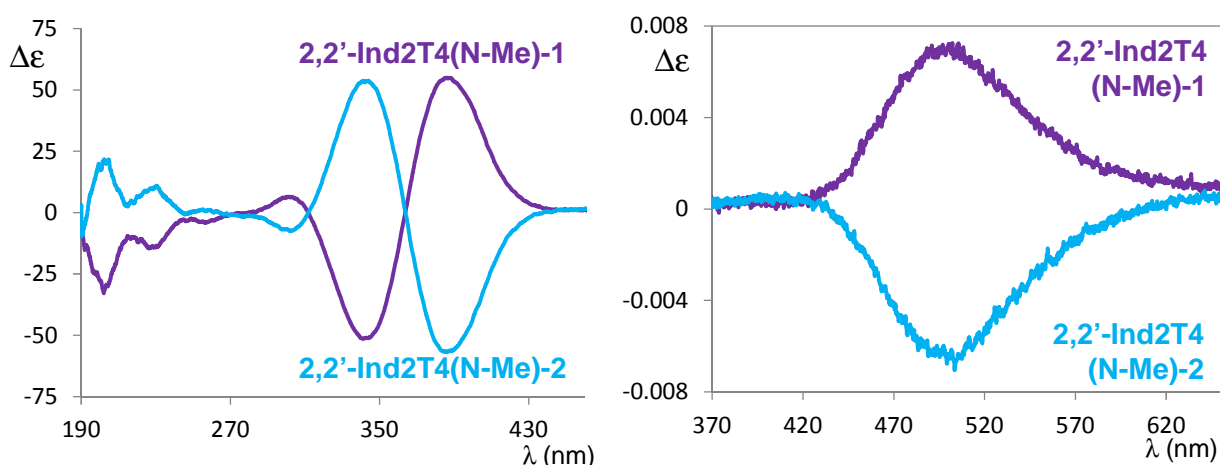


Figure 51. CD and CPL measurements of 2,2'-Ind2T4(N-Me)-1 (violet line, 1.02×10^{-4} M) and 2,2'-Ind2T4(N-Me)-2 (light blue line, 1.09×10^{-4} M) recorded in ACN.

CD and CPL measurements of the 2,2'-Ind2T4(N-Me) enantiomers were performed by Prof. Giovanna Longhi. Signals are perfectly specular and also in this case enantiopure antipodes emit circularly polarized light (Figure 51).

The same research group has also carried out VCD experiments that have allowed to assign the absolute configuration by comparison between the experimental spectra and those obtained by theoretical computations (Figure 52).

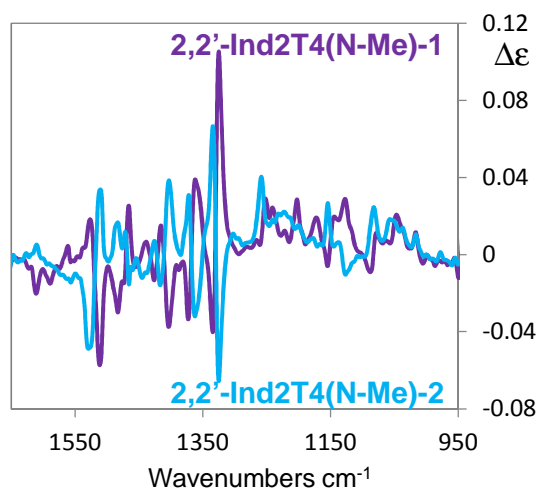


Figure 52. VCD spectra recorded in CDCl_3 . 2,2'-Ind2T4(N-Me)-1 (0.094 M) and 2,2'-Ind2T4(N-Me)-2 (0.096M)

In this way the (+) configuration has been assigned to the first 2,2'-Ind2T4(N-Me)-1 enantiomer eluted in HPLC separation.

3.2.2 A Corollary Study: Temperature Effect on Rotational Barrier of Indole-based Monomer with 3,3'- Connectivity

The temperature effect on the torsional angle between the two moieties of a monomer with the 3,3'-bis-indole scaffold was studied (Figure 53) by means of differential pulse voltammetry (DPV). Such a scaffold has lower racemization barrier than its 2,2'- homologous, as confirmed by theoretical studies. Measurements were carried out both in ACN and DCM as solvents; but experimental details are available in the experimental section at paragraph 2.1.4.

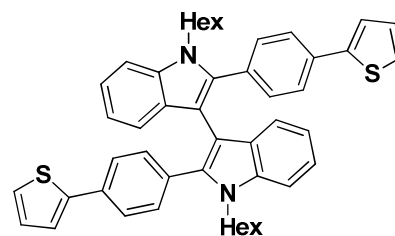


Figure 53. The indole-based monomer with 3,3'- connectivity under study

As depicted in Figure 54 below, the temperature increase results in a decrease of the rotational barrier and an increase of the reciprocal interaction between the two redox centres (*i.e.* the distance between the first twin peak corresponding to processes localized on the bis-indole core increases).

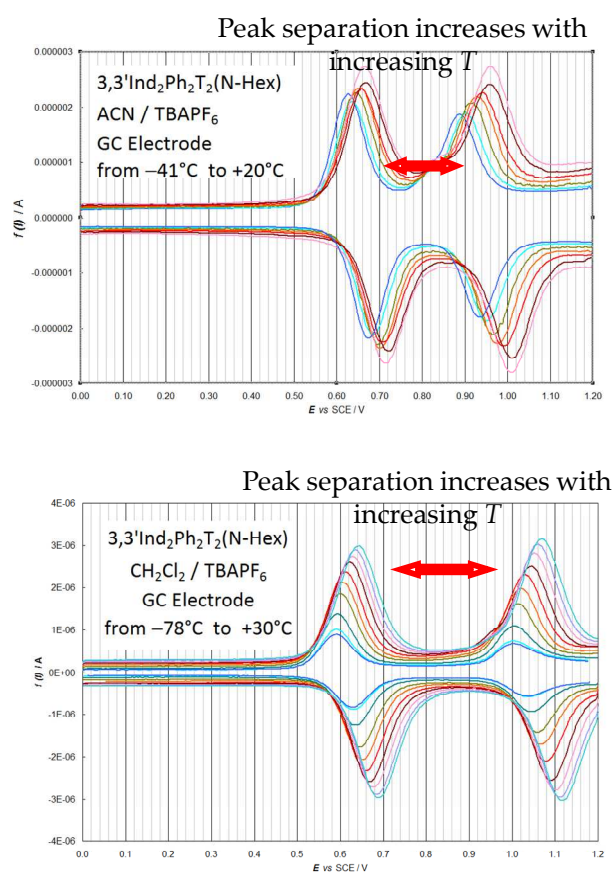


Figure 54. Forward and reverse DPV scans on twin peak system, gradually increasing the cell temperature. Studies in ACN above and in DCM below

3.3 Inherently chiral spider-like oligothiophenes with β,β' -bithiophene core

Features of this family has been described in the Introduction at the paragraph 1.4.5.

In summary this kind of molecules are fully constituted by thiophene rings and chirality originates from the β,β' interconnection between the two equal halves.

Inherently chiral spider like oligothiophenes have been synthesized according to the previous structures named spider like oligothiophenes [21] in which the link between the two equal moieties is α,α' type. In the latter case molecule are achiral due to the low racemization barrier that does not impair the free rotation between the torsional angle.

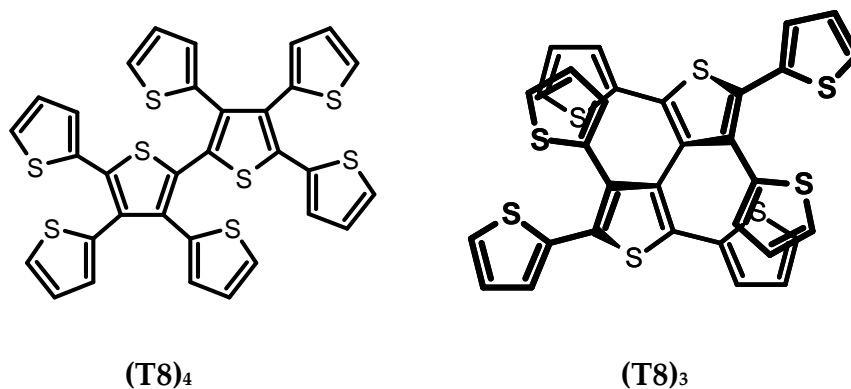


Figure 55. On the right: the inherently chiral spider like molecule object of study in this work.
On the left: the corresponding spider like molecule for comparison

The examined molecule in this work, named (T8)₃, is represented in Figure 55.

Theoretically studies performed by Simone Casolo at Università degli Studi di Milano have revealed that the torsional angle between the two equal moieties is of about 91°. The three thiophenes are conjugated (flat), while the other 'side' thiophene is at 103°. The four α -conjugated thiophene terminals are the preferred sites for radical cation formation, suitable for electrooligomerization. Moreover the energy barrier is sufficiently high (about 68 kcal mol⁻¹) to yield stable enantiomers that can be separated, stored and characterized.

Electrochemical characterization of monomer and oligomers has been carried out in three different media: ACN, DCM and BMIMPF₆ and on three different electrode surfaces: GC, Pt, Au. CV features of the monomer (Figure 56) show two oxidations peaks both in ACN and DCM solvents and only one signal in the BMIMPF₆ medium.

The medium effect is also evident on the oxidation peak potentials, that are shifted at more positive values, while the effect of changing electrode supports appears negligible (unlike in the electrodeposition process, see later).

The two redox peaks correspond to two equivalent but slightly interacting redox sites and are chemically and partially electrochemically irreversible (*i.e.* electronic transfer barrier not too high).

In the case of DCM, peaks are more distant than those recorded in ACN due to the shielding effect of this solvent on the positive charges of the generated radical cation.

Electrooligomerization takes place fast and regular, both cycling around the first or the second oxidation peak. The oligomer generated by cycling around the whole twin peak system has a faster, but less controlled growth. Electrodeposition is better in ACN than in DCM due to the high solubility of formed oligomers in the second solvent; instead when BMIMPF₆ is used, the process is more controlled because of it proceeding slower than the other two cases, and the obtained films are more regular and homogeneous. Regarding the influence of electrode surfaces in the electrodeposition, the best support for the electrooligomerization of (T8)₃ monomer, albeit possibly non-innocent in the first monolayer orientation, is the gold electrode consistently with the high affinity of sulfur for gold (Figure 57).

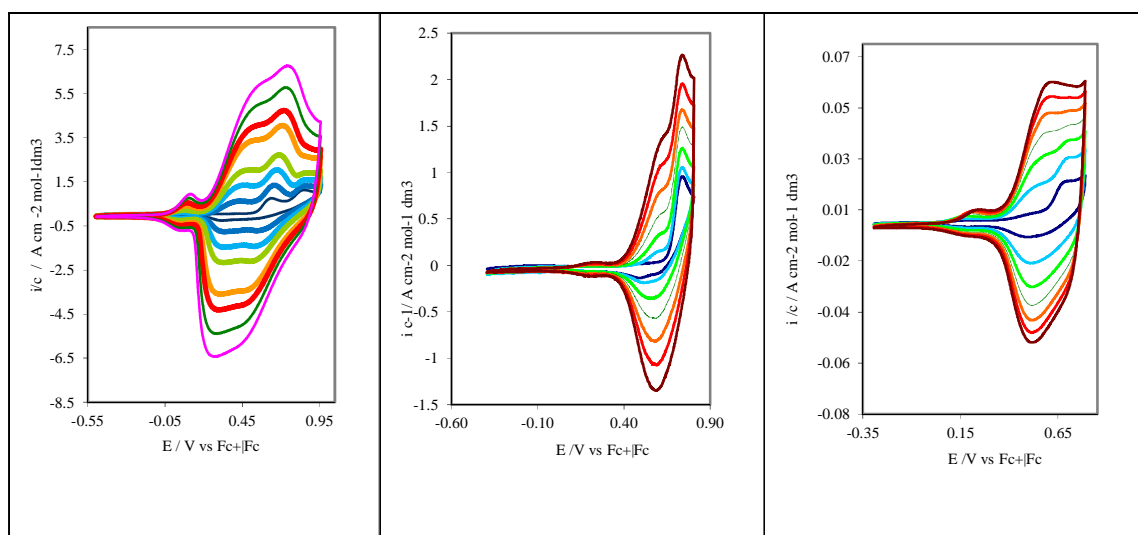


Figure 57. CV features of the (T8)₃ oligomers electrodeposited on Au electrode in the three used media: from left to right ACN, DCM and BMIMPF₆

Films resulted to be stable both in all tested solvents and on all electrodic surfaces upon repeated potential scans in a monomer-free solution and have shown a remarkable charge trapping effect.

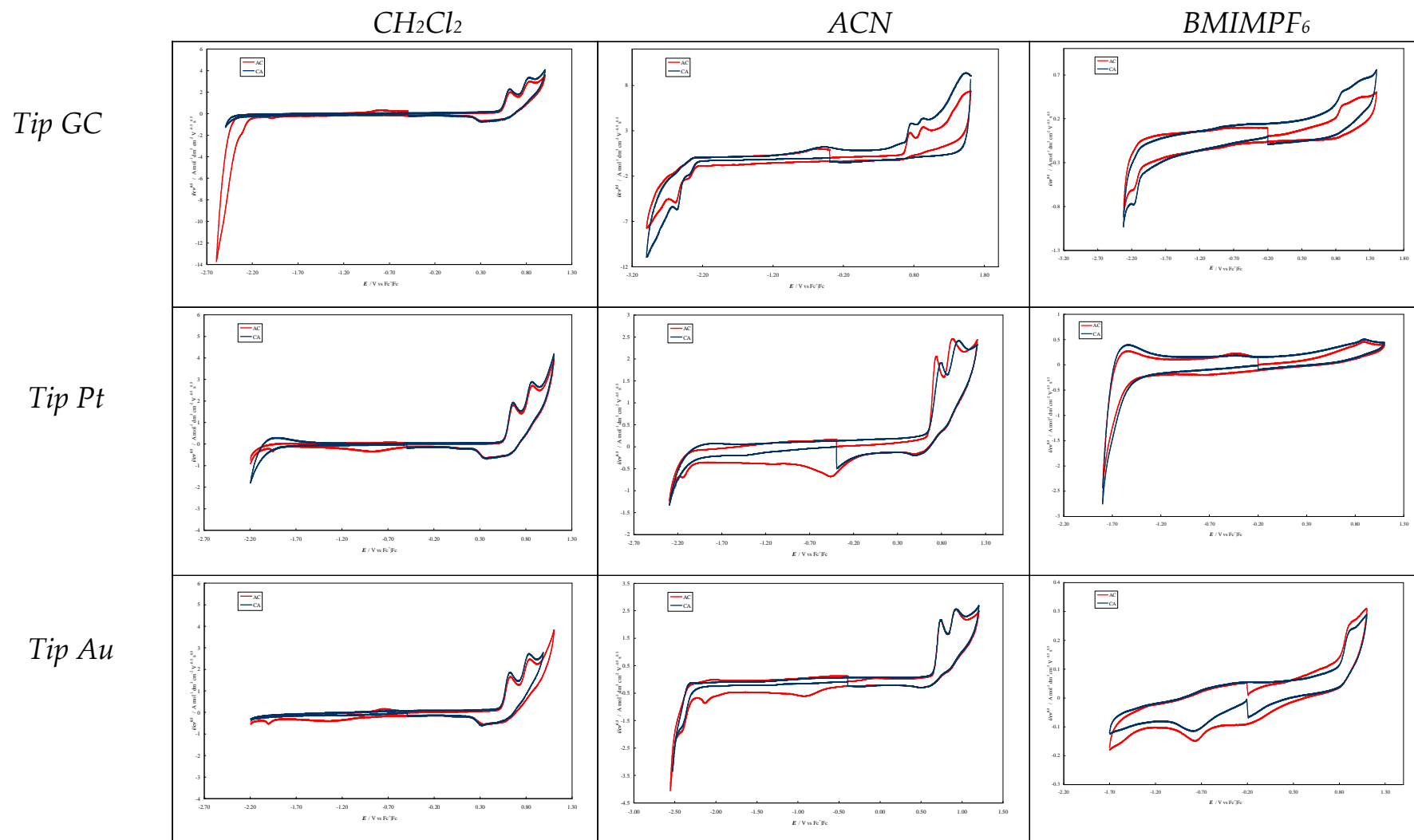


Figure 56. CV patterns of $(T8)_3$ monomer recorded in the three indicated media on GC, Pt and Au electrodes at 200 mV s^{-1} . Potential values were referred to the standard redox couple Fc^+/Fc . In red anodic-cathodic scans, in blue cathodic-anodic scans.

Among the oligomer films characterized in this work, (T8)₃ oligomers show a particularly neat electrochromic effect (Figure 58). Electrochromism is defined as a reversible color change of a material as a function of applied voltage. This process is due to the redox behavior of the electrochromic material.



Figure 58. Electrochromism of the (T8)₃ oligomer on ITO working electrode
(on the left: oligomer doping, on the right: oligomer undoping)

In particular (T8)₃ oligomer displays a green color in the doped state becoming orange in the undoped one. This means that films can be exploited for their using for example in the so called electrochromic devices (ECDs). ECDs consist of a two-electrode electrochemical cell. They include an ion-conducting liquid or solid electrolyte medium sandwiched between two electrode surfaces coated with organic or inorganic electrochromic materials, chosen for their electrical and optical properties. Their purpose is the generation of a variable-color system that can be changed in a controllable fashion for potential applications as displays, smart windows or in other technologies [22].

This phenomenon also corresponds to a net and reversible variation of the *UV-vis* spectrum of the (T8)₃ oligomer between the neutral and polaronic state, observed in spectroelectrochemistry tests carried out in cooperation with Dr. Monica Panigati at Università degli Studi di Milano. Oligothiophenes belong to the vast class of conjugated systems with non-degenerate ground-state limiting forms (aromatic and quinoid) The formation of doping-induced charged states, paramagnetic radical ions (polarons) or

diamagnetic di-ions (bipolarons) and intra/intermolecular π -dimers is associated with chain relaxation that alters the π -electrons distribution along and leads to electronic levels within the energy gap of the neutral material. Thus new electronic bands are characteristic for the doped state.

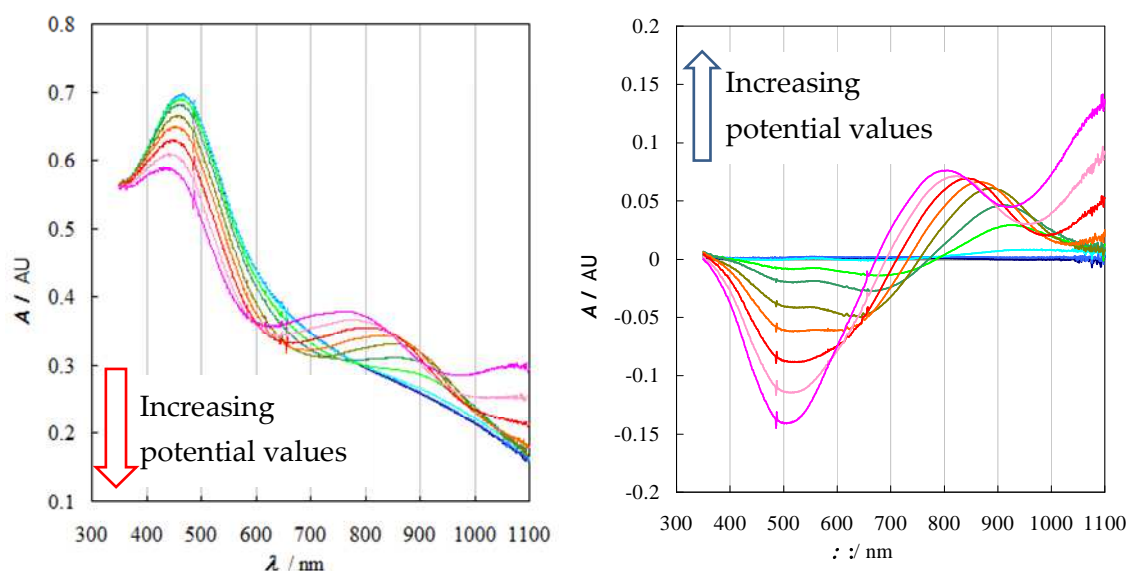


Figure 59. On the left: combined Vis/NIR data collected by *in situ* spectroelectrochemistry spectra on a (T8)₃ film (deposited on a ITO electrode) reported at constant potential intervals. On the right: Vis/NIR spectra plotted as differences with respect to the spectrum of the neutral film

In situ spectroelectrochemistry experiments for the (T8)₃ oligomer has been carried out with ITO as working electrodes in ACN + TBAPF₆ 0.1 M. Spectra are reported in Figure 59. Unfortunately results are not as satisfactory as in the case of T₄BT₂ films due to the low affinity of the (T8)₃ oligomer for the ITO surface, in fact within a few recordings the deposited molecular material moved away from the electrode surface. Figure 59 shows a decreasing intensity of the band associate with the π - π^* transition in the neutral state at low wavelength. This decrease starts at the electrochemical potential where anodic current onset occurs in the corresponding CV trace. Increasing the potential results in further and progressive bleaching of the band, accompanied by a loss of its vibronic fine structure. Conversely, a growth of two doping-induced bands is observed at higher wavelengths corresponding to more conjugated polaronic and bipolaronic states respectively.

The (T8)₃ racemate has been resolved into its enantiomers (Figure 60) at analytical level at room temperature on a chiral stationary phase: the chromatograms have been registered by using two detectors, a UV-Vis (in black) and a circular dichroism (in blue).

From these results it seems that the two antipodes are stable (absence of a plateau between the two signals).

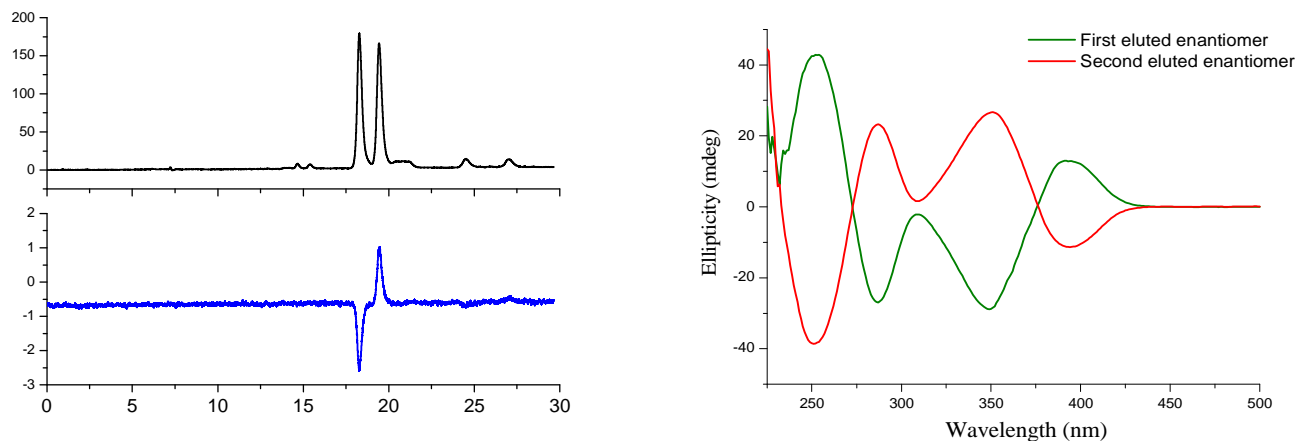


Figure 60: (T8)₃, CSP: Chiralpak IB-3 250 x 4.6 mm I.D. + Chiralpak IB-3 250 x 4.6 mm I.D. ; eluent: *n*-hexane-dichloromethane-ethanol 100/5/0.2; flow-rate: 1.0 cm³/min; temperature: 25°C; detection: UV (black) and CD (blue) at 350 nm. $k_1 = 1.61$, $\alpha = 1.11$, $R_s = 2.15$. CD in chloroform at 25°C

Unfortunately it was very difficult to obtain in adequate quantities both enantiomers in order to well characterize them.

3.3.1 Enantiorecognition Tests

As in the former study [5] on T₄BT₂ enantiopure films, enantiorecognition tests were carried out by means of CV and EIS (explained at paragraphs 3.1.2 and 3.1.3).

Electrodeposition of (T8)₃ monomer is very efficient in the BMIMPF₆ ionic liquid and on gold electrode, as just said above, granting high homogeneity and regularity in the resulted films. The same protocol used to check the discrimination properties of T₄BT₂ antipodes was also employed for the (T8)₃ enantiomeric films.

So chiral surfaces were electrodeposited on screen-printed gold electrodes in BMIMPF₆ employing the same (S)-(-)- and (R)-(+)-N,N-dimethyl-1-ferrocenyl ethylamine as chiral electroactive probes. Results are reported in Figure 61.

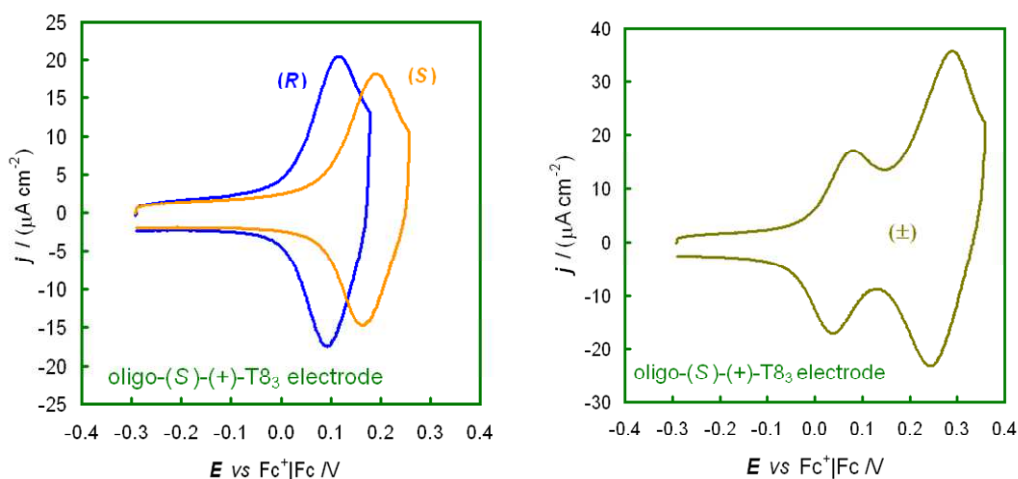
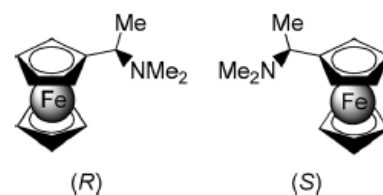


Figure 61. Enantioselective CV tests for the oligo-(S)-(+)-(T8)₃ film coated electrode with (R)- and (S)-chiral redox probes (8 mM) on the left and with the (±)-racemic redox probe on the right.

Potential scan rate: 50 mV s⁻¹

On bare gold electrode both (S)- and (R)- chiral probes exhibit a typical diffusion-controlled process with a formal potential of $E^{\circ'} = -0.01$ V vs. Fc⁺ | Fc.

On the oligomer-film-coated electrodes (36 oligomerization potential cycles, 12 mM (T8)₃ at 50 mV s⁻¹) the enantiomeric oligo-(S)-(+)-(T8)₃ film displays an exceptional enantiodiscrimination ability towards the (R)- and (S)- N,N-dimethyl-1-ferrocenyl ethylamine probes, with a formal potential difference of ~ 75 mV between the two antipodes (Figure 61, on the left). The separation between the two enantiomer peaks is much more pronounced (more than 200 mV) employing racemic probe (Figure 61, on the right).

The oligo (*R*)-enantiopure film electrode gave a good response in terms of potential separation when (*S*)- and (*R*)-chiral probes were used, indeed the peak separation between the two enantiomers is about 100 mV. Unfortunately the CV current values in the case of (*S*) probe are lower than the (*R*) one, which may be attributed to the quite low enantiomeric excess (*ee* 86%) of the monomer due to the difficulty in the chiral HPLC separation (Figure 62).

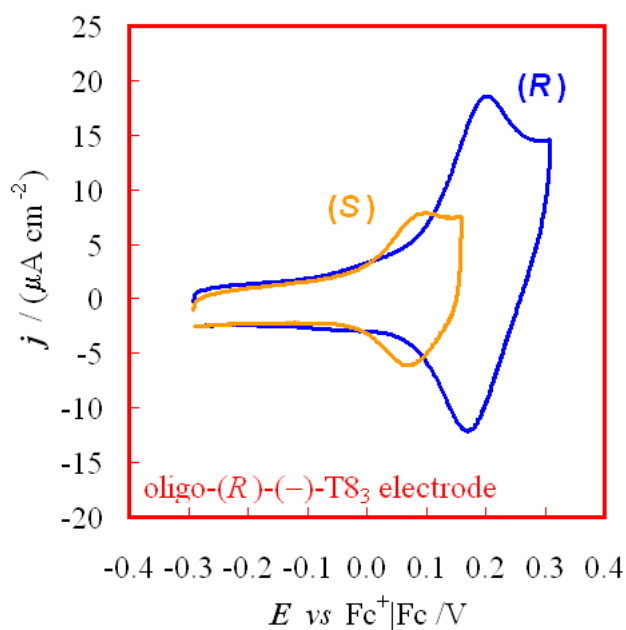


Figure 62. Enantiorecognition CV tests for the oligo-(*R*)-(-)-(*T8*)₃ film coated electrode with (*R*)- and (*S*)-chiral redox probes (8 mM)

Enantiorecognition tests were carried out by means of EIS in the same conditions described at paragraph 3.1.3. Results are depicted in Figure 63.

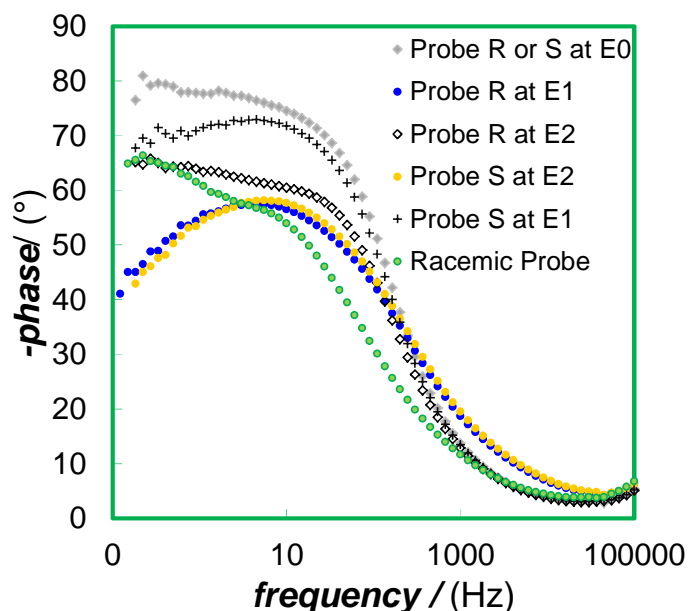


Figure 63. Bode phase plots representative of enantiorecognition tests conducted on oligo-(S)-(+)-(T8)₃ electrodes in BMIMPF₆ in presence of chiral ferrocene-based probes.

Spectra were recorded at different potential values named E_0 , E_1 , E_2 representative respectively of: the peak potential of chiral probes on bare electrode ($E_0 = 0.01$ V *vs* Fc⁺|Fc) and the peak potential of each probe enantiomer ($E_1 = 0.07$ V *vs* Fc⁺|Fc V and $E_2 = 0.17$ V *vs* Fc⁺|Fc) recorded on electrode covered by (T8)₃ homochiral films.

For comparison it is moreover indicated the spectra of (*R*) probe recorded on gold bare electrode.

In green Bode plot on (S)-(+)-(T8)₃ enantiopure film in presence of racemic probe

As in the case of T₄BT₂ films, EIS measurements have proved a useful tool to estimate the enantiorecognition capability of these inherently chiral materials.

Recording Bode spectra at E_0 value (Figure 63) on chiral electrode surfaces in presence of (*R*) or (*S*) probes, the signals obtained are perfectly superimposable recalling a situation of an electrode coated with a conductive polymer layer in contact with a solution containing no redox couple.

When spectra were recorded at E_1 and E_2 values (Figure 63) corresponding to the peak potentials of each probe enantiomer (*i.e.* in the region where each probe is active), as in the previous study, they are perfectly superimposed although plots have been recorded at

different potential values. This means that both chiral probes are involved in a charge transfer process characterized by the same time constant.

This interpretation is also confirmed when Bode spectra are recorded on the same surface for each enantiomer at the other enantiomer's own potential (*i.e.* E_1 for probe *S* and E_2 for probe *R*); in this case the EIS diagrams are not superimposable, consistently with the former assumptions.

The spectrum recorded for (*R*) probe at E_2 potential value recalls a process with high resistance coherently with the hypothesis that at this potential the probe is already active. For (*S*) probe the situation is the opposite: in fact at E_2 value this probe is not yet active inducing a low resistance process.

Enantio-recognition tests were also carried out in presence of a racemic mixture of chiral probes. In the Bode diagram (the green in Figure 63) it is appreciable the presence of two phase peaks. The first peak possibly corresponds to the favorite electron transfer process involving the (*R*) probe and the second one is related to (*S*) probe. The potential applied is the E_2 value necessary to activate both redox probes.

These outstanding enantio-recognition results are very important because they confirm the generality of the inherent chirality concept which does not depend from the chemical nature of the atropisomeric scaffold. We hope to be able to confirm it also by the scheduled enantio-recognition tests on the indole-based inherently chiral films.

3.4 Inherently Chiral Electroactive Macrocycles [23, 24]

Very recently, it has been found that FeCl_3 oxidation of T_4BT_2 monomer (paragraph 3.1.1) generates a series of cyclic oligothiophenes (the largely prevailing ones being dimers and trimers). When produced from enantiopure starting materials, all of them must be inherently chiral macrocycles constituted by a single D_n symmetric stereoisomer.

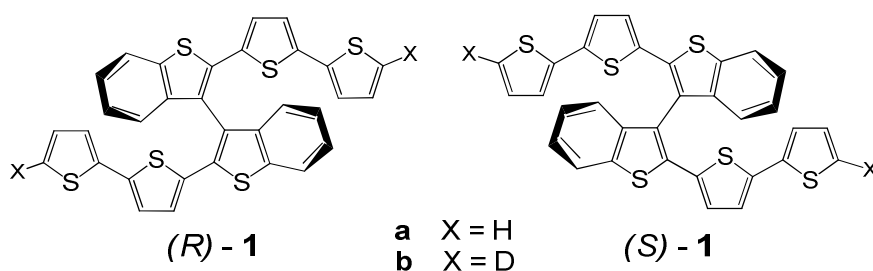


Figure 64. The inherently chiral enantiomeric monomers employed in the present research.

The preliminary experiments have been carried out on racemic (\pm)- T_4BT_2 (Figure 61 (a)). Extraction with THF in a Soxhlet apparatus to remove some insoluble iron-containing materials, gives an orange residue (50% yields in weight), composed by dimers (67%), trimers (27%), tetramers (2%) and pentamers (less than 1%), on the basis of peak intensity in Laser Desorption Ionization (LDI) mass spectrum (Figure 65).

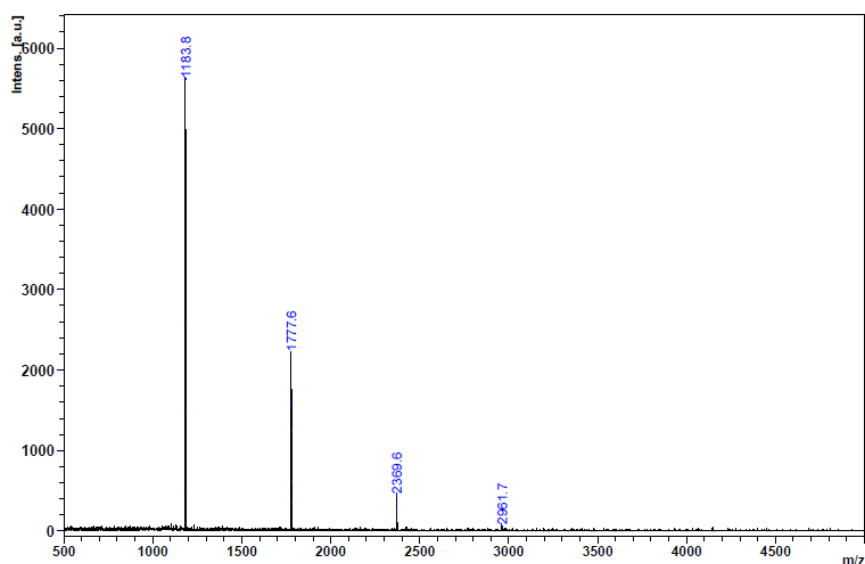


Figure 65. High resolution LDI mass spectrometry of the residue obtained after Soxhlet extraction with THF in the range $m/z = 500$ -5000.

High Resolution LDI (HR-LDI) experiments show that the molecular weights and the isotopic patterns of all the components of the mixture are in agreement with formulas having two hydrogen atoms less than the expected values for linear oligomers (Figure 66), as if the thiophene terminals of the oligomers would have undergone an unexpected FeCl_3 promoted intramolecular coupling.

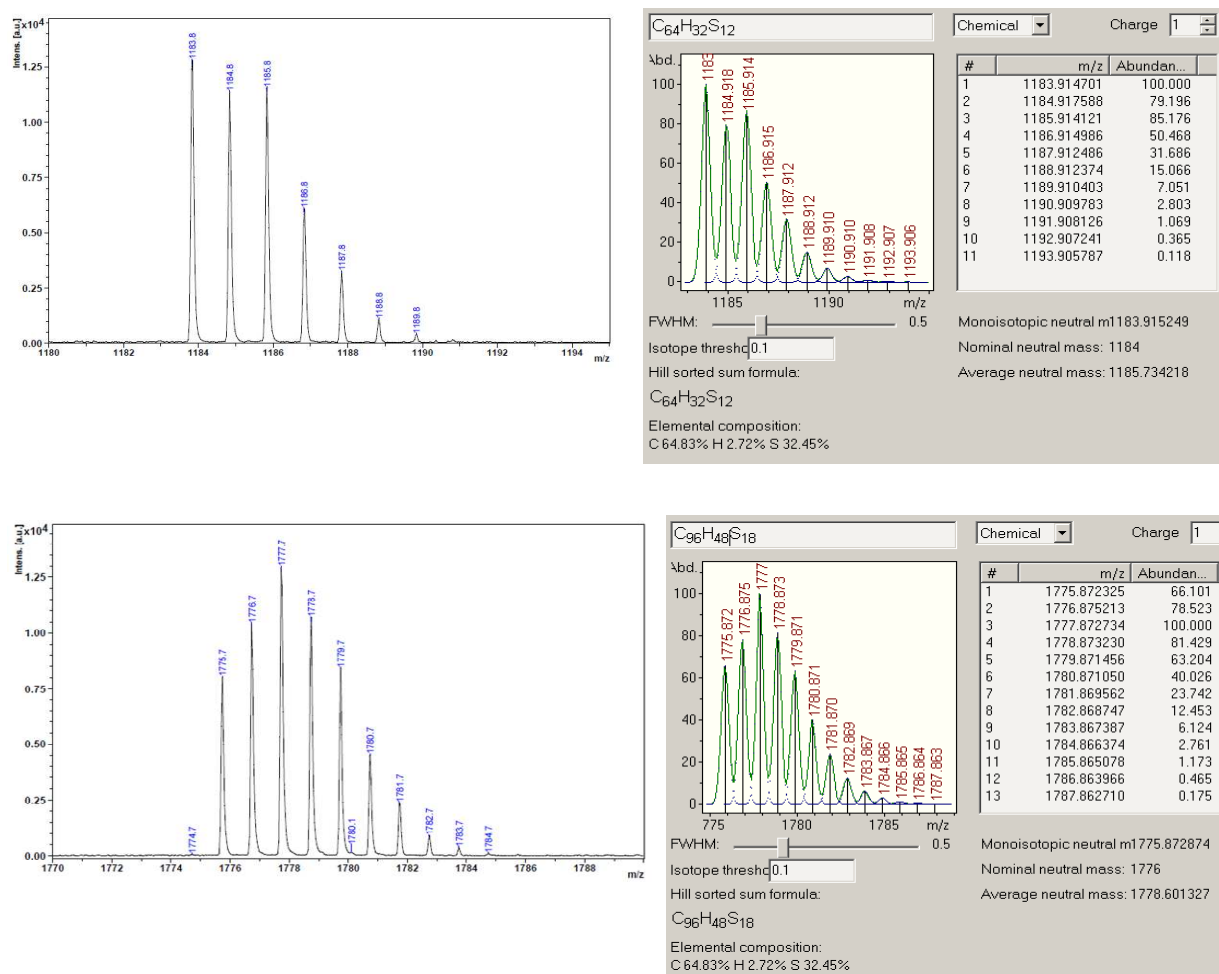


Figure 66. Above: experimental (left) and calculated ($C_{64}H_{32}S_{12}$, right) HR LDI mass spectra of dimer in the range $m/z = 1180-1195$. Experimental (left) and calculated ($C_{96}H_{48}S_{18}$, right) HR LDI mass spectra of trimer in the range $m/z = 1770-1790$.

To prove this hypothesis, we submitted to the same $FeCl_3$ treatment the dideuterated compound (\pm)- T_4BT_2 (Figure 64(b)), prepared by quenching with D_2O the dianion of (\pm)- T_4BT_2 , obtained in turn by lithiation of the latter with $n-BuLi$ excess, in the presence of N,N,N',N' -tetramethyl-ethylenediamine, in THF solution, at $-78^\circ C$. We found (HR-LDI) that the deuterium had been totally lost, thus proving the cyclic structure of the oligomers. The same cycles also constitute a large fraction of the electrodeposited oligomer films. The cyclic *vs* linear electrodeposited oligomer ratio appears to depend on the electrode surface material ($GC \gg ITO$).

In this frame, we considered as primary target the isolation of the most abundant oligomers present in the mixture resulting from the FeCl_3 oxidation of both the enantiopure antipodes of $(\pm)\text{-T}_4\text{BT}_2$ [5].

The oxidation of racemic $(\pm)\text{-T}_4\text{BT}_2$ is expected to afford diastereomeric mixtures of cyclic oligomers produced by homochiral or heterochiral couplings: a pair of D_2 symmetric enantiomers and a C_{2h} symmetric meso compound in the case of the dimer and two diastereomeric racemates, one D_n and one C_1 symmetric, in the case of the trimer.

Accurate column chromatography let us isolate the enantiopure dimer $(S,S)\text{-(-)}$ -dimer and the $(S,S,S)\text{-(+)}$ - trimer from $(S)\text{-(+)-T}_4\text{BT}_2$ and, specularly, the $(R,R)\text{-(+)}$ -dimer and the $(R,R,R)\text{-(-)}$ -trimer from $(R)\text{-(-)-T}_4\text{BT}_2$, in 15% and 8% isolation yields, calculated on 1a, respectively for dimers and trimers. (Figure 67). The enantiomeric purity of the four compounds was checked and demonstrated by analytical HPLC on a chiral stationary phase (Fig. 68).

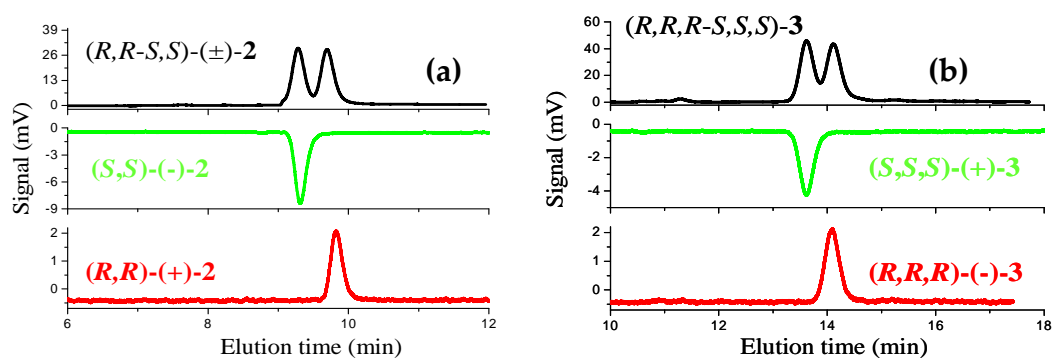


Figure 68. a. Analytical HPLC enantiomeric purity check on a chiral stationary phase of $(S,S)\text{-(-)}$ -2-dimer (green) and $(R,R)\text{-(+)}$ -2-dimer (red); racemate (2, black) prepared from pure enantiomers. CSP: Chiralpak IB-3 (250 mm x 4.6 mm I.D.) + Chiralpak IB-3 (100 mm x 4.6 mm I.D.); eluent: acetone:ethanol-100:60; flow rate: 1 cm^3/min ; temperature: 5°C; detector: UV (black) and CD (green/red) at 410 nm. **b.** Enantiomeric purity check of $(S,S,S)\text{-(+)}$ -3-trimer (green) and $(R,R,R)\text{-(-)}$ -3-trimer (red); racemate (3, black) prepared from pure enantiomers. Conditions are the same reported for case a

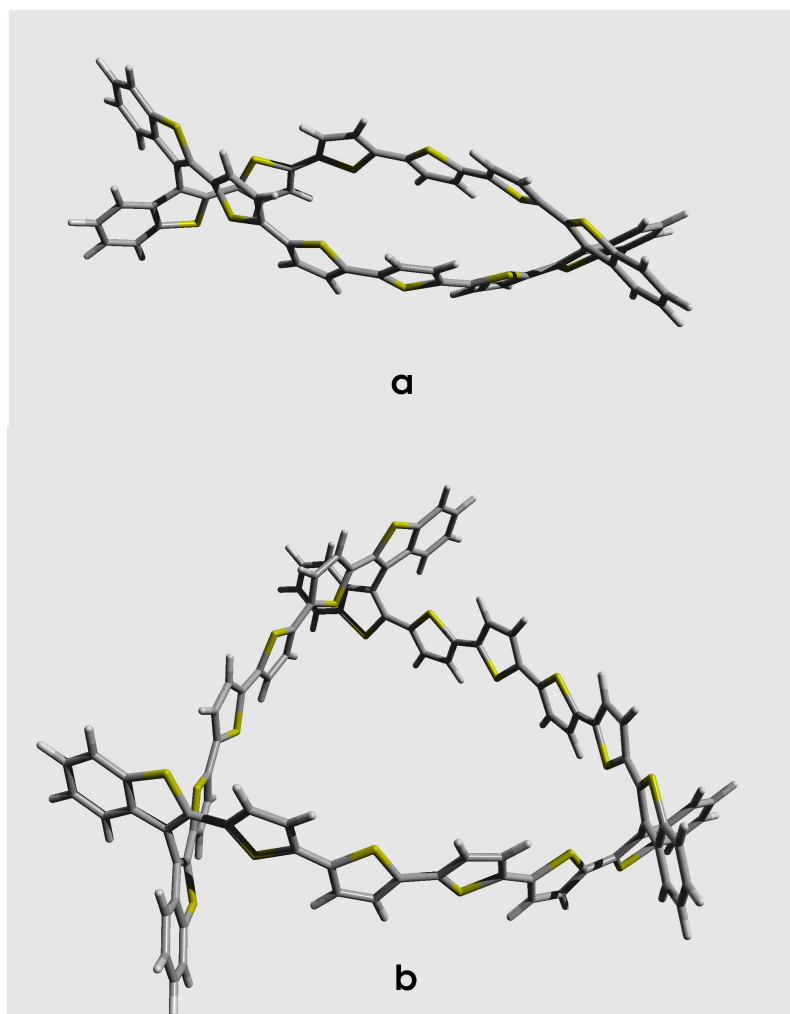


Figure 67. Calculated structures of: **a.** (*R,R*)-dimer and **b.** (*R,R,R*)-trimer performed by Dr. Rocco Martinazzo at Università degli Studi di Milano using Density Functional Theory (DFT) calculations in the generalized gradient approximation, employing the Perdew-Burke-Ernzerhof functional to handle exchange-correlation effects

The ^1H and ^{13}C NMR spectra of enantiopure cyclodimers and trimers (Figure 66) unequivocally proved the D_2 and D_3 symmetry of the molecules. According to stereotopism rules, only four coupled signals for the benzothiophene ring protons and four doublets for the protons in β -position of the two thiophene rings directly connected to it are observed in the ^1H NMR spectra (Figure 69), while only sixteen signals are observed in the ^{13}C NMR spectra.

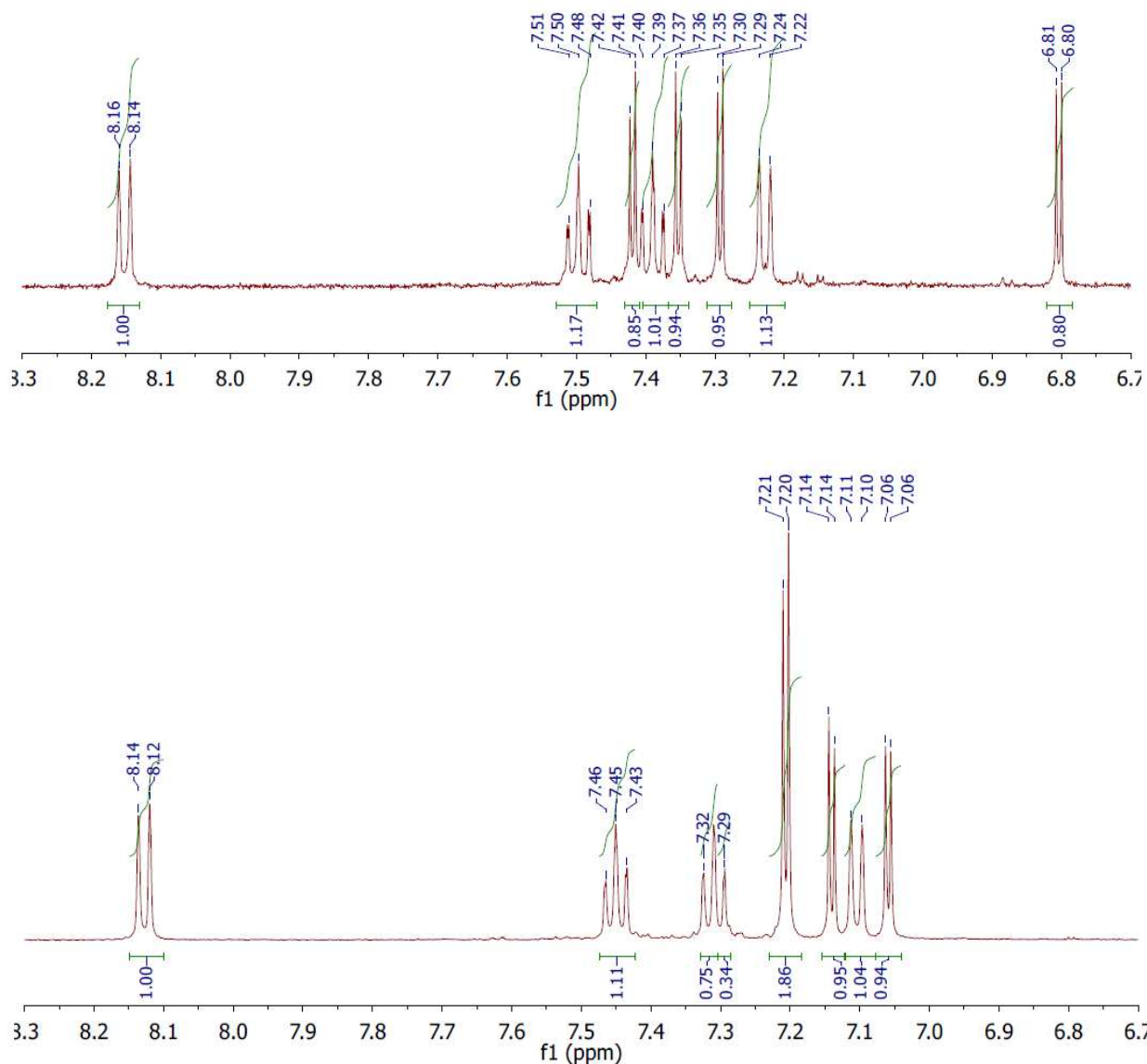


Figure 69. ^1H NMR (above) of $(R,R/S,S)$ -dimer ($d_6\text{DMSO}$, $40\text{ }^\circ\text{C}$).
 ^1H NMR (below) of $(R,R,R/S,S,S)$ -trimer ($d_6\text{DMSO}$, $40\text{ }^\circ\text{C}$).

From the spectroscopic point of view, both dimer and trimer display absorption maxima significantly red-shifted with respect to that observed for the T_4BT_2 monomeric unit, and attributable to the spin allowed π - π^* transition ($\lambda_{\text{max}} = 423\text{ nm}$, $\epsilon = 5.3 \times 10^4\text{ M}^{-1}\text{ cm}^{-1}$, for dimer, $\lambda_{\text{max}} = 447\text{ nm}$, $\epsilon = 1.3 \times 10^5\text{ M}^{-1}\text{ cm}^{-1}$, for trimer and $\lambda_{\text{max}} = 372\text{ nm}$, $\epsilon = 4.8 \times 10^4\text{ M}^{-1}\text{ cm}^{-1}$ for T_4BT_2 in CH_2Cl_2 solution). This feature is in agreement with the extended π -conjugated system involving the six α -linked thiophene units. However it is interesting to note that the absorption maximum of dimer is slightly blue-shifted with respect to that of the

corresponding linear α -sexithiophene ($\lambda_{\text{max}} = 445 \text{ nm}$, $\epsilon = 5.0 \times 10^4 \text{ M}^{-1} \text{ cm}^{-1}$) [25]. This is mainly due to the constraint of the atropisomeric scaffolds, which bends outwards the two sequences of the six α -linked thiophene units in dimers with consequent conjugation loss. A sterically more relaxed situation characterizes trimers, where the rings of the α -sexithiophene sequences are coplanar, with remarkable gain in conjugation extent. However, the broad features of the absorption spectra indicate that dimer and trimer still maintain conformational flexibility in the ground state.

3.4.1 Chiroptical Properties of Enantiopure Ringlets

The most fascinating structural features of these compounds are, however, their chiral electroactive cavities, characterized by different internal sizes and shapes, small and elliptical in the case of dimer (the major and minor axis lengths are about 17.7 and 5.8 Å respectively) and quite large, equilateral triangular, in the case of trimer (side of the triangle: ~17.9 Å long; geometrical height: ~17.0 Å).

The chiroptical manifestations of the antipodes of dimer and trimer are outstanding, as expected, since produced by extended inherently dissymmetric chromophores (Figure 70 and Table 3).

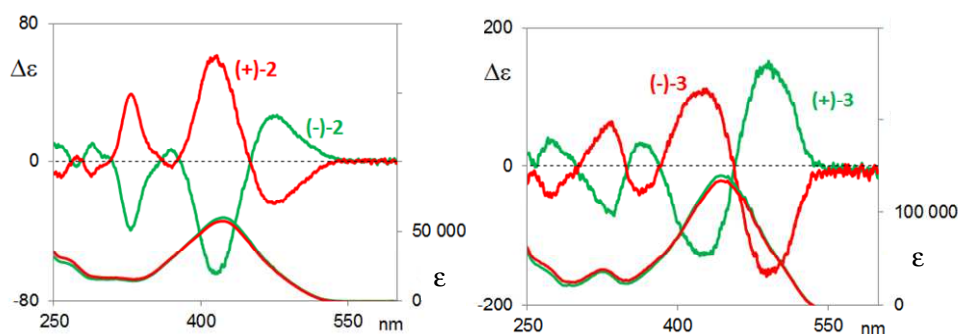


Figure 70. CD and UV spectra of (*S,S*)-(-)-2-dimer and (*R,R*)-(+)-2-dimer (6.0×10^{-6} M) and of (*S,S,S*)-(+)-3-trimer and (*R,R,R*)-(-)-3-trimer (3.0×10^{-6} M). Spectra of enantiomers with *S* stereogenic axes configuration are in green, with *R* configuration in red

DIMER (2)	TRIMER (3)
(-)-2: $[\alpha]_{D^{25}} = -132$ ($c = 0.10$ g/100 cm ³)	(+)-3: $[\alpha]_{D^{25}} = +2254$ ($c = 0.08$ g/100 cm ³)
(+)-2: $[\alpha]_{D^{25}} = +132$ ($c = 0.11$ g/100 cm ³)	(-)-3: $[\alpha]_{D^{25}} = -2316$ ($c = 0.04$ g/100 cm ³)

Table 3. Optical rotation values for (*S,S*)-(-)-dimer and (*R,R*)-(+)-dimer and of (*S,S,S*)-(+)-trimer and (*R,R,R*)-(-)-trimer

Preliminary experiments on enantiopure dimer and trimer have been focused: *i*) to evaluate their Circularly Polarized Luminescence (CPL) activity; *ii*) to check their enantio-recognition capability in front of classical ferrocene-based chiral probes.

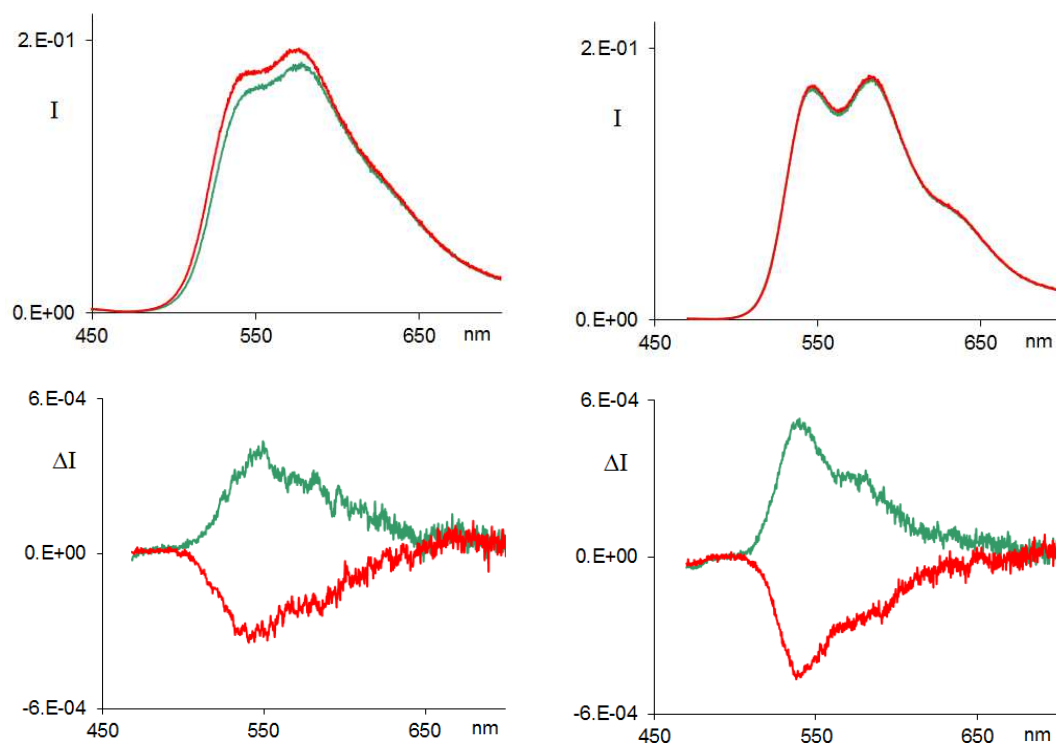


Figure 71. Above: emission spectra of (–)-dimer (green) and (+)-dimer (6.0×10^{-6} M) and of (+)-trimer (green) and (–)-trimer (3.0×10^{-6} M) in aerated toluene solution at room temperature. Emission spectra were corrected for emission spectral response (detector and grating) by standards correction curves. Below: CPL of (–)-dimer and (+)-dimer and CPL of (+)-trimer and (–)-trimer under the same conditions. Spectra of enantiomers with (*S*) stereogenic axes configuration are in green, with (*R*) configuration in red

Fluorescence and CPL simultaneous measurements have been carried out in a toluene solution, at *r.t.* ($\lambda_{\text{exc}} = 450$ nm for dimer and 470 nm for trimer). Upon optical excitation both dimer and trimer display intense orange-yellow vibrationally structured emission at $\lambda_{\text{em}} = 545, 573$ nm and 542, 580 nm respectively. These structured emissions are consistent with the planar quinoid-like structure proposed for the singlet excited-state of oligothiophenes [26]). The Stokes shift ($\Delta = 122$ nm) observed for dimer, larger than that observed for trimer ($\Delta = 96$ nm), suggests that the ground state of the latter better matches the quinoid-like geometry of the excited state requiring less conformational

reorganization. This feature is in agreement with the more planar conformation of the α -sexithiophene sequences in trimer as indicated by DFT calculations and absorption features. The extent of backbone rigidity in the excited state has a significant impact on the photoluminescence quantum yields (Φ_F), which are found to be 16% and 37% for dimer and trimer respectively. The more accessible non-radiative deactivation pathways, favored by torsional vibration motions and responsible for the lower quantum yields observed for dimer, match the high steric constrain of this species, both in ground and excited states. The CPL emission is notable, with an anisotropy g factor close to $3 \cdot 10^{-3}$, comparable with what observed in other inherently chiral molecules like helicenes. [27]

These properties suggest possible applications of these materials in chiroptical devices.

Tests of the enantio-recognition capability of the enantiopure macrocycles have been performed on gold screen printed electrodes in BMIMPF₆, employing the (*S*)-(-)- and (*R*)-(+)-*N,N*-dimethyl-1-ferrocenylethylamine as chiral probes.

On the bare gold electrodes enantiomeric chiral probes result in the same CV pattern, a diffusive reversible peak at a formal potential very similar to the ferrocene one. Coating the electrodes with the enantiomers of dimer and trimer outstanding enantio-recognition is achieved (Figure 72).

In particular,

- the electrodes coated with the enantiomeric (*R,R*)-(+)- and (*S,S*)-(-)-cyclodimers result in specular separation of enantiopure (*R*)- and (*S*)-chiral probes, with a E_{pa} separation of ~ 90 mV;
- a slightly larger E_{pa} separation (~ 110 mV) is obtained with the electrodes coated with enantiomeric (*R,R,R*)-(-)- and (*S,S,S*)-(+)-cyclotrimers.

It is worthwhile noticing that, unlike the performances of the films displayed by electrooligomerization of enantiopure T₄BT₂, [5] the CV peak morphology resembles a reversible diffusional process (distance of 60–70 mV between forward and backward peak

even at low scan rates) rather than a solid state one (specular forward and backward peaks). This could point either to a different mode in the approach of the probe molecule to the gold surface within the film and/or to the fact that the reaction occurs on the film surface, slightly charged at the potential at which the electron transfer takes place.

Finally, the enantioselection performance in the case of experiments with the (\pm)-racemic chiral probe is spectacular:

- the electrodes coated with (*S,S*)-(-)-dimer result in a 190 mV E_{pa} separation;
- also in this case, the electrodes coated with enantiopure (*S,S,S*)-(+)-trimer perform slightly better than those coated with the corresponding dimer, resulting in an impressive 210 mV E_{pa} separation.

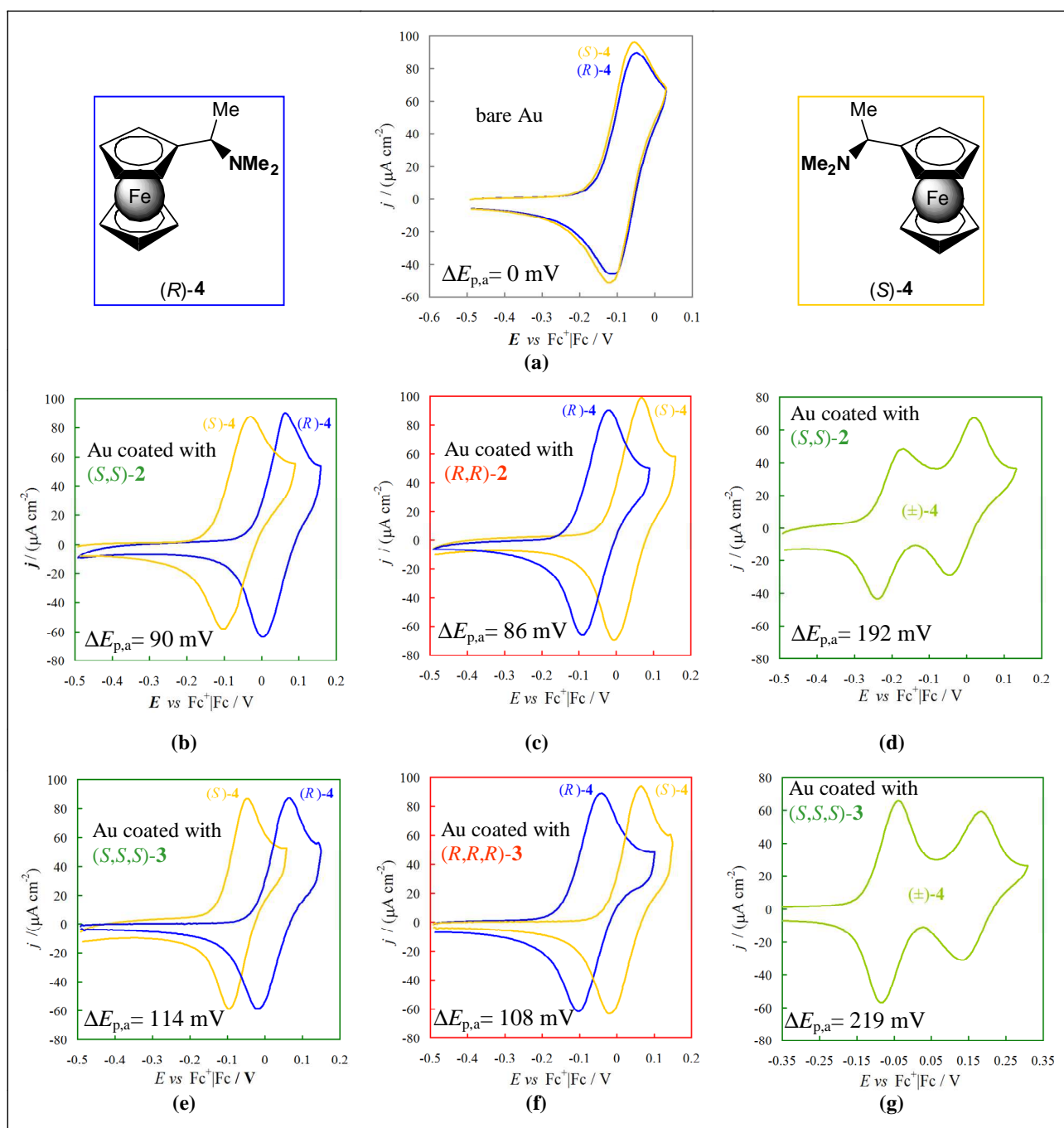


Figure 72. Enantioselective electrocatalysis tests with enantiopure (S)-probe (dark yellow curves), enantiopure (R)-probe (blue curves) and (±)-racemic probe (green curve) on **a.** bare Au and on enantiopure films of: **b.** (S,S)-dimer (green); **c.** (R,R)-dimer (red); **d.** (S,S)-dimer (green); **e.** (S,S,S)-trimer (green); **f.** (R,R,R)-trimer (red); **g.** (S,S,S)-trimer (green)

3.4.2 Electrochemistry of Chiral Macrocycles in BMIMPF₆

Films of enantiopure and racemic dimer and trimer, drop-casted on screen printed electrodes are electroactive and conducting, affording reversible and repeatable oxo-reduction cycles when tested in BMIMPF₆. The CV of enantiopure dimer displays a peculiarly sharp oxidation peak which is lost in racemic one, pointing to a better supramolecular organization. In all cases the activation of the redox sites strongly depends on the scan rate, in accordance with slow doping/undoping processes similar to those shown by oligothiophene films (Figure 73).

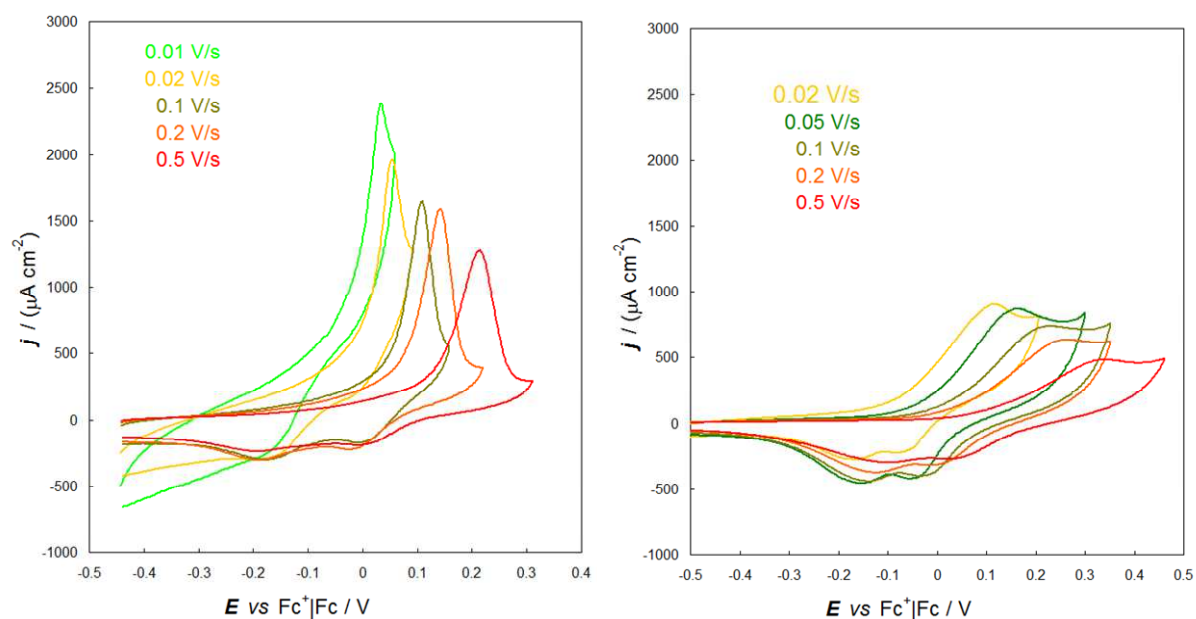


Figure 73. Scan rate effect on the electroactivity test of the films of drop-casted (*R,R*)-(+)-dimer (left) and (*S,S,S*)-(+)-trimer (right) on screen printed Au in BMIMPF₆

3.4.3 Characterization of Cavities also as Racemates: Electrochemistry of Racemate Macrocycles in Traditional Solvents

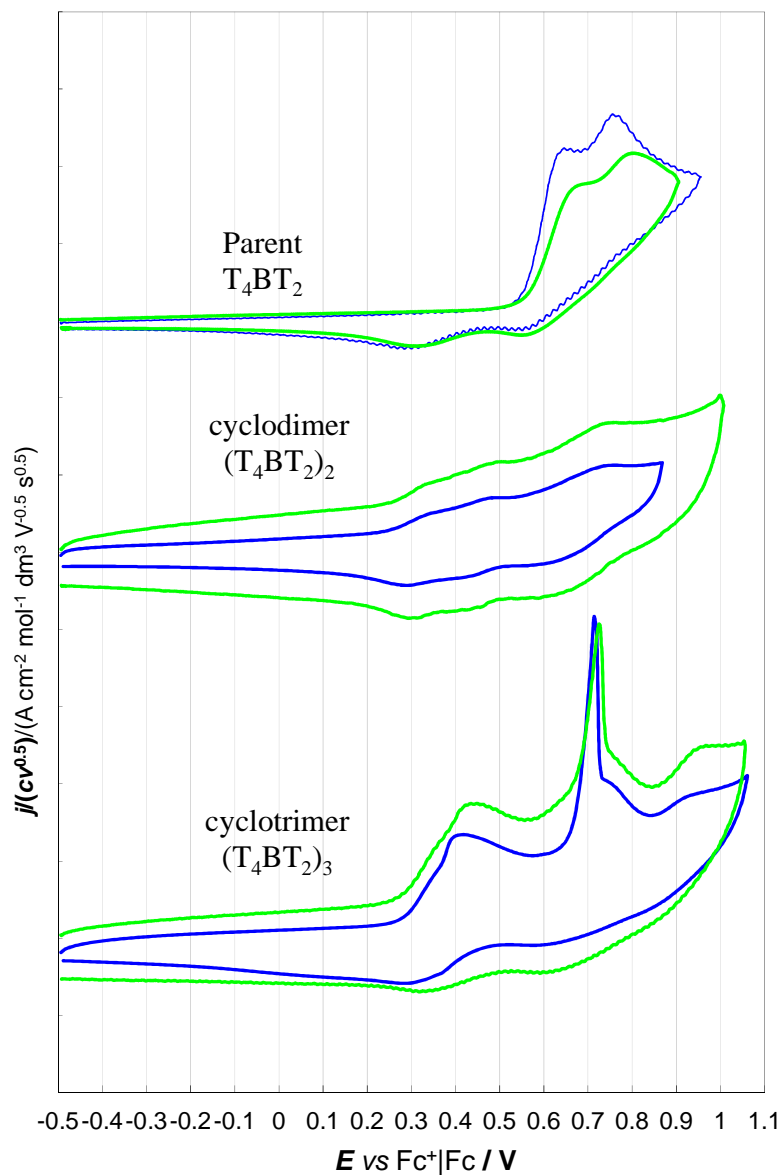
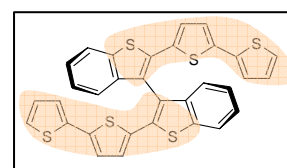


Figure 74. Synopsis of normalized CV patterns of racemic: T₄BT₂ monomer, cyclic dimer and cyclic trimer recorded in CH₂Cl₂ + TBAPF₆ 0.1 M on GC electrode both at 0.05 V s⁻¹ (blue line) and 0.2 V s⁻¹ (green line) potential scan rates. Substances concentration: 5·10⁻⁴ M

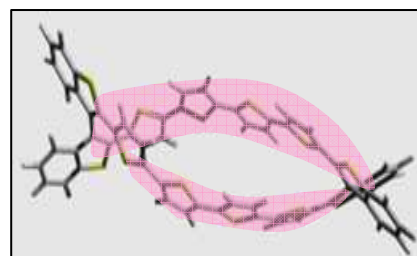
As already mentioned, benchmark T₄BT₂ shows two closely separated first oxidation peaks, corresponding to two equivalent and slightly interacting redox centers. Consistently, the first



oxidation peak potential, 0.64 V(Fc⁺|Fc), is similar to that of linear terthiophene T₃ (~0.58 V(Fc⁺|Fc)) [20]. A reduction peak is only perceivable in ACN, pointing to a HOMO-LUMO gap intermediate between a linear terthiophene and tetrathiophene (as said in the paragraph 3.1.1).

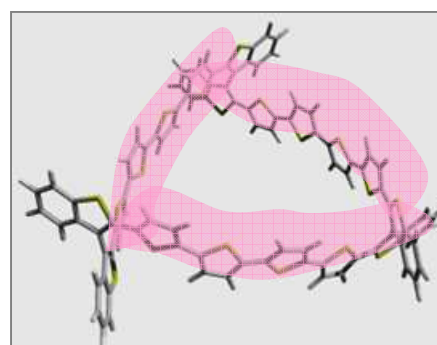
The cyclodimer features a first two-peak system followed by a single peak resulting from the merging of two very close ones (according to convolution), consistently with the presence of two (slightly twisted) hexathiophene chains, each of them accommodating two subsequently generated positive charges, and slightly reciprocally interacting in the 3D space.

Actually the first oxidation peak potential (0.34 V *vs* Fc⁺|Fc) and the separation between (average) first and second oxidation (0.34 V) are consistent with a distorted linear hexathiophene chain (considering that $E_{pl,a}$ is ~-0.43 V(Fc⁺|Fc) for T₄ and ~-0.28 V(Fc⁺|Fc) for T₆, and that $E_{pII,a} - E_{pl,a}$ is ~0.44 V for T₄ and ~0.22 V for T₆).



Unlike parent T₄BT₂, oxidations are chemically reversible, consistently with the lack of free thiophene α positions with the extended π system. The reduction peak is now well visible in CH₂Cl₂, this, too, demonstrates an improved conjugation of the cyclodimer with respect to the starting monomer.

The same considerations could be applied more or less to the mixture of racemate cyclotrimers, more complex, but also featuring two multiple peak systems separated by ~0.34 V(Fc⁺|Fc), with $E_{pl,a} = 0.34(\text{shoulder}) - 0.41$ V(Fc⁺|Fc); moreover a third peak can be perceived before the background at 0.93 V(Fc⁺|Fc) (actually linear T₆ chains can accommodate a third charge at ~-0.88 V(Fc⁺|Fc)).



The smaller splitting of the first oxidation peak system might be consistent with lower interchain interactions. Moreover an intriguing reproducible presence of a sharp peak

could point to some solid state process and/or a sudden molecular rearrangement. These peculiar features are currently under study. For comparison linear dimer (Figure 76) and cyclotetramer (Figure 77) were tested in the same conditions.

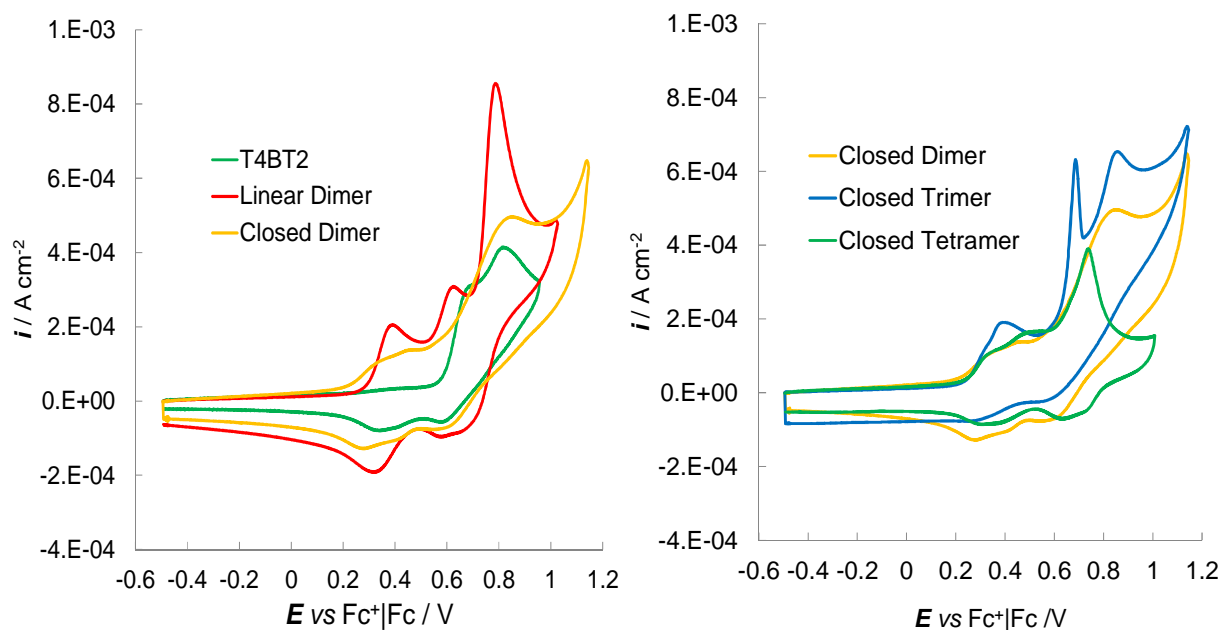


Figure 75. On the left: CV patterns of T4BT₂ monomer (green line), closed dimer (orange line) and linear dimer (red line) recorded in CH₂Cl₂+ TBAPF₆ 0.1 M at 200 mVs⁻¹ on GC electrode. On the right: CV patterns of closed dimer (orange line), closed trimer (light blue line) and closed tetramer (green line) recorded in the same above conditions. Substances concentrations: 5·10⁻⁴ M

In the case of linear dimer (red line in Figure 75 on the left) it is evident that there is no peak splitting in the first two oxidation peaks unlike the case of closed dimer consistently with the absence of interchain interaction due to the loss of cyclization. The third oxidation peak corresponds to the α -positions available for the oligomerization.

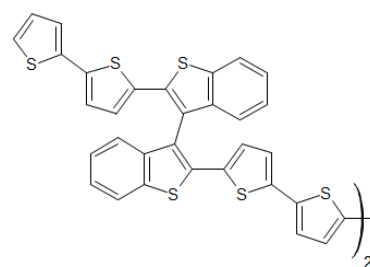


Figure 76. Molecular structure of linear dimer T4BT₂-LD

A splitting of the first oxidation peak is also observed for the cyclotetramer; intriguingly, it is higher than both those observed for the cyclodimer and the cyclotrimer.

We are planning a deeper investigation on this nice case of reciprocally interacting multiple and symmetrical redox centers.

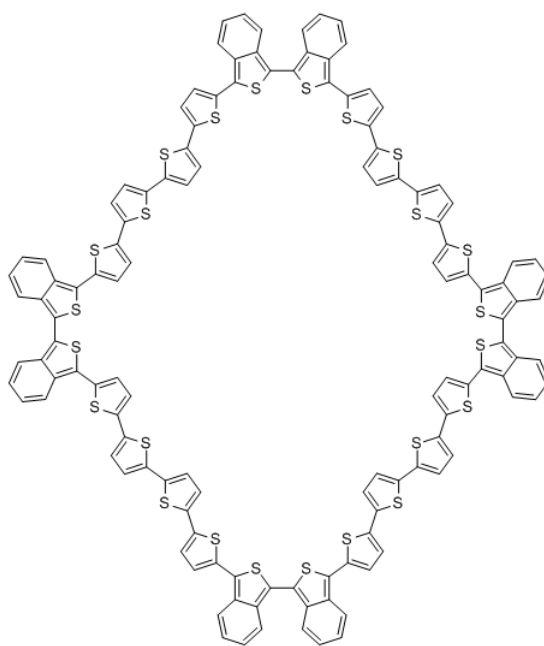
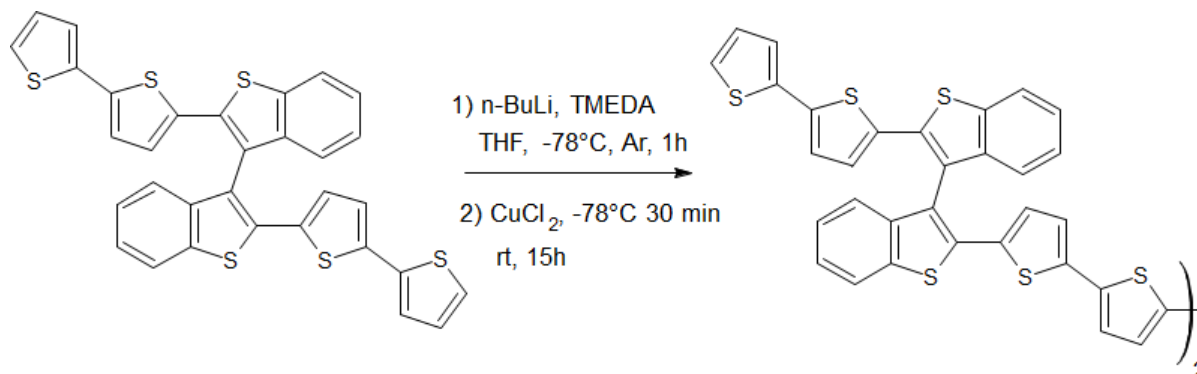


Figure 77. Chemical structure of closed tetramer

3.4.4 Focusing on Linear Dimers

The chemical synthesis of liner dimer T₄BT₂-LD is here below represented:



The reaction yield is about 30%, with the possibility to recover more or less 50% of the starter T₄BT₂ monomer. The separation of the racemic T₄BT₂-LD into enantiomers was successfully achieved at the semi-preparative scale level by HPLC on a chiral stationary phase, but in low quantities due to the scarce reaction yield (Figure 78). Together with the two enantiomers (LD-1 and LD-2) a meso form (51%) is also obtained.

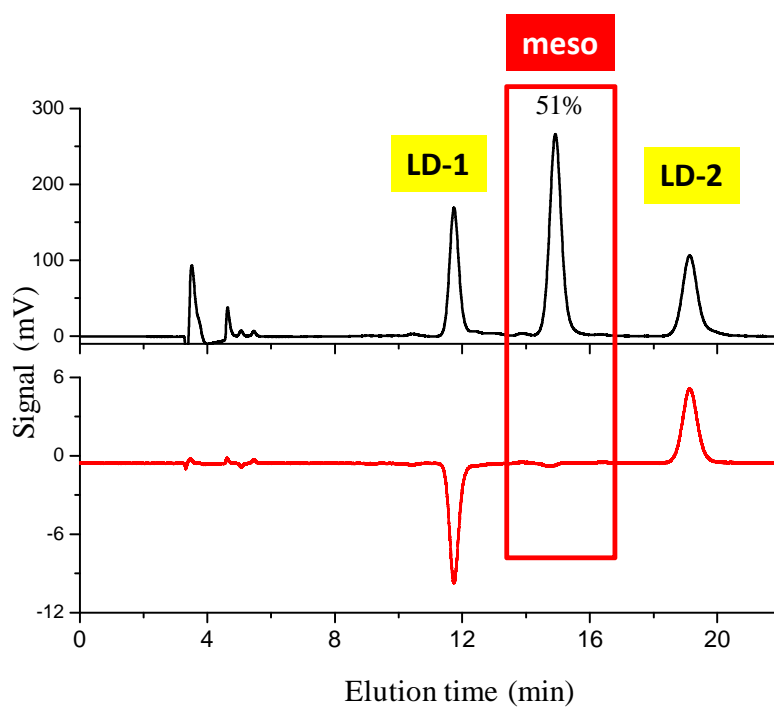


Figure 78. Enantiomeric separation of racemic T₄BT₂-LD. CSP: Chiralpak IB 250 mm x 4.6 mm I.D.. Eluent: *n*-hexane-CH₂Cl₂-ethanol: 100:10:2. Flow rate: 1 cm³ min⁻¹. Temperature: 25°C. Detector: UV (black) and CD (red) at 360 nm

Optical rotation measurements have evidenced higher values for linear dimer (LD) enantiomers than the closed dimer (CD) ones index of high chirality manifestations.

CLOSED DIMER	LINEAR DIMER
CD-1: $[\alpha]_{D^{25}}(\text{CHCl}_3) = -132$	LD-1: $[\alpha]_{D^{25}}(\text{CHCl}_3) = +1010$
CD-2: $[\alpha]_{D^{25}}(\text{CHCl}_3) = +132$	LD-2: $[\alpha]_{D^{25}}(\text{CHCl}_3) = -1360$

In progress is the optimization of the reaction and the subsequently fully characterization of the two enantiopure antipodes.

The difference between the closed dimer and the linear dimer is also evidenced in terms of ^1H NMR spectra.

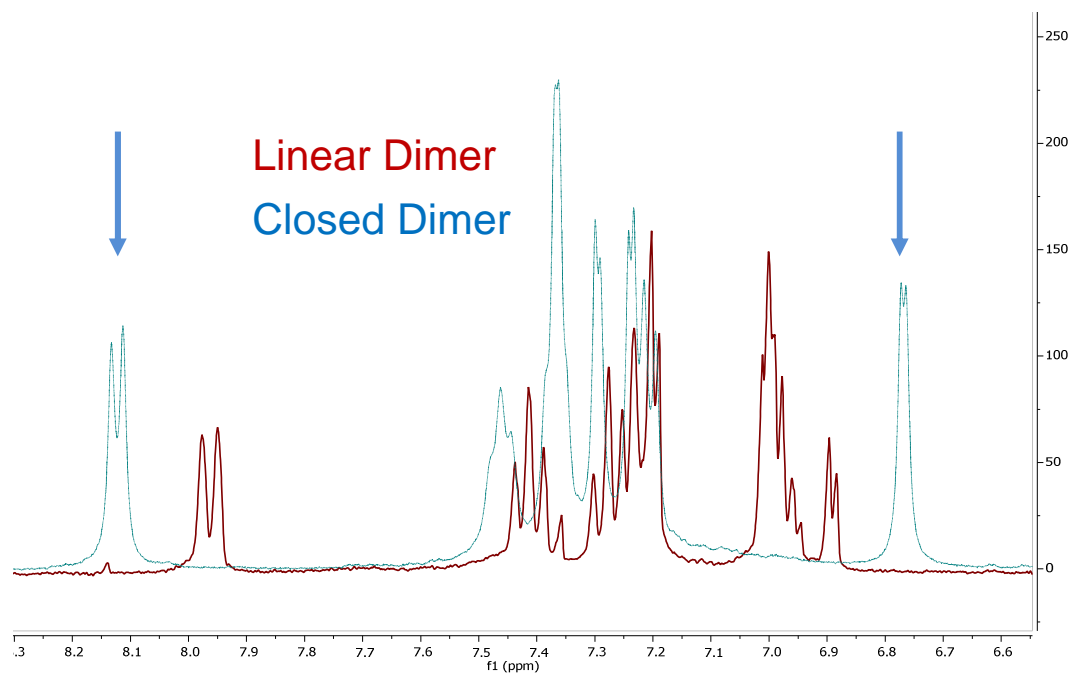


Figure 79. ^1H NMR spectra of linear dimer (d_6DMSO , $40\text{ }^\circ\text{C}$, red line) and closed dimer (d_6DMSO , $40\text{ }^\circ\text{C}$, blue line) superimposed for comparison

Respect to the ^1H NMR spectrum of closed dimer, the presence can be observed of a new doublet in the ^1H NMR spectrum of linear dimer corresponding to the proton in α position of the thiophene ring available for the oligomerization, and a doublet that became a triplet related to the proton in β position.

As expected, racemic $\text{T}_4\text{BT}_2\text{-LD}$ shows good attitude to electrooligomerization in traditional solvents like CH_2Cl_2 and ACN cycling around the third peak (Figure 75, on the left). Resulting films were very stable if tested in monomer-free solutions upon several redox cycles and exhibit a neat charge trapping effect.

3.4.5 Racemic Trimer Tested as a Donor in a Bulk-heterojunction Solar Cell

Parallely to T₆BT₂ (paragraph 3.1.5), the racemic trimer has also been tested as a donor in a bulk-heterojunction solar cell. The procedure was the same explained at the paragraph 3.1.5 and also in this case measurements have been carried out in cooperation with Istituto ENI Donegani (Novara).

The racemic trimer has shown the best performance in terms of efficiency. The highest obtained value (1.4 %,table 4) was observed when the trimer was used as donor in a mixture with PCBM (Figure 80).

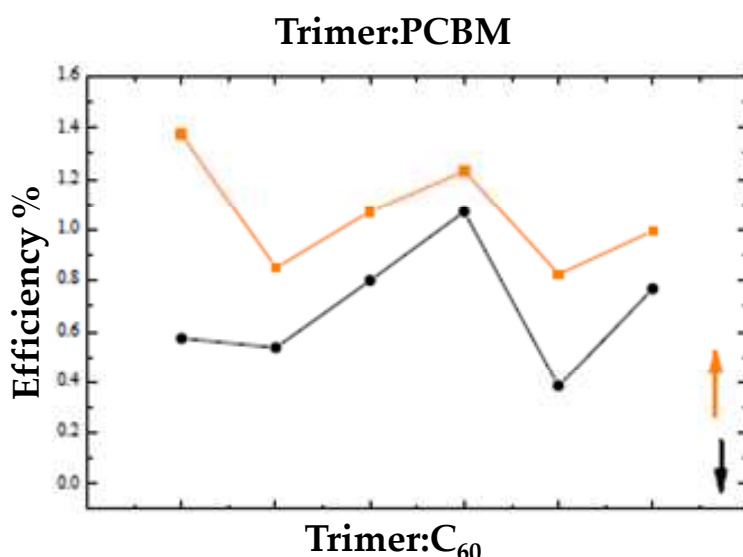


Figure 80. Efficiency values displayed by six cells prepared with two blends: *i*) (T₄BT₂)₃:PCBM (orange line) and *ii*) (T₄BT₂)₃:C₆₀ (black line)

Donors	η_{\max} %
Poli-T4 + C ₆₀	0.4
Poli-T4 + PCBM	1.2
Tri-T4 + C ₆₀	1.1
Tri-T4 + PCBM	1.4
Poli-T6 + C ₆₀	0.022
Poli-T6 + PCBM	0.30

Table 4. Comparison between different efficiency values obtained using the indicated blend

The results obtained employing the racemic trimer as donor can be considered satisfactory even if they do not reach the performances displayed by the standard blend P3HT:PCBM (~3.2% efficiency value). In fact they were obtained in the very first experiments, without optimization of the experimental conditions (evaporation and deposition techniques).

Reproducibility in the experimental set-up strictly depends on the film morphology and on the roughness of the film surfaces.

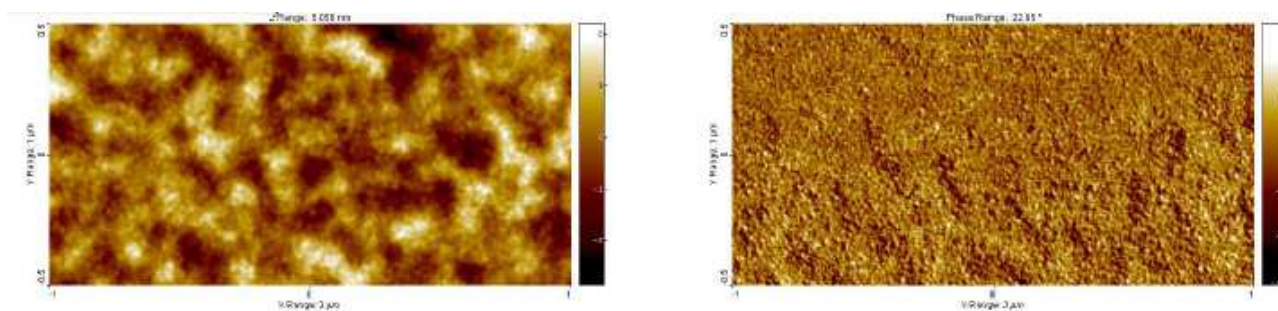


Figure 81. AFM images of the film obtained using the blend (T₄BT₂)₃:PCBM.

The RMS factor in case of (T₄BT₂)₃:PCBM blend is the lowest obtained, consistently with the best results displayed using this blend (Figure 81).

In conclusion the new oligothiophene macrocycles are not only aesthetically charming but operationally active molecules.

They display an impressive pool of outstanding properties as enantiopure antipodes and even as racemates. They idealize conducting polymers without ends, with electronic properties tunable with the cycle dimensions, competitive (even in cost) with popular molecular materials such as poly-3-hexyl-thiophene. Ringlets offer electrosensitive cavities of different sizes for selective inclusion of guest molecules and tuning the electric potential, they undergo reversible variations of both color and torsional angles.

The first α -cyclo[n]thiophenes, reported by Bäuerle *et al.* [28-35] a few years ago, were obtained in very low yields and achiral. Instead, the new cyclic oligomers characterized in our work are obtained in high yield and in a few steps from unexpensive reagents; moreover, combination of chirality with electroactivity makes these new cavities unique in the current library.

In the light of the fact that it has been demonstrated that the chemical and electrochemical oligomerization of T₄BT₂ monomer generates a series of interesting macrocycles (from dimer to hexamer), other oligomerization products generated from monomers with different atropisomeric scaffold (*e.g.* chemical nature) or different terminal bi-thiophenic units were analyzed.

For example the chemical oxidation of 2,2'-Ind₂T₄(N-Me) monomer chiefly consists of cyclic dimers instead in the case of (T₈)₃ monomer only linear oligomers are generated due to geometrical reasons. Work is in progress to characterize both chemically and electrochemically these new macrocycles in order to test their properties both as racemate and enantiopure antipodes (*e.g.* the enantio-recognition capability, or in solar cell as donor).

3.5 Study of the DET Process of Model Organic Halides in BMIMPF₆ Ionic Liquid

In the last years our research group, in collaboration with Padova University, has been performing a detailed mechanistic investigation on the electrocatalytic cleavage of carbon-halogen bonds, a process of fundamental and applicative interest in the analytical, synthetic and environmental fields. A lot of interpretative/predictive guidelines were thus developed, particularly concerning the process modulation by (a) the stepwise or concerted nature of the DET mechanism (as a function of the electrode surface, of the nature of the halogen atom, and of the molecular structure of RX) [36] and (b) the double layer structure (as a function of the nature and bulkiness of the supporting electrolyte ions) [37]. Recently, in order to both complete and support the above interpretative scheme, our attention has been focused on the solvent role, comparing aprotic solvents with protic organic solvents, and evidencing the attractive peculiarities of the latter, which dramatically enhance the electrocatalytic properties of silver and gold surfaces for the process. This study was the subject of my 5-year thesis research project [38].

With this background, we have decided to extend this study to room temperature ionic liquids (RTILs), which are currently raising considerable interest on account of their advantages over traditional organic solvents, including negligible vapour pressure, high intrinsic conductivity and easy recyclability. Moreover, RTILs appear attractive in the frame of the above mechanistic studies on account of their two-fold role as both solvent and supporting electrolyte, and of their high viscosity. In this frame, within this research a study was carried out on the reduction of model organic halides on glassy carbon GC, Au and Ag electrodes (behaving as non-catalytic, moderately catalytic, and highly catalytic electrodes, respectively, for the process under study, in traditional solvents), by a combination of cyclic voltammetry and electrochemical impedance spectroscopy, evaluating (i) whether the catalytic effects also persist in ionic liquids and to what extent, and if there is any relationship with the nature of the electrode material; (ii) whether in

ionic liquids the same relations previously observed in traditional media still hold between catalytic effects and molecular structure of the halide.

3.5.1 Electrochemical characterization: BMIMPF₆ vs ACN

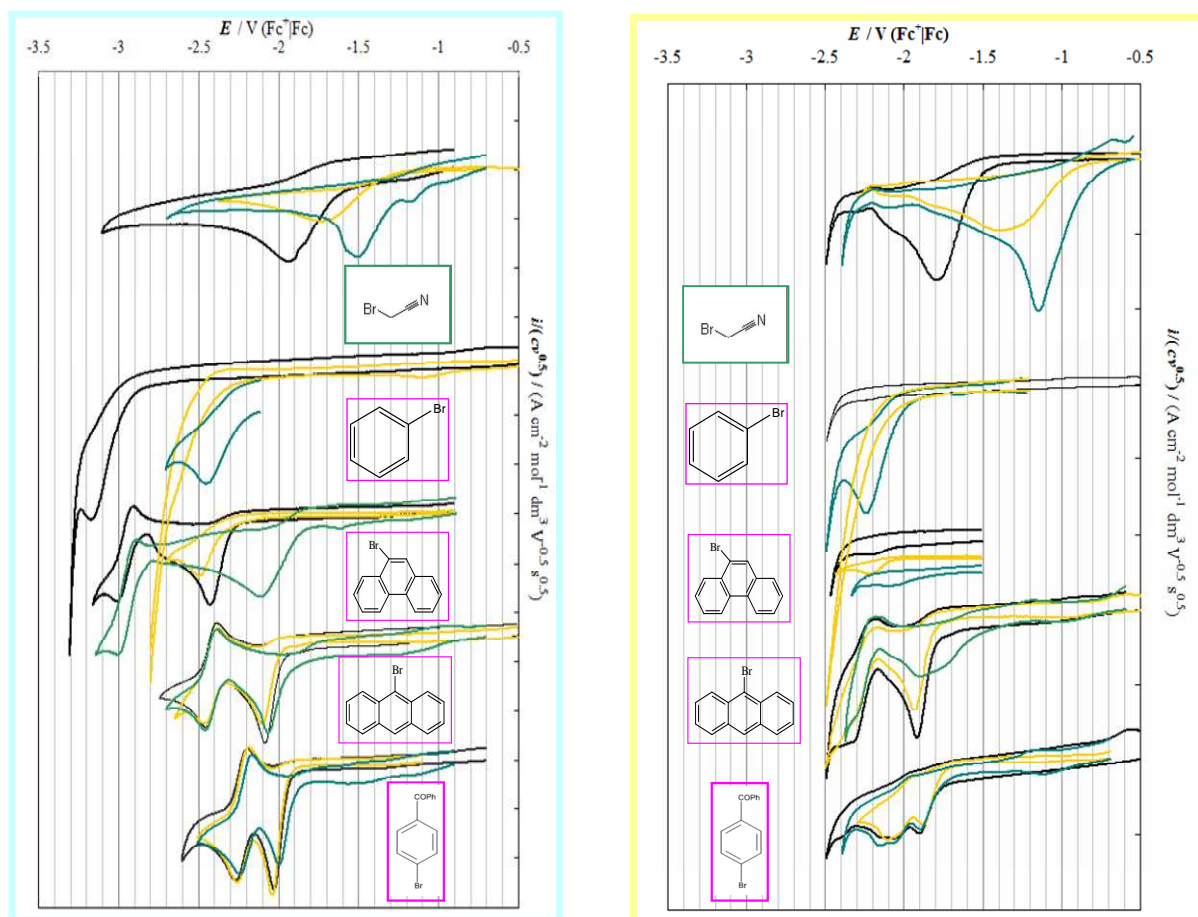


Figure 82. Synopsis of CV patterns recorded in ACN + TBAPF₆ (on the left) and in BMIMPF₆ (on the right) for model organic halides represented at the side of the figures (concentrations: $7.5 \cdot 10^{-4}$ M in ACN and $7.5 \cdot 10^{-3}$ M in BMIMPF₆) at 200 mVs^{-1} on GC (black line), Au (yellow line) and Ag (green line) electrodes. Potentials are referred to the standard redox couple Fc^+/Fc

The model organic halides chosen for this study were the following ones, in ascending order of mechanistic κ parameter, accounting for the DET mechanism and rate determining step¹ :

- bromo-acetonitrile (the only aliphatic molecule),
- bromobenzene,
- 9-bromophenanthrene
- 9-bromoanthracene
- 4-bromo-benzophenone

Parallel CV experiments were performed on the above molecules in a traditional medium (ACN + TBAPF₆) and in a room temperature ionic liquid with the same counter anion, BMIMPF₆.

It is interesting to notice that even working in the ionic liquid with a ten-time higher concentration results in lower current intensities (~1/10) than those obtained when ACN solvent was used, consistently with the huge viscosity difference between the two media (220 cP *vs* 0.343 cP).

The CV experiments are summarized in Figure 82. The results point to the following features:

- the same concerted and stepwise mechanism observed for the investigated molecules in the traditional ACN solvent is maintained in the ionic liquid;
- even after intersolvental normalization, all reduction peak potentials appear significantly less negative in BMIMPF₆;

¹ κ values can range between 0 and 1. κ values below 0.3-0.35 generally indicate a concerted mechanism, implying concurrent electron transfer and bond cleavage, with the electron transfer as the rate determining step; this mechanism is typically thermodynamically more favourable and kinetically less favourable. Higher κ values indicate a stepwise mechanism, implying a first electron transfer step resulting in a radical anion intermediate, followed by a second chemical step of bond cleavage. The higher the κ value, the more kinetically determining is the chemical step upon the electron transfer one. This mechanism is typically thermodynamically less favourable and kinetically more favourable. [Abdirisak A. Isse, Patrizia R. Mussini and Armando Gennaro, *J. Phys. Chem. C*, **2009**, 113, 14983]

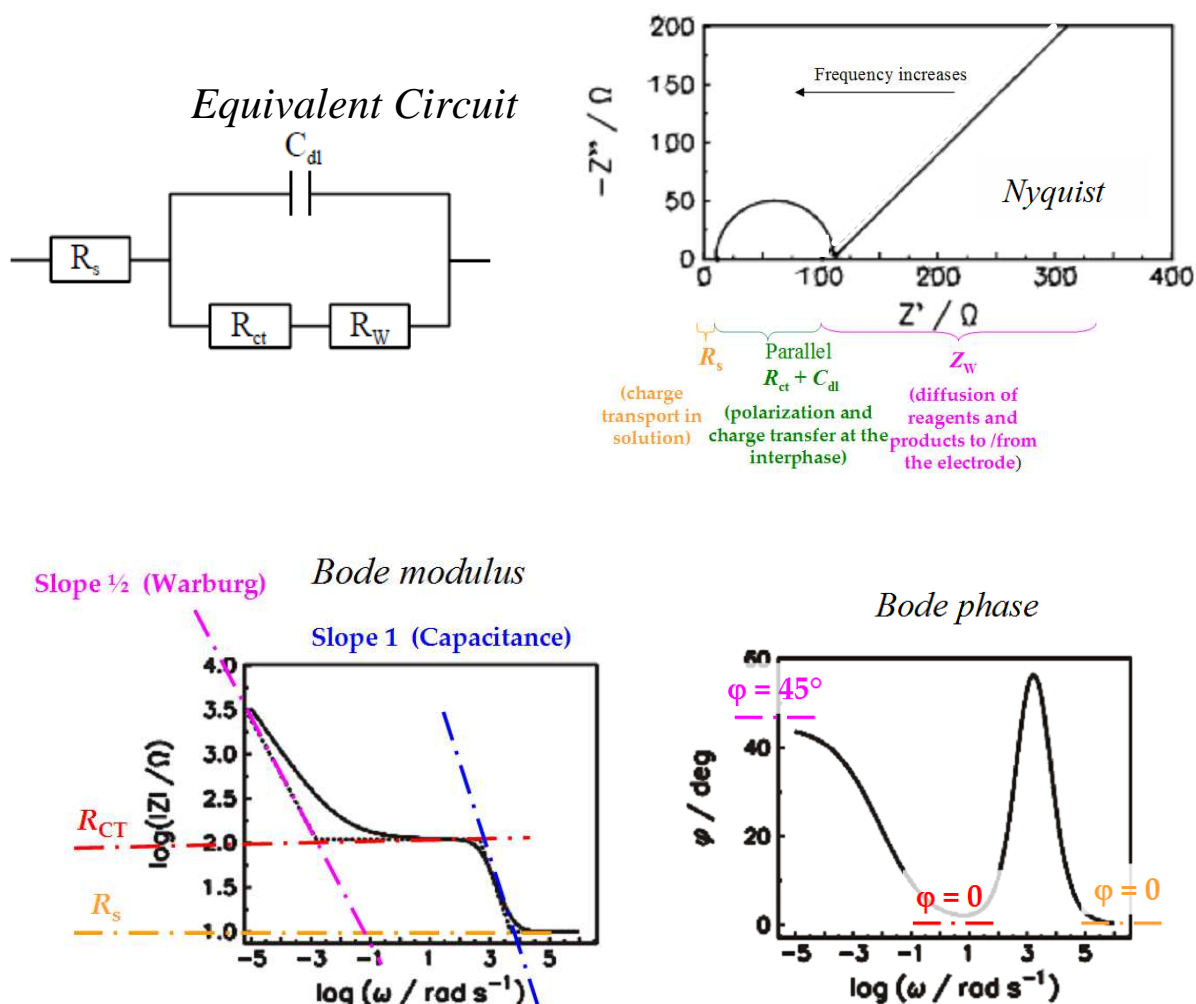
- the positive shift is particularly conspicuous in the concerted case (bromoacetonitrile);
- in the same concerted case, BMIMPF₆ results in much higher catalytic effects with respect to ACN, both on Ag and Au electrodes.
- the chemical reversibility of the second reduction peak concerning the aromatic system of aryl halide substrates decreases in the ionic liquid (a feature similar to that observed for protic solvents in our cited former study on the effect of protic and aprotic traditional solvents on the carbon-halide electrocatalytic cleavage);
- as in ACN, catalytic effects on Ag increase with decreasing κ , *i.e.* with increasing importance of the electron transfer step, in the stepwise series.

The highest catalytic effect is observed for the concerted case.

3.5.2 EIS Characterization: BMIMPF₆ vs ACN

EIS studies have been carried out, for the first time in our knowledge, in the context of mechanistic studies of carbon-halide bond cleavages, aiming to verify whether it is possible to find a relationship between the κ parameter obtained by CV measurements and the EIS parameter R_{CT} accounting for the electron transfer activation barrier.

A classical Randles equivalent circuit also including a Warburg impedance term to account for semi-infinite reactant diffusion was taken into consideration, with the implications summarized in the scheme below:



It must be preliminarily noted that in all experiments an additional capacitance C in parallel with the R_s element accounting for electrolyte resistance was actually observed (Figure 83, focusing on the highest frequency range). This might be associated to the geometric cell capacitance, which in this case could be perceivable because of the short distance between the electrodes in our operating conditions. This would imply a high C , resulting in low capacitive reactance, which therefore becomes significant in the parallel with R_s).

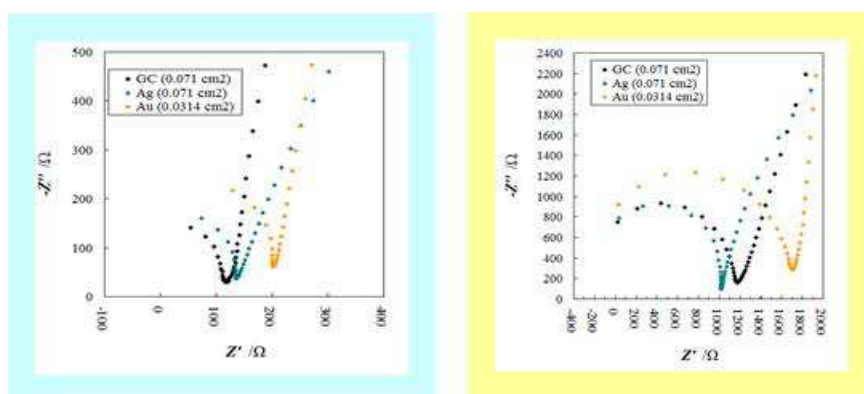


Figure 83. Nyquist plots obtained focusing on the high frequencies to highlight R_s parameter of the two systems: ACN (on the right) and BMIMPF₆ (on the left)

Figures 84 and 85 report selected EIS results in ACN + 0.1 M TBAPF₆ and BMIMPF₆, respectively.

According to our working assumption, R_{CT} should be proportional to the activation energy barrier, increasing with decreasing κ , *i.e.* with increasing kinetic influence of the ET activation barrier. Actually, looking at the four examples in ACN medium collected in Figure 5, the highest R_{CT} is observed in the concerted case (the one also resulting in the highest electrocatalytic effects).

In the BMIMPF₆ case R_{CT} and especially R_s values (the latter evidenced in Figure 4) appear to be higher with respect to parallel ACN cases. Unfortunately only two systems could be satisfactorily characterized; in such systems, R_{CT} appears to exhibit the expected correlation with the DET mechanism at least on Au, and, albeit less evidently, GC.

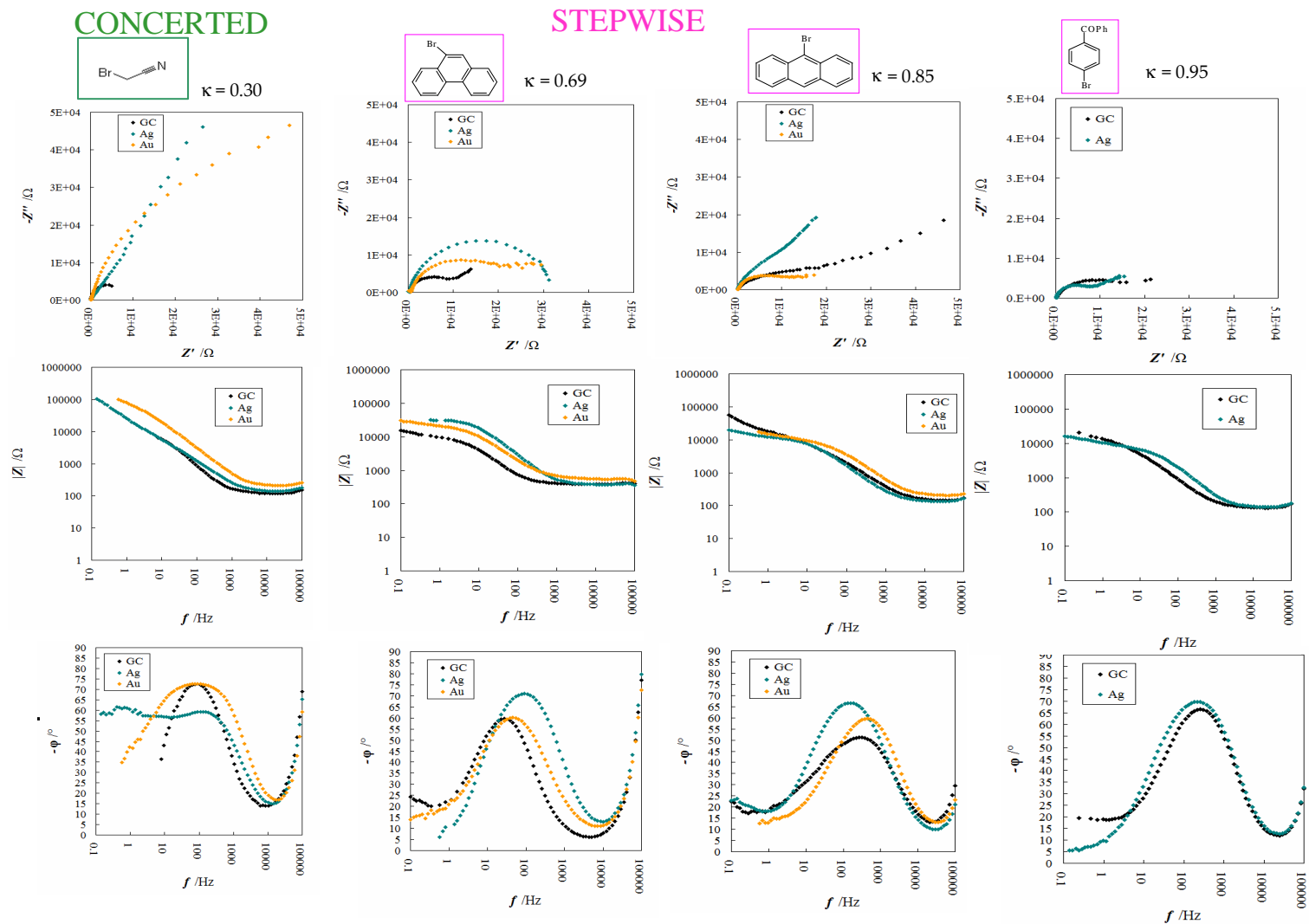
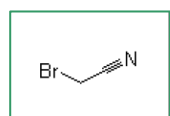
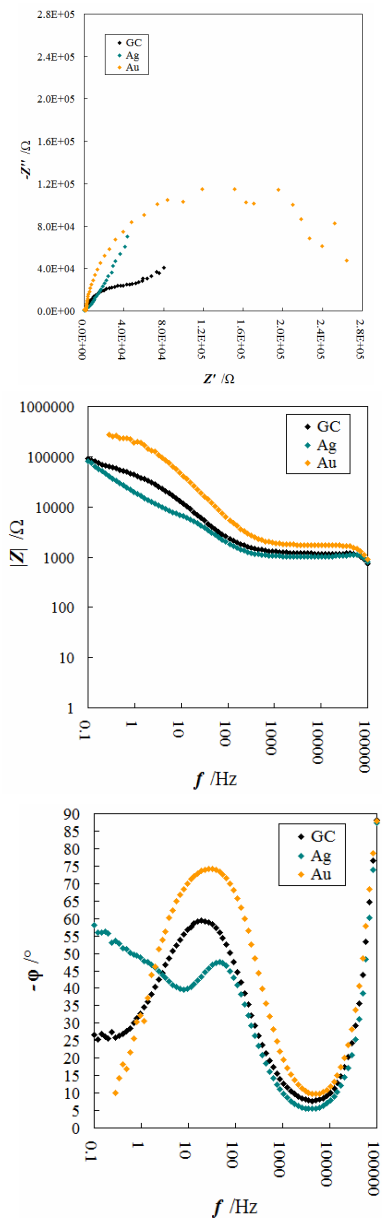


Figure 84. Nyquist, Bode modulus and Bode phase diagrams for the reduction a series of organic bromides representative of concerted and stepwise mechanisms, on Ag (green), Au (yellow) and GC (black) in ACN + 0.1 M TBAPF₆.

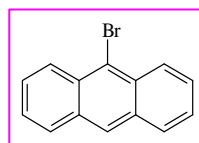
CONCERTED



$\kappa = 0.30$



STEPWISE



$\kappa = 0.85$

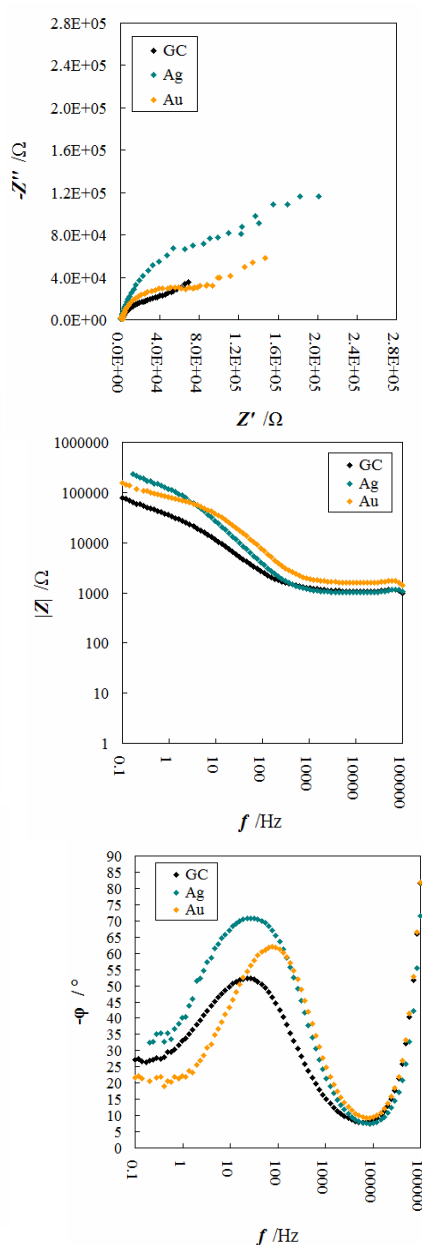


Figure 85. Nyquist, Bode modulus and Bode phase diagrams for the reduction of two organic bromides representative of concerted and stepwise mechanisms, on Ag (green), Au (yellow) and GC (black), in BMIMPF₆

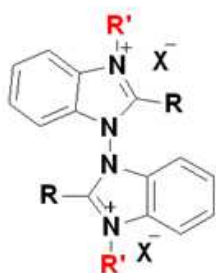
The study will be completed with more model molecules, but it already points to attracting potentialities of EIS as investigation technique complementary to voltammetry in DET mechanistic studies.

3.6 Inherently Chiral Ionic Liquids

The final part of the thesis has been dedicated to the development of a new class of chiral ionic liquids named 'inherently chiral ionic liquids' (ICILs) obtained by combining the common properties of the commercial achiral ionic liquids with the concept of inherent chirality.

In these frame three different families of mono- and di-alkylated ICILs have been synthesized:

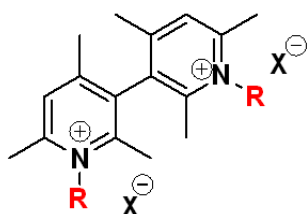
- 1,1'-Bis(benzimidazolium) salts



- 2,2'-Bis(benzimidazolium) salts



- 3,3'-Bis(pyridinium) salts



3.6.1 1,1' Bis-benzimidazole-based Inherently Chiral Ionic Liquids

3.6.1.1 2,2'-Dialkyl-1,1'-Bis-benzimidazole Scaffolds

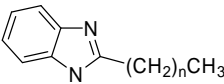
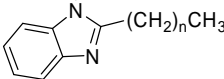
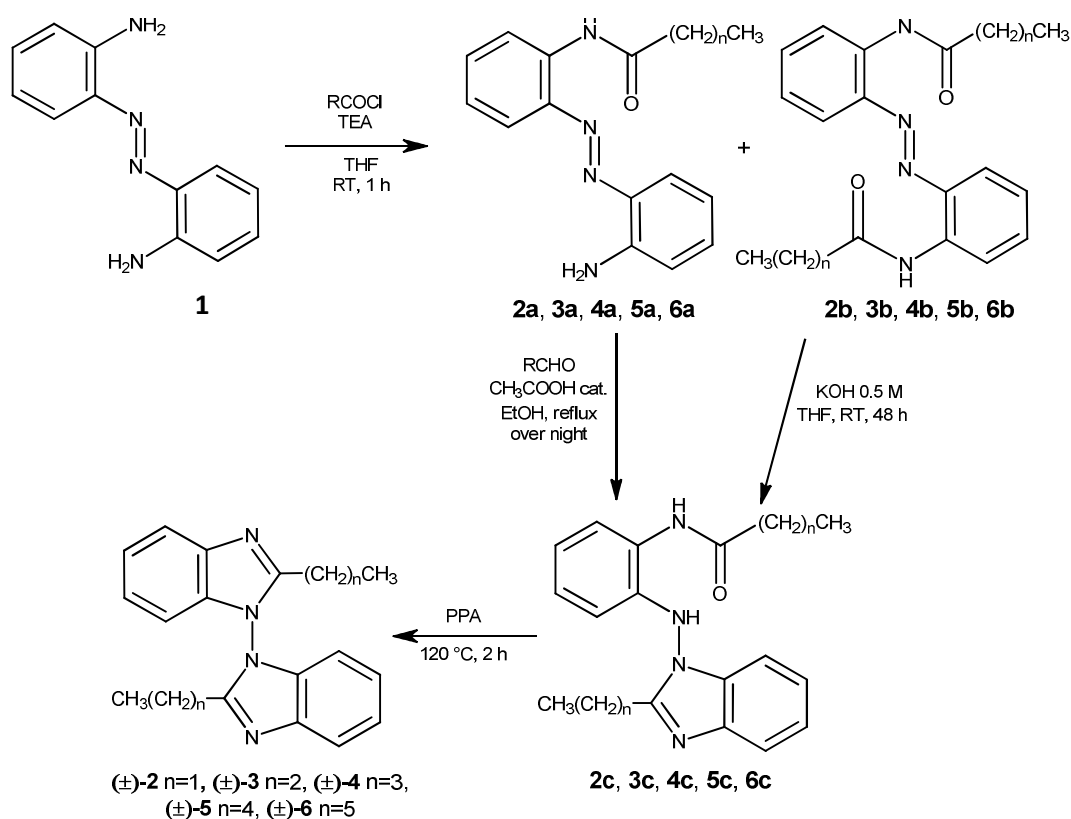
	Compound	n
	(1)	(0)
	2	1
	3	2
	4	3
	5	4
	6	5

Table 5. Summary of all 2,2'-dialkyl-1,1'-bibenzimidazole scaffolds synthesized

a. Synthesis

The general scheme for the synthesis of the 2,2'-dialkyl-1,1'-bibenzimidazoles (**2-6**; **1** is a commercial product) is reported below:



Scheme 2. Preparation of 1,1' bisbenzimidazole scaffolds

Calculated structures and torsional angles for the scaffold series are collected in Figure 86.

Theoretical calculations were performed by Prof. Marco Pierini, Università di Roma 'La

Sapienza'. All structures seem to have a high racemization barrier suitable for separation of enantiomers.

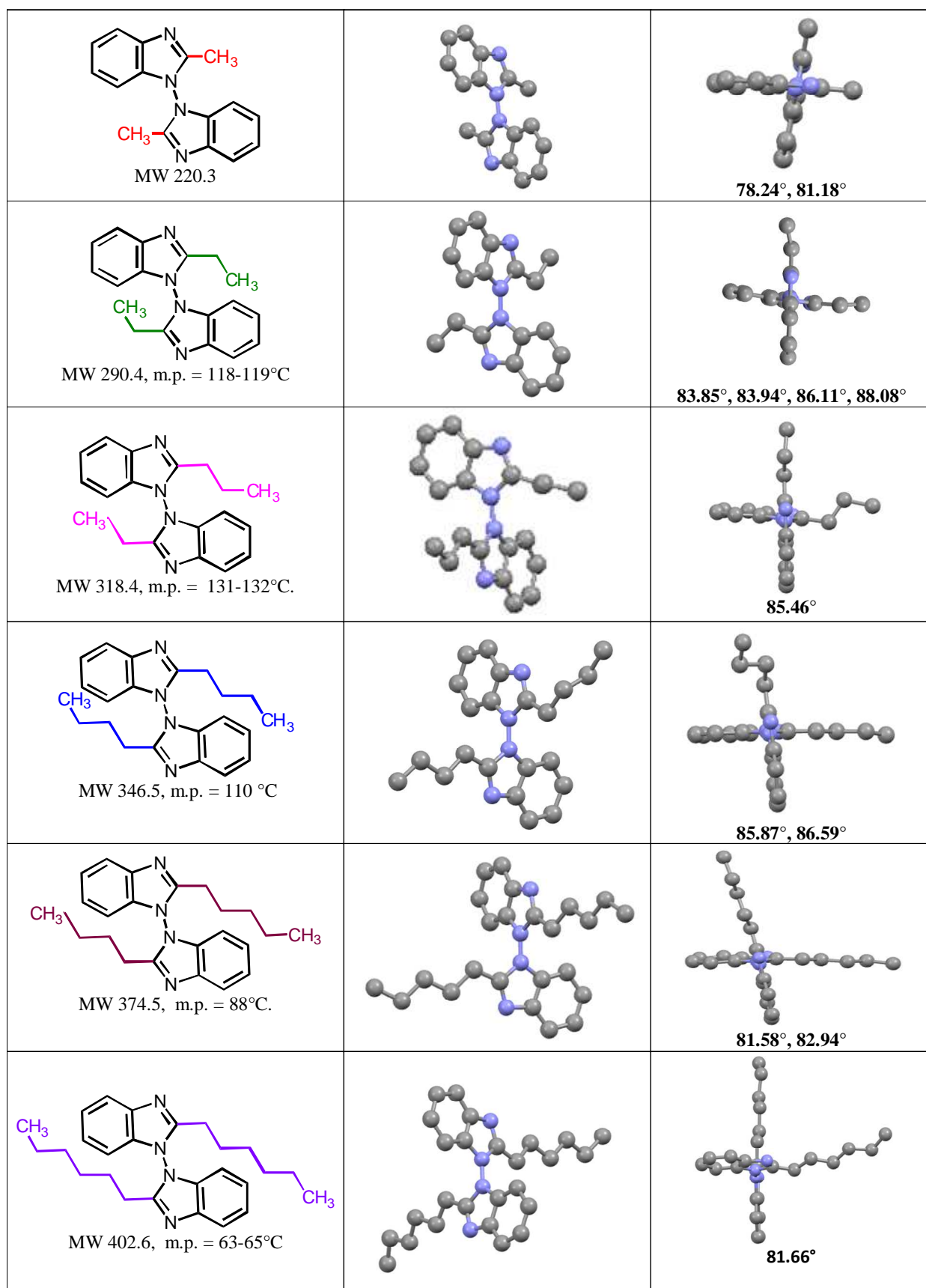


Figure 86. 1,1'-bis-benzimidazole scaffold calculated structures

b Enantiomer separation and absolute configuration assignment

(performed by Dr. Roberto Cirilli, Istituto Superiore di Sanità, Rome and Prof. Marco Pierini, Università di Roma La Sapienza)

Racemic mixtures of **1-6** (Table 5) were resolved on a semipreparative scale under the operating conditions resumed in Table 6, using a commercially available 250 mm x 10 mm I.D. Chiralpak AD column (Figure 87), a PerkinElmer 200 LC pump equipped with a Rheodyne injector, a 500 μ L sample loop, a PerkinElmer LC 101 oven and a Waters 484 detector (Waters Corporation, Milford, MA, USA).

Table 6. Chromatographic conditions for the semipreparative enantioseparation of **1-6**. Column: Chiralpak AD (250 mm x 10 mm I.D); flow-rate: 5.0 cm³ min⁻¹; detector: UV at 290 nm.

Compound	Mobile phase	Column temperature (°C)	A ^a /V ^b
1	n-hexane-ethanol 100:10	40	20/0.5
2	n-hexane-ethanol 100:10	25	10/0.5
3	n-hexane-ethanol 100:10	25	3/0.1
4	n-hexane-2-propanol 100:10	10	1/0.1
5	n-hexane-2-propanol 100:10	10	2/0.2
6	n-hexane-ethanol 100:10	10	3/0.2

^a amount of sample (in mg) resolved in a single semipreparative run.

^b volume of sample (in cm³)

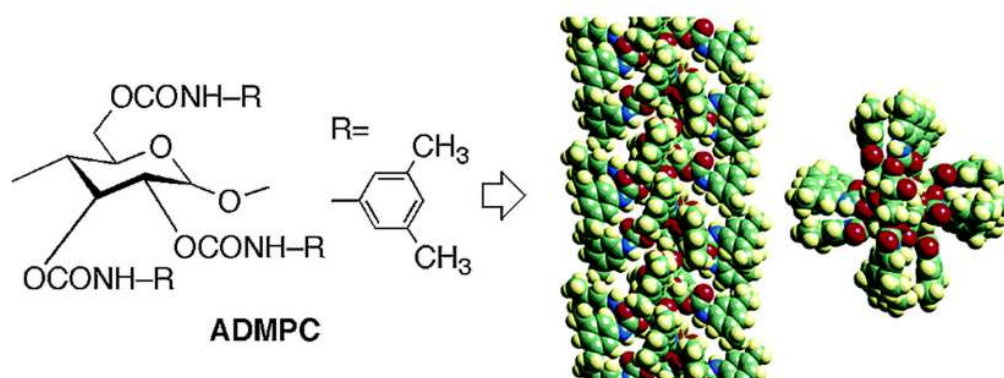


Figure 87. Amylose tris-(3,5-dimethylphenylcarbamate) as chiral stationary phases (CSPs)

Resolution was good in all cases and several mg of both enantiomers were collected in a pure state ($ee > 98\%$).

The molecular structures of the enantiomers of **6** were determined by X-ray analysis. Suitable crystals of both enantiomers were obtained by crystallization from ethyl acetate/*n*-hexane. An ORTEP view of (*M*)-**6** and (*P*)-**6** is illustrated in Figure 88.

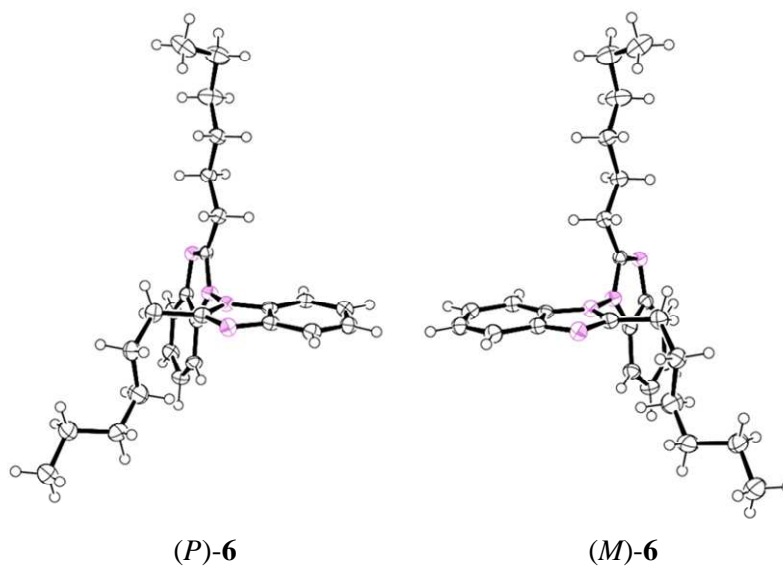


Figure 88. An ORTEP view of the molecular structures of (*P*)-**6** and (*M*)-**6**

As expected, the dihedral angle between the two intersecting planes described by two heteroarene rings is close to 90° .

Knowing the absolute configuration of the enantiomers of **6**, the assignment of the absolute configuration of enantiomers of **1-5** was empirically established by CD correlation method. As can be seen in Figure 89, the replacing of the *n*-hexyl group by shorter *n*-alkyl groups did not produce significantly alteration in the spectral location of the maximum and minimum of the representative CD bands recorded in ethanol solution. At 250 nm the negative ellipticity could be related to the (*M*) absolute configuration and the specular positive CD signal to the (*P*) configuration of **1-6**.

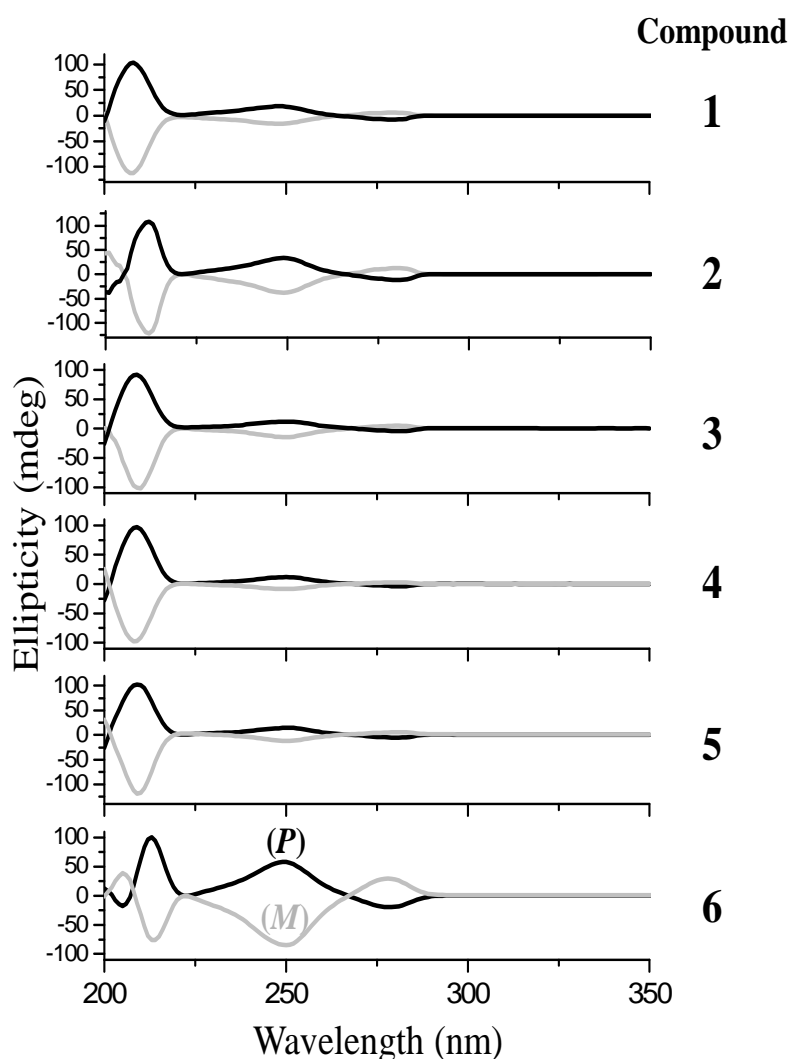


Figure 89. CD spectra of the enantiomers of **1-6** dissolved in ethanol

As a consequence, at the same wavelength and mobile phase condition, the sign of the CD signal of a chiroptical detector on-line recorded during enantioselective HPLC analysis is expected to unambiguously trace the enantiomer elution order. As described below, the correctness of this approach was confirmed by comparing the HPLC chromatograms of non-racemic samples of known enantiomeric composition with those of pure enantiomers.

Influence of length of the 2,2'-alkyl chains on retention, enantioselectivity and elution order of (*P*) and (*M*) enantiomers.

Table 7 lists the chromatographic data obtained by HPLC resolution of **1-6** on the Chiralpak AD-3 CSP using the mixtures *n*-hexane–2-propanol 100:10 and *n*-hexane–ethanol 100:10 (hereafter denoted as mpA and mpB, respectively) as mobile phases and setting the column temperature at 25°C. Through their inspection some relevant evidences, pointing to a clear involvement of the 2,2'-*n*-alkyl side chains in the retention and enantio-recognition mechanisms of the atropisomeric compounds may be stressed.

Table 7. Effect of mobile phase on retention, *k*, and enantioseparation factors, α , of the compounds 1-6

Compound	Eluent	k_1 (AC) ^a	k_2 (AC)	α
1	mpA	3.82 (<i>M</i>)	4.63 (<i>P</i>)	1.21
	mpB	4.90 (<i>M</i>)	11.16 (<i>P</i>)	2.28
2	mpA	1.65 (<i>M</i>)	2.29 (<i>P</i>)	1.39
	mpB	1.74 (<i>M</i>)	5.38 (<i>P</i>)	3.09
3	mpA	1.50 (<i>M</i>)	1.63 (<i>P</i>)	1.09
	mpB	1.72 (<i>M</i>)	2.33 (<i>P</i>)	1.35
4	mpA	1.27 (<i>P</i>)	1.38 (<i>M</i>)	1.09
	mpB	1.08 (<i>M</i>)	1.13 (<i>P</i>)	1.05
5	mpA	0.98 (<i>P</i>)	1.27 (<i>M</i>)	1.30
	mpB	0.99 (<i>P</i>)	1.13 (<i>M</i>)	1.14
6	mpA	0.80 (<i>P</i>)	0.98 (<i>M</i>)	1.23
	mpB	0.76 (<i>P</i>)	1.20 (<i>M</i>)	1.58

^a Absolute configuration.

Flow-rate, 1 cm³ min⁻¹; temperature, 25 °C; detection, UV at 250 nm

Under mpA condition, the retention of both (*P*) and (*M*) enantiomers on the AD-3 CSP decreased as the length of the alkyl groups increased. For the series of analytes **2-6** the reducing was moderate but regular while passing from methyl (compound **1**) to ethyl

(compound 2) it was much more pronounced. It is worthwhile noticing by comparing the CD traces recorded at 250 nm and depicted in Figure 90 that the enantiomer elution order switched passing from the compound bearing *n*-propyl to those with longer alkyl groups. The (*M*)-enantiomers of 1-3 were eluted before than (*P*)-enantiomers and showed negative sign of the CD chromatographic peak. As expected, positive sign of the CD peaks for the less retained enantiomers of 4-6 were associated to the (*P*) configuration.

When ethanol was replaced by 2-propanol in the normal-phase eluent, the variation trend of the retention times was quite similar but with some substantial differences. Firstly, passing from compound 1 to compound 2, the *k* values reduced in a much more pronounced way. Secondly, only for the (*M*)-enantiomer of compounds 5 and 6 it was noted that the relevant retention factors came back to increase rather than progress in reducing. The (*M*)-5 enantiomer was slightly more retained than (*M*)-4 (*k* = 1.13 vs. *k* = 1.08) whereas the (*P*)-enantiomer followed the usual decreasing trend. The retention of (*M*)-6 further increased (*k* = 1.20) and maintained higher than the (*P*)-form (*k* = 0.76).

This suggests a direct and favorable contact between the alkyl portion of 5 or 6 and the CSP, which was not observable in the case of 4.

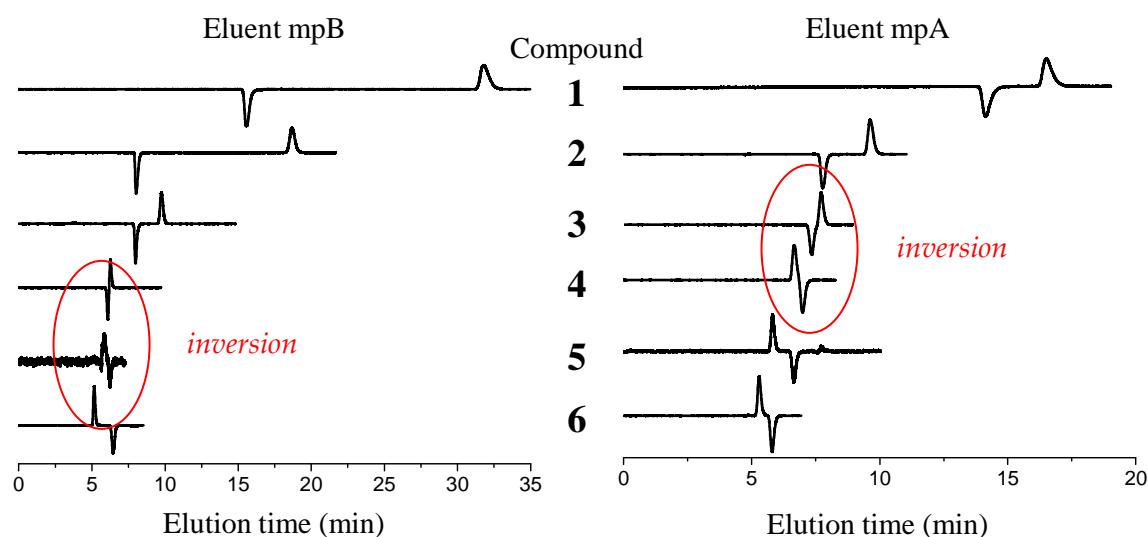


Figure 90. Typical chromatograms illustrating the differences in enantioselection and retention of 1-6 on the AD-3 CSP. Column, Chiralpak AD-3 250 mm x 4.6 mm I.D.; mobile phase, *n*-hexane-ethanol 100:10 (eluent mpB) and *n*-hexane-2-propanol 100:10 (eluent mpA); temperature, 25 °C; detection, CD at 250 nm

Thermodynamic aspects concerning the elution and enantioseparation processes of (P) and (M) enantiomers

(Prof. Roberto Cirilli, Istituto Superiore di Sanità, Rome and Prof. Marco Pierini, Università di Roma La Sapienza)

Retention and resolution of enantiomers by HPLC on CSP are thermodynamically governed processes depending on the summative contribution of repulsive and non-covalent attractive intermolecular interactions occurring between selector and selectand enantiomers. When an enantiomer resolution is observed, the retention and enantioselectivity factors may be related to the column temperature by the following equations:

$$\ln k = -\Delta H^\circ/RT + \Delta S^\circ/R + \ln \phi \quad (1)$$

$$\ln \alpha = -\Delta\Delta H^\circ/RT + \Delta\Delta S^\circ/R \quad (2)$$

where ΔH° and ΔS° are the enthalpy and the entropy of adsorption, respectively, $\Delta\Delta H^\circ$ and $\Delta\Delta S^\circ$ are the differences in enthalpy and entropy of adsorption of the more and less retained enantiomers onto stationary phase, ϕ is the phase ratio, R is the gas constant and T the absolute temperature.

According to equation 2, it is useful to stress that, in all cases of enantioselective HPLC separations in which both the terms $\Delta\Delta H^\circ$ and $\Delta\Delta S^\circ$ are characterized by equal sign, it will exist a particular temperature, named isoenantioselective temperature (T_{iso}), at which the enthalpic and entropic contributions to chiral recognition cancel out each other and the enantiomers coelute (*i.e.* at which $\alpha=1$). The value of T_{iso} can be promptly computed by the equation (3):

$$T_{iso} = \Delta\Delta H^\circ/\Delta\Delta S^\circ \quad (3)$$

Thus, for temperatures above T_{iso} the separation of enantiomers is entropy-controlled ($|T\Delta\Delta S^\circ| > |\Delta\Delta H^\circ|$). Importantly, by transition from entropic to enthalpic domain (or vice versa), the elution order of the enantiomers will be reversed.

Typically, chiral HPLC separations are enthalpy-controlled because the chromatographic discrimination is usually carried out at temperatures lower than that of isoelution. This is particularly true for polysaccharide-based stationary phases, because the temperature range of applicability recommended by its manufacturers is fairly narrow and close to room temperature (about 0 – 45 °C).

However, since the inversion of the elution order occurring in the case of a low T_{iso} may severely compromise the study of chiral recognition mechanism making impossible the correlation between absolute configuration and retention [39], the thermodynamics of the investigated enantioseparation process should be fully elucidated.

According to this, each racemic compound **1-6** was submitted to a temperature-dependent study between 15 °C and 45 °C on the AD-3 CSP. The retention and enantioselectivity values were calculated in 5 °C increments over the temperature range selected, using mpA and mpB as eluents.

Figure 91 shows the α vs. T and $\ln k$ vs. $1/T \times 10^3$ plots obtained. The $\Delta\Delta H^\circ$ and $\Delta\Delta S^\circ$ terms were calculated by regression analysis of the highly linear $\ln k$ vs. $1/T \times 10^3$ plots ($R^2 > 0.990$ irrespectively by the employed mobile phase) [40].

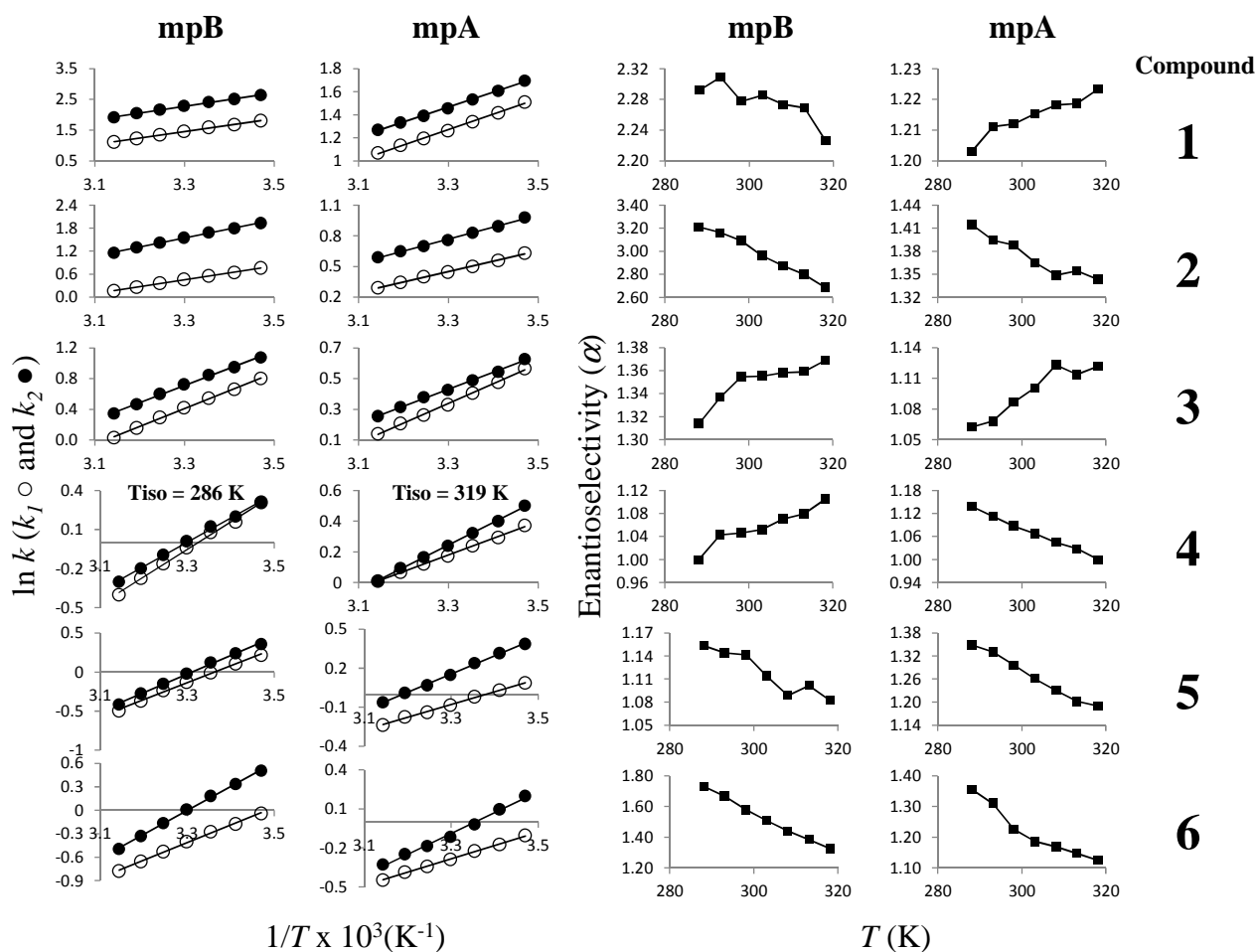


Figure 91. Plots of $\ln k$ vs. $1/T \times 10^3$ and α vs. $1/T$ for **1-6** with different mobile phases. Temperature, 15 - 45 °C; mobile phase, *n*-hexane-ethanol 100:10 (eluent mpB) and *n*-hexane-2-propanol 100:10 (eluent mpA); for other chromatographic conditions see Table 6

The found thermodynamic parameters, as well as the calculated isoelution temperatures, are summarized in Table 8.

Entry	Compound	Eluent	$\Delta\Delta H_{(P)-(M)}^\circ$ (kcal mol ⁻¹)	$\Delta\Delta S_{(P)-(M)}^\circ$ (cal mol ⁻¹ K ⁻¹)	<i>T</i> _{iso} (K)
1	1	mpA	0.09	0.68	132
2		mpB	-0.16	1.11	-
3	2	mpA	-0.32	-0.42	761
4		mpB	-1.10	-1.49	742
5	3	mpA	0.37	1.39	263
6		mpB	0.21	1.28	162
7	4	mpA	0.76	2.38	319
8		mpB	0.51	1.78	286
9	5	mpA	0.82	2.24	366
10		mpB	0.41	1.13	362
11	6	mpA	1.14	3.38	337
12		mpB	1.64	4.59	357

Table 8. Thermodynamic data.

On the basis of these findings it was clear that, in the explored range of temperatures, the chiral resolutions were entropy-controlled for the compounds **1** and **3** eluted with mpA and **1**, **3** and **4** eluted with mpB (Table 8, entries 1,2,5,6,8) (i.e. $|T\Delta\Delta S^\circ| > |\Delta\Delta H^\circ|$). With the only exception of racemate **1**, when eluted with mpB, all the other enantioseparations were characterized by $\Delta\Delta H^\circ$ and $\Delta\Delta S^\circ$ terms of equal sign, independently from the used mobile phase (Table 8). This means that for all racemates **1-6** eluted with mpA, and for racemates **2-6** eluted with mpB, it is possible to calculate a correspondent T_{iso} values (for a rank of these data see Table 8). From inspection of their values it is easy to note that, by excluding the case of racemate **4**, for which they were found $T_{iso}=46^\circ\text{C}$ for elution with mpA and $T_{iso}=13^\circ\text{C}$ for elution with mpB, all the other computed T_{iso} are largely far away from the explored temperature range 15-45°C (i.e. the coalescence temperatures fall beyond the practical range of the AD-3 CSP). This means that only for **4** it is expected that a coalescence of peaks of its enantiomers occurs when T_{iso} is achieved, as in fact it can be actually seen in the chromatograms registered at the temperature of 45°C for elution with mpA and at the temperature of 15°C for elution with mpB (Figure 92).

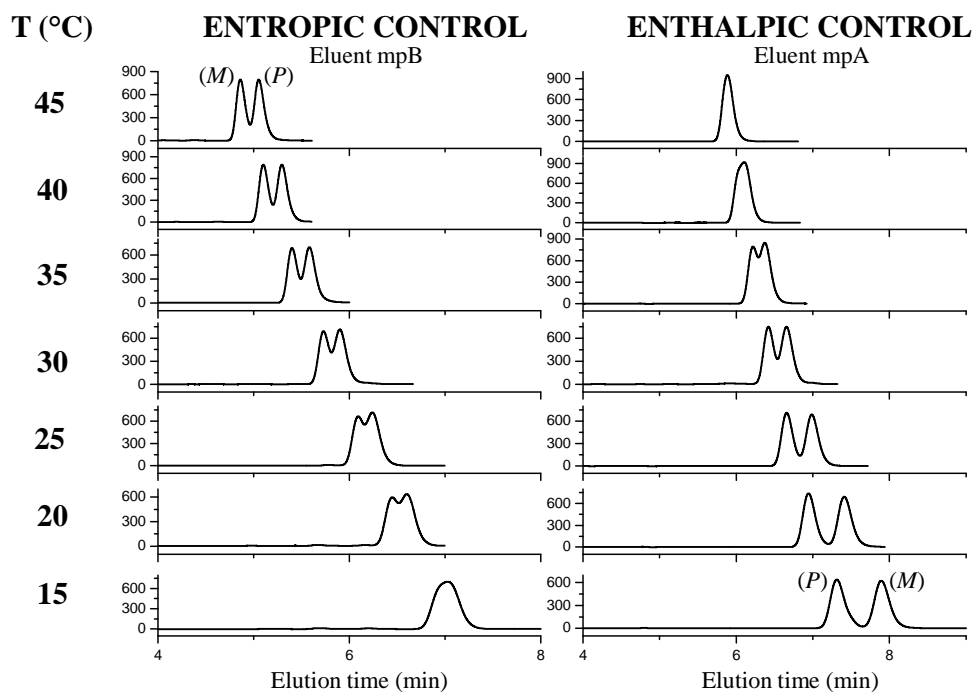


Figure 92. Variable-temperature HPLC of **4** in entropic and enthalpic domain. Temperature, from 45 °C (top) to 15 °C (bottom); mobile phase, *n*-hexane-ethanol 100:10 (eluent mpB) and *n*-hexane-2-propanol 100:10 (eluent mpA); for other chromatographic conditions see Table 6

Just looking at the $\Delta\Delta H^\circ$ values listed in Table 8, the change of the elution order of the enantiomers as a function of 2,2'-n-alkyl chains length should take place with both the mobile phases mpA and mpB when passing from racemate **2** to **3** (*i.e.* when $\Delta\Delta H^\circ$ reverses its sign), namely, in significant advance with respect to the experimental elution orders found using both the above mobile phases at an established constant temperature (*i.e.* when $\Delta\Delta G^\circ$ reverses its sign, condition that occurs passing from racemate **3** to **4** with mpA and from racemate **4** to **5** with mpB).

This points to a significant role played by the entropy in the global process of enantiorecognition (Figure 93), which is certainly and strictly related to a progressive, but differential, involvement of the alkyl chains mobility of the enantiomers in the discrimination mechanism.

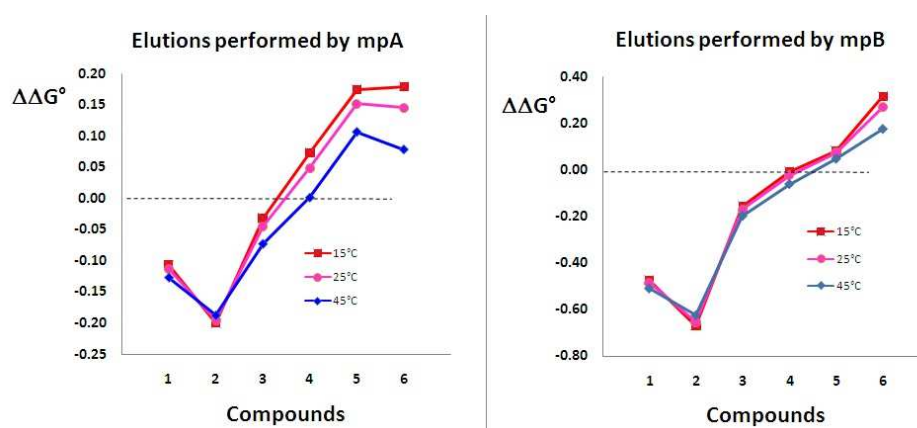


Figure 93. $\Delta\Delta G^\circ$ as a function of the increase of length of the alkyl chains in **1-6**

In order to shed light on this subject we analyzed each enantiorecognition by splitting out from the related $\Delta\Delta G^\circ$ amounts the contributions coming from the individual enantiomers (*P*) and (*M*) ($\Delta G_{(P)}^\circ$ and $\Delta G_{(M)}^\circ$), as well as the related enthalpic ($\Delta H_{(P)}^\circ$ and $\Delta H_{(M)}^\circ$) and entropic ($\Delta S_{(P)}^\circ$ and $\Delta S_{(M)}^\circ$) inputs. The ΔH° and ΔS° amounts governing the retention processes of each enantiomer of compounds **1-6** were obtained as the slope of linear plots $\ln k$ vs. $1/T \times 10^3$ (Figure 91) in the first case and $RT \times \ln k$ vs. T in the second one (plots are not shown) ($R^2=0.997$ were the relevant correlation coefficients, each of which averaged on 24 linear correlations involving both the employed mobile phases). The enthalpic and

entropic terms obtained (Table 9) were evaluated as a function of the progressive increase of length of the alkyl chains in **1-6** (Figure 94).

Eluent	Compound	$\Delta H_{(M)}^\circ$ (kcal mol ⁻¹)	$\Delta S_{(M)}^\circ$ (cal mol ⁻¹ K ⁻¹)	$\Delta G_{(M)}^\circ$ (25°C) (kcal mol ⁻¹)	$\Delta H_{(P)}^\circ$ (kcal mol ⁻¹)	$\Delta S_{(P)}^\circ$ (cal mol ⁻¹ K ⁻¹)	$\Delta G_{(P)}^\circ$ (25°C) (kcal mol ⁻¹)
mpA	1	-2.65	-6.2	-0.80	-2.57	-5.5	-0.92
	2	-2.02	-5.8	-0.30	-2.34	-6.2	-0.50
	3	-2.55	-7.7	-0.25	-2.19	-6.4	-0.29
	4	-2.91	-9.1	-0.19	-2.15	-6.7	-0.14
	5	-2.76	-8.8	-0.14	-1.94	-6.6	0.02
	6	-3.18	-10.6	-0.01	-2.04	-7.3	0.13
mpB	1	-4.18	-10.9	-0.92	-4.34	-9.8	-1.41
	2	-3.56	-10.9	-0.32	-4.66	-12.4	-0.98
	3	-4.64	-14.5	-0.31	-4.43	-13.3	-0.48
	4	-4.20	-14.0	-0.03	-3.69	-12.2	-0.05
	5	-4.71	-15.6	-0.05	-4.30	-14.5	0.02
	6	-6.08	-20.1	-0.09	-4.45	-15.5	0.18

Table 9. Thermodynamic data related to elution of single enantiomers of 1-6

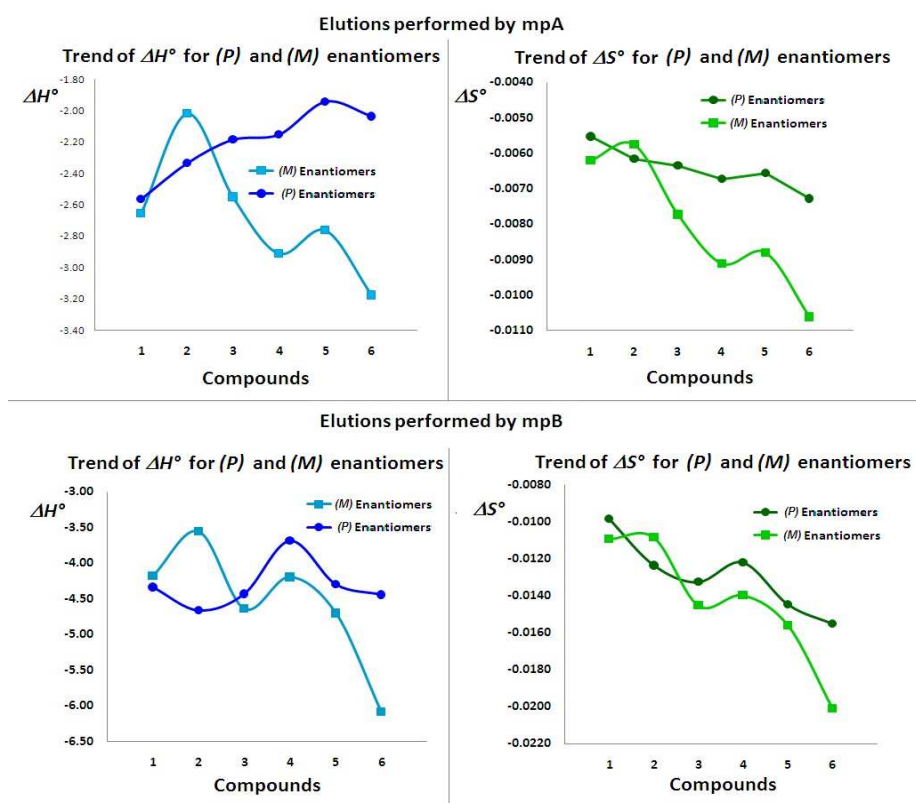


Figure 94. ΔH° and ΔS° for (M) and (P) enantiomers as a function of the increase of length of the alkyl chains in 1-6

In the case of elutions performed with mpA the really different chromatographic behaviour of the (*P*) enantiomers with respect to their optical isomers (*M*) is particularly evident and easy to be rationalized. In fact, under an enthalpic point of view, when the aliphatic moiety changed from methyl to hexyl, the solute-CSP interactions engaged by (*P*) enantiomers achieved a modest but steady deterioration (*i.e.* the $\Delta H_{(P)}^\circ$ values systematically rise, becoming less negative, see Figure 94 and Table 9) while, the opposite trend was registered in the case of (*M*) enantiomers. This demonstrates that the (*M*) enantiomers interacted with the AD-3 CSP in a progressively more intense and favourable way (*i.e.* the $\Delta H_{(M)}^\circ$ systematically achieve more negative values, the only macroscopic exception being represented by the case of compound **2** when compared to **1**). Thus, it seems logical to assume that the opposite enthalpic behaviour reflects a really different geometric complementarity between the two kind of enantiomers and the chiral selector (scarce for (*P*) and really good for (*M*)), much more marked than could be envisioned by looking at the experimental values of α (see Table 7). As an example, by assuming a negligible $\Delta \Delta S^\circ$ contribution to recognition ($\Delta \Delta G^\circ \cong \Delta \Delta H^\circ$) for racemate **6** the computable α factors would achieve values of 7.3 and 17.5 using mpA and mpB, respectively, as mobile phases.

By thinking again in terms of enthalpy about the kind of interaction established between enantiomer and stationary phase, the growing number of methylene groups within the selectand molecule seems to lead to a progressive increase of steric interference in case of (*P*) enantiomers and instead to an improve of geometrical complementarity (and therefore of recognition) in case of (*M*) enantiomers. Therefore any progressive improve of interaction should essentially arise from a direct and growing contact between the alkyl frameworks of the enantiomers and the stationary phase. So, that it should be expected that the stronger the bond established between selectand and CSP, the greater will be the reduction of conformational freedom experienced by the chains (*i.e.* the mobility of chains will be at least partially frozen). As a consequence, to a more favorable interaction enantiomer-CSP (more negative ΔH_x°) should correspond a more negative (and then,

unfavourable to the retention) value of ΔS_X° (subscript X denotes (*P*) or (*M*)). Coherently, this is just what was observed by looking at the plots reported in Figure 94 and data collected in Table 9, where the decrease of ΔS_X° (to which, however, always also contribute the loss of rotational and translational freedom degrees due to the chromatographic association selector-selectand) is much more marked for the (*M*) enantiomers than for (*P*) ones. Thus, the contributions afforded to $\Delta G_{(P)}^\circ$ and $\Delta G_{(M)}^\circ$ by the respective enthalpic and entropic terms (Table 9), provides the justification for the fact that the resulting experimental $\Delta\Delta G^\circ$ are only moderately different from zero ($\Delta\Delta G^\circ$ values were never greater than 0.2 kcal mol⁻¹ in module, while amounts of $\Delta\Delta H^\circ$ achieved values up to 1.1 kcal mol⁻¹, always considered in absolute sense, Figure 95). The observed trend of both ΔH_X° and ΔS_X° also suggests that, in order to perform the effective enantiorecognition of compounds **1-6**, and so also give rise to the partial freezing of their alkyl chains (which is much more effective for those in (*M*) than in (*P*) enantiomers), Chiralpak AD-3 CSP must expose to these stereoisomers a conformation endowed with chiral cavities of quite wide sizes, suitable to allow the entrapping of relevant portions of selectand's chains.

All the above considerations may be substantially reiterated in the case of elution performed by mpB, with the noticeable difference that the change of co-solvent from isopropyl alcohol to ethanol greatly strengthens the enthalpic contributions ΔH_P° and ΔH_M° favorable to the association, and therefore also markedly strengthens the entropic contributions $\Delta S_{(P)}^\circ$ and $\Delta S_{(M)}^\circ$, which, instead, act in opposition to the retention (the values increased on average by a factor 1.7 for (*M*) and 2.0 for (*P*), with respect to those found by elution with mpA, see Figure 94 and data in Table 9).

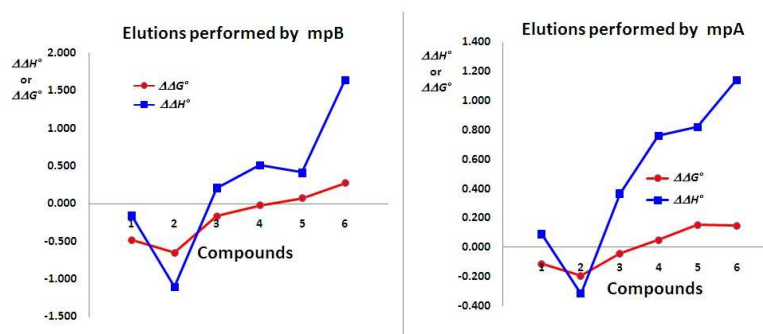


Figure 95. $\Delta\Delta H^\circ$ and $\Delta\Delta G^\circ$ as a function of the increase of length of the alkyl chains in **1-6**

c. Racemisation barrier

DFT computations demonstrated that the racemisation barrier of this system is higher than 40 kcal mol⁻¹. This implies that the two enantiomer are indefinitely stable at room temperature.

Actually, with **1** the enantiomeric excess remained unchanged within 116 h, even upon heating in decalin to 100 °C (Figure 96)

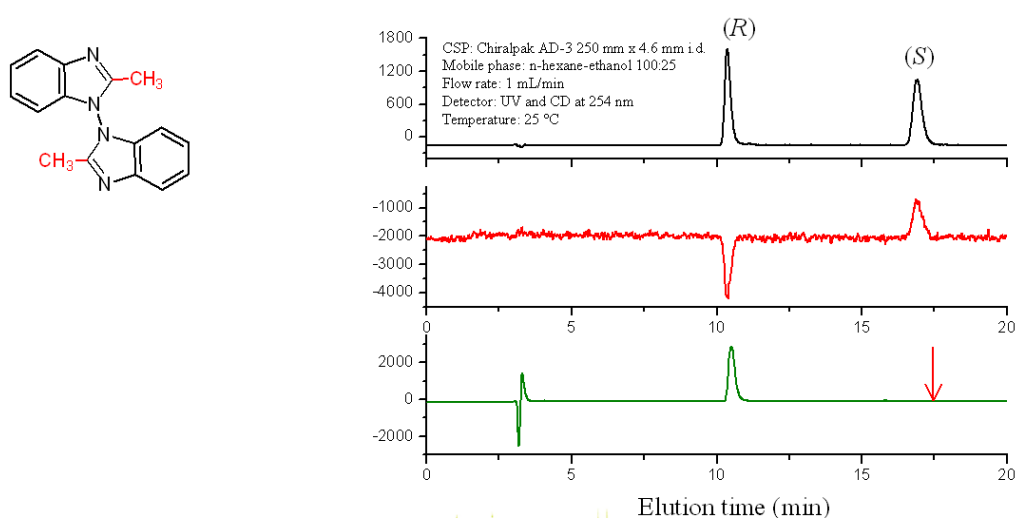
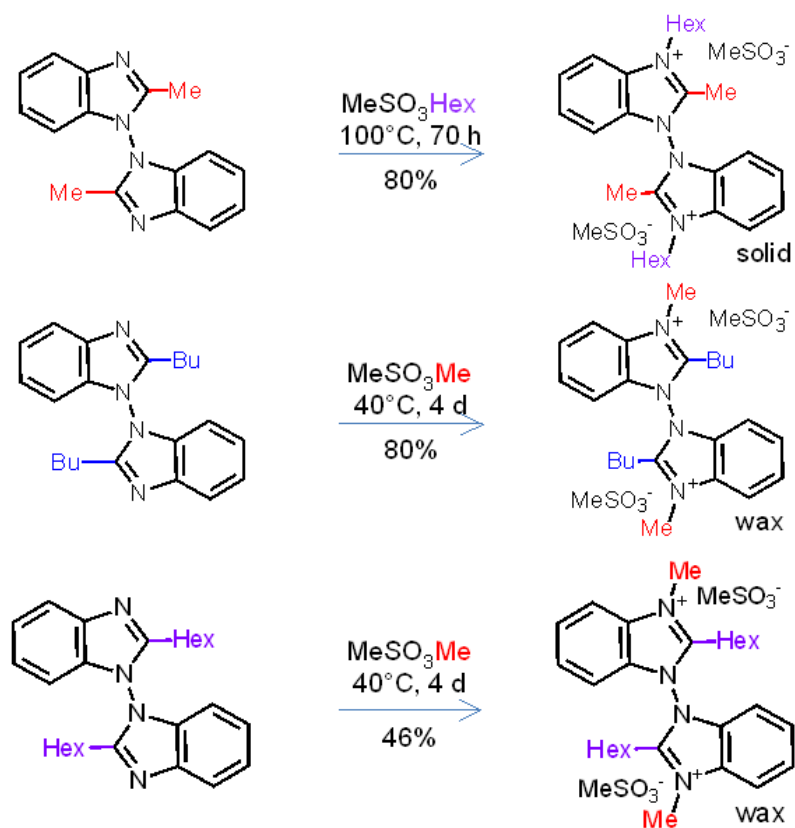


Figure 96. Check of thermal stability of enantiopure **1**

3.6.1.2 1,1' Bis-benzimidazolium Salts

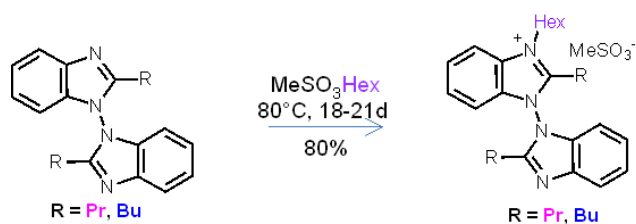
Synthesis

Alkylation of the 1,1'-bisbenzimidazole scaffolds has been achieved in the selected cases and with the synthetic pathways depicted in Scheme 3



Scheme 3. Dialkylations of 1,1' bis-benzimidazole scaffolds

In all other cases, alkylation reaction was not complete; sometimes the mono-alkylated salt was formed (Scheme 4)



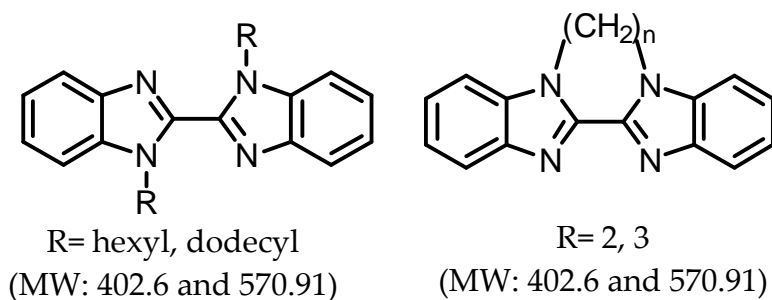
Scheme 4. Monoalkylations of 1,1' bis-benzimidazole scaffolds (with overall longer alkyl chains)

while, in other cases, some degradation was observed.

The use of microwaves does not improve yields. Overall, the reaction does not appear clean.

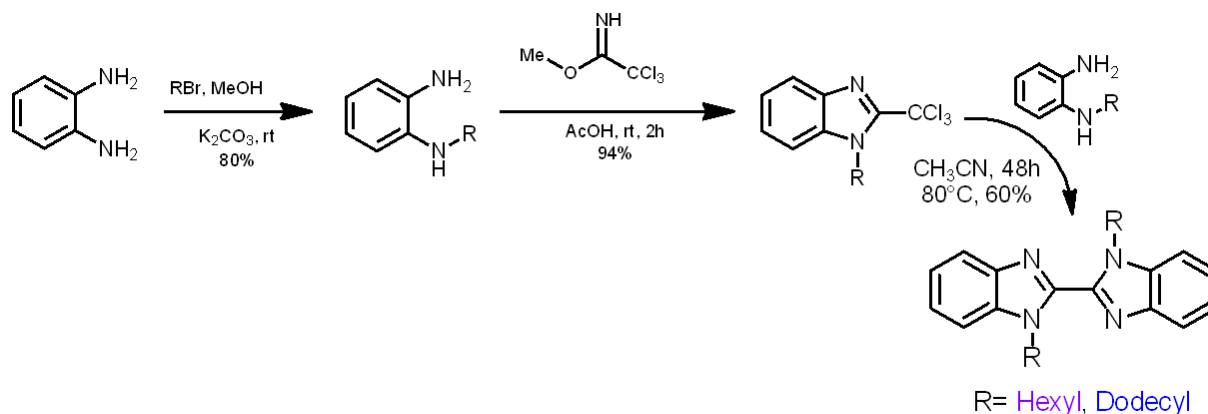
3.6.2 2,2' Bis-benzimidazole-based Inherently Chiral Ionic Liquids

3.6.2.1 2,2' Bis-benzimidazole Scaffolds



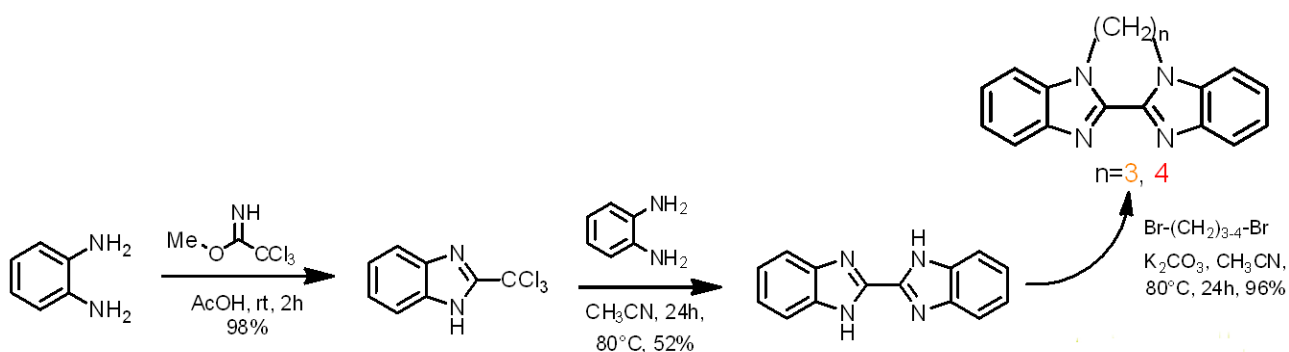
Synthesis

The preparation of 2,2' benzimidazole scaffolds, along the route described in Scheme 5, appears easier and cleaner and easier scalable than that of 1,1' ones.



Scheme 5. Preparation of 2,2' bisbenzimidazole scaffolds

2,2' bisbenzimidazole scaffolds featuring a bridging alkyl chain instead of two separated alkyl chains have also been easily prepared according to the route represented in Scheme 6:



Scheme 6. Preparation of bridged 2,2' bisbenzimidazole scaffolds

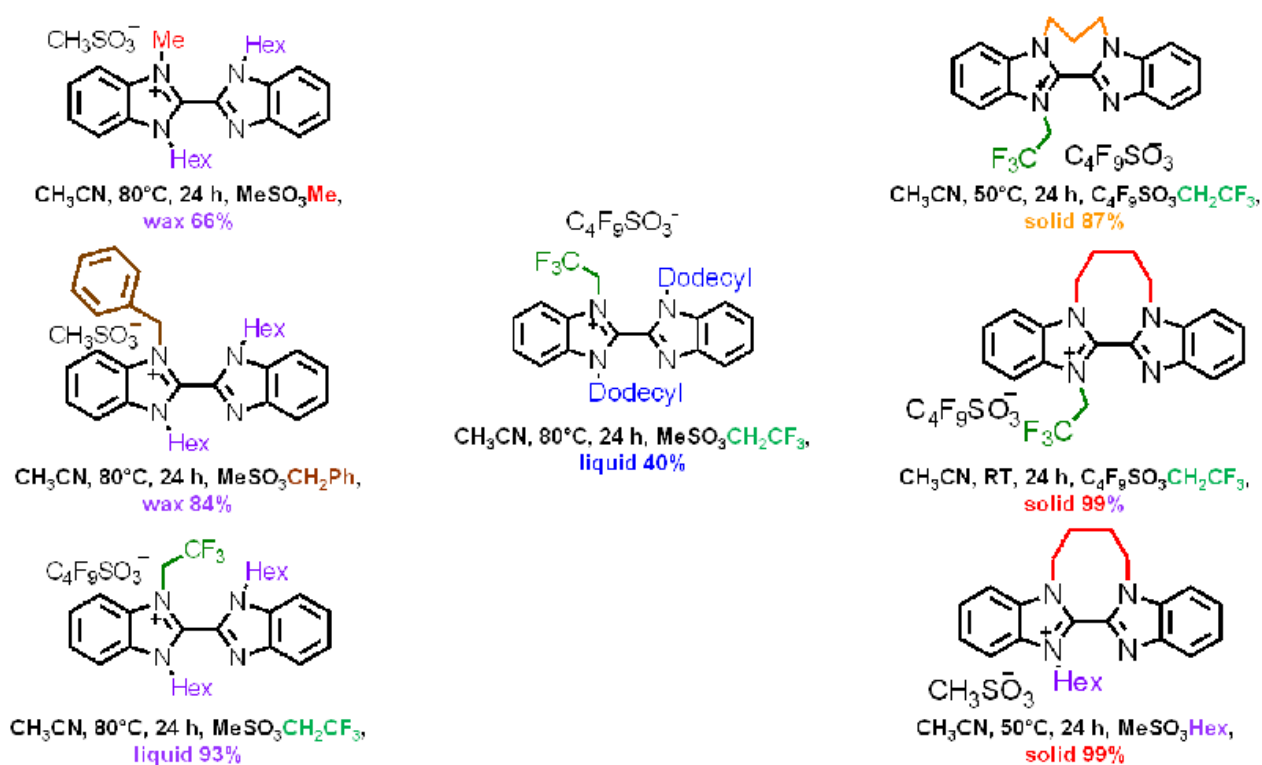
Unlike the 1,1' scaffolds, theoretical computations point to the 2,2' ones having a much lower interconversion barrier, so that they are not configurationally stable as such, nor after simple alkylation, as we will see, but only after double alkylation.

This applies to both the dialkylated ones and also surprisingly, to the bridged ones (which can undergo enantiomer interconversion notwithstanding the additional constraint, by a 'flapping' movement of the two heteroaromatic moieties).

3.6.2.2 2,2' Bis-benzimidazolium Salts

Synthesis

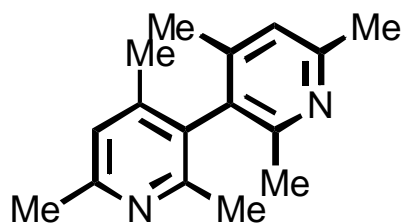
Unfortunately, all the 2,2' bis-benzimidazolium scaffolds invariably afforded monoalkylation only. Different alkylating agents were used, yielding the salts collected in Scheme 7:



Scheme 7. A synopsis of the 2,2' bis-benzimidazolium salts obtained

In spite of their featuring a single alkylated unit, several of the 2,2'-bis-benzimidazolium salts are liquid at room temperature, as desired. However, they unfortunately lack configurational stability, having racemization energy barriers $\Delta E^\ddagger \sim 13\text{-}22$ kcal mol⁻¹ (Semiempirical level and/or DFT B3LYP/6-31G* level).

3.6.3 3,3'-Bis-Collidine Scaffold

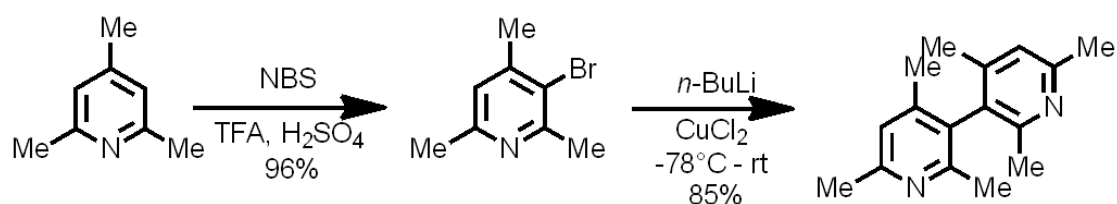


MW 240.35

Synthesis

3,3'-Bis-collidine is known in literature. According to a 1968 Russian paper, its synthesis can be achieved through pyrocondensation of collidine on white hot platinum coil, at 200°C, for 7 days.

However, it can also be obtained along the pathway in Scheme 8.



Scheme 8. Synthesis of 3,3'-bis-collidine

3,3' bis-collidine exists in two enantiomers (Figure 97) having a very high interconversion barrier of ~42.5 kcal/mol and therefore stable at room temperature.

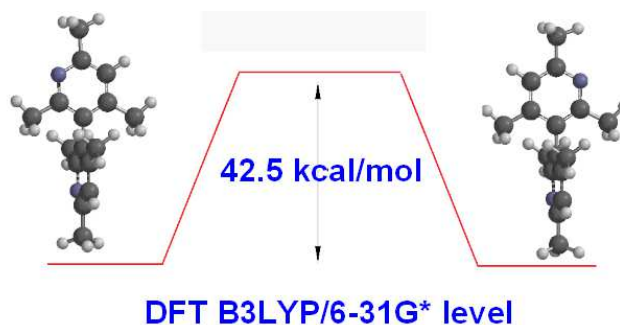


Figure 97. The two stable enantiomers of biscollidine and their racemization barrier

In particular, we have achieved successful resolution of the racemate obtained by the synthesis described in the former paragraph, by fractional crystallization of the diastereomeric salts with *o,o*-dibenzoyl-tartaric acids (Figure 98).

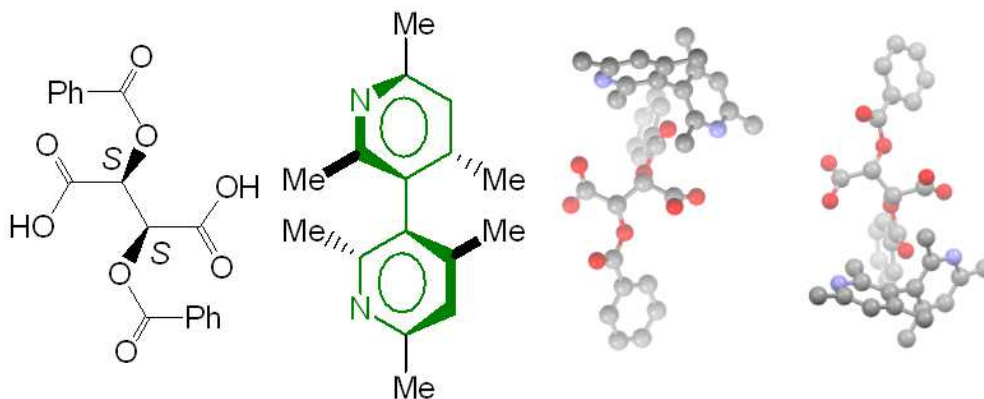


Figure 98. Diastereomeric salts of 3,3'-bis-collidine with *o,o*-dibenzoyl-tartaric acids

The purity of the separated enantiomers was tested by analytical chiral HPLC (Figure 99); moreover, their CD spectra appear quite symmetrical (Figure 100)

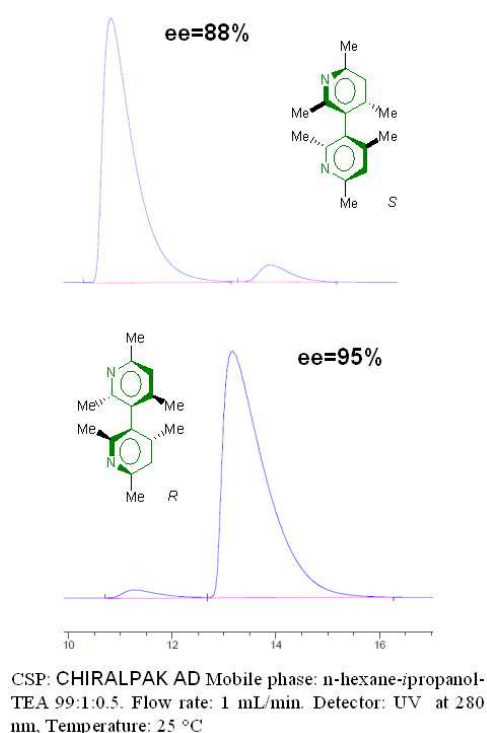


Figure 99. Analytical Chiral HPLC purity test of the 3,3'-bis-collidine enantiomers separated by fractional crystallization as *o,o*-dibenzoyl-tartaric acid salts

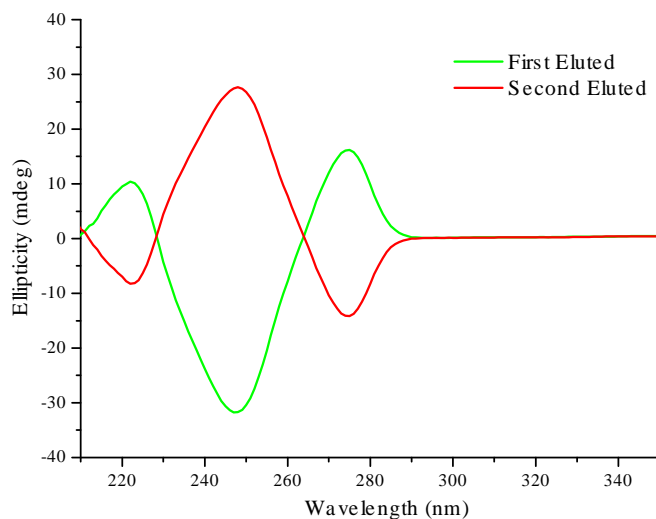
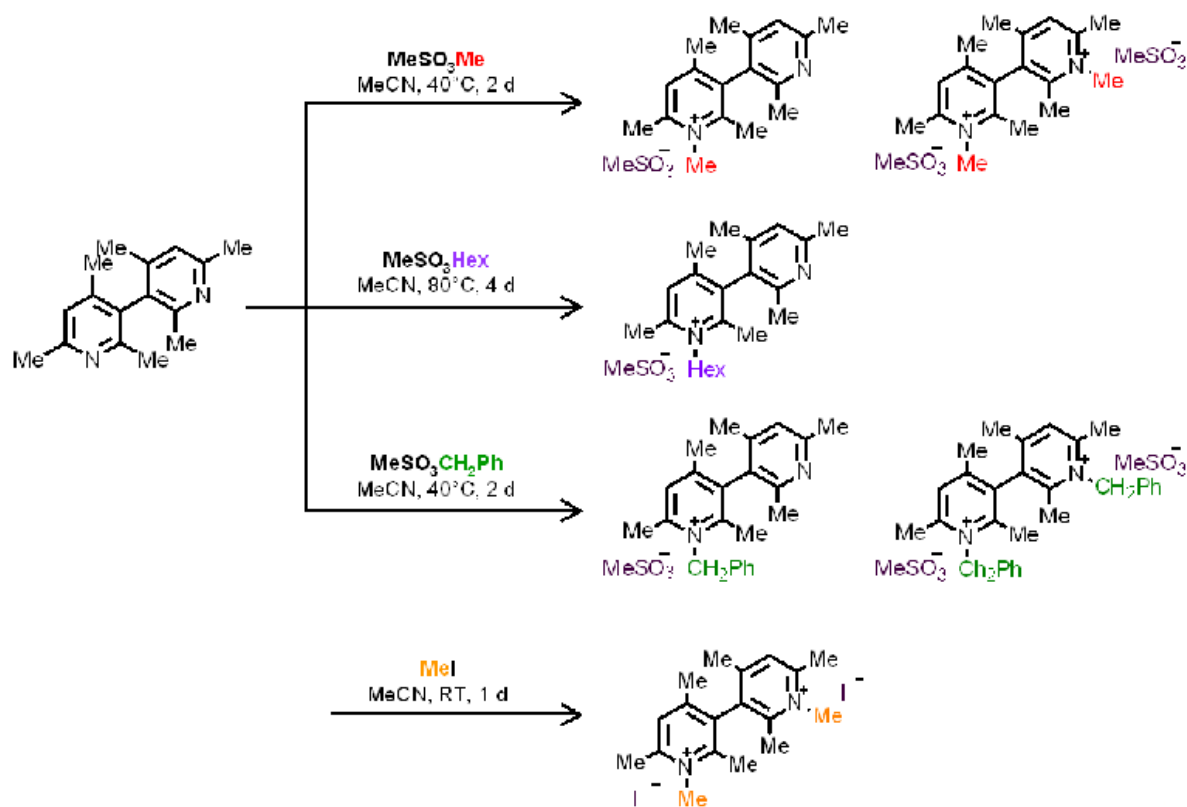


Figure 100. Circular Dichroism spectra of the 3,3'-bis-collidine enantiomers separated by fractional crystallization as *o,o*-dibenzoyl-tartaric acid salts

3.6.3.1 3,3' Bis-collidinium Salts

Synthesis



The precursor biheteroaromatic scaffolds and the corresponding salts have been characterized by cyclic voltammetry on GC electrode in ACN + 0.1 M TEABF₄, with the aim of:

- obtaining guidelines for structure *vs* electronic properties rationalization, particularly concerning the role of racemization barrier/effective conjugation, as well as alkyl substituent bulkiness, counteranion, *etc.*;
- providing an indication of the available potential window when working in such media, alone or as cosolvents.

3.6.4 Electrochemical Characterization of Biheteroaromatic Scaffolds

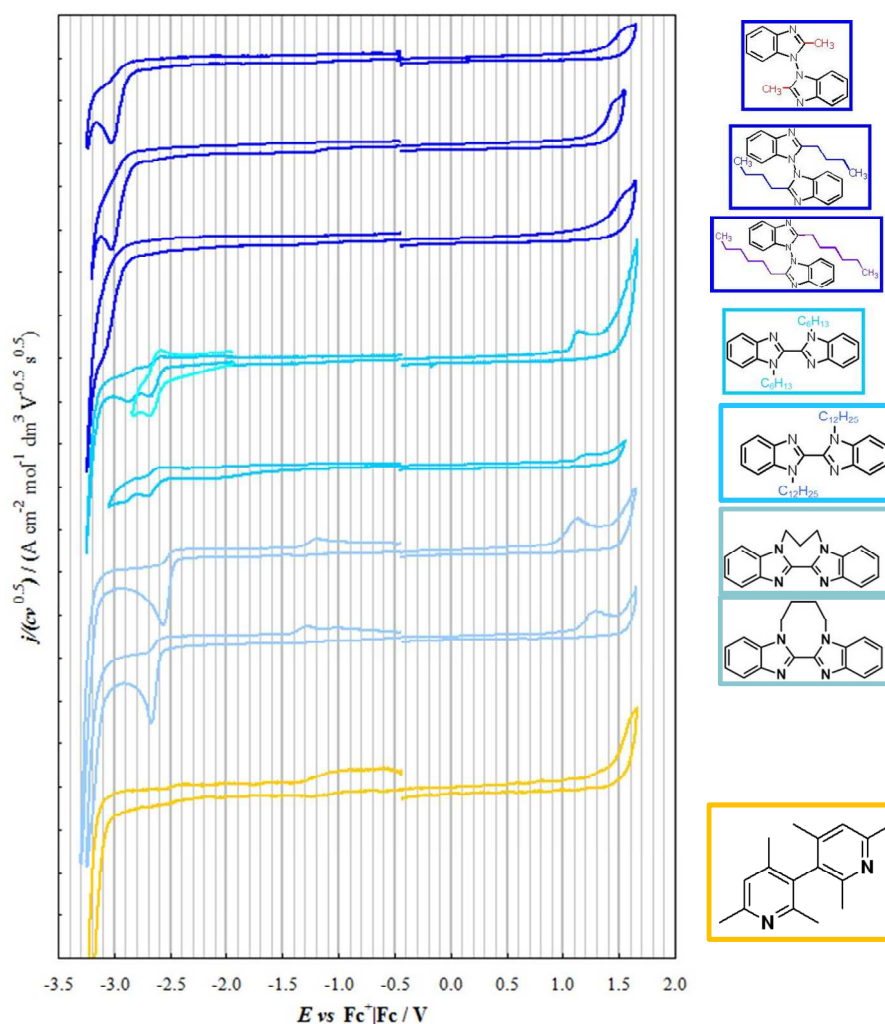


Figure 101. Synopsis of CV features of inherently chiral scaffolds whose molecular structures are depicted at the side of the figure. All signals were recorded in ACN + TEABF₄ 0.1 M at 200 mV s⁻¹ potential scan rate on GC electrode. All potential values are referred to the standard redox couple Fc⁺|Fc

Figure 101 evidences that all synthesized scaffolds have a large potential window, a very interesting feature for their use as chirality inductors in electrochemical experiments.

Comparing the CV features of each scaffold family the following features emerge:

- **1,1'-bis-benzimidazoles** display a racemization barrier of $\sim 40 \text{ kcal mol}^{-1}$.

First reduction and first oxidation peaks are close to the boundaries of the available potential windows, consistent with very low effective conjugation deriving from the high energy barrier. The effect of alkyl chain length is very slight, with the potential window slightly widening with increasing chain length, possibly as a consequence of higher sterical hindrance. Thus the largest potential window is obtained when hexyl chains are used to functionalized the two nitrogen atoms of the atropisomeric core ($E_g \sim 4.5 \text{ eV}$, the third CV pattern in blue).

- **2,2'-bis-benzimidazoles** exhibit the narrowest potential window of all scaffold families: both first reduction and first oxidation peaks are shifted to less extreme potentials, pointing to higher effective conjugation between the scaffold moieties, which is in accordance with the lower computed racemization barriers. Twin quasi-reversible reduction peaks are also visible (in unbridged 2,2' systems), which could correspond to two equivalent, significantly interacting redox centres (fifth and sixth light blue CV patterns).

It is worthwhile noticing that bridging alkyl substituents result in a different reduction mechanism with respect to simple alkyl chains. Actually bridging alkyl substituents appear to destabilize the first ET product, which reacts much more rapidly. Moreover, the 3-term bridge results in a significantly lower E_g with respect to the 4-term one, consistently with its lower calculated racemization barrier (pale blue CV pattern).

- **3,3'-bis-collidine** is the most promising scaffold, corresponding to the highest computed racemization barrier ($42.5 \text{ kcal mol}^{-1}$) and, consistently, yielding the

largest potential window in CV experiments ($E_g \sim 4.8$ eV, yellow line). First reduction and oxidation are in this case barely perceptibly as background shoulders, consistent with very low effective conjugation.

It is worthwhile noticing that these inherently chiral scaffolds can be employed, even without salification, as chirality inductors in stereoselective processes, either dissolved in achiral commercial ionic liquid media or, together with a supporting electrolyte, in traditional solvents.

3.6.5 ICILs vs Scaffolds

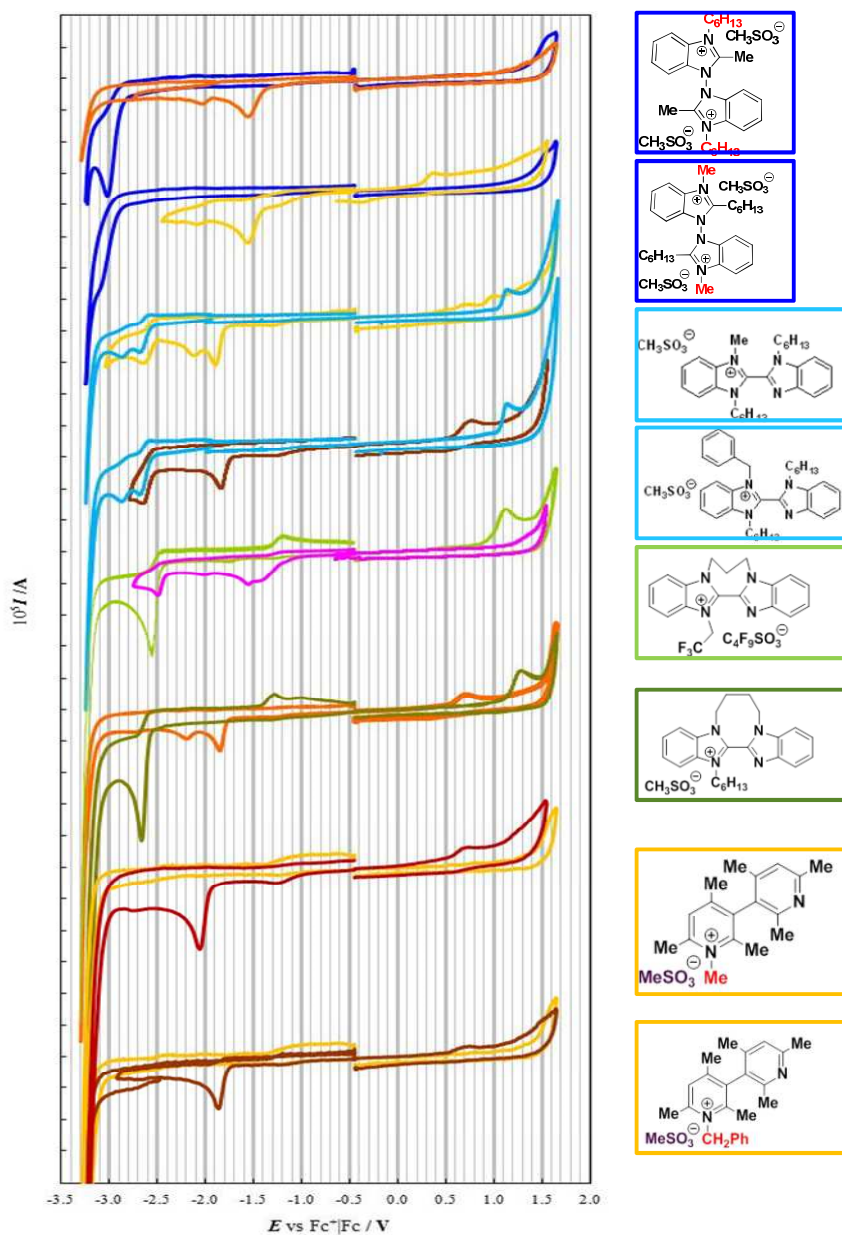


Figure 102. Synopsis of CV features of ICILs whose molecular structures are indicated at the side of the figure. All signals were recorded in ACN + TEABF₄ 0.1 M at 200 mV s⁻¹ potential scan rate on GC electrode. All potential values are referred to the standard redox couple Fc⁺|Fc. The CV patterns of the ICILs are here superimposed to those of the corresponding scaffolds

From all CV patterns (Figure 102) it is evident that quaternarization of the imidazole and pyridinium rings results in a huge positive shift of the first reduction potentials. In other words, the alkylated compounds appear significantly more oxidable than the original

scaffolds. Thus, the ICILs show a narrower potential window than the corresponding scaffolds.

In particular, in alkyl-monosubstituted scaffolds the first reduction peaks are nearly at the same potential (-1.8–1.9 V *vs* Fc⁺|Fc), no matter the nature of the scaffold, of the alkyl group and of the counterion.

In the dialkylated case the first reduction peak is even more positive (-1.55 V *vs* Fc⁺|Fc) and a second peak is perceived at -2 V, while the original scaffold peak has disappeared.

It is also worthwhile mentioning that the new bis-benzimidazolium salts appear significantly more reactive (in particular, more reducible) than the commercially available imidazolium salt BMIMPF₆. This can be explained as a consequence of their higher conjugation, arising from their having a benzimidazolium rather than an imidazolium cation, and also, possibly, from some residual conjugation between the two moieties across the central node.

3.6.6 First Electrooligomerization Test using a 3,3'-Bis-collidinium Derivative as Supporting Electrolyte

In view of testing the new ICILs as media for electrooligomerizations, a preliminary electrooligomerization study was carried out using as deposition media commercial CILs; the only easily available were:

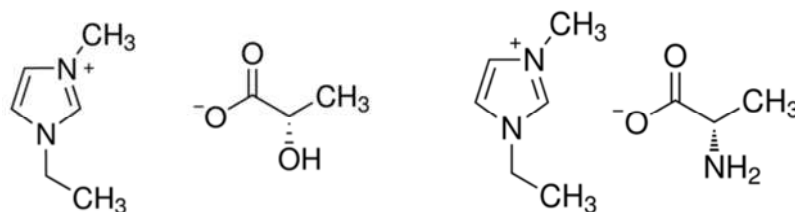


Figure 103. Commercially available CILs

1-ethyl-3-methylimidazolium-*L*-(+)-lactate (Figure 103 on the left) and 1-ethyl-3-methylimidazolium-*S*-2-aminopropionate (Figure 103 on the right). Unfortunately, all of them imply chirality to stem from a chiral anion. In any case, no electrooligomerization at all took place, probably on account of the anion bulkiness.

Thus, to preliminarily check whether electrooligomerize could take place in the presence of the new ICILs under development, racemic 3,3'-di-methylbis-collidinium salt (Figure 104) has been tested as 0.1 M supporting electrolyte in ACN for the electrooligomerization of the T₄BT₂ inherently chiral monomer, parent molecule of the new class of inherently chiral monomers applied to the preparation of highly enantioselective electrode surfaces, as described in former paragraphs [5, 23, 24].

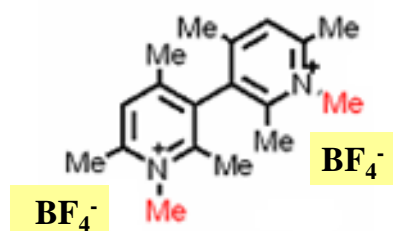


Figure 104. The 3,3'-bis-collidinium salt employed as supporting electrolyte in the electrochemical oligomerization

A first test was carried out using the same ICILs represented in Figure 104 with methanesulfonate (MeSO_3^-) as counteranion. Unfortunately the MeSO_3^- anion appeared to prevent oligomerization of T_4BT_2 monomer (the counteranion is suspected to be responsible). So the double BF_4^- salt of the same cation was prepared *via* ion exchange of the corresponding di-iodide one.

Using the BF_4^- salt very regular and virtually unlimited electrooligomerization was observed. The obtained films are very stable after several redox cycles, both on GC and on ITO electrodes. Their CV features resemble those obtained carrying out the electropolymerization in commercial BMIMPF_6 ionic liquid (Figure 105). These results are promising in view of future electrochemical reactivity studies in bulk ICILs.

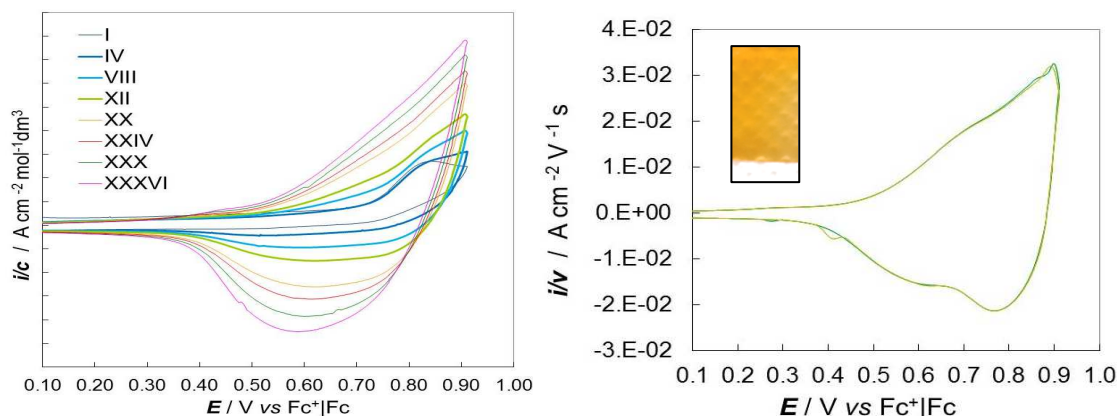
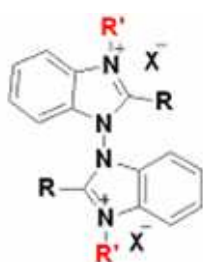


Figure 105. On the right: CV features of the oligomerization (36 cycles) of (±)-T₄BT₂ monomer employing the 3,3'-bis-collidinium salt as supporting electrolyte 0.1 M +ACN. On the right: stability cycles in a monomer free solution, in the inset: oligo-(±)-T₄BT₂ film deposited on an ITO electrode

Synthetic work is in progress both to lower the melting points of the new salts (most of which are still too high) and to scale up the synthesis of the ones most promising so far, to afford electrochemistry experiments in 100% ICIL, of course exploiting the low-volume optimized protocols (paragraph 3.1.2). In particular, we plan to study electropolymerization of enantiopure T₄BT₂ in 100% enantiopure biscollidinium ICIL with suitable counteranion, evaluating the enantiodiscrimination properties of the medium.

In conclusion, the features of the three new classes of inherently chiral ionic liquids available so far are the following ones.

- **1,1'-bis-benzimidazolium di- (or mono-) alkyl salt family**



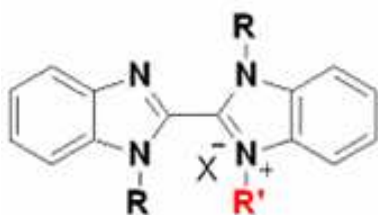
-Very high racemization barrier.

-Very stable enantiomers, neatly separated by preparative HPLC.

-Most of the salts are solid or wax-like at room temperature, since so far double alkylation has succeeded only when either R or R' chains were short ones.

However, they could be used as chirality inductors both as high-percentage co-solvents, or as chiral supporting electrolytes.

- **2,2'-bis-benzimidazolium mono-alkyl salt family**



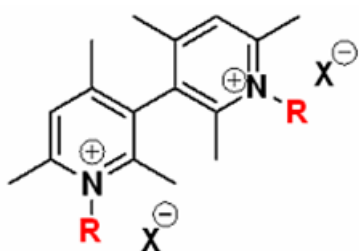
-Easy synthesis, albeit only mono-alkylation has been so far obtained.

-Some of the salts have low melting point and are waxes or oils at room temperature.

-Much lower racemization barriers than 1,1' family and as a consequence enantiomers are unstable at room temperature

The insertion of a bridge of three or four carbon atoms between the two nitrogen atoms does not impair the free rotation so the separation of stable enantiomer is also in this case impossible. Moreover, surprisingly the bridge results in chemical irreversibility of the first reduction process (unlike the case of separate alkyl chains).

- **3,3'-bis-collidinium di- (or mono-) alkyl salt family**



-Easy synthesis of the parent un-alkylated scaffold from inexpensive starting reagents.

-Easy separation of the scaffold enantiomers by fractional crystallization of diastereomeric salts with o,o-dibenzoyl-tartaric acids; this would afford low-cost synthesis of enantiopure salts.

-Low melting points could be obtained, affording liquid salts.

-They display the highest racemization barriers in the three families.

-First test of electrooligomerization using a 3,3'-bis-collidinium salt as supporting electrolyte gives a promising response while evidencing the powerful influence of the anion choice on the oligomerization process.

References

- [1] F. Sannicolò, S. Rizzo, T. Benincori, W. Kutner, K. Noworyta, J. W. Sobczak, V. Bonometti, L. Falciola, P. R. Mussini, M. Pierini, *Electrochim. Acta*, **2010**, 55, 8352
- [2] G. Schiavon, S. Sitran, G. Zotti, *Synth. Met*, **1989**, 32, 209
- [3] K. Meerholz, J. Henze, *Electrochim. Acta*, **1996**, 41, 1839
- [4] B. M. W. Langeveld-Voss, R. A. J. Janssen and E. W. Meijer, *J. Mol. Struct.*, **2000**, 521, 285
- [5] F. Sannicolò, S. Arnaboldi, T. Benincori, V. Bonometti, R. Cirilli, L. Dunsch, W. Kutner, G. Longhi, P. R. Mussini, M. Panigati, M. Pierini, and S. Rizzo, *Angew Chem. Int. Ed.*, **2014**, 53, 2623
- [6] J. Heinze, B.A. Frontana-Uribe, S. Ludwigs, *Chem. Rev.* **2010**, 110, 4724
- [7] F. Entres, D. MacFarlane, A. Abbott, *Electrodeposition from Ionic Liquids*, Weinheim, **2008**
- [8] Y Pang; X. Li; H. Ding; G. Shi; L. Jin; *Electrochimica Acta*, **2007**, 52, 6172
- [9] J. D. Morrison, H. S. Mosher, *Asymmetric Organic Reactions*, Prentice-Hall, Englewood Cliff New Jersey, **1971**
- [10] IUPAC, Compendium of Chemical Terminology, 2nd ed. (the 'Gold Book'), **1997**
- [11] C. Gabrielli, O. Haas, H. Takenouti, *J. Appl. Electrochem.*, **1987**, 17, 82
- [12] M. M. Musiani, *Electrochimica Acta*, **1990**, 35, 1665
- [13] PhD Thesis Valentina Bonometti 'Electrochemistry for the development of innovative three-dimensional and chiral thiophene-based organic semiconductors' **2011/2012**
- [14] A.J. Bard, L.R. Faulkner, *Electrochemical Methods: Fundamentals and Applications*, 2nd ed., Wiley, New York, **2001**
- [15] L.D. Pulfrey, *Photovoltaic Power Generation*, New York, Van Nostrand Reinhold, **1978**
- [16] J. Nelson, *Current Opinion in Solid State and Materials Science*, **2002**, 6, 87.
- [17] J.J.M. Halls, R.H. Friend, M.D. Archer, R.D. Hill, ed. *Clean electricity from photovoltaics*, London: Imperial College Press., **2001**
- [18] D. Kearns, M. Calvin, *J. Chem. Phys.*, **1958**, 29, 950

- [19] F. Yang *et al.*, *Nature Materials*, **2005**, 4, 37
- [20] K. Meerholz, J. Heinze, *Electrochimica Acta*, **1996**, 41, 1839
- [21] T. Benincori, V. Bonometti, F. De Angelis, L. Falciola, M. Muccini, P. R. Mussini, T. Pilati, G. Rampinini, S. Rizzo, F. Sannicolò, S. Toffanin, *Chem. Eur. J.*, **2010**, 16, 9086
- [22] I.F. Perepichka, D.F. Perepichka, *Handbook of Thiophene-based materials: Applications in Organic Electronics and Photonics*, **2009**, Wiley, Chichester, ISBN 978-0-470-05732-2
- [23] F. Sannicolò; P. Mussini; T. Benincori; R. Cirilli; S. Abbate; S. Arnaboldi, S. Casolo; E. Castiglioni; G. Longhi; R. Martinazzo; M. Panigati; M. Pappini; E. Q. Procopio; S. Rizzo, *Chemistry A European J.*, **2014**, 10, 15261
- [24] F. Sannicolò, S. Arnaboldi *et al.* Patent. Appl. MI2014A000948
- [25] W. M. Sears, C. D. MacKinnon, T. M. Kraft, *Synth. Met.*, **2011**, 161, 1566
- [26] M. Takayanagi, T. Gejo, I. Hanazaki, *J. Phys. Chem.*, **1994**, 98, 12893
- [27] S. Abbate *et al.*, *J. Phys. Chem. C*, **2014**, 118, 1682
- [28] F. Zhang *et al.*, *Chem. Sci.* 2, **2011**, 781
- [29] F. Zhang, P. Bäuerle, *J. Am. Chem. Soc.*, **2007**, 129, 3090
- [30] P. Bäuerle *et al.*, *Angew. Chem Int. Ed.*, **2007**, 119, 367
- [31] A. Kaiser, P. Bäuerle, *Top. Curr. Chem.*, **2005**, 249, 127
- [31] J. Casado *et al.*, *J. Raman Spectroscopy*, **2004**, 35, 592
- [32] G. Fuhrmann, T. Debaerdemaeker, P. Bäuerle, *Chem. Commun.*, **2003**, 948
- [33] G. Fuhrmann, J. Krömer, P. Bäuerle, *Synth. Met.*, **2001**, 119, 125
- [34] J. Krömer *et al.*, *Angew. Chem. Int. Ed.*, **2000**, 112, 3623
- [35] A. Mishra, C.-Q. Ma, J. L. Segura, P. Bäuerle, in *Thiophene-based materials*, I. F. Perepichka, D. Perepichka Eds. (John Wiley & Sons Ltd, Chichester, UK, **2009**), vol. 1, pp. 74-97
- [36] A. A. Isse, P. R. Mussini, A. Gennaro, *J. of Phys. Chem. C* , **2009**, 113, 14983
- [37] A. Gennaro; A. A. Isse; E. Giussani, P. R. Mussini; I. Primerano; M. Rossi, *Electrochimica Acta*, **2013**, 89, 52

- [38] S. Arnaboldi, A. Gennaro, A. A. Isse, P. R. Mussini, *Electrochimica Acta*, **2014**, submitted
- [39] Z. Jiang, V. Schurig, *J. Chromatogr. A.*, **2008**, 262, 1186
- [40] J.N. Akanaya, D.R. Taylor, *Chromatographia*, **1988**, 25, 639

4. Appendix: Removal of Cl^- Impurities from Ionic Liquids by AgCl Deposition on Silver Electrode [1]

Chloride impurities in ionic liquids, which can be present even in huge amounts depending on the IL synthetic route, are particularly critical for electrochemical processes; thus, their abatement is often mandatory.

For example, the ionic liquid used in most experiments in this PhD thesis (BMIMPF_6) contains several amount of chlorides, causing poor success in several electrochemical experiments. In particular this impurity can affect the electrooligomerization process influencing the morphology of the resulting films (for instance by involvement in the doping/undoping processes); they can result in severe irreproducibility of CV peak potentials and of electrolysis conditions if an $\text{Ag}|\text{AgCl}$ pseudo-reference electrode is used instead of a true reference electrode (typically, when working on screen printed electrodes); their specific adsorption can alter the performance of electrocatalytic electrodes, such as Ag and Au in our DET studies concerning organic halides; in the same studies, when working with organic bromides, a significant presence of chloride impurities can result in unwanted, fast nucleophilic substitution of the leaving group of the molecule under study. Moreover Cl^- signals, if present in large amount, are clearly visible in the anodic regions, making the CV pattern interpretation more difficult.

Such a huge impact of the IL halide impurities has prompted application of different analytical techniques to their quantitative determination, but, surprisingly, very few approaches to the electrochemical abatement of IL halide impurities have so far appeared. One of them involves Cl^- electrooxidation to Cl_2 , on Pt anode, at constant potential, in a divided cell [2]. A more recent, similar study deals with both Cl^- and Br^- concurrently [3], in a cell divided by an anion exchange membrane, the cathodic compartment being filled with HNO_3 or HBF_4 solutions in order to provide convenient anions to replace the

eliminated halide ions. The working potential is +1.6 V (*vs.* Ag|AgCl) at room temperature in the bromide case and +1.4 V (*vs.* Ag|AgCl) at 80 °C in the chloride one. The electrolytic process must be followed by a treatment with ethylene gas to capture the electrogenerated Br₂ and Cl₂; the resulting halogenated products are then volatilized under vacuum. On the whole, the working conditions (high potential and temperature, strong acid, ethylene gas, halogenated products to be volatilized, multiple step) appear far from mild and easily scalable.

In this context, we have developed a very simple but effective protocol consisting in performing the electrooxidation process on a silver anode. Silver oxidation to silver chloride allows to operate at a very mild potential and room temperature, while the oxidation products directly grow on the Ag electrode as a compact, stable layer. Actually the process coincides with the electrolytic production of a Ag|AgCl electrode, a very favourable process in ionic liquids (which, as we have already mentioned, are very good media for electrodepositions). The process proceeds at room temperature, at very mild potentials, with nearly ideal current efficiencies, and with negligible side effects on the electrolyzed IL. The chloride impurities are quantitatively captured and accumulated on the silver wire and eliminated by simply extracting the resulting Ag|AgCl electrode from the solution, with no need of subsequent treatments.

Concerning the counter reaction, the choice of a Pt cathode in the presence of a sufficient amount of residual water in the IL implies hydrogen evolution with concurrent pH increase; this could be beneficial to the IL, too, since most ILs have H⁺ impurities besides halide ions. The electrolytic process can be monitored by a second smaller Ag electrode, provided that suitable calibration is previously made in the same conditions.

Thus, to evaluate the chloride amount before, during, and after the abatement process, the multitechnique voltammetric protocol on Ag and GC electrodes described in the experimental section (paragraph 2.1.7) was applied, similar to one previously proposed in the literature [4], but with some modifications, particularly the much milder accumulation

potential. The linear dynamic ranges (either considering current or charge) afford safe application of the standard addition technique (SAT) for quantification of chloride concentration, of course selecting the appropriate voltammetric technique according to the concentration range. A chloride content of *ca.* 0.7 ppm and 4÷7 ppm was thus estimated for BMIMPF₆ 98.5% and 97.0% purity (Figure 1a and 1d), respectively. Interestingly, a significant variation in the chloride amount (*e.g.* 4÷7 ppm for BMIMPF₆ 97.0%) was detected in different batches of the same IL purchased in different times. A huge amount of chlorides (*ca.* 0.01 mol dm⁻³) was estimated in the 98% 'BASF-Quality' BMIMBF₄ sample by comparing its chloride peak current with the aforementioned calibration plots for BMIMPF₆.

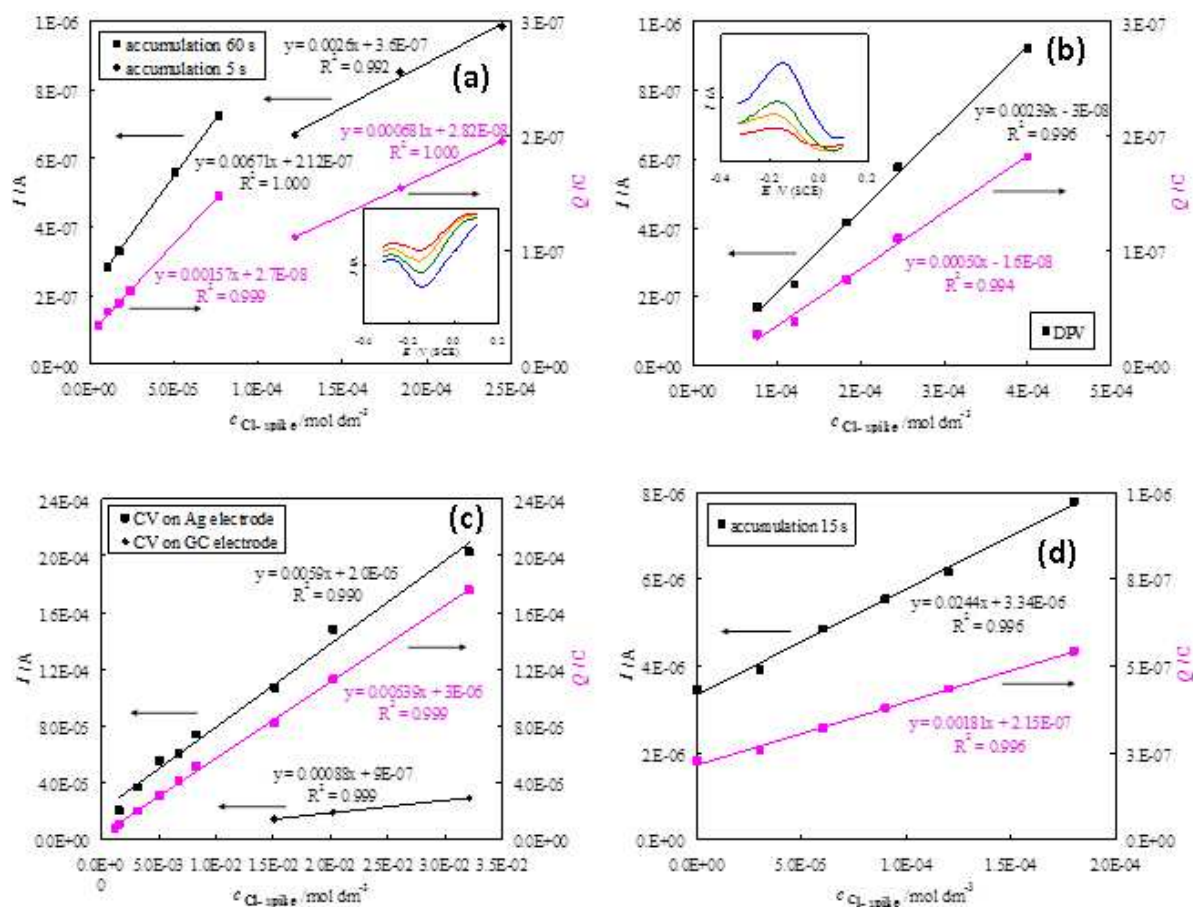


Figure 1. Calibration curves in BMIMPF₆ >98.5% for $5 \cdot 10^{-6} + 3.2 \cdot 10^{-2}$ mol dm⁻³ added chlorides from a TEACl standard solution, employing different voltammetric techniques at increasing concentrations ((a), CSV; (b), DPV; (c), CV). Insets: examples of CSV (a) and DPV (b) patterns used for the calibration. (d) Standard addition technique plot for commercially available BMIMPF₆ >97.0%. Cathodic stripping: 0.4 and 0.1 V (*vs.* SCE) deposition potential for (a) and (d) respectively. Working electrode: Ag disk (0.071 cm²), GC disk (0.031 cm²)

Abatement of the chloride impurities has been performed both on an artificially spiked IL (0.032 M Cl⁻ added to the purest BMIMPF₆), and on pristine 98% 'BASF-Quality' BMIMBF₄ (Figure 2) by constant-potential electrolysis on an Ag pigtail working electrode at 0.2 V (*vs.* SCE) at room temperature. The counter electrode, in the same IL, was inserted in a jacket ending with a porous frit. In fact we had observed that the reduction process at the counter electrode can result in brown coloring which we associated with products of dialkylimidazolium reduction when only low amounts of water are present [2]. However, it was sufficient to insert a few drops of water in the counter electrode compartment to prevent such a process, turning to hydrogen evolution with concurrent acidity

consumption, as confirmed by pH measurements. The latter process would be a desirable complementary reaction that could be exploited working in undivided cell in the case of an ionic liquid having acidic impurities concurrently with the chloride ones.

The electrodeposition process was very regular, actually a typical feature of IL media [5-7]. Starting currents depended on the starting chloride concentrations and IL viscosity (typically $3\text{-}4\cdot 10^{-4}$ A for the spiked BMIMPF₆ and $8\text{-}9\cdot 10^{-4}$ A for pristine BMIMBF₄) and regularly decreased with decreasing chloride concentration, monitored by periodical scans on the analytical Ag disk electrode, pointing to a first-order kinetics, implying

$$\ln(c/c_0) = \ln(Q/Q_0) = -kt \quad (3)$$

where Q and Q_0 are the DPV or CV peak charges at time t and $t = 0$ respectively, and a concentration-independent halving time of

$$t_{1/2} = \ln 2/k \quad (4)$$

Fitting the experimental data with equation (3) yields (a) $k = 5\cdot 10^{-5}$ s⁻¹ implying from equation (4) $t_{1/2} = 1.3\cdot 10^4$ s in the case of artificially spiked 0.032 M BMIMPF₆ and (b) $k = 1.2\cdot 10^{-4}$ s⁻¹ and $t_{1/2} = 5.9\cdot 10^3$ s in the case of pristine 98% BMIMBF₄ (Figure 3). The differences in the rate constants can be attributed to the lower viscosity of the BF₄⁻ derivate. The charge passed (obtained by integrating the current *vs* time characteristics) appeared to be consistent with the concentration decrease monitored by voltammetric techniques, and the charge passed for chlorides below the CSV limit of detection was only slightly higher than the theoretical one, implying a nearly quantitative current yield for the desired AgCl formation reaction. In our conditions (implying a working electrode surface : IL volume ratio of about 1.4-1.6 cm⁻¹) this typically required *ca.* 12 hours, which is however not a problem since the process is well controlled and can safely proceed overnight, just like when performing the first step of bielectrolytic Ag|AgCl electrode preparation according to the classical protocol [8]. In any case, a shorter time could be achieved by increasing the above operating ratio. The final solution is colorless as at the beginning, its CSV pattern satisfactory, and no significant pH change is observed, provided that the counter electrode is inserted in the separated jacket. The chloride impurities are then removed by simply

extracting the Ag|AgCl electrode, from which the Ag wire can be easily recovered by sandpaper treatment or immersion in NH_3 solution.

There is no apparent limit in the concentration of chloride impurities to be abated, consistently with the conductivity of the AgCl film and the slow process rate.

As an example, the DPV and CSV monitoring of the electrolysis concerning pristine 98% BMIMBF₄ is provided in Figure 2. In particular DPV was used to follow the first part of the electrolysis, and CSV for the last part, at very low chloride concentrations. Incidentally, it can be observed that the shape of DPV peaks is no more canonical above *ca.* 0.0005 M.

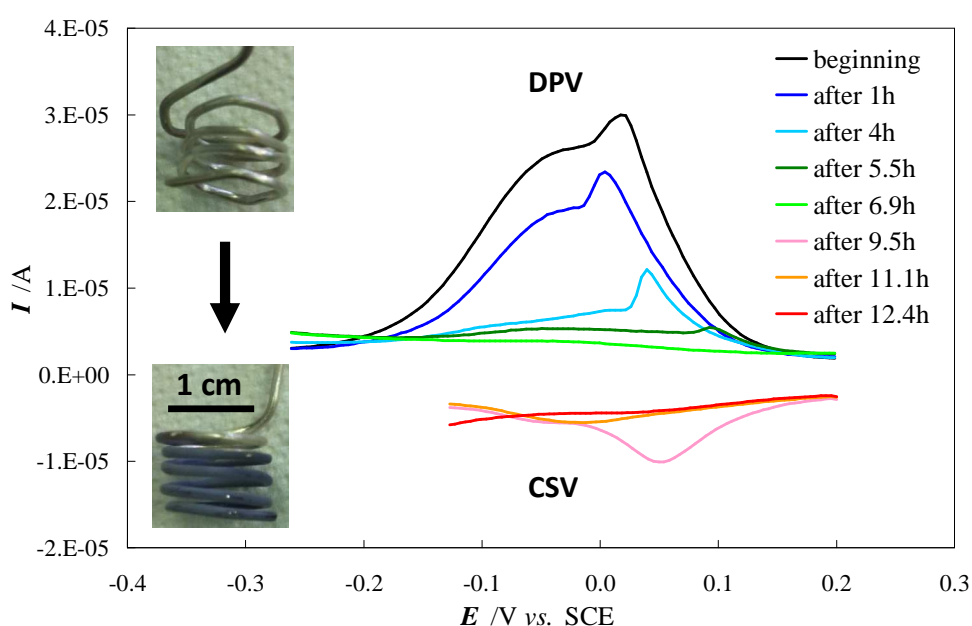


Figure 2. DPV and cathodic stripping voltammograms, CSV, on Ag disk electrode (0.071 cm^2) recorded during the electrolysis of Cl^- in 0.003 dm^3 BMIMBF₄ using a Ag wire as anode (before and after the electrolysis, in the two pictures). Constant potential electrolysis at 0.2 V (*vs.* SCE). Stripping parameters: 0.2 V (*vs.* SCE) deposition potential, 120 s accumulation time

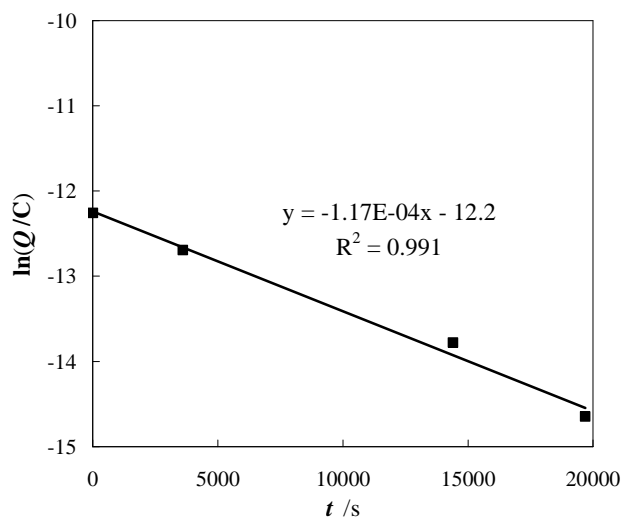


Figure 3. Ln Q vs t plot for the chloride abatement in BMIMBF₄ ionic liquid, and related regression curve

References

- [1] S. Arnaboldi, M. Magni, P. R. Mussini, A. Gennaro, A. A. Isse, *Electrochemistry Communications*, **2014**, submitted
- [2] L. Xiao, K.E. Johnson, *J. Electrochem. Soc.*, **2003**, 150, E307
- [3] Z. Li, Z. Du, Y. Gu, L. Zhu, X. Zhang, Y. Deng, *Electrochem. Comm.*, **2006**, 8, 1270.
- [4] C. Villagran, C. E. Banks, C. Hardacre, R.G. Compton, *Anal. Chem.*, **2004**, 76, 1998
- [5] M. Freemantle, *An Introduction to Ionic Liquids*, Royal Society of Chemistry, London, **2009**
- [6] P. Hapiot, C. Lagrost, *Chem. Rev.*, **2008**, 108, 2238
- [7] F. Endres, D. MacFarlane, A. Abbott, *Electrodeposition from Ionic Liquids*, Wiley-VCH, Weinheim, **2008**
- [8] D. I. J. Ives, G. J. Ianz, *Reference electrodes, theory and practice*, Academic Press, New York and London, **1961**

Conclusions

The originality and applicative relevance of the results obtained in this thesis work greatly exceeded the expectations of the initial research plan, which was of prevalingly fundamental character, being aimed to the detailed study in ionic liquids, emerging media for safe and environmentally friendly chemical and electrochemical processes, of two important electrochemical model processes, namely radical-cation based electrooligomerizations of thiophene-based monomers and radical-anion based cleavage of the carbon halide bond.

The turning point was choosing as monomer substrates for the oligomerization research line, in cooperation with the research group of Professor Sannicolò, thiophene-based monomers endowed with inherent chirality, *i.e.* implying a stereogenic element not external to, but coinciding with, the whole electroactive backbone, derived from a tailored torsion originating in the molecule by the insertion of atropisomeric scaffolds. Therefore both chirality and electroactivity are stricly connected, originating from the same element, which constitutes the main part of the molecule. Moreover, as we have verified, such property is fully transmitted to the oligomers obtained by the monomer electrooxidation. Thus, the 'inherent chirality' concept has turned out to afford molecular materials endowed with powerful chirality manifestations plus an unprecedented pool of other outstanding properties.

Thus, in the first part of this research, electrooligomerization in ionic liquids of the first inherently chiral monomer afforded to evidence and exploit the outstanding enantiodiscrimination ability of the resulting inherently chiral electroactive films, providing the first electrode surfaces able to neatly discriminate the antipodes of chiral probes in terms of difference in the signal potentials, rather than, as in former literature attempts, in current intensities (which did not afford to quantify enantiomeric excesses in

chiral probes).^{2,3} Very importantly, such properties are of general character: we have shown that they hold with different chiral probes, also of pharmaceutical interest like DOPA and ofloxacin, and in different media and with different electrode supports (albeit the combination ionic liquid + screen printed supports is the optimal one). Furthermore, we have shown such response to be linear with concentration. These features can afford for instance evaluation of enantiomeric excesses on cheap, disposable electrodes, or as a postchromatographic electrochemical sensor, and opens the way to chiral voltammetry.

However, such results, albeit of outstanding importance in the analytical field, only represent a facet of the polyhedral innovation potential of the new materials studied in our research.

In fact we discovered that the oligomer films electrodeposited or chemically synthesized from several inherently chiral monomers mostly consisted of *cyclic* oligomers (mainly dimers and trimers) rather than linear ones. This provides an entirely new class of inherently chiral electroactive oligothiophene macrocycles, soluble in organic solvents and therefore easily processable, of simple synthesis from unexpensive reactants, endowed with an exceptional pool of properties, which prompted us to submit a patent application⁴:

As racemates:

- highly and reversibly electroactive,
- idealizing conducting polymers without end, with no defectivity connected with active terminals;

² F. Sannicolò, S. Arnaboldi, T. Benincori, V. Bonometti, R. Cirilli, L. Dunsch, W. Kutner, G. Longhi, P. R. Mussini, M. Panigati, M. Pierini, and S. Rizzo, *Angew Chem. Int. Ed.*, **2014**, 53, 2623

³ F. Sannicolò; P. Mussini; T. Benincori; R. Cirilli; S. Abbate; S. Arnaboldi, S. Casolo; E. Castiglioni; G. Longhi; R. Martinazzo; M. Panigati; M. Pappini; E. Q. Procopio; S. Rizzo, *Chemistry A European J.*, **2014**, 10, 15261

⁴ F. Sannicolò, S. Arnaboldi *et al.* Patent. Appl. MI2014A000948

- energy parameters similar to popular semiconductors employed in photovoltaic applications (and more expensive), and modulable by structure design; promising preliminary results for the trimer as donor in bulk heterojunction solar cells;
- the electrooligomerization process also takes place on alternative flexible supports like ITO/PET, a useful feature for application in solar flexible organic cells;
- photoactive as demonstrated by recently photocurrent experiments;
- electrochromic;
- displaying charge-trapping effects;
- providing cavities functionalized with S and N heteroatoms, which, like for instance cyclodextrins, can act as hosts for a variety of guests, including semiconductors of complementary properties;
- showing outstanding 3-D character and ability to oligomerize, so that they can be used as comonomers to obtain fast and regular polymerization of monomers of interesting functional properties but poor oligomerization ability (as in molecular imprinted polymers for use in piezogravimetric sensors by our partner group at the Institute of Physical Chemistry of the Polish Academy of Science, Warsaw).

As enantiomers (the new ringlets, in which electroactivity and chirality are strictly interconnected, are an outstanding addition to the library of dissymmetric organic cavities. The preparative enantioseparation of the monomer racemate is not a severe limitation given the capacity of modern chiral technologies to resolve racemates at the level of several kilograms):

- impressive polarized light rotation angles and circular dichroism spectra;
- torsional angles and chirality manifestations reversibly modulable by the electric potential ('breathing chirality');
- circularly polarized luminescence;
- outstanding enantiodiscrimination ability as chiral electrodes, as already mentioned;

- very recently, self-supported membranes have been obtained (Figure on the left)



starting from a chiral monomer deposited on ITO electrodes. The film was completely removed from the electrode surface by cycling in a solution of water and 0.1 M lithium perchlorate. The potential applications could be for example in medicinal chemistry, as chiral separation membranes. Further

investigations are in progress to fully characterise these membranes.

Of course the above outstanding and unforeseen results prompted us to concentrate our efforts on the electrooligomerization process rather than the halide-carbon cleavage one, to explore and exploit the potentialities of the new class of inherently chiral electroactive cyclic oligomers.

However, an interesting CV and EIS reactivity study has been carried out in ionic liquid concerning the C-X reductive cleavage by dissociative electron transfer in a series of model organic bromides of different structures (accounting for different dissociative electron transfer mechanisms). The results of this original study afford a first extension to the world of ionic liquids of our former mechanistic studies concerning the above fundamental process in traditional solvents. Moreover, to our knowledge, the study provides the first example of EIS application to such mechanistic issues.

Finally, having verified the general validity and effectiveness of the inherent chirality approach, and considering our concern for ionic liquids, we have started, again in cooperation with Professor Sannicolò's group, and with the support of Fondazione Cariplo (as in the case of inherently chiral oligomers) a further research line, concerning the implementation of inherent chirality in new-concept ionic liquids, with the target of obtaining new, attractive media for chemical and electrochemical processes, possibly of cheap and simple synthesis, affording safe, mild and environmentally friendly operating

conditions, as intrinsic to the ionic liquid class, combined with powerful chirality manifestations. In this research line the inherent chirality property is being implemented by a tailored torsion in the ionic liquid cationic scaffold, according to three alternative approaches (based on 1,1'-bis-benzimidazole, 2,2'-bis-benzimidazole, and 3,3'-bis-collidine scaffolds, respectively), which are under comparative evaluation, mostly based on electrochemical studies, affording rationalizing guidelines for structure-properties relationships in the new molecule classes.

Finally, as a corollary work in the ICIL development, a very simple, cheap and effective 'Egg of Columbus' protocol to completely remove chlorides impurities from commercial ionic liquids was developed. Commercially available ionic liquids often contain huge amounts of halide impurities which derive from the synthetic process and that can dramatically affect chemical and above all electrochemical processes. Several approaches have been so far proposed in the literature to solve the problem, none of them satisfactory. Our protocol affords complete abatement of the chloride impurities in a single step, at room temperature, at very mild potentials, with nearly ideal current efficiencies, and with negligible side effects on the electrolyzed IL. It practically coincides with the electrolytic preparation of a Ag|AgCl electrode, a very regular and safe process in the IL medium. The chloride impurities are thus captured and accumulated on the silver wire and eliminated by simply extracting the resulting Ag|AgCl electrode from the solution, with no need of subsequent treatments. The process is carried out in a divided cell when the water and acidity content is low, but it could offer the nice opportunity to simultaneously abate acidic impurities (when present) together with chloride ions. Moreover, it appears of general validity for halide ions, affording simultaneous purification, for instance, from bromide and chloride traces.

Of course many further developments can be thought of, starting from the above summarized results. Particularly urgent and desirable appear, on one side, the achievement and applicative experimentation of the new inherently chiral ionic liquids

under development; on the other side, a more complete elucidation and full exploitation, with ionic liquid media as valuable tools, of the outstanding applicative potentialities of the new class of inherently chiral electroactive cyclic oligomers, both as racemates and as enantiomers, in a wide range of in photovoltaic, optoelectronic, and sensor applications.

Acknowledgements



fondazione
c a r i p l o

Grants no. **2011-0417** (inherently chiral electrodes) and
no. **2011-1851** (inherently chiral ionic liquids).

Dr. Mirko Magni, Dr. Elisa Lo Bello, Dr. Sephira Riva, Dr. Valentina Bonometti

Electrochemistry Group of Università degli Studi di Milano

**Prof. Francesco Sannicolò, Prof. Benincori Tiziana, Dr. Voichita Mihali,
Dr. Simona Rizzo**

Organic Chemistry Group of Università degli Studi di Milano

Dr. Monica Panigati, Dr. Elsa Quartapelle

Università degli Studi di Milano

Spectroscopy and Synthesis

Prof. Włodzimierz Kutner, Prof. Krzysztof Noworyta

IPC PAS, Warsaw, Poland.

Prof. Andrea Penoni

Organic Chemistry group of Università dell'Insubria Sede di Como

Indole synthesis

Prof. Armando Gennaro, Dr. Abdirisak Ahamed Isse

Mechanistic Studies, Università degli Studi di Padova

Dr. Roberto Cirilli

Dip. del Farmaco, Ist. Superiore di sanità, Roma

Racemate resolution at analytical and preparative level by chiral HPLC

Prof. Marco Pierini,^a Dr. Rocco Martinazzo^b

^aUniversità di Roma La Sapienza, Roma

^bUniversità degli Studi di Milano

Theoretical computations

Prof. Sergio Abbate, Prof. Giovanna Longhi, Dott. Ettore Castiglioni

Dipartimento di Scienze Biomediche e Biotecnologie, Università di Brescia

Solid-state circular dichroism

